Study of the cryopreservation-related stresses in the lactic acid bacterium Lactobacillus delbrueckii subsp. bulgaricus through a global and multi-scale approach

Julie Meneghel

université PARIS-SACLAY

NNT : 2017SACLA030

AgroParisTech
INSTITUT DES SCIENCES ET INDUSTRIES DU VIVANT ET DE L'ENVIRONNEMENT
PARIS INSTITUTE OF TECHNOLOGY FOR LIFE, FOOD AND ENVIRONMENTAL SCIENCES

Study of the cryopreservation-related stresses in the lactic acid bacterium *Lactobacillus delbrueckii* subsp. *bulgaricus* through a global and multi-scale approach

Thèse de doctorat de l'Université Paris-Saclay
préparée à l'Institut des sciences et industries du vivant et de l'environnement (AgroParisTech)

École doctorale n°581 Agriculture, alimentation, biologie, environnement et santé (ABIES)
Spécialité de doctorat: Sciences de la vie et de la santé

Thèse présentée et soutenue à Paris, le 12 octobre 2017, par

Julie Meneghel

Composition du Jury :

Pascale Serror Directeur de recherches, INRA Jouy-en-Josas – Institut MICALIS	Président
Laurent Beney Professeur, AgroSupDijon – UMR PAM	Rapporteur
Andrea Gomez-Zavaglia Directeur de recherches, CONICET– CIDCA	Rapporteur
George John Morris Président Directeur Général, Asymptote	Rapporteur
Muriel Mercier-Bonin Chargé de recherches, HDR, INRA Toulouse – UMR TOXALIM	Examinateur
Fernanda Fonseca Directeur de recherches, INRA Grignon – UMR GMPA	Directeur de thèse
Paul Dumas Directeur de recherches émérite, CNRS – Synchrotron SOLEIL	Co-Directeur de thèse

INRA Grignon, UMR 0782 GMPA, Avenue Lucien Brétignières, 78850 Thiverval-Grignon
Synchrotron SOLEIL, lignes de lumière SMIS et DISCO, 91190 Gif-sur-Yvette

Thèse de doctorat

« À trop se soucier de l'achèvement des choses,
On n'entreprend jamais rien »

François I^{er},
à propos de la construction du Château de Chambord

This statement, pronounced by François I^{er} during the building of the Château de Chambord, could probably be translated to:

Worrying too much about the completion of things,
One never engages in anything.

REMERCIEMENTS (ACKNOWLEDGEMENTS)

Tout d'abord, je souhaiterais remercier chaleureusement Andrea Gomez-Zavaglia, Directrice de Recherches du CIDCA CONICET argentin ainsi que Laurent Beney, Professor à AgroSup Dijon, d'avoir accepté la tâche de rapporteur de ces travaux. Merci également à Muriel Mercier-Bonin, Chargée de Recherches à l'INRA de Toulouse, à Pascale Serror, Directrice de Recherches à l'INRA de Jouy-en-Josas, ainsi qu'à John Morris de faire partie de ce jury de thèse et d'examiner mes travaux.

Je voudrais ensuite remercier le laboratoire GMPA de l'INRA de Grignon, dirigé par François Boué puis Pascal Bonnarme, pour m'avoir accueillie et offert des conditions de travail optimales. Merci également au Synchrotron SOLEIL de m'avoir offert un accès permanent à son site ainsi qu'un bureau lors de mes séjours ponctuels.
Parlant de conditions de travail optimales, je remercie vivement le département CEPIA de l'INRA (Caractérisation et Elaboration de Produits Issus de l'Agriculture), ainsi que l'Université Paris-Saclay *via* le programme interdisciplinaire IDI, pour avoir chacun co-financé ce projet doctoral. Enfin, j'adresse de sincères remerciements à l'école doctorale ABIES, au travers de Cyril Kao puis d'Alexandre Pery qui l'ont dirigée, une école doctorale humaine et souciante de chacun de ses doctorants. Je la remercie surtout au travers d'Irina Vassileva, pour son écoute bienveillante et son soutien qui ont énormément compté pour moi.

Maintenant, j'adresse un immense et sincère remerciement à Fernanda Fonseca et Stéphanie Passot, respectivement directrice et chargée de recherches au GMPA et co-directrice et co-encadrante de ma thèse. Merci pour tous vos précieux enseignements, conseils et encouragements ! Merci aussi à Paul Dumas et Frédéric Jamme, scientifiques au Synchrotron SOLEIL et respectivement co-directeur et co-encadrant de ma thèse. J'ai énormément appris à vos côtés, tant sur un plan scientifique que personnel et humain ! Merci à vous quatre de m'avoir laissé une grande autonomie au quotidien, mais aussi le choix parmi les vastes possibilités d'investigation permises par ce projet ainsi que les moyens adéquats pour leur réalisation. Merci enfin pour votre disponibilité, votre patience, et d'avoir mis la main à la pâte côté manipes et de ne jamais avoir compté vos heures à SOLEIL, fussent-elles diurnes ou nocturnes !
Un grand merci également à Séverine Layec, Enseignant-chercheur AgroParisTech, Maarten van de Guchte, Directeur de Recherches à l'INRA de Jouy-en-Josas, et Ganesh Sockalingum, Professeur à l'Université de Reims Champagne-Ardenne, pour m'avoir conseillée et accompagnée tout au long de cette thèse en tant que membres de comité de cette thèse. Merci en particulier à

Maarten pour m'avoir confié la souche *L. bulgaricus* ATCC 11842 qui m'aura finalement considérablement servi ! ainsi qu'à Ganesh pour avoir aimablement proposé d'effectuer (puis effectué !) quelques tests Raman.

Côté SOLEIL, je remercie toute l'équipe SMIS et toute l'équipe DISCO pour m'avoir chaleureusement accueillie à chacun de mes séjours au Synchrotron et pour m'avoir fait découvrir la physique de pointe. Ça a toujours été un réel plaisir pour moi d'échanger avec vous et de travailler à vos côtés. Un grand merci donc, et ce tout particulièrement à Christophe Sandt, Stéphane Lefrançois et Wiliam André côté SMIS, et à Matthieu Réfrégiers côté DISCO.

D'un point de vue un peu plus spécifique des travaux qui ont été effectués, j'adresse un chaleureux remerciement à Stéphanie Cénard, technicienne au GMPA jusqu'à la réussite de son concours et son envol dans le Sud (qui sont arrivés trop tôt !). Merci pour m'avoir d'abord formée à la microbio du GMPA, puis pour avoir partagé la paillasse avec moi et m'avoir soutenue dans les nombreuses récoltes, lavages cellulaires et CinAc ! Merci également d'avoir toujours accepté de me filer un coup de main dans les coups de bourre ! Ta bonne humeur au quotidien a été communicante et précieuse, pareil pour ta fermentite aigue (surtout pour le brassage) que tu as su me transmettre 😉 ! Pour son importante contribution à mon projet de thèse, son travail impeccable, sa douceur et sa gentillesse, je souhaite remercier vivement Jiawei Xu d'avoir choisi d'effectuer son stage UTC à mes côtés. J'ai beaucoup apprécié cette expérience d'encadrement et te souhaite bonheur et réussite !

Côté formation, je tiens à remercier toutes les personnes qui ont donné de leur temps pour me transmettre leur savoir-faire : Pascale Lieben pour la spectro infrarouge, Sébastien Dupont pour la spectrofluorimetrie à Dijon, Caroline Pénicaud pour l'ASE et la GC-MS ainsi qu'Armelle Delile et Brigitte Pollet lors d'éventuels soucis sur ces appareils, Marielle Bouix et Sarah Ghorbal pour la cytométrie en flux, Eric Dugat-Bony pour la transcripto, Christophe Monnet et Séverine Layec pour la génomique comparative, Jérôme Delettre pour la protéo… Merci aussi Jérôme pour les toutes dernières manipes in extremis et le gardiennage ponctuel de la bête !

Merci à nouveau à Stéphane Lefrançois de s'être autant impliqué dans les travaux de conception du microscope inversé et des multiples petits équipements qui ont été d'une utilité cruciale. Merci aussi encore une fois à Christophe Sandt pour avoir toujours eu une oreille attentive, un conseil ou une solution pertinente en cas de besoin ! Merci à vous deux pour votre générosité.

Pour leur travail administratif indispensable, mais aussi pour leur disponibilité, leur grande amabilité et l'approvisionnement en chocolats et pâte à tartiner, je remercie également Laurence Fruchart, Thierry Feugnet et Evelyne Philippe, gestionnaires au GMPA. Merci aussi à Michel Savy pour les dépannages informatiques, à Bruno Perret pour avoir fait des adaptations logicielles sur-

mesure, et aux gars de l'atelier pour le soutien logistique (Jérôme Bussière, David Lévêque et Frédéric Lecornué) !

Pour en finir avec le GMPA, je souhaite remercier l'ensemble de son personnel que j'ai pu côtoyer, des personnes avec chacune desquelles j'ai pu entretenir des liens souvent amicaux. Je pense en premier lieu à mes compatriotes de bureau : Hélène et Greg (Grogware), puis Sichao, Michele, Marine, Florence et Phuong. Ç'a vraiment été chouette d'avoir passé bout de temps plus ou moins (mais jamais assez !) long à vos côtés ! Les voisins tout proches de la plateforme et autres thésards ont également largement contribué à rendre le travail quotidien au GMPA plus qu'agréable : Solenne (Mich'Miche), Vincent (Chaton), Vincent (Bibiche), Nadège (Nadou), David (Dave), Salma (Princesse au petit pois), Hélène (Bidochette), Florian, Gilles, Mathieu (Batman), Daniela, Phuong et les expatriés de Malices au 2ème étage : Thuy Minh, Julien, Benoît, Thomas, Marc et Bernadette. Également les stagiaires, avec la fournée « Batman contre Joker » et la performance remarquée de Thomas, Gautier, Eugénie et Lucille, puis la fournée musicienne et épicurienne avec Hubert, Marianne et Hélène, mais encore Florent (Robin). Et enfin bien d'autres membres du GMPA, dont la Ronneba et ses jeux de mots incroyables, Steven Le Feunteun, Thomas Cattenoz, Claire Saulou, Sandra Helinck, Isabelle Souchon, Catherine Béal, Violaine Athès, Marwan Moussa, François Boué, Evelyne Lutton, Dominique Swennen, Alberto Tonda, Anne-Sophie Sarthou, Jessie Castellote, Eric Spinnler, Françoise Irlinger, Daniel Pique pour n'en citer que quelques-uns… Les dégustations hebdomadaires d'AOP fromagères vont me manquer !

Maintenant je voudrais remercier l'ensemble des personnes qui ont contribué à rendre mon quotidien en dehors du labo des plus agréables et inoubliables ! D'abord (et à nouveau) Greg, Bibiche, Chaton, Nadou et Mich'Miche, pour les apéros, tartiflettes, fondues… clin d'œil particulier à Greg pour sa cultissime blague du poil et à sa maman pour m'avoir confié la garde de sa chatte 😉 ! Et plus récemment Mathieu pour ses calembours et autres jeux de mots, Florence pour m'avoir tenue à jour des actualités scientifiques dignes des Ig Nobels et fait découvrir de nouveau horizons musicaux (parfois douteux avec les rappeurs sensibles, les collectionneurs de canards et les amoureux de l'Aveyron), et pour m'avoir tirée d'affaire *in extremis* dans mon duel de mise en page contre Word !! Anna-Karen, Amélie, Anne-Cécile, Audrey et Luciana ! Puis l'ensemble des grignonais, avec qui les activités « home-made » (slack-line, piscine, ventrigliss, cinéma en plein air), et celles plus sportives (l'escalade, les randos et les courses à pied, parfois dans la boue), les excursions (Bruxelles, Lille, Grenoble, le Jura pour la percée du vin jaune, Fort-Mahon, Dijon, Grande-Synthe, Les Deux Alpes, Strasbourg, Cambridge, les fêtes de l'Huma…), Hero Corp, les repas, les barbecues, les cours d'œno avec Cyrielle et les « vrais » villageois, mais surtout les apéros et les tranches de poilade n'ont pas manqué ! Je pense donc à tous les habitants de la « cité ! » de Grignon ainsi qu'à ses affiliés, notamment Damien (RamDam la grenouille),

Gaspard (Gaspou), Clémence (Ravière), Guigui, Oliv', Marie, Aurore, Leticia, Karen, Anne-Lise, Leticia, Romain, Fiona et Nith, mais surtout, surtout, les déesses du 2A, mes colocataires de choc et ami(e)s : Anaïs, Laure, Ophélie et Arthur (ben…oui, lui aussi !). Merci pour votre générosité, les moults repas, cinés et DVD partagés ensemble, nos discussions enrichissantes et votre réconfort sans faille, même dans les moments qui ont pu être rudes ! C'est une chance pour moi d'avoir pu (et de pouvoir) compter sur vous !

Enfin, je voudrais remercier les personnes qui m'ont accompagnée d'un peu plus loin, mais qui ont toujours été présentes pour moi, déjà bien avant cette thèse : les dijonnaises Annikou, Annabulle et Jennie, les daixois Guillaume Poby et Matthieu Bato, et les Agrosupiens Seb, Zizie, Lucie, Neyla et Helena. Je n'oublie pas non plus Thibaud pour qui j'ai une pensée toute particulière, lui qui a contribué à ce que je m'engage dans ce projet de thèse. Last but not least, un immense merci à ma famille et aux personnes tout proches de celle-ci, qui m'ont apporté soutien et encouragements constants, ainsi que des refuges bien ressourçants ! Merci Maman, Romain, Aurélie-Anne et André.

PUBLICATIONS AND COMMUNICATIONS

Published works in peer-reviewed journals

Fonseca F, **Meneghel J**, Cénard S, Passot S and Morris JG (2016). Determination of intracellular vitrification temperature for unicellular microorganisms under conditions relevant for cryopreservation. PLoS ONE 11(4): e0152939.

Meneghel J, Dugat-Bony E, Fonseca F, Irlinger F, Loux V, Vidal M, Passot S, Béal C, Layec S and Fonseca F (2016). Draft genome sequence of *Lactobacillus delbrueckii* subsp. *bulgaricus* CFL1, a lactic acid bacterium isolated from French handcrafted fermented milk. Genome Announc 4(2): e00052-16.

Meneghel J, Passot S, Dupont S and Fonseca F (2017). Biophysical characterisation of the *Lactobacillus delbrueckii* subsp. *bulgaricus* membrane during cold and osmotic stress and its relevance for cryopreservation. Appl Microbiol Biotechnol 101: 1427-1441.

Meneghel J, Passot S, Cénard S, Réfrégiers M, Jamme F and Fonseca F (2017). Subcellular membrane fluidity of *Lactobacillus delbrueckii* subsp. *bulgaricus* under cold and osmotic stress: heterogeneity is related to sensitivity. Appl Microbiol Biotechnol, 101:6907-6917.

Deuscher Z, Bonny JM, Boué F, Cheynier V, Clerjon S, Devaux MF, **Meneghel J**, Guillon F, Jamme F, Le Feunteun S, Passot S, Réfrégiers M, Rogniaux H, Ropartz D, Thévenot J, Vallverdu-Queralt A and F Canon (2018). Selected case studies presenting advanced methodologies to study food and chemical industry materials: from the structural characterization of raw materials to the multisensory integration of food. Innov Food Sci Emerg Technol.

Experimental reports – synchrotron SOLEIL (Saint-Aubin, France)

Meneghel J, Passot S, Cénard S, Lefrançois S, André W, Fonseca F and Dumas P (2014). Proposal n° 20131066. Biophysical responses of isolated bacteria to environmental stresses by using synchrotron infrared microscopy study: the first step of microfluidic approach. SMIS beamline.

Meneghel J, Passot S, Cénard S, Réfrégiers M, Fonseca F and Jamme F (2014). Proposal n° 20140401. *In-situ* and heterogeneity analysis of membrane fluidity of lactic acid bacteria (LAB) exposed to various stressful treatments by using UV fluorescence polarization. DISCO beamline.

Meneghel J, Passot S, Cénard S, Lefrançois S, Borondics F, Fonseca F and Dumas P (2016). Proposal n° 201408998. In situ synchrotron FTIR micro-spectroscopy to analyse the biophysical responses of small clusters of bacteria to hyperosmotic stress occurring during freezing. SMIS beamline.

Meneghel J, Passot S, Lieben P, Borondics F, Fonseca F and Dumas P (2016). Proposal n°20150220. A new inverted microscope setup coupled with synchrotron ATR-FTIR spectroscopy for an in-situ analysis of

the response of small groups of bacterial cells to an osmotic stress encountered during freezing. SMIS beamline.

Da Silva Pinto M, **Meneghel J**, Gohon Y, Ropers MH, Passot S, Fonseca F, Froissard M, Pénicaud C, Roblin P, Perez J and Boué F (2016). Proposal n° 20160299. Model biological membranes: Small, Wide-Angle X-ray Scattering, and Grazing Incidence X-ray Diffraction for better understanding of bacterial cells degradation during freezing and dehydration. SWING beamline.

Scientific vulgarization

Meneghel J, Fonseca F, Passot S, Lefrançois S, Jamme F, Borondics F and Dumas P (2016). New development on the SMIS beamline for a non invasive analysis of single bacterial cells. *Towards bioeconomy*, in "INRA-SOLEIL – 10 years of partnership" document (p.54-55), synchrotron SOLEIL, Gif-sur-Yvette, France (http://www.cepia.inra.fr/en/Tools-and-Resources/SOLEIL-Synchrotron/INRA-SOLEIL-10-years-of-partnership).

Froissard M, Fonseca F, Gohon Y, **Meneghel J**, Passot P, Pénicaud C, Jamme F and Réfrégiers M (2016). Lipid cell structure imaging and membrane fluidity measurement in single living microorganisms. *Towards bioeconomy*, in "INRA-SOLEIL – 10 years of partnership" document (p. 58-59), synchrotron SOLEIL, Gif-sur-Yvette, France (http://www.cepia.inra.fr/en/Tools-and-Resources/SOLEIL-Synchrotron/INRA-SOLEIL-10-years-of-partnership).

Oral communications

Meneghel J, Passot S, Jamme F, Dumas P and Fonseca F. *In situ* and time-evolved characterisation of the physiological and biophysical responses of *Lactobacillus bulgaricus* to environmental stresses following stabilization process. *AMMAC seminar (CEPIA division, INRA)*, March 31, 2015, Paris, France.

Meneghel J, Xu J, Cenard S, Sockalingum G, Passot S, Dumas P and Fonseca F. Comprendre la réponse au stress osmotique chez les bactéries lactiques grâce à la spectroscopie Raman. *XXI^{è} Journées du groupe français de spectroscopies vibrationnelles (GFSV)*, June 17-19, 2015, Reims, France.

Meneghel J, Passot S, Jamme F, Réfrégiers M, Cénard S, Dumas P and Fonseca F. Mapping membrane fluidity by fluorescence anisotropy to better understand bacterial tolerance to osmotic and cold stresses encountered during freezing. *52nd annual meeting of the Society for Cryobiology*, July 26-29, 2015, Ostrava, Czech Republic. Awarded a "Student Travel Award" based on the extended abstract submitted for the oral communication.

Meneghel J, Passot S, Jamme F, Réfrégiers M, Cénard S, Xu J, Dumas P and Fonseca F. Dynamic characterisation of membrane biophysical properties to better understand bacterial tolerance to osmotic and cold stresses encountered during freezing. *Microbial stress meeting: from molecules to systems*, Nov. 12-14, 2015, Sitges, Spain.

Meneghel J, Passot S, Jamme F, Réfrégiers M, Cénard S, Xu J, Dumas P and Fonseca F. Apport de la lumière synchrotron dans l'étude de la réponse aux stress chez les bactéries lactiques. *Journée des doctorants du laboratoire Génie Microbiologique des Procédés Alimentaires (GMPA)*, Feb. 11, 2016, Grignon, France.

Meneghel J, Passot S, Cénard S, Réfrégiers M, Jamme F, and Fonseca F. Mapping membrane fluidity in single bacterial cells to study the impact of cryopreservation and its related stresses. *Physics and Biological Systems*, Oct. 24-26, 2016, Palaiseau, France. Invited speaker.

Posters

Meneghel J, Xu J, Jamme F, Passot S, Dumas P and Fonseca F. Dynamic characterisation of membrane biophysical properties is crucial for improving the tolerance of lactic acid bacteria to osmotic and cold stresses encountered during freezing. *Journée des doctorants de l'Ecole Doctorale ABIES*, April 14-15, 2015, Paris, France. Obtention du prix du meilleur poster.

Meneghel J, Lefrançois S, Passot S, Jamme F, Dumas P and Fonseca F. Challenges underlying the *in situ* analysis of single bacterial cells by synchrotron FTIR spectromicroscopy. *16th European Conference on the Spectroscopy of Biological Molecules (ECSBM)*, Sept. 6-10, 2015, Bochum, Germany.

Meneghel J, Dumas P, Lefrançois S, Passot S and Fonseca F. Towards the analysis of single bacterial cells in aqueous environment by Fourier transform infrared spectroscopy. *11th Soleil Users' Meeting (SUM16)*, Jan. 21-22, 2016, Saint-Aubin, France.

Others

Participation in the written contest "My professional project in 3000 signs" – ABIES Doc'Avenir Forum, Feb. 22, 2017, Paris (awarded the 3rd prize).

LIST OF ABBREVIATIONS

2DGE:	two-dimensional gel electrophoresis
AA:	amino acid
asym:	asymmetric IR vibration modes
ATCC:	American type culture collection
ATR:	attenuated total reflectance
BioMiP:	bio-products, food, micro-organisms and processes
CDM:	chemically defined medium
cF:	carboxyfluorescein
CFA:	cyclic fatty acid
CFU:	colony-forming unit
CL:	cardiolipin (= diphosphatidylglycerol)
CPA:	cryoprotective agent
CSP:	cold-shock protein
DISCO:	dichroism, imaging, mass spectrometry for chemistry and biology
DMSO:	dimethyl sulfoxide
DNA:	deoxyribonucleic acid
DSC:	differential scanning calorimetry
DSMZ:	German collection of microorganisms and cell cultures
EPS:	exopolysaccharides
FA:	fatty acid
FTIR:	Fourier transform infrared spectroscopy
Ge:	Germanium
HGT:	horizontal gene transfer
HSP:	heat-shock protein
IIF:	intracellular ice formation
INRA:	national institute for agricultural research
IR:	infrared radiation
LAB:	lactic acid bacteria
LN_2:	liquid nitrogen
LTA:	lipoteichoic acids
LURE:	laboratory for the use of electromagnetic radiation
MCT:	mercury cadmium telluride
MRS broth:	growth medium for lactobacilli elaborated by de Man, Rogosa and Sharpe in 1960
NCBI:	national centre for biotechnology information
NMR:	nuclear magnetic resonance
PA:	phosphatidic acid
PDMS:	polydimethylsiloxane

PG:	phosphatidylglycerol
PHASTER:	phage search tool – enhanced release
PI:	propidium iodide
RNA:	ribonucleic acid
S/N ratio:	signal-to-noise ratio
SFA:	saturated fatty acid
S-layer:	surface-layer
SMIS:	spectroscopy and microscopy in the infrared using synchrotron
SOLEIL:	optimized light source of intermediate energy to LURE
SR:	synchrotron radiation
sym:	symmetric IR vibration modes
UFA:	unsaturated fatty acid
UV:	ultraviolet radiation
VBNC:	viable but non culturable
WTA:	wall teichoic acids
ZnSe:	zinc selenide
ZPD:	zero path difference

LIST OF SYMBOLS

C12:0:	dodecanoic acid = lauric acid
C14:0:	tetradecanoic acid = myristic acid
C15:0:	pentadecanoic acid
C16:0:	hexadecanoic acid = palmitic acid
C16:1:	hexadecenoic acid = *e.g.*, palmitoloeic acid (cis-9 unsaturated)
C17:1:	heptadecenoic acid
C18:0:	octadecanoic acid = stearic acid
C18:0-OH:	*hydroxyoctadecanoic acid* = hydroxystearic acid;
C18:1:	octadecenoic acid = *e.g.*, oleic acid (cis-9 unsaturated)
C18:2:	octadecadienoic acid = *e.g.*, linoleic acid (cis-9, cis-12 unsaturated)
C19:0 cyc:	methylenoctadecanoic acid = *e.g.*, dihydrosterculic acid (9,10 cyclization)
d:	spatial resolution
d_p:	penetration depth of the evanescent wave (in ATR FTIR configuration)
G+C%:	guanine-cytosine content
k:	force constant of a chemical bond
M:	molar (mol L^{-1})
Mb:	mega (10^6) base pairs
mOsm L^{-1}:	milliosmoles per litre

$T_{c\ ice}$:	ice crystallization temperature
T_g:	glass transition temperature
T_g':	glass transition temperature of the maximally cryoconcentrated solution
$T_g'e$:	extracellular T_g'
$T_g'i$:	intracellular T_g'
tm:	time necessary to reach the maximum acidification rate in milk (in min)
$T_{m\ ice}$:	ice melting temperature
$T_{m\ lip}$:	membrane lipid melting temperature
$T_{n\ ice}$:	ice nucleation temperature
$T_{s\ lip}$:	membrane lipid solidification temperature
T_{stor}:	storage temperature
δ:	bending IR vibration modes
ν:	stretching IR vibration modes
§:	paragraph

MICROORGANISMS CITED

C. pleistocenium:	*Carnobacterium pleistocenium*
E. coli:	*Escherichia coli*
L. acidophilus:	*Lactobacillus acidophilus*
L. buchneri:	*Lactobacillus buchneri*
L. bulgaricus:	*Lactobacillus delbrueckii* subsp. *bulgaricus*
L. casei:	*Lactobacillus casei*
L. plantarum:	*Lactobacillus plantarum*
Lc. lactis:	*Lactococcus lactis*
S. cerevisiae:	*Saccharomyces cerevisiae*
St. thermophilus:	*Streptococcus thermophilus*

Other microorganisms cited but not abbreviated:

Bifidobacterium animalis subsp. *lactis*
Geobacter sulfurreducens
Planococcus halocryophilus
Streptococcus mutans
Yarrowia lipolytica

A FEW DEFINITIONS

Direct vat inoculation: direct inoculation method in which frozen concentrated bacterial pellets are directly added to the fermentation tanks, as opposed to subculturing or back-slopping in which a small portion of the previous batch is used as starter.

Enantiomers: stereoisomers (*i.e.*, molecules of the same chemical formula) whose mirror images are non-superposable. Both enantiomers of lactic acid are L-lactic acid and D-lactic acid; a 1:1 mixture thereof is called racemic.

Frequency: Number of complete vibrations lapsed in one second; **Wavenumber**: Number of waves executed in a given distance (or reciprocal of wavelength); **Wavelength**: Length of one complete vibration.

Gram-negative/Gram-positive prokaryotes: prokaryotes may be classified into two major groups based on the structure of their envelope; Gram-negative prokaryotes are characterised by a thin peptidoglycan wall (5-10 nm) surrounding the cytoplasmic membrane that is additionally surrounded by an outer membrane, while Gram-positives have a unique cytoplasmic membrane surrounded by a thick peptidoglycan wall (20-80 nm). The name originates from the "Gram staining", in which the crystal violet primary staining of cells is retained after acetone or ethanol decolourization in Gram-positive cells, and not in Gram-negatives.

Lactic acid bacteria (LAB): also referred to as Lactobacilalles, this group of bacteria is a taxonomic order encompassing various genera (including *Lactobacillus*, *Lactococcus*, *Oenococcus*, *Streptococcus*…) that share common characteristics, among which the production of lactic acid as the major metabolic end product of carbohydrate fermentation.

Locus tag: gene identifier.

Orthologous genes (or orthologs): Genes in different genomes that evolved from a common ancestral gene and usually retain the same function.

LIST OF FIGURES

FOREWORD

BIBLIOGRAPHIC REVIEW – PART I

BIBLIOGRAPHIC REVIEW – PART II

BIBLIOGRAPHIC REVIEW – PART III

EXPERIMENTAL APPROACH

RESULTS – PART I

RESULTS – PART II

RESULTS – PART III

RESULTS – PART IV

CONCLUSIONS & PERSPECTIVES

APPENDICES

LIST OF TABLES

FOREWORD

BIBLIOGRAPHIC REVIEW – PART 1

BIBLIOGRAPHIC REVIEW – PART 1I

BIBLIOGRAPHIC REVIEW – PART 1II

RESULTS – PART I

RESULTS – PART II

RESULTS – PART III

RESULTS – PART IV

APPENDICES

TABLE OF CONTENTS

FOREWORD

Table I-1: Detailed taxonomic lineage of *Lactobacillus delbrueckii* subsp. *bulgaricus* down to the strain level

Taxonomic rank or level	***L. bulgaricus***
Domain	Bacteria
Phylum	Firmicutes
Class	Bacilli
Order	Lactobacillales
Family	Lactobacillaceae
Genus	*Lactobacillus*
Species	*Lactobacillus delbrueckii*
Subspecies	*Lactobacillus delbrueckii* subspecies *bulgaricus*
Strain (examples)	*Lactobacillus delbrueckii* subspecies *bulgaricus* ATCC 11842, ATCC BAA-365, 2038, CFL1, CIDCA 333…

FOREWORD

Lactobacillales, commonly referred to as lactic acid bacteria (LAB), have been used for centuries in the fermentation of meat, vegetables, fruit beverages and dairy products. Today, the market of starter cultures is continuously growing due to the development of health benefits products associated with fermentation. The importance of LAB in food and feed technology is linked to their production of large amounts of lactic acid out of carbohydrates. In addition, other metabolites may be produced during fermentation and include organoleptic compounds (flavours, exopolysaccharides…) and growth limiting substances (bacteriocins used in biopreservation) leading to a high diversity of final commercialized products.

The industrial interest for LAB also arises from their ability to produce high quantities of lactic acid from renewable resources with enantiomeric purity, whereas chemical production uses petrochemicals and results in racemic mixtures of D- and L-lactic acid (Eiteman and Ramalingam 2015). Applications of lactic acid span from food preservative, personal care additive (moisturizing, pH regulating and skin-lightning properties) and platform ingredient for the production of valuable chemicals such as lactate esters and polylactic acid (PLA), which are respectively biodegradable non-toxic solvents and a biodegradable polymer used in food packaging. In particular, PLA is benefiting from a fast-growing market with 25,000 tons produced in Europe in 2011 that is expected to reach 650,000 tons in 2025[1].

Lactobacillus delbrueckii subsp. *bulgaricus* (*L. bulgaricus*) belongs to the taxonomic order Lactobacillales, and therefore to LAB, whose detailed taxonomic lineage is given in **Table I-1**. This Gram-positive, non sporulating, obligate homofermentative and facultative anaerobic bacteria catabolizes few carbohydrates (lactose, glucose and fructose according to Weiss *et al*. (1983), and also cellobiose and mannose in some strains according to Felis and Pot (2014), and El Kafsi *et al*. (2014), respectively) to produce lactic acid as end product of the Embden-Meyerhof glycolysis pathway. *L. bulgaricus* is of interest to the food industry as a dairy starter. Its major use is in protocooperation with *Streptococcus thermophilus* (*St. thermophilus*) in producing yoghurt. It is also used for manufacturing Swiss and Italian-type cheeses.

[1] NNFCC (British bioeconomy consultancy company), 2011: http://www.soci.org/-/media/Files/Conference-Downloads/2011/BioPlastics-2011/BioPlastics_2011_The_market_for_second_generation_PLA.ashx?la=en (accessed November 2016).

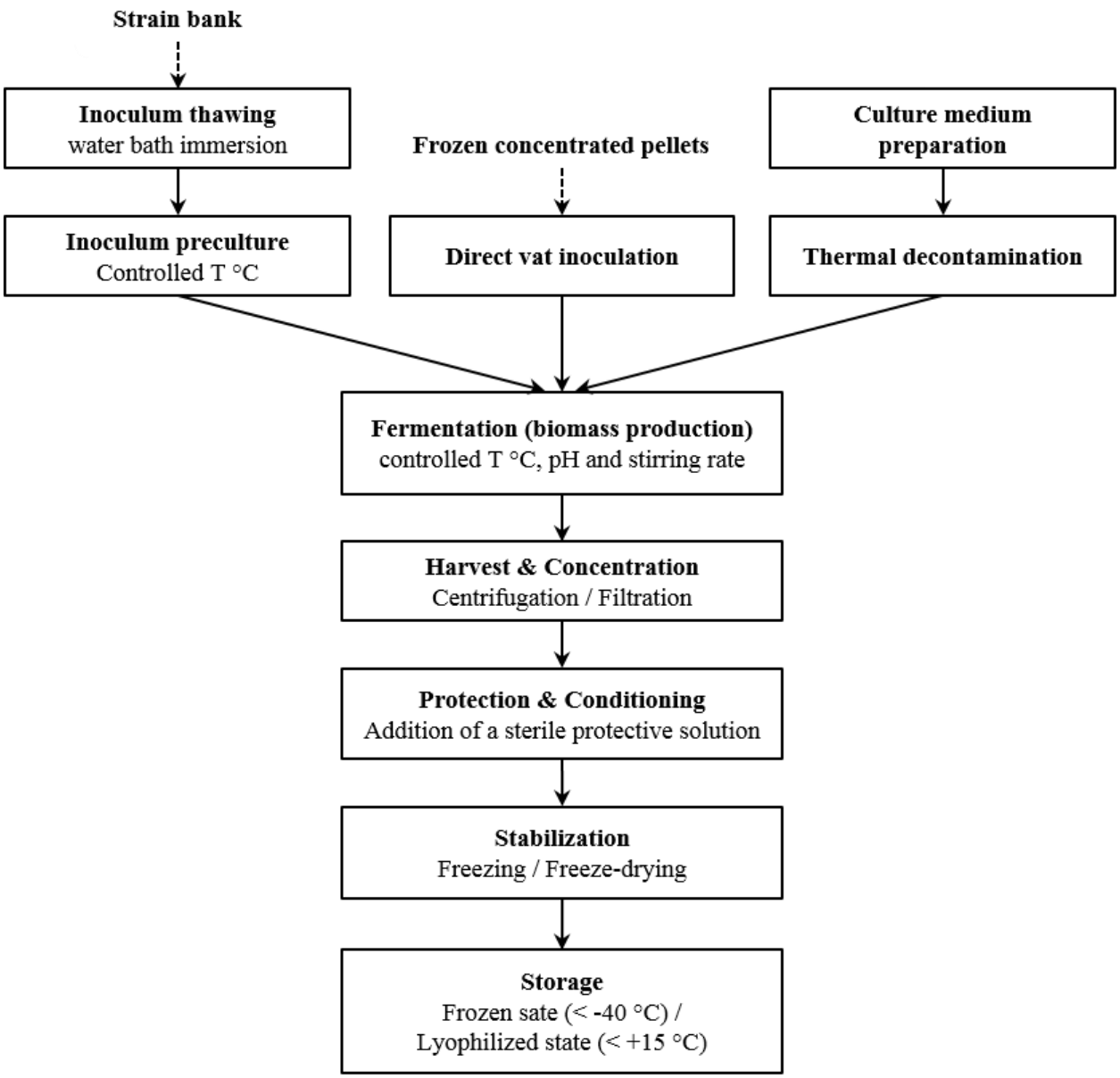

Figure I-1: Flow diagram of the general industrial production process of *Lactobacillus delbrueckii* subsp. *bulgaricus* (adapted from Beal *et al*., 2008).

Yogurt was originally prepared empirically to expand the shelf-life of milk by ancient civilizations in several regions of the world (Fisberg and Machado 2015). It has become nowadays one of the most popular industrial products and benefits from dynamic R&D in France. According to Syndifrais (French national dairy manufacturers union), the volume of yoghurts and fermented milks sold in 2016 came close to 1 million tons (slightly over 930,000 tons) and generated almost 2 billion Euros (1,922,608 k€) of economic income. In parallel, there is an increasing consumption of Swiss and Italian-type cheeses worldwide, especially Mozzarella. Fonterra, the New-Zealand dairy giant has indeed opened new Mozzarella plants in 2015 to double its cheese production and meet the demand in Asia and Middle East[2]. These types of cheese require thermophilic starter cultures and have also intensified the production demand for *L. bulgaricus*.

The flow diagram of **Fig. I-1** represents the general industrial production process of *L. bulgaricus* starters. It consists in inoculating a liquid culture medium with a preculture propagated from a pure thawed inoculum or by direct vat inoculation. When bacterial growth reaches the desired physiological state, cells are harvested and concentrated by centrifugation or filtration and a sterile protective solution is added for subsequent long-term stabilization by freezing or freeze-drying.

Cryopreservation is one of the possible ways for preserving live microorganisms and maintaining their functionalities over a long period of time. It involves freezing and keeping in the frozen state a cell suspension in the presence of a protective matrix containing cryoprotective agents (CPAs). Cells longevity ranges from one to more than 30 years (She and Petti 2015), although infinite preservation at temperatures below -135 °C (lower limit for ice crystals growth) is theoretically possible (Hubálek 1996). The dairy, brewery, winery and bakery industries rely to a large extent on cryopreservation for storing and exploiting their own culture collections. However, despite the use of cryoprotective agents, freeze-thawing is still responsible for cell damages leading to lethality and degradation of the technological properties of cells. Trying to understand the cryopreservation-related damages in the LAB *L. bulgaricus* and to reduce them has indeed been a research topic of the GMPA laboratory (INRA, Grignon) for more than 15 years, especially within BioMiP[3] team (Fonseca *et al*. 2000; Fonseca *et al*. 2016) in which I carried out my PhD work.

More recently, a partnership was initiated between BioMiP team and the French synchrotron radiation facility SOLEIL[4] (Gif-sur-Yvette). Synchrotron radiation is an extremely bright light extending from the far-infrared to hard X-rays. It can be used to explore matter for fundamental and applied research in various fields of activity such as physics, chemistry, environmental sciences, medicine and biology. Collaboration

[2] http://www.agweb.com/article/fonterra-completes-new-mozzarella-plant-to-supply-global-markets-naa-dairy-today-editors/ (accessed November 2016).

[3] BioMiP, acronym for Bioproducts, Food, Micro-organisms and Processes (Bioproduits, Aliments, Micro-organisms et Procédés in French), is one of the four research teams of the GMPA laboratory (INRA, Grignon) whose main research topics include the production and stabilisation of micro-organisms with technological interest for the food industry (https://www6.versailles-grignon.inra.fr/gmpa_eng/Research-teams/BioMiP).

[4] SOLEIL, acronym for Optimized Light Source of Intermediate Energy to LURE (Laboratory for the Use of Electromagnetic Radiation) (Source Optimisée de Lumière d'Energie Intermédiaire du LURE; Laboratoire pour l'Utilisation du Rayonnement Electromagnétique), means "sun" in English (https://www.synchrotron-soleil.fr/en).

between BioMiP team and the SMIS[5] beamline of SOLEIL synchrotron started in 2011. The aim was to expand the expertise on the characterisation of microorganisms in response to preservation processes by moving to high spatial resolution analyses, and thus address population heterogeneity issues. This project extended from infrared to ultraviolet radiations with further collaborations with the DISCO[6] beamline, and gave rise to numerous oral communications and to the publication of two scientific articles (Passot *et al*. 2014; Passot *et al*. 2015).

In this framework, my PhD thesis aimed at contributing to the understanding of the mechanisms of LAB cryoinjury through a multi-disciplinary and multi-scale approach. In this respect, the first objective of my PhD work was to study the response of *L. bulgaricus* to cryopreservation-related stresses by physiological, genomic and biophysical characterisations. The second and challenging objective was to investigate the relative importance of single cell responses comparatively to the population responses to these stresses.
This work was focused on three starting hypotheses:

- Cryopreservation may be considered as a combination of different stresses: cold and osmotic;
- The cell membrane, but also other constituents of the envelope, as well as cell proteins are the main targets of bacterial cell cryoinjury;
- The investigation at population and single cell levels give different and relevant information, important for basic science and for technological applications.

The present manuscript is divided into four parts: a bibliographic review, an experimental approach, a results and discussion section, followed by conclusions and perspectives.

The **BIBLIOGRAPHIC REVIEW** focuses on three axes describing (i) the physical events taking place during the freeze-thawing process and their biological consequences, (ii) the ways for improving LAB cryo-resistance and (iii) the application of Fourier transform infrared (FTIR) spectroscopy for the analysis of biological samples and the identification of stress markers.
The **EXPERIMENTAL APPROACH** then describes the main phases of the work that was conducted, mentioning the experimental methods employed for each phase and the parameters measured. More details on the material and methods used are given in each chapter of results and discussion, and complementary information may be found in **Appendix I**.
The **RESULTS & DISCUSSION** section then develops four topics in the form of scientific articles that are either published or in construction for an expected imminent submission. In **CHAPTER I**, an analysis

[5] SMIS, acronym for Spectroscopy and Microscopy in the Infrared using Synchrotron, is a beamline at SOLEIL synchrotron that delivers high-brilliance infrared radiation in the 2.5 – 100 µm spectral range (https://www.synchrotron-soleil.fr/en/beamlines/smis).
[6] DISCO, acronym for Dichroism, Imaging, mass Spectrometry for Chemistry and biOlogy, is a vacuum-UV to visible beamline at SOLEIL synchrotron, optimized in the 60 – 700 nm spectral range with conservation of the natural polarization of the light (https://www.synchrotron-soleil.fr/en/beamlines/disco).

of the growth kinetics and cryoresistance of three *L. bulgaricus* strains presenting different phenotypes is presented. Besides, genomic characteristics explaining the differences observed are tentatively provided through a genomic comparison. This study involved the sequencing of the genome of *L. bulgaricus* CFL1 and resulted in the selection of growth conditions leading to one cryosensitive strain and one cryoresistant strain to be studied in the rest of the work. Then, in **CHAPTER II**, the quantification of biological response of the two selected strains of *L. bulgaricus* to the main cryopreservation-related stresses – cold and osmotic – is provided. A deep characterisation of the biophysical properties of their plasma membrane is also proposed and related to biological properties. In **CHAPTER III** the membrane fluidity, a key biophysical property of bacterial cells, is quantified at a single-cell level to bring a deep insight into the cell response mechanisms to cryopreservation stresses, and to discuss inter-cellular and intra-cellular population heterogeneity in response to cold and osmotic stresses. Finally, methodological developments are described in **CHAPTER IV** that aimed at analysing bacteria in an aqueous environment by FTIR spectroscopy at two spatial resolutions: groups of a few thousands of cells and individual cells. The comparison of both approaches for identifying markers of stress and for determining the relevance of heterogeneity in cryoresistance behaviour, is finally presented. Supplementary results may also be found in **Appendices II** and **III**.

Eventually, a **CONCLUSIONS & PERSPECTIVES** section summarises the main results obtained, and gives some perspectives for future work.

BIBLIOGRAPHIC REVIEW

BIBLIOGRAPHIC REVIEW

CONTENTS

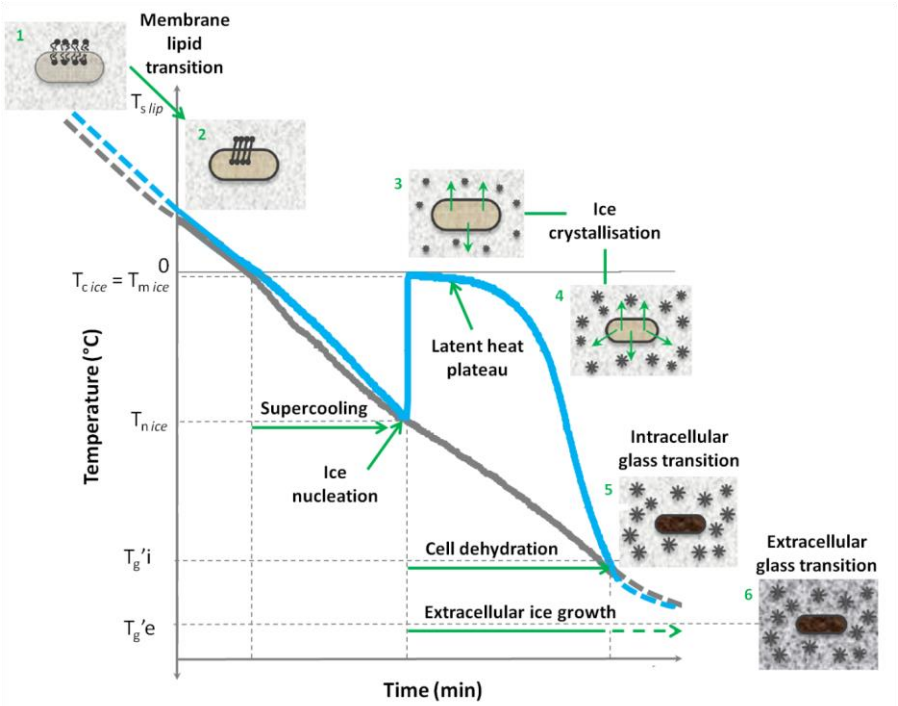

Figure II.1-1: Typical cooling profile measured inside a 2-mL cryogenic vial containing a bacterial suspension (blue) and on the surface of the cooling module of a controlled rate freezer (gray) programmed to cool at a 2 °C min^{-1} rate (EF600-103, Asymptote, Cambridge, UK). The cooling profile is illustrated by schematic representations of the main physical events taking place in the bacterial suspension during freezing (adapted from Fonseca *et al*. 2016); $T_{s\,lip}$, $T_{n\,ice}$, $T_{c\,ice}$ (= $T_{m\,ice}$), T_g'i, T_g'e are the temperatures of membrane lipid solidification, ice nucleaction, ice crystallization (= ice melting), intracellular glass transition and extracellular glass transition, respectively.

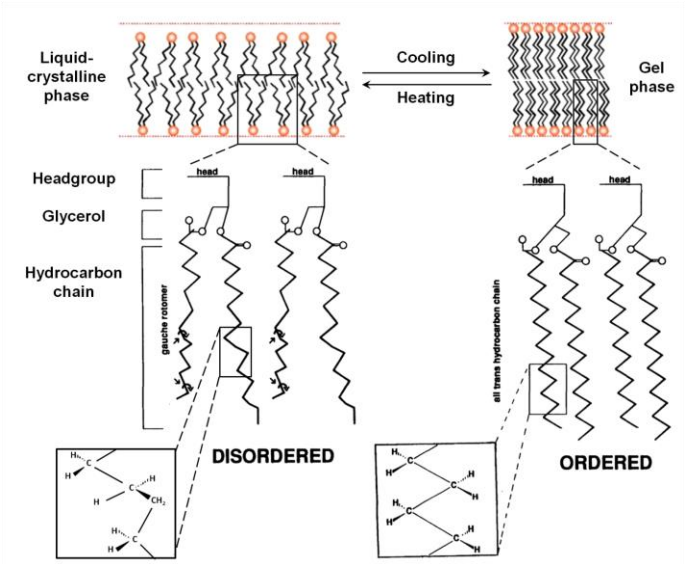

Figure II.1-2: Schematic representation of membrane lipid transition from the disordered liquid-crystalline phase characterised by the presence of methyl groups in gauche conformation (left) to the ordered gel phase with all trans conformation (right) (adapted from Borchman *et al*. 1991 and Dr. M. Blaber's website, Lecture 14: Membranes, structure of membrane proteins: http://www.mikeblaber.org/oldwine/BCH4053/Lecture14/Lecture14.htm, 2001).

I. Freezing lactic acid bacteria

Upon culture and harvest, the LAB culture exhibits a number of viable cells with defined technological properties. To maintain such quality parameters on a long time-scale, preservation processes are applied. However, they paradoxically lead to cell degradation and freeze-thawing complies with this reality.
This first part of the state of the art presents a description of the physical events governing the freezing process and their consequences on LAB cell structure and biological activity.

1.1. Physical events taking place during freeze-thawing of LAB

To understand why freeze-thawing may lead to important cellular damage, a review of the physical transitions taking place within cells and their surrounding medium throughout this process will first be given. Three sequential temperature-dependent steps of the freeze-thawing protocol will be considered: (i) from harvest to low positive temperatures (chilling), (ii) during freezing until storage temperatures are reached (iii) and during storage and thawing. To illustrate the phase transitions occurring during chilling and freezing (i and ii), a diagram adapted from Fonseca *et al*. (2016) is presented in **Fig. II.1-1**.

1.1.1. Chilling: membrane lipid phase transition

At the end of cell production by fermentation, the culture is harvested and rapidly cooled down to 4-5 °C in order to stop the metabolic activities. Chilling often results in membrane lipid solidification ($T_{s\ lip}$ from diagrams 1 to 2, **Fig. II.1-1**). Membrane lipid solidification is the transition of the acyl chains from a disordered fluid state, referred to as the liquid-crystalline phase, to an ordered rigid state, called the gel phase. The upper part of **Fig. II.1-2** schematically illustrates a membrane lipid phase transition caused by temperature decrease. In the liquid-crystalline phase, consecutive methyl groups of the lipid hydrocarbon chains may adopt gauche rotamers (illustrated in the lower part of **Fig. II.1-2**) (Borchman *et al*. 1991). Such conformation results in an uncompressed bilayer with minimum van der Waals interactions between adjacent hydrocarbon chains. Liquid-crystalline bilayers are therefore characterised by a high degree of disorder and fluidity. On the contrary, when the environmental temperature decreases, hydrocarbon chains adopt a straight all-trans conformation. This densely packed state maximizes van der Waals interactions and the membrane becomes ordered and rigid.
The temperature of membrane lipid phase transition may be assessed by Fourier transform infrared (FTIR) spectroscopy, differential scanning calorimetry (DSC) or nuclear magnetic resonance (NMR). While DSC and NMR require sample preparation (extraction) (McGibbon *et al*. 1985; Lewis *et al*. 1987), FTIR spectroscopy advantageously enables such determination on intact cells. Membrane lipid transition temperatures range from 33 to 35 °C in thermophilic bacteria (Oldenhof *et al*. 2005; Gautier *et al*. 2013), from 5 to 23 °C in mesophilic bacteria (Leslie *et al*. 1995; Ulmer *et al*. 2002; Molina-Höppner *et al*. 2004; Ragoonanan *et al*. 2008; Laczkó-Dobos and Szalontai 2009), and around -30 °C in the membrane lipids extracted from the psychrophilic bacterium *Micrococcus cryophilus* (McGibbon *et al*. 1985).

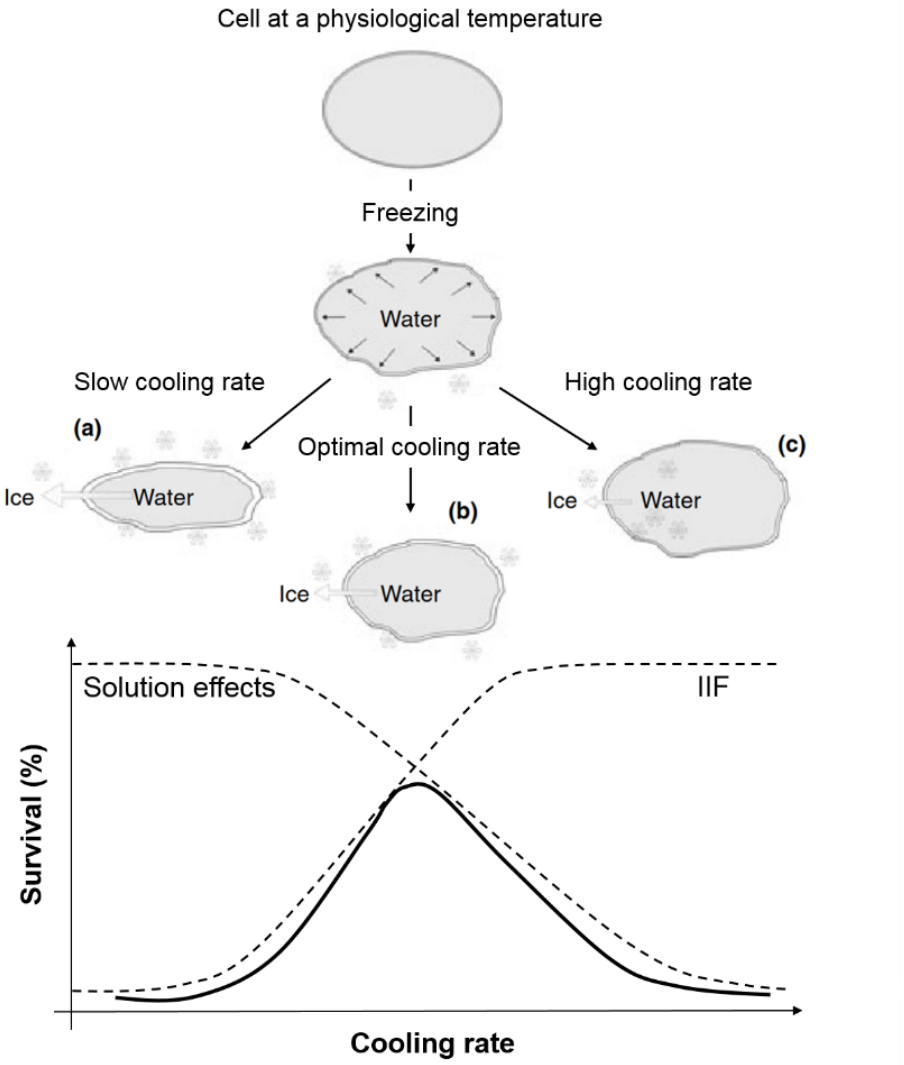

Figure II.1-3: Schematic illustration of cell injuries following freezing at different cooling rates and the resulting hypothetical cell survival according to the two-factor hypothesis of Mazur (1972). Water efflux and solution effects dominate at slow cooling rates (**a**), intracellular ice freezing (IIF) dominate at high cooling rates (**c**), both leading to minimum cell survival (solid line). Optimal cooling rate is located in between (**b**), where IIF and solution effects are minimal (adapted from Mazur, 1977, Hubàlek, 1993 and Santivarangkna *et al*. 2008b).

To function properly, cellular processes occurring at the membrane level (transport, enzymatic reactions) require membrane lipids to be in a liquid-crystalline state (Beney and Gervais 2001; Mykytczuk *et al*. 2007). Metabolic activities may therefore be greatly affected below the membrane solidification temperature ($T_{s\ lip}$), and the low $T_{s\ lip}$ of psychrophilic bacteria constitutes a cold-adaptive mechanism for their membrane to remain in the liquid-crystalline state below 0 °C.

1.1.2. Freezing: ice crystallization-related phenomena

Following the chilling step, several physical events take place during freezing and frozen storage.

i. The two-factor hypothesis

According to the two-factor hypothesis formulated by Mazur and colleagues (Mazur 1970; Mazur *et al*. 1972), freezing injury is the result of two competing mechanisms that depend on the cooling rate applied (**Fig. II.1-3**). Damages associated with long exposures of cells to the cryoconcentrating medium, termed the solution effects, dominate at low rates (**Fig. II.1-3a**). On the contrary, water efflux is greatly limited at high cooling rates and intracellular ice formation (IIF) responsible for lethal damages may occur in rapidly frozen eukaryotic cells (**Fig. II.1-3c**). However, in cryopreserved LAB it was clearly evidenced that at very high cooling rates, no intracellular ice was formed.

Several studies on LAB cryopreservation showed that high cooling rates either (i) better preserved the viability than slow cooling rates (Tsvetkov and Shishkova 1982; Morice *et al*. 1992; Fonseca *et al*. 2001), (ii) did not lead to significant survival differences (Foschino *et al*. 1996) or (iii) depended on the microbial species (Péter and Reichart 2001) and strain (Smittle *et al*. 1972) under investigation. High cooling rates lead to variable results, owing to the difficulty of accurately controlling them and due to the stochastic event of ice nucleation. Optimal cooling rates between 1-10 °C (**Fig. II.1-3b**) have been reported for various microorganisms: *Saccharomyces cerevisiae* (*S. cerevisiae*) in distilled water (Mazur 1970) or *S. cerevisiae*, *Candida utilis*, *Escherichia coli* (*E. coli*) and *Lactobacillus plantarum* (*L. plantarum*) in a water-glycerol solution (Dumont *et al*. 2003; Dumont *et al*. 2004). Besides, the American Type Culture Collection (ATCC), the German Collection of Microorganisms and Cell Cultures (DSMZ, Smith *et al*. 2008) and other authors (De Paoli 2005; Prakash *et al*. 2013; She and Petti 2015) recommend a slow and controlled cooling rate (1 to 5 °C min^{-1}) for a successful cryopreservation. Applying slow cooling rates allows reproducible freezing protocols but research is still needed to understand the biological responses of LAB to slow cooling, and thus propose optimized cryopreservation protocols.

ii. Freezing at a slow cooling rate

The temperature profile monitored in a slowly frozen bacterial suspension (blue curve in **Fig. II.1-1**) shows the existence of a first phase of temperature decrease to subzero values before ice nucleation. This is referred to as a supercooling event. The extent of supercooling depends on the cooling profile and sample dimensions (volume, concentration) (Morris 2007). High concentrated samples thus tend to remain liquid at lower temperatures than isotonic samples.

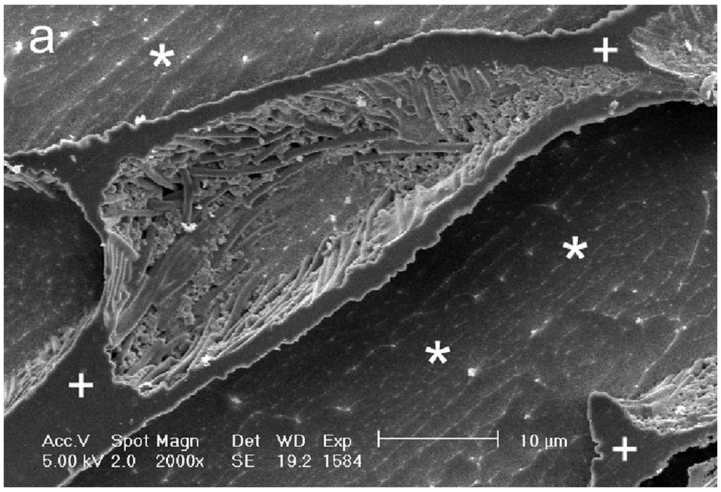

Figure II.1-4: Cryo scanning electron microscopy picture of a frozen *Lactobacillus delbrueckii* subsp. *bulgaricus* sample. Cells are confined to the liquid cryoconcentrated matrix (+) surrounded by ice crystals (*) (Clarke *et al*. 2013).

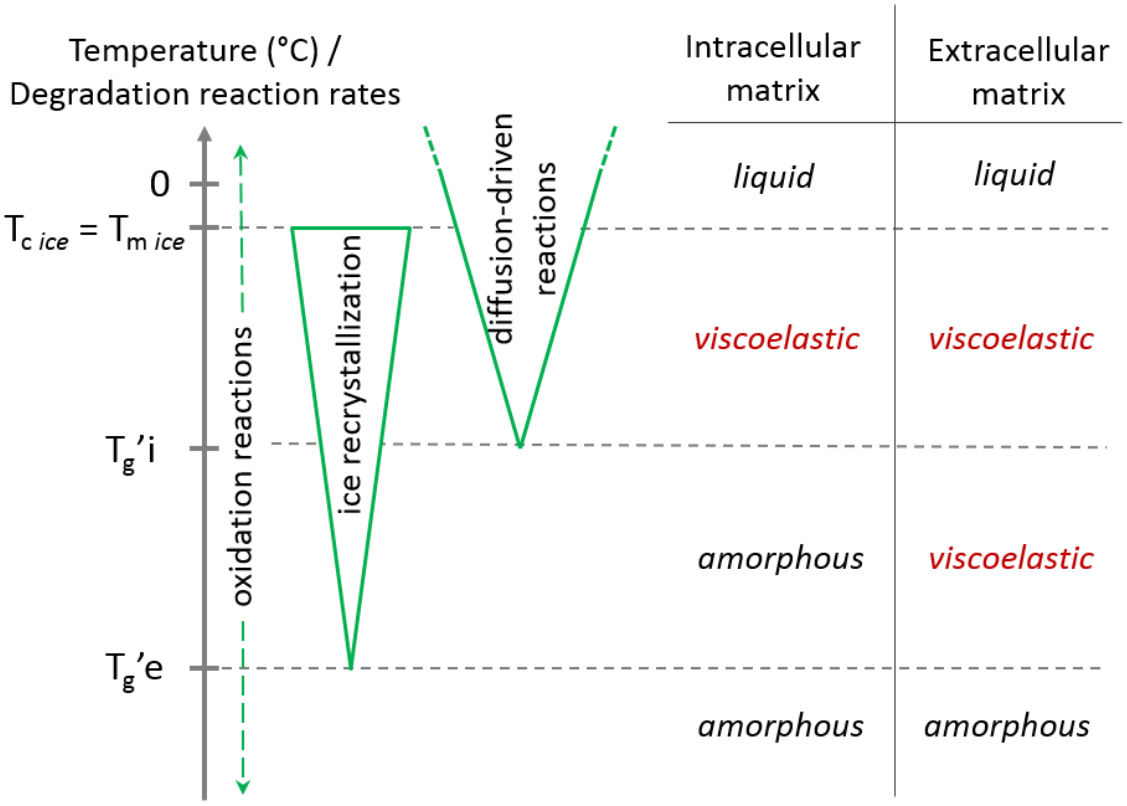

Figure II.1-5: Degradation reaction rates as a function of temperature and state of the intracellular and extracellular matrices.

Ice nucleation is an endothermic and stochastic process. When it occurs ($T_{n\,ice}$ and diagram 3, **Fig. II.1-1**), the sample temperature rises to its melting point ($T_{m\,ice}$, 0 °C for pure water; < 0 °C otherwise) and a large water fraction is converted into ice (Morris and Acton 2013). A temperature plateau is thus observed, termed the "latent heat plateau". When most of the freezable water crystallized, heat absorption associated with this transition declines and the sample temperature decreases again.

Ice grows from nucleation spots by accumulation of water molecules diffusing towards the ice-solution interface. Cells are excluded from this interfacial zone in the cryoconcentrating matrix (Fonseca *et al*. 2006; Clarke *et al*. 2013, **Fig. II.1-4**), and are believed to suffer only slightly from this mechanical constraint. Moreover, no IIF was experimentally detected in cryopreserved LAB at slow cooling rates (Fonseca *et al*. 2016).

The other consequence of extracellular ice formation is the withdrawal of unbound water from the suspension. This leads to an increased concentration in extracellular solutes, thus exerting an osmotic stress on cells. In case of sufficiently slow cooling rates, osmotic equilibration of intracellular compartments with the extracellular medium occurs by water efflux (Mazur 1984) (diagrams 3 to 5, **Fig. II.1-1**). This intracellular water loss goes on until the intracellular compartment becomes maximally freeze-concentrated and vitrifies (T_g'i, diagram 5, **Fig. II.1-1**) (Fonseca *et al*. 2016). The cell is then osmotically irresponsive. This means that the cytoplasm has physical properties of a solid, and that further extracellular cryoconcentration will not result in further intracellular osmotic equilibration. The temperature value of T_g'i depends on the cell type and the composition of the suspending medium (Fonseca *et al*. 2016). The cryoconcentration of the extracellular compartment actually continues until the extracellular matrix reaches its maximally cryoconcentrated state and vitrifies (T_g'e, diagram 6, **Fig. II.1-1**). Below this temperature, which depends on the composition of the extracellular medium, the viscosity is extremely high ($10^{12\text{-}14}$ Pa s) and diffusion-driven degradation reactions are considered to be hindered.

1.1.3. Storage and thawing

Storage enables long-term sample stability provided that storage temperature is low enough ($T_{stor} < T_g$'e). Otherwise, physical events leading to cell degradation occur, and these types of events are similar to those occurring during thawing. For instance, if ice crystallization was incomplete during freezing, undesired ice recrystallization may occur during a storage conducted at a temperature above T_g'e and during thawing when temperatures exceed T_g'e. This phenomenon caused cell plasmolysis in *L. bulgaricus* (Fonseca *et al*. 2006). This phenomenon has minor effect for slow cooling rates, since the initial unfrozen fraction is limited. In such a case, as temperature is increased during thawing, the physical events that occurred during freezing are reversed: first the mobility in the extracellular matrix is recovered, followed by the recovery of mobility in the intracellular matrix. Fonseca *et al*. (2003) also showed that damaging oxidative reactions took place during the storage at -20 °C of bacterial suspensions slowly cooled (1°C min^{-1}). Degradation reactions (ice recrystallization and other diffusion-driven reactions, oxidation) occur at a rate that depends on temperature, as depicted in **Fig. II.1-5**.

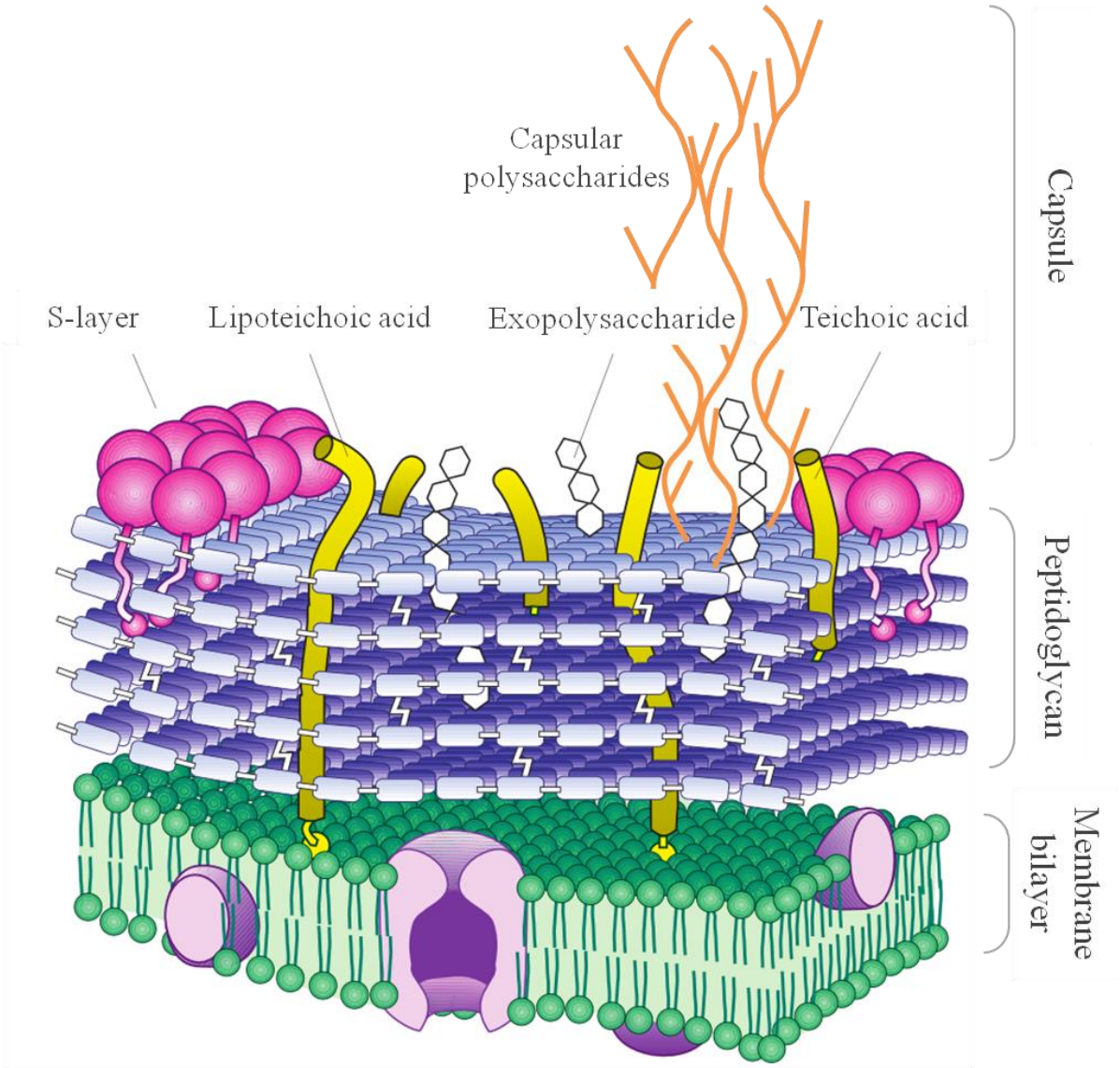

Figure II.1-6: Schematic representation of the cell envelope of a Gram-positive bacterium emphasizing on the cell wall and its various constitutive elements. The peptidoglycan is here represented with parallel-oriented disaccharide strands (adapted from Delcour *et al*. 1999).

Also, the extra amount of ice formed between $T_g'i$ and $T_g'e$ during freezing results in the exposure of cells to increased osmolarities between $T_g'i$ and $T_{m\ ice}$ during storage and/or thawing. When ice melts, cells are suspended back in the initial medium of low osmolarity.

Sum up of the physical events taking place during freeze-thawing of LAB:

A **slow freezing process** exerts two main stresses on bacterial cells, namely **cold stress** and **osmotic stress** as cryoconcentration increases until $T_g'i$. Mechanical constraints are negligible when freezing bacteria (absence of IIF and very limited interactions, if any, between extracellular ice crystals and cells) and oxidative degradation reactions may be neglected provided that storage conditions are optimal. Studying the effects of cold and osmotic stresses appears essential to elucidate the damage mechanisms associated with cryopreservation.

1.2. Degradation of cell structures following freezing

The physical events occurring during freezing affect cellular structures and components. Before reviewing these degradation processes, the general LAB cell structure under normal physiological conditions and their main functions are presented.

1.2.1. LAB cell structure

From the exterior to the interior, a LAB cell consists of (i) a cell wall, (ii) a membrane – both constituting the cell envelope which is schematically presented in **Fig. II.1-6** – and (iii) the intracellular medium: a crowded cytoplasm containing diffuse nucleic acids, proteins and other essential components (nutrients, metabolites) but exempt of membrane-bound organelles.

i. The cell wall structure and functions

The cell wall of Gram-positive bacteria is a complex structure composed of peptidoglycan, polysaccharides, teichoic acids and proteins. The peptidoglycan is a thick (20 – 80 nm) scaffold of repeating disaccharide units of varying length (from 3 to 250) cross-linked by amino acid bridges (Dmitriev *et al*. 2005; Vollmer *et al*. 2008). The disaccharide units consist of N-acetyl glucosamine (GlcNAc) and N-acetyl muramic acid (MurNAc), whose orientation with respect to the cell membrane (parallel or perpendicular) is still debated (Vollmer *et al*. 2008). The peptidoglycan confers rigidity and shape to the bacterial cell. It also prevents the cell from plasmolyzing or bursting under mild osmotic perturbations of the environment (*i.e.*, hypertonic or hypotonic conditions, respectively) (Dmitriev *et al*. 2005). Despite this apparent massive structure, the cell wall is not a barrier to the passage of molecules smaller than approximately 55 kDa (Koch 1998). Most small molecules, such as disaccharides, therefore freely diffuse through the cell wall of bacteria.

Wall polysaccharides

Polysaccharides sprinkle the cell wall and extend to the cell surface. Three different types of wall polysaccharides exist, although the distinction is not always clear (Kleerebezem *et al*. 2010; Chapot-Chartier and Kulakauskas 2014): capsular polysaccharides (CPS), cell wall polysaccharides (WPS) and exopolysaccharides (EPS). CPS form a thick layer surrounding the bacterial cell surface (the capsule) that is maintained *via* covalent binding to the peptidoglycan (Roberts 1996, **Fig. II.1-6**). WPS, in contrast, may not be covalently bound to the peptidoglycan, and do not form a thick external surrounding layer. Finally, EPS are loosely associated to the cell surface or excreted. All three types of wall polysaccharides are involved in cell interactions with the environment (other microorganisms, bacteriophage, host, adhesion) (Kleerebezem *et al*. 2010; Chapot-Chartier and Kulakauskas 2014), cell division and morphology (Chapot-Chartier and Kulakauskas 2014) and the cold-stress response as antifreeze-agents (Boetius *et al*. 2015). The production of extracellular wall polysaccharides production by LAB, including *L. bulgaricus*, is also appreciated by the dairy industry for conferring natural thickening properties to fermented products (Behare *et al*. 2009).

Teichoic acids

Lipoteichoic acids (LTA) and wall teichoic acids (WTA) are linear polyanionic glycophosphate polymers anchored to the membrane or the cell wall, respectively (**Fig. II.1-6**). Teichoic acids are major constituents of cell walls of Gram-positive bacteria, also involved in cell interactions with the environment, cell division and morphology. In addition, they provide the cell wall with a pool of cations due to their anionic character, used for proper enzyme functioning (Chapot-Chartier and Kulakauskas 2014). Interestingly, Vinogradov *et al*. (2015) recently launched an investigation into the wall polysaccharides of an industrial *L. bulgaricus* strain (Ldb17). They did not find any LTA and identified only small amounts of short-chain WTA. On the other hand, Räisänen *et al* (2007) isolated LTA from four other *L. bulgaricus* strains, whose structural differences were linked to varying degrees of phage-resistance. These studies suggest strain variability in the composition of teichoic acids in *L. bulgaricus*.

Cell wall proteins

Cell wall proteins are either bound to the peptidoglycan (wall proteins) or to membrane lipids (membrane anchored proteins), and are also involved in cell interactions with the environment (Kleerebezem *et al*. 2010; Chapot-Chartier and Kulakauskas 2014). An *in silico* analysis aiming at localizing proteins in *L. bulgaricus* was performed using the SurfG+ software (Barinov *et al*. 2009) on the genomes of three *L. bulgaricus* strains (ATCC 11842, ATCC BAA-365 and 2038). It revealed that 6-8 % of total proteins are wall proteins, and 15-16 % are membrane proteins, corresponding to about 90-140 and 230-290 wall and membrane proteins, respectively (Tardy-Corvet *et al*., unpublished data).
A surface layer (S-layer) that is made of a continuous lattice of packed proteins is commonly found in Gram-positive bacteria. Diverse functions were attributed to the S-layer (including protection against various

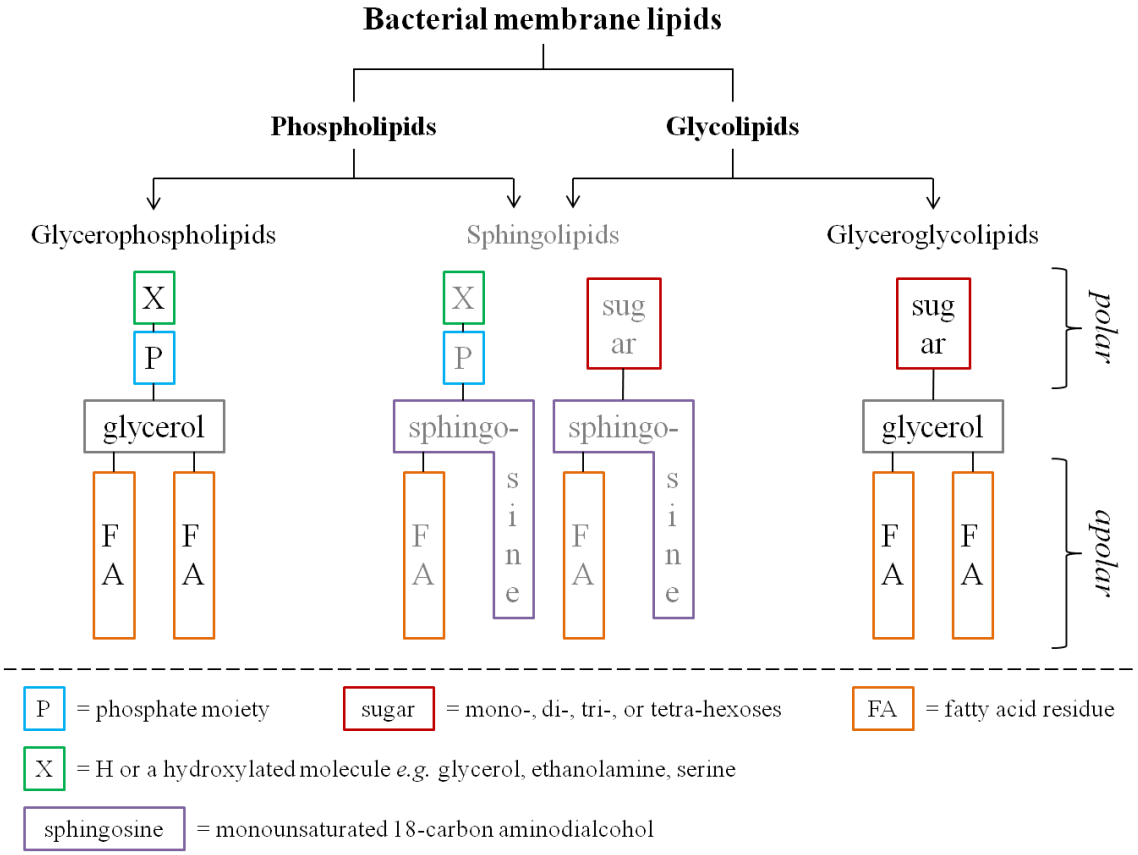

Figure II.1-7: Classification of bacterial membrane lipids. Glycerophospholipids and glyceroglycolipids are constitutive of the membrane of lactobacilli; not sphingolipids, which are therefore typed in gray.

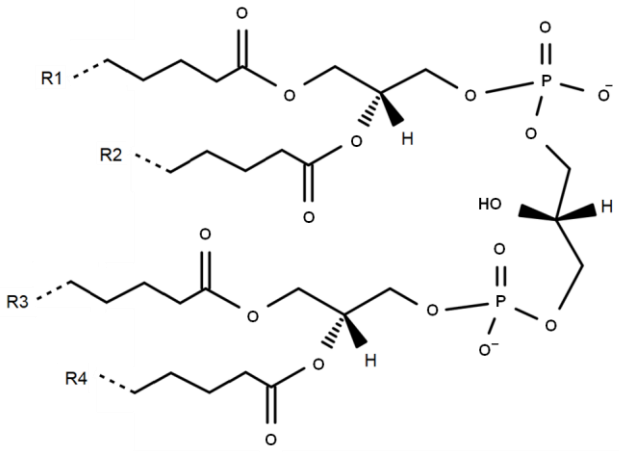

Figure II.1-8: Generic cardiolipin molecule. R1 to R4 refer to fatty acyl residues. Adapted from LIPID MAPS, http://www.lipidmaps.org/data/LMSDRecord.php?LMID=LMGP12010000

environmental perturbations), but genomic studies revealed that *L. bulgaricus* does not produce S-layers (Hynönen and Palva 2013; Johnson *et al*. 2015).

ii. The membrane structure and functions

The membrane is a 7 – 8 nm thick self-assembly of phospholipids and glycolipids in a closed bilayer sprinkled with proteins. Polar heads of membrane lipids are outwardly oriented in order to minimize the contact between water and the hydrophobic acyl chains (Beney and Gervais 2001). The principal role of the membrane bilayer is to act as a semi-permeable barrier. It enables the passage of specific molecules, while restricting that of others. Small hydrophobic (O_2, CO_2) and small uncharged polar molecules (alcohols) thus passively diffuse through the membrane. Channels may facilitate the entry of specific molecules, such as aquaporins with water. Larger polar molecules require specific transport facilitators (*e.g.*, lactose permease) and active transport involving the consumption of energy (*e.g.*, ATP hydrolysis) is required to pump uncharged molecules and ions through the membrane against their concentration or electrochemical gradient.

Membrane lipids

Membrane lipids are divided into two categories, as shown in **Fig. II.1-7**: phospholipids that contain a phosphate group, and glycolipids, which are phosphorous-free and contain a carbohydrate portion. In most prokaryotes, such as lactobacilli, the only lipid species representative of each category are glycerophospholipids and glyceroglycolipids, respectively. Sphingolipids, which may contain either a phospho-hydroxylated headgroup or a carbohydrate portion, are indeed absent from lactobacilli membranes (Olsen and Jantzen 2001; Sohlenkamp and Geiger 2016).

Glycerophospholipids and glyceroglycolipids are composed of a glycerol backbone, two hydrocarbon chains and a polar headgroup. Regarding the first lipid class (glycerophospholipids), this headgroup is made of a phosphate moiety either free (phosphatidic acid, PA) or linked to a hydroxylated molecule: glycerol (phosphatidylglycerol, PG), ethanolamine (phosphatidylethanolamine, PE), or serine (phosphatidylserine, PS) for the most common LAB membrane glycerophospholipids. The transesterification of two PGs catalyzed by a phospholipase D results in the formation of diphosphatidylglycerol, also called cardiolipin (CL) (Schlame 2008). The general structure of CL is presented in **Fig. II.1-8**.

In the second lipid class (glyceroglycolipids), the headgroup is a carbohydrate portion, containing up to four hexose moieties (Iwamori *et al*. 2011). Glyceroglycolipids are exclusively located in the external membrane leaflet and are therefore likely involved in interactions of cells with their environment (Alberts *et al*. 2002). Exterkate and colleagues (1971) established the glycerophospholipid composition of *L. bulgaricus*as the following: 54 % PG, 32 % lysyl-PG (PG carrying a lysine residue), 7 % CL, 2 % PA and the last 5 % remained unidentified. More recent studies on the subject additionally identified several glyceroglycolipids in three *L. bulgaricus* strains (Gómez-Zavaglia *et al*. 2000; Tymczyszyn *et al*. 2005).

The fluid mosaic model proposed by Singer and Nicolson (1972) represents the constant movement of lipids within the membrane: they diffuse laterally and rotate permanently at a very fast rate. Under physiological conditions, a few seconds are sufficient for a membrane lipid to laterally diffuse from one extremity of the

Table II.1-1: Literature review on membrane lipid domains reported in rod-shaped bacteria

Membrane lipid domain	Main component(s)	Bacterial species	References
Polar & septal lipid domains	Anionic lipids, especially cardiolipin (CL)	*Escherichia coli*	Mileykovskaya and Dowhan (2000) Koppelman *et al.* (2001) Romantsov *et al.* (2008)
		Bacillus subtilis	Kawai *et al.* (2004) López *et al.* (2006) Seydlová *et al.* (2013)
		Pseudomonas putida	Bernal *et al.* (2007)
Lipid spirals	Phosphatidylglycerol (PG)	*Bacillus subtilis*	Barák *et al.* (2008) Hachmann *et al.* (2009) Muchová *et al.* (2010) Muchová *et al.* (2011)
Lipid rafts	Lipids from the isoprenoid family & flotillin-like proteins	*Bacillus subtilis*	Donovan and Bramkamp (2009) López and Kolter (2010)
		Bacillus halodurans	Zhang *et al.* (2005)
Illustration adapted from Barák and Muchová (2013)	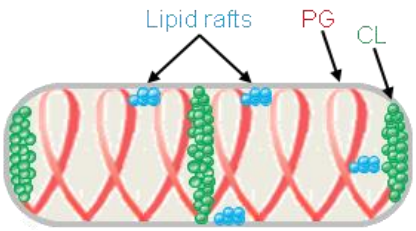		

PG: phosphatidylglycerol; CL: cardiolipin

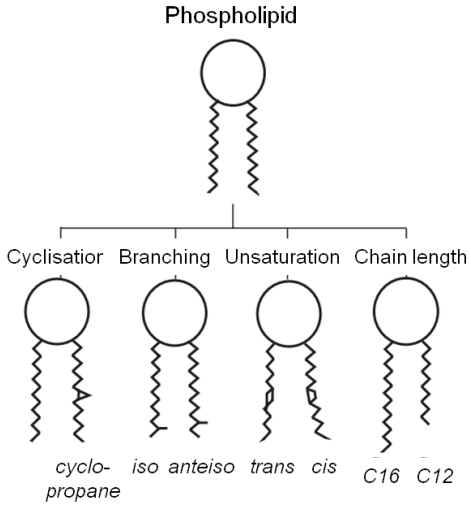

Figure II.1-9: Schematic representation of the possible phospholipid fatty acyl conformations found in biological membranes (adapted from Mykytzcuk *et al.* 2007).

bacilli to the other (a speed of 2 µm s^{-1} was estimated, Berg *et al*. 2002). It may even transfer from one leaflet to the other by a flip-flop motion, but this is much less frequent and fast. However, recent evidences for the existence of lipid domains in prokaryotes questioned this model, being in favour of a more complex and structured organization (**Table II.1-1**). In the Gram-positive *Bacillus subtilis* (*B. subtilis*), polar and septal regions of the cell were found to be enriched in anionic phospholipids, especially CL (Kawai *et al*. 2004; López *et al*. 2006; Seydlová *et al*. 2013). A spiral-like organization of PG extending along the long axis of this bacterium was also evidenced (Barák *et al*. 2008; Hachmann *et al*. 2009; Muchová *et al*. 2010), and the existence of domains similar to eukaryotic lipid rafts was suggested (Donovan and Bramkamp 2009; López and Kolter 2010).

Membrane fatty acids and fluidity

The two remaining carbon atoms of the interfacial glycerol are esterified with two fatty acids (FA). In bacterial membranes, their length is usually comprised between 12 to 24 carbon atoms (Mykytczuk *et al*. 2007). Fatty acyl chains may be saturated, harbour one or several double bonds, or other less common hydrocarbon chain modifications such as cyclization or methyl branching (Mykytczuk *et al*. 2007, **Fig. II.1-9**). A phospholipid molecule is often composed of one saturated and one unsaturated FA (Denich *et al*. 2003). These different types of fatty acyl conformation have an influence on the stability of the membrane by modulating the van der Waals interactions existing between neighbouring chains. Interactions and thus lipid stability and rigidity are favoured by long, saturated, noncyclized and unbranched FA chains, and vice versa (Denich *et al*. 2003). The unsaturation level of bacterial membranes has especially been reported to give an estimation of membrane fluidity in bacteria (Alvarez-Ordóñez *et al*. 2008). When grown in MRS broth, the major membrane FA of *L. bulgaricus* appear to be, on average and in decreasing order: C18:1, C16:0, C19:0 cyc, C16:1 and C14:0 (**Table II.1-2**, bold font) and therefore mainly account for the resulting membrane fluidity. However, the non-negligible inter-strain differences existing with high standard deviations between the five strains considered in **Table II.1-2**, probably indicate important differences in terms of membrane fluidity and concomitant other membrane biophysical properties between strains, at the origin of different levels of cryoresistance (Beney and Gervais 2001).

Membrane proteins

Membrane proteins are bound to the membrane or anchored *via* one or several transmembrane domains, and are involved in several cellular functions. These functions include transport, chemical reactions, sensing of environmental perturbations (*via* receptors), quorum sensing and cellular division. To function properly, membrane proteins must be in a native state (*i.e.*, properly folded, similarly to any other water-soluble protein). In addition, it is generally assumed that a fluid membrane is required for full enzymatic activity of integral proteins (McElhaney 1982; Uribe and Sampedro 2003), but it is difficult to prove since the modulation of membrane fluidity (by playing on environmental temperature, hydration or solutes concentration) will concomitantly affect enzymatic activity.

Table II.1-2: Membrane fatty acid composition of different strains of *Lactobacillus delbrueckii* subsp. *bulgaricus* grown in MRS broth

Strain	C12:0	**C14:0**	C15:0	**C16:0**	**C16:1**	C17:1	C18:0	**C18:1**	C18:2	C18:0-OH	**C19:0 cyc**	**Reference**
9LB	tr	3.2	-	**18.8**	**13.8**	1	1.1	**35.8**	-	-	**25.5**	Veerkamp, 1971
CIDCA 331	0.2	6.4	0.7	**30.9**	**15.5**	0.9	0.8	**23.7**	2.7	4.1	**14**	Gomez-Zavaglia *et al*. 2000
CIDCA 332	0.5	6.5	0.4	**16.6**	**15**	-	0.3	**23.6**	4.4	4.4	**7.2**	
CIDCA 333	0.2	6.9	0.9	**26.2**	**15.6**	1.5	0.9	**30.3**	1.4	3.1	**12.8**	
CFL1	tr	**5**	2	**18**	2	-	3	**48**	3	-	**14**	Gautier *et al*. 2013
average	0.3	**5.6**	1.0	**22.1**	12.4	1.1	1.2	**32.3**	2.9	3.9	**14.7**	
st. dev.	0.2	**1.5**	0.7	**6.2**	5.8	0.3	1.0	**10.2**	1.2	0.7	**6.7**	

"-": the FA was not detected or not analysed; "tr": trace amounts of the FA were detected; the four major FA constituting the membrane of each *L. bulgaricus* strain are typed in bold.

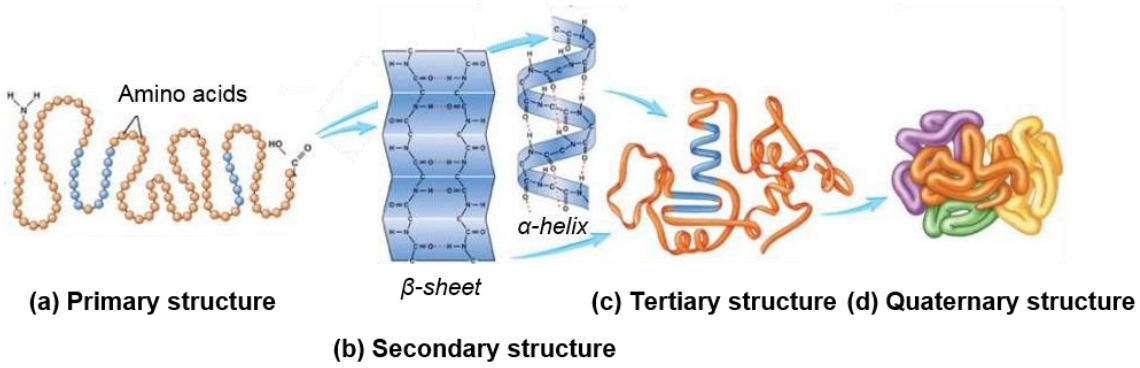

Figure II.1-10: Schematic of the four levels of protein structure (adapted from McGraw-Hill higher education website, http://www.mhhe.com/biosci/ap/ap_prep/chemH5.html, 2007).

Table II.1-3: Sequenced chromosomal genomes of *Lactobacillus delbrueckii* subsp. *bulgaricus* strains and their principal genomic characteristics (size, overall G+C content, and number of proteins; source: NCBI). Strains' origin is mentioned.

Strain	Origin	Size (Mbp)	G+C %	Proteins	Reference
ATCC 11842[a]	Bulgarian yoghurt	1.865	49.7	1626	van de Guchte *et al*. 2006
ATCC BAA-365	French starter	1.857	49.7	1625	Makarova *et al*. 2006a
PB2003/044-T3-4	Human vaginal isolate	1.977	50.0	1773	Durkin *et al*., 2010 (unpublished)
2038	Japanese starter	1.873	49.7	1618	Hao *et al*. 2011
CNCM I-1632	American starter	1.768	49.9	1603	McNulty *et al*. 2011
CNCM I-1519	American starter	1.797	49.9	1678	McNulty *et al*. 2011
VIB27	Yogurt	1.853	49.8	1692	El Kafsi *et al*. 2014
VIB44	Yogurt	1.818	49.7	1617	El Kafsi *et al*. 2014
CRL871	Argentinian yoghurt	2.061	49.1	1361	Laiño *et al*. 2015
Lb1-WT	Danish sarter	1.790	49.9	1641	Sørensen *et al*. 2016
Lb1-GS-1	Danish starter	1.743	49.9	1578	Sørensen *et al*. 2016
MN-BM-F01[b]	Dairy fan[c]	1.875	49.7	1630	Yang *et al*. 2016
ND04	Fermented camel milk	1.862	49.6	1547	Zhong *et al*. 2016 (submitted)
LBB.B5	Bulgarian yoghurt	1.778	49.8	1587	Urshev *et al*., 2016
DSM 20080	Yoghurt	1.868	49.8	1617	Kim & Yi, 2017 (unpublished)

[a] strain ATCC 11842 may also be referred to as DSM 20081, JCM 1002 or NCDO 1489, depending on the hosting culture collection (ATCC for ATCC 11842, American Type Culture Collection, Manassas, VA, USA; DSMZ for DSM 20081, Deutsche Sammlung von Mikroorganismen und Zellkulturen, Leibniz, Germany; JCM for JCM 1002, Japan Collection of Microorganisms, Tsukuba, Japan; NCFB for NCDO 1489, National Collection of Food Bacteria, Reading, UK).
[b] Strain MN-BM-F01 was originally identified as *Lactobacillus acidophilus* and subsequently reclassified as *L. bulgaricus*; similarly, strain ND02 was originally identified as belonging to the *bulgaricus* subspecies of *Lactobacillus delbrueckii* (Sun *et al*. 2011), but was later reclassified in the *lactis* subspecies following the work of El Kafsi *et al*. (2014).
[c] Dairy fan is a traditional Chinese fermented dairy.

iii. The intracellular content

A dense cytoplasm

The cytoplasm is a dense solution containing proteins, nucleic acids and metabolites. In 1991, Cayley *et al*. estimated that the concentration of proteins and RNA in the model bacterium *E. coli* under physiological conditions were close to 200 and 75 mg mL^{-1}, respectively. Recent single-cell proteomics techniques with very high throughput and sensitivity revealed that protein abundances could reach up to 10^5 in individual cells (Taniguchi *et al*. 2010). Considering a single cell represents a volume of less than two femtoliters (1.8 10^{-15} L, or 1.8 μm^3, Cayley *et al*. 1991) and is able to theoretically synthesize 4000 to 5000 different proteins (source: NCBI; http://www.ncbi.nlm.nih.gov/genome/?term=Escherichia+coli), it is reasonable to consider the cytoplasm as a highly crowded place (McGuffee and Elcock 2010). Compared to *E. coli*, the genome of *L. bulgaricus* encodes approximately 1600 proteins only, but it is very likely that the density of its cytoplasm is similar. Mika *et al*. (2014) compared the translational diffusion of cytoplasmic proteins in the LAB *Lactococcus lactis* and *E. coli*. The values they found under isotonic conditions were close, which reinforces the hypothesis of a dense cytoplasm also in Gram-positive bacteria.

Cytoplasmic proteins

Cytoplasmic proteins exert specific and various biological functions (biosynthesis, transport, replication…). Depending on the protein localization, size and function, the native structure encompasses four different levels of specific arrangements (**Fig. II.1-10**). The primary structure is the amino acid (AA) sequence of the protein (**Fig. II.1-10a**). In some parts of this sequence, neighbouring AA may interact through hydrogen bonding and arrange into characteristic secondary structures (α-helices, β-sheets protein, **Fig. II.1-10b**). Larger scale folding of the whole AA sequence makes up the tertiary structure (**Fig. II.1-10c**) as a result of covalent and non-covalent interactions (disulfide bridges, and van der Waals and hydrogen bonds, respectively). Several individual entities may as well assemble to form multimers (the quaternary structure, **Fig. II.1-10d**). If one level of this complex arrangement is compromised due to perturbations, the functionality of the protein may be lost. Environmental stress may cause reversible or permanent protein denaturation, depending on the nature and strength of the perturbation.

Nucleic acids

Nucleic acids comprise DNA (the genome) and RNAs (the transcriptome), which carry the genetic information for long-term storage and translation into proteins, respectively. The genome of *L. bulgaricus* consists of a diffuse circular double stranded chromosome plus a possible plasmid (small circular DNA molecule capable of self-replication and harbouring non essential genes conferring novel properties to their host) (Azcárate-Peril and Raya 2002; Lee *et al*. 2007). To date, the genome of fifteen *L. bulgaricus* strains has been sequenced, of which almost two thirds in the last 4 years (**Table II.1-3**). Considering these fifteen genomes, the following characteristics emerge: average length of 1.85 ± 0.08 Mb, average G+C content of 49.7 % ± 0.2 %, and about 1600 encoded proteins. Comparatively to other Lactobacilli species, *L. bulgaricus*

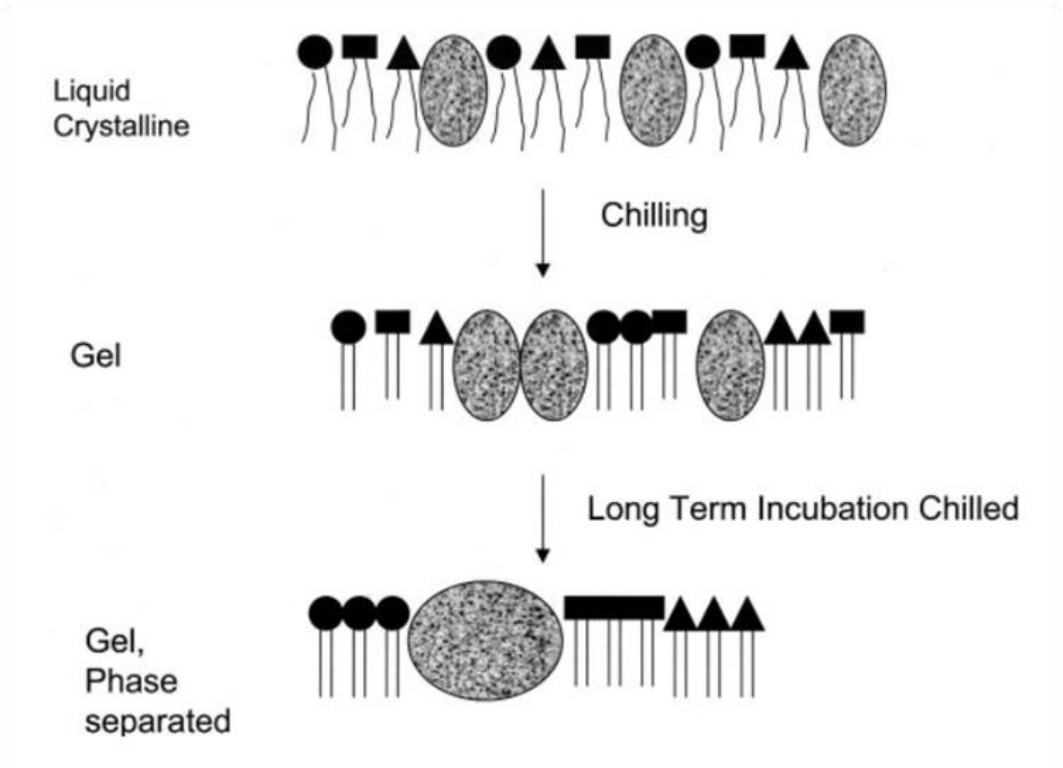

Figure II.1-11: Schematic illustration of membrane lipid lateral phase separation caused by lipid transition from the liquid crystalline to gel phase upon chilling. Each symbol (▲, ●, ■) represents different phospholipid species (Tablin *et al*. 2001).

falls within the lower range of genome size (spanning from 1.38 to 3.42 Mb) and encoded proteins (spanning from 1349 to 3241) and within the higher range of G+C content (spanning from 32 to 55 %) (Holzapfel and Wood 2014; Wassenaar and Lukjancenko 2014).

Despite its stability, the DNA may be damaged by freezing protocols (Romanazzi *et al*. 2015). Degradation of RNA in vivo, apart from natural decay, may result from chemical (antibiotics, membrane-damaging agents, Hg^{2+} ions…) and physical agents (UV radiation, oxidation…) (Deutscher 2003; Wurtmann and Wolin 2009).

1.2.2. Main targets of freeze-injury

This general cell structure may be compromised under unfavourable environmental conditions. The freeze-thawing process is thus responsible for the alteration of cellular structures, targeting particularly membrane lipids and cell proteins. The damages induced by a freezing process may be categorized according to damages associated with low temperatures and water transport across the membrane. This is described in the following.

i. Damages associated with low temperatures

The primary consequences of lowering environmental temperature are the decrease of enzymatic activities and the phase transition of membrane lipids to an ordered gel state. This transition is accompanied by a membrane rigidification which may be evaluated by fluorescence anisotropy through a decreased mobility of specific probes introduced inside the bilayer (Mykytczuk *et al*. 2007). Phase transition occurs over a temperature range depending on the specific thermodynamic properties of each membrane lipid species. Membrane lipids containing saturated and/or long chain fatty acyl residues undergo phase transition at higher temperatures than those containing unsaturated and/or short chain residues. This results in the coexistence of fluid and rigid phases at intermediate temperatures causing membrane lateral phase separation (Quinn 1985; Tablin *et al*. 2001; Beney and Gervais 2001) and exclusion of proteins from the rigid gel phase (Letellier *et al*. 1977). Such segregation of lipid species and proteins was illustrated by Tablin *et al*. (2001) and is presented in **Fig. II.1-11**. Phase separation would, in turn, cause protein aggregation leading to their inactivation (Tablin *et al*. 2001). It is also responsible for some lethal membrane permeabilization, but to our knowledge, no such studies have focussed on LAB.

Below zero degrees, distinguishing the putative impacts of cold stress from those associated with the apparition of ice is difficult (Beal *et al*. 2008). Authors claimed that no damage occurs to bacteria in samples at subzero temperatures, unless they freeze (Nei 1973). More recently, Moussa *et al*. (2008) and Simonin *et al*. (2015) evidenced the damaging effects of low temperatures on the viability of different microorganisms including the prokaryote *E. coli*, by comparing the consequences of freezing and supercooling to the same temperature. They ascribed these damaging effects to increased membrane permeability and cold lability of proteins.

ii. Damages associated with cryoconcentration and water transport

Ice formation leads to an increased extracellular solutes concentration that triggers the efflux of water from the cells' cytoplasm. Two types of injury may result from this water transport: injuries that are directly associated with mechanical constraints of water escaping through the envelope, and the chemical consequences of the concentrating intracellular and extracellular media.

Mechanical constraints associated with the water efflux through the cell envelope

With erythrocytes as models, Meryman (1968) postulated that cells behave as passive osmometers during freezing until a certain point, with cell volume reduction concomitant to cryoconcentration of the extracellular medium. Beyond this point, additional cryoconcentration would not result in further cell volume reduction, due to a pressure gradient developing across the membrane until its permeabilization (Meryman 1968). Tymczyszyn *et al*. (2005) evaluated this critical pressure at constant temperature in *L. bulgaricus* for external NaCl concentrations exceeding 1.2 M, resulting in a cellular volume loss of 20 %. According to Dumont *et al*. (2003), slow cooling rates and thus slow cryoconcentration rates allow cells to lose water at a rate that avoids membrane destabilisation. The state of the membrane (in the liquid-crystalline or gel phase) upon water efflux is another parameter that must be considered because it influences membrane permeability (Tymczyszyn *et al*. 2005). Furthermore, Gautier *et al*. (2013) have related cryoresistance to a low lipid phase transition temperature (T_m) in *L. bulgaricus*. According to the authors, a low T_m ensures more flexible membrane properties and facilitates water efflux upon freezing.

Chemical constraints resulting from cryoconcentration and water loss

Cryoconcentration and water efflux from cells directly increase the concentration of extracellular solutes and intracellular components. Salts may precipitate, resulting in a modification of the intracellular pH. High electrolyte concentrations may cause the destabilization and consequently the inactivation of macromolecules whose structure relies on non-covalent interactions: proteins and nucleic acids. In case of irreversible destabilization, enzymatic activities, protein synthesis and replication capacity may be lost upon thawing. Nevertheless, injuries resulting from high solutes concentration may rather be exerted on cell membrane than intracellular components, according to Leibo *et al*. (1970).

Sum up of the degradation of cell structures following freezing:

Cryopreservation-related cellular injuries seem to result mainly from the **loss of membrane integrity**. Understanding the impacts of the main stresses associated with freezing (cold and osmotic stresses) seems difficult when considering the scarcity of works reporting such approaches on bacteria. Studying separately cold and osmotic stresses would increase the understanding of the underlying damage mechanisms, enable to identify critical points and improve LAB preservation procedures.

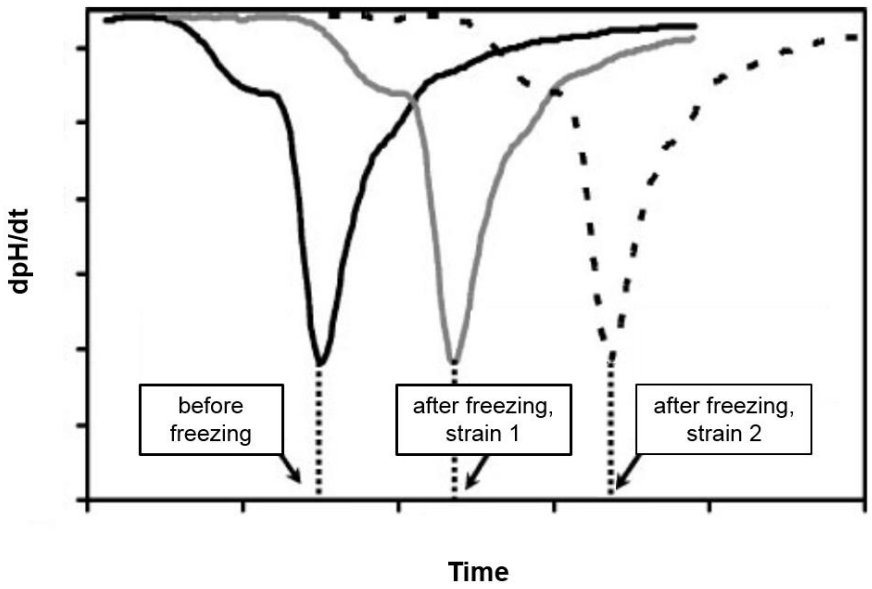

Figure II.1-12: Derivatives of hypothetical acidification activity curves of two LAB samples before freezing (solid black curve) and after freeze-thawing for strain 1 (grey curve) and strain 2 (dashed curve). The acidification activity loss following freeze-thawing is greater for strain 2 compared to strain 1, indicating its higher sensitivity to the freezing process applied (adapted from Fonseca *et al*. 2006).

1.3. Biological responses of LAB following freezing

The evolution of environmental conditions and the physical events associated with freezing are responsible for cellular structures modification and frequently induce loss of cell integrity. These, in turn, have a direct impact on cellular biological responses.

1.3.1. Assessment of the technological properties of LAB

The quality of LAB concentrates is generally evaluated through viable cell density and functionality, of which the acidifying activity is the major one. Depending on the specific technological properties desired, other metabolic activities may be looked for, such as flavouring, texturing or proteolytic properties. A high-quality LAB concentrate thus at least presents high viable cell density and acidifying activity.

Culturability

The density of viable bacterial cells is commonly assessed by the classical plate count method, while the most probable number (MPN) is more appropriate to low numbers of bacteria and therefore to evaluate the level of contaminants in foods for instance (Sutton 2010; Fakruddin *et al*. 2013). The plate count method enumerates the number of cells that are capable of replication on a defined solid medium under optimal growth conditions, and the measured parameter is thus often referred to as "culturability". Bias to this method exist, since it does not consider viable but non culturable (VBNC) cells. Besides, individual bacterial cells or clusters of bacteria arranged in chains or packets will both result in the formation of one colony, thus underestimating the total number of viable cells. Nevertheless, evaluating bacterial culturability through the plate count method remains the reference.

Acidifying activity

The acidifying activity of LAB results from glycolysis through the Embden-Meyerhof pathway. It is part of the central metabolism of LAB and informs about the general physiological state of cells. *L. bulgaricus* and other homofermentative LAB produce lactic acid as main end-product of glycolysis. Their acidifying activity may thus be evaluated by measuring the concentration of lactic acid in the growth medium, or by measuring its pH. Traditional measurements of both parameters are performed statically and do not provide dynamical information of the culture.

To remediate this, Spinnler and Corrieu (1989) proposed a method to characterise the acidifying activity of LAB in real time, based on a continuous pH measurement: the CinAc system. This system affords the possibility to acquire and exploit a high quantity of pH data in real-time, and to create the corresponding acidifying kinetics. Various descriptors may be retained to characterise the acidifying activity of LAB samples and to compare different experimental conditions. One of them is the time necessary to reach the maximum acidification rate in milk (tm, expressed in minutes), low values of tm describing a fast acidifying LAB sample, and thus a high bacterial acidifying activity. Such descriptors enable, for instance, strain performances to be compared, and the evolution of the acidifying activity of LAB to be monitored at any stage during the production process. This is illustrated in **Fig. II.1-12** which depicts the acidifying activity

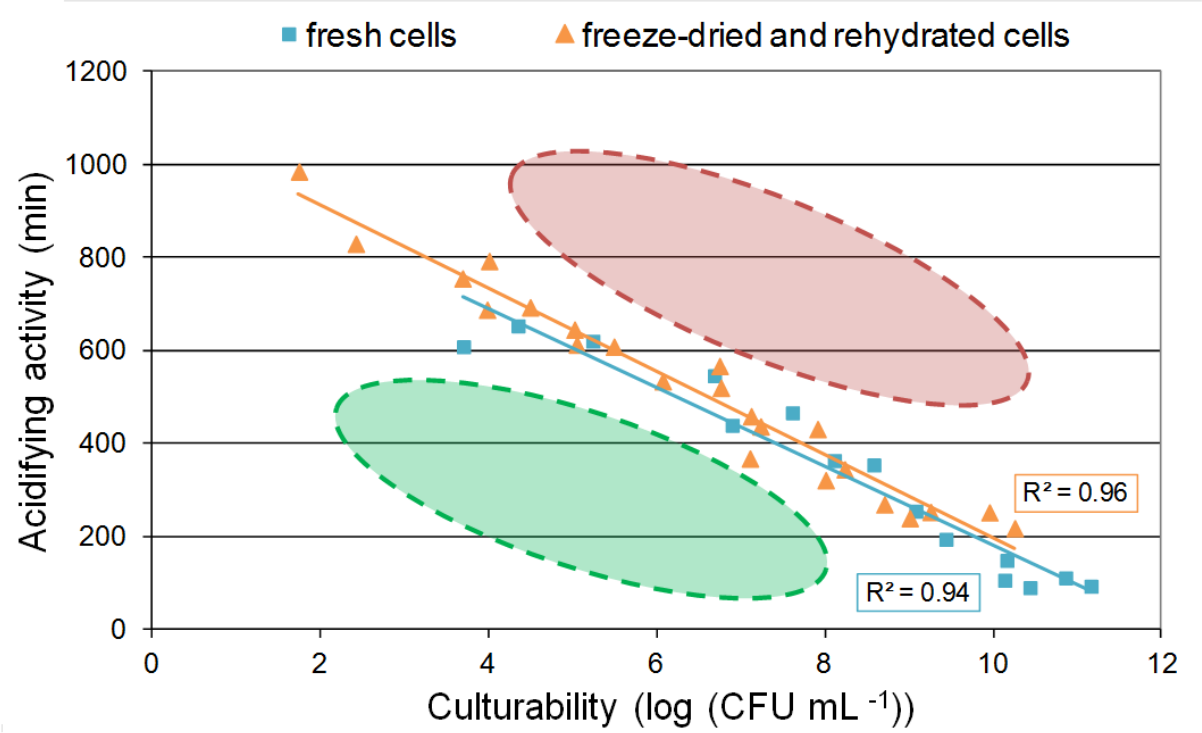

Figure II.1-13: Relationship between culturability and acidification activity of LAB for serial dilutions of *L. bulgaricus* CFL1 in the fresh state (blue squares) and after freeze-drying (orange triangles) from several biological replicates. The red and green zones illustrate the putative impact of a stressful treatment on the biological response of LAB, selecting the least (red) and most active (green) cell survivors (courtesy of Fernanda Fonseca, unpublished data).

loss following freeze-thawing of two strains with different cryosensitivities. The evaluation of the impact of preservation protocols such as cryopreservation on LAB functionality has thus been extensively studied by monitoring the tm with the CinAc system (Picque *et al*. 1992; Fonseca *et al*. 2000; Beal *et al*. 2001; Gautier *et al*. 2013).

Furthermore, plotting the acidifying activity of serial dilutions of a fresh LAB sample in standardized culture conditions gives a linear equation with species and strain specific parameters (Sodini *et al*. 2000; Wang *et al*. 2005a). This is represented in **Fig. II.1-13**, in which the blue squares correspond to serial dilutions of *L. bulgaricus* CFL1 from several biological replicates. By performing this experiment after applying a stressful treatment, three locations for the data point are possible with respect to the initial linear equation plot, giving valuable information on the biological response of LAB following this process or any other treatment:

- on the line → survivors retained their initial acidifying activity, only cell concentration varies. Such is the case of the data presented in **Fig. II.1-13** in orange triangles, corresponding to serial dilutions of *L. bulgaricus* CFL1 after freeze-drying from several biological replicates;
- above the line, in the red zone → the survivors present a weakened acidifying activity;
- below the line, in the green zone → the treatment selected survivors presenting a high initial acidifying activity that was retained throughout the treatment.

Therefore, culturability and acidifying activity give complementary information and are both important to characterise the technological properties of LAB.

1.3.2. Species and strain dependence

Due to the application of different growth conditions and freezing procedures, it is difficult to compare the cryoresistance of LAB from different published studies. However, this is possible with studies involving several LAB species and/or strains that were submitted to the same experimental conditions. **Table II.1-4** summarizes some of them, and shows substantial interspecies variability (To and Etzel 1997; Fonseca *et al*. 2000; Gómez-Zavaglia *et al*. 2000) but also intraspecies variability at the subspecies and strain levels (Smittle *et al*. 1972; Kim *et al*. 1999; Fonseca *et al*. 2000; Gómez-Zavaglia *et al*. 2000; Rault *et al*. 2007; Bravo-Ferrada *et al*. 2015).

Interspecies variability may originate from differing cell sizes and shapes. Some authors have linked bacterial cryoresistance to the surface area-to-volume ratio that could facilitate water transport across the cells upon freezing (Fonseca *et al*. 2000; Dumont *et al*. 2004). For instance, *St. thermophilus*, a cryoresistant species of LAB, exhibited a surface area-to-volume ratio four times higher than the cryosensitive *L. bulgaricus* CFL1 (Fonseca *et al*. 2000). Cell size and shape are generally similar within the same species or subspecies suggesting that cryoresistance variability may originate from other factors, including membrane lipid composition and biophysical properties, and/or protein composition and conformation.

Table II.1-4: Variability in LAB cryoresistance: culturability and acidification activity losses following freeze-thawing.

LAB species and strain	Growth conditions	Freezing procedure	Culturability loss (%)	Acidification activity loss (h)	Ref.
L. bulgaricus NCS1	Unstirred milk bottles at 37 °C for 12 h	Concentration (10^9 CFU mL^{-1} in NFMS); LN_2 immersion for 24 h	95	73*	Smittle *et al.* 1972
L. bulgaricus NCS3			54	31*	
L. bulgaricus NCS4			0	8*	
Lc. lactis subsp. *cremoris* D11 (1)	Stirred and pH-controlled spinner flasks of Elliker broth (1, 2) or MRS (3) at 32 (1, 3) or 38 °C (2) until early stationary phase	Freezing on dry ice; storage at -20 °C overnight	5	0.8	To and Etzel 1997
St. thermophilus CH3TH (2)			-80	0.8	
Lc. casei subsp. *pseudoplantarum* UL137 (3)			10	1	
Lc. lactis subsp. *lactis* MM210	Culture in MEB-Ll broth at 30 °C	Pellet suspended in 10-mL broth frozen at -60 °C for 24h	60	-	Broadbent and Lin, 1999
Lc. lactis subsp. *lactis* FG2			45	-	
Lc. lactis subsp. *cremoris* MM160	Culture in MEB-Lc broth at 30 °C		45	-	
Lc. lactis subsp. *cremoris* MM310			37	-	
Lc. lactis subsp. *lactis* LL41-1	Anaerobic growth in M17 medium + 0.5% glucose at 30 °C	Freezing to -20 °C for 24 h	75	-	Kim *et al.* 1999
Lc. lactis subsp. *cremoris* LC10-1			90	-	
St. thermophilus PB18	Stirred and pH-controlled whey-based medium in a 2L-fermentor at 42 °C until the end of the logarithmic phase	Concentration 1:1 (g cell pellet:g supernatant); Freezing to -20 °C at 0.75 °C min^{-1}	-	NS	Fonseca *et al.* 2000
St. thermophilus CFS2			-	NS	
L. delbrueckii subsp. *lactis* CFS3			-	0.3	
L. delbrueckii subsp. *bulgaricus* CFL1			-	4.0	
L. bulgaricus CIDCA 331	MRS broth at 37 °C until the stationary phase	Concentration (10^8 CFU mL^{-1} in MRS); Freezing to -20 °C	0	2.0	Gomez-Zavaglia *et al.* 2000
L. bulgaricus CIDCA 332			0	0.0	
L. bulgaricus CIDCA 333			33	3.0	
L. delbrueckii subsp. *delbrueckii* ATCC 9649			59	0.5	
L. delbrueckii subsp. *lactis* CIDCA 132			4	1.0	
L. delbrueckii subsp. *lactis* CIDCA 133			0	1.5	
L. helveticus ATCC 15807			22	0.0	
L. acidophilus CIDCA 134			0	1.0	
L. bulgaricus CNRZ 208T	MRS broth at 42 °C for 22 h	Freezing to -80 °C for 24 h with 15 % glycerol	4.8†	-	Rault *et al.* 2007
L. bulgaricus CFL1			10.4†	-	
L. bulgaricus CIP 101027T			-2	-	
L. delbrueckii subsp. *lactis* ITG LL57			1.5†	-	
L. plantarum UNQLp 133	MRS broth at 28 °C and pH 6.5 for 48 h	Freezing to -20 °C for 30 days with 20 % sucrose	60	-	Bravo-Ferrada *et al.* 2015
L. plantarum UNQLp 65.3			50	-	
L. plantarum UNQLp 155			98	-	

* acid production loss in frozen-thawed cells compared to fresh cells (%); † dead cells increase (measured as PI-stained cells, %) *Lc.*: *Lactococcus*; *St.*: *Streptococcus*; *L.*: *Lactobacillus*; *L. bulgaricus*: *Lactobacillus delbrueckii* subsp. *bulgaricus* NS: not significant; NFMS: non fat milk solids; "-": the parameter was not assessed.

Sum up of the first part of the bibliographic review:

Freezing is a stressful process for LAB (cold temperatures; high osmolarities) that **mainly targets the cell envelope** but studies remain scarce and lack precision. The degradation of cell structures leads to the deterioration of LAB functionality (acidifying activity) and to lethality. Responses might be very different from one LAB species to another and even within the same species or subspecies. Correlating biophysical characterisation to biological activity assessments appears as an interesting approach to identify the targets of cryoinjury and to quantify the extent of cell degradation. **Comparing strains with different cryoresistances** might also give valuable information to elucidate the mechanisms of cell injury following freezing.

To reduce these damages, several strategies exist. They either rely on triggering active or passive cell responses to enhance the capacity of bacteria to resist the freeze-thaw process or to protect them, respectively, and are developed thereafter.

Table II.2-1: Active cellular responses improving LAB cryoresistance by the induction of modifications related to membrane lipids and proteins.

	LAB species and strain	Growth production parameters leading to improved cryoresistance	Parameters explaining the improved cryotolerance	Reference
Membrane lipid composition & membrane properties	*Lc. lactis* subsp. *lactis* (MM210 & FG2) *Lc. lactis* subsp. *cremoris* (MM160 & MM310)	25-min heat shock at 42 °C (subsp. lactis) or 39 °C (subsp. cremoris) 2-h cold shock at 10 °C	Increased cycC19:0; decreased C18:1 Increased UFA:SFA (↘ C16:0 & slight ↗ C16:1 for all strains; ↗ C18:1 for FG2 and MM310)	Broadbent and Lin, 1999
	L. acidophilus CRL 640	Growth at suboptimal temperature (25 °C)	Increased C18:2 & C16:0; decreased C14:0 & cycC19:0	Fernandez-Murga *et al.* 2000
	St. thermophilus CFS2	Addition of oleic acid to the growth medium	Increased UFA:SFA (in particular ↗ C20:1)	Beal *et al.* 2001
	L. acidophilus RD758	Growth at suboptimum pH (pH 4.5 & 5) and temperature (30 °C)	Increased C16:0 and cycC19:0; decreased C18:0	Wang *et al.* 2005a
		8-h cold incubation at 26 °C prior to harvest	Increased UFA and slight increased CFA	Wang *et al.* 2005b
	L. bulgaricus CFL1	30-min acidification at pH 5.25 prior to harvest	Slight decreased UFA:SFA & CFA:SFA	Streit *et al.* 2008
		Cell harvest by microfiltration	Increased UFA:SFA & CFA:SFA: ↗ membrane fluidity	Streit *et al.* 2011
		Growth in a nutrient rich medium (compared to a low nutrient medium)	Decreased $T_{m\,lip}$ due to an increased UFA:SFA ratio	Gautier *et al.* 2013
			Increased membrane fluidity, especially around 0 °C	Passot *et al.* 2014
	L. buchneri R1102	Harvest in exponential growth phase	Increased UFA:SFA: ↗ membrane fluidity	Louesdon *et al.* 2015
Proteome	*L. acidophilus* CRL 639	Growth at suboptimal temperature (25 °C)	Induction of 6 proteins including a putative antifreeze protein & repression of 8 proteins	Lorca and Font de Valdez, 1998
		Growth at suboptimal temperature (25 °C) Growth at 37 °C until stationary phase	Induction of 3 proteins Induction of 2 proteins	Lorca and Font de Valdez, 1999
	St. thermophilus CNRZ302	2 to 4-h cold incubation at 20 °C	7-kDa cold induced proteins, likely CSPs (95% identity with other LAB Csps)	Wouters *et al.* 1999
	L. plantarum NC8	Overproduction of cold shock proteins: CspL, CspP and CspC	CSPs involved in: cold adaptation (CspL, ↗ growth at 8 °C); cryoadaptation (CspP, significant between 4 and 8 FT cycles); starvation adaptation (CspC, growth resumed more rapidly after nutrition deprivation)	Derzelle *et al.* 2003

II. Improvement of the cryoresistance of LAB

The physical events occurring during freeze-thawing result in the alteration of cellular structures and constituents and directly affect cellular biological activity. In LAB, freeze-thawing induces losses of cellular viability or culturability and acidifying activity to various extents. Different strategies were identified in order to limit cell degradations and enhance freeze-thaw resistance by inducing active or passive cellular responses. Active responses are induced by modulating the fermentation and post-fermentation conditions and passive responses involve the optimisation of cryoprotection, freeze-thawing and storage conditions. The second part of the bibliographic review presents an overview of these two strategies for improving LAB cryoresistance.

2.1. Improvement of LAB cryoresistance by triggering active cell responses

Modifying the conditions of fermentation (growth) and post-fermentation (but before freezing) may lead to important alteration of bacterial physiological state, including their capacity to resist to a freeze-thawing procedure. Therefore, numerous studies have optimized the processing conditions applied before freezing and/or introduced specific nutrients in order to improve the cryoresistance of LAB. Researchers have long realized that such levers generate active cellular responses leading to the modification of cellular constituents, especially the membrane lipids and cell proteins.

2.1.1. Active cell responses influencing membrane lipid composition and membrane properties

The homeoviscous adaptation is probably the most familiar cellular adaptive mechanism. It was formulated by Sinensky in 1974 and refers to the adaptability of cell membrane fluidity with temperature. It describes the fact that sub- and supra-optimal growth temperatures lead to the biosynthesis of membrane fatty acyl residues with lower and higher phase transition temperatures, respectively. This way, the cell membrane remains in a constant and optimal state of fluidity, whatever the environmental temperature.

According to **Table II.2-1**, a sub-optimal growth temperature, a cold incubation or a cold-shock upon harvest are frequently performed to improve LAB cryoresistance. As a general rule, such process modifications led to an increased unsaturated to saturated (UFA:SFA) ratio (Broadbent and Lin 1999; Wang *et al*. 2005b), an increased content in poly-unsaturated fatty acyl residues (Fernández Murga *et al*. 2000), and/or a higher concentration of cyclic fatty acids (Wang *et al*. 2005a). Surprisingly, a heat-shock has also been reported to improve the cryoresistance of *Lc. lactis* subsp. *lactis* and *cremoris*, by increasing the proportion of saturated fatty acyl residues in their membrane at the expense of unsaturated ones (Broadbent and Lin 1999). Nevertheless, the cross-resistance has rather been ascribed to the synthesis of heat-shock proteins (HSP), since addition of erythromycin, a protein synthesis inhibitor, suppressed the resistance improvement conferred by heat-shocking (Broadbent and Lin 1999). Growth at sub-optimal pH and an acid-shock have also modified the membrane fatty acid composition and improved the cryoresistance of *L. bulgaricus* CFL1 (Streit *et al*. 2008) and *Lactobacillus acidophilus* RD758, respectively (Wang *et al*. 2005a). Heat and acid cross-protections to freezing damage are part of mechanisms referred to as heterologous adaptation.

Table II.2-1 (Continued): Active cellular responses improving LAB cryoresistance by the induction of modifications related to membrane lipids and proteins.

	LAB species and strain	Growth production parameters leading to improved cryoresistance	Parameters explaining the improved cryotolerance	Reference
Proteome	*L. acidophilus* RD758	8-h cold incubation at 26 °C prior to harvest	Induction of 4 proteins (cold acclimation protein; Clp protease; pyruvate kinase; endopeptidase); 1 repressed (trigger factor for cell division)	Wang *et al*. 2005b
	L. bulgaricus CFL1	30-min acidification at pH 5.25 prior to harvest	Induction of 11 proteins (involved in energy and nucleotide metabolism, higher synthesis of stress proteins); reduction of 10 proteins (involved in protein metabolism, plus a Clp protease)	Streit *et al*. 2008
	L. plantarum L67	6-h cold incubation at 5 °C prior to harvest	Induction of thirteen proteins (involved in cell growth, energy, stress response, signal transduction and transcription)	Song *et al*. 2014
Unidentified cellular components	*L. bulgaricus* (NCS1, NCS2 & NCS3)	Addition of Tween 80 to the growth medium	not investigated	Smitle *et al*. 1972
	Lc. lactis subsp. *lactis* IL1403	48-h cold incubation at 8 °C prior to freezing	not investigated	Panoff *et al*. 1995
	Lc. lactis subsp. *lactis* (LL40-1, LL41-1 & LL43-1)	2-h cold incubation at 10 °C prior to freezing, or harvest in stationary phase	not investigated	Kim *et al*. 1999
	Lc. lactis subsp. *cremoris* (LC10-1, LC11-1 & LC12-1)	Harvest in stationary phase for strains LC10-1 and LC11-1 only	not investigated	
	L. bulgaricus CIP 101027T	24-h cold adaptation at 28 °C prior to freezing	not investigated	Panoff *et al*. 2000
	L. bulgaricus CFL1	30-min acid adaptation at pH 5.15 prior to freezing	not investigated	Streit *et al*. 2007
		Centrifugation conditions + acid adaptation	not investigated	Streit *et al*. 2008
		Growth at low pH (5) and late harvest (end of log, stationary or late stationary phases)	not investigated	Rault *et al*. 2010

Lc.: *Lactococcus*; *St*.: *Streptococcus*; *L*.: *Lactobacillus*; *L. bulgaricus*: *Lactobacillus delbrueckii* subsp. *bulgaricus*
SFA, UFA, CFA: saturated, unsaturated, cyclic fatty acids, respectively; Tm: membrane lipid phase transition temperature (°C); CSPs: cold shock proteins; FT: freeze-thaw.

Another common lever appears to be the addition of specific molecules to the growth medium. They are metabolized by the cell and reused as building blocks for the membrane. Lipid molecules are thus frequently used for this purpose. The addition of oleic acid and Tween 80 (an emulsifier containing oleic acid) to the growth medium of LAB was shown to increase their membrane UFA content and their cryoresistance (Beal *et al*. 2001). Similarly, by growing *L. bulgaricus* in a nutrient-rich medium (that contains, among others, Tween 80), compared to a nutrient-poor medium, an increased membrane UFA:SFA ratio was obtained (Gautier *et al*. 2013). With such particular membrane lipid composition, cells moved to a gel phase only at very low temperatures (below 0 °C). The increased cryoresistance observed in this culture condition was ascribed to the maintenance of the cell membrane in a fluid state close to the nucleation temperature, thus facilitating water efflux upon ice formation. These conclusions were corroborated afterwards by a direct measurement of membrane fluidity by fluorescence anisotropy (Passot *et al*. 2014).

Some post-fermentation conditions enhancing the cryotolerance of LAB have also been reported. They rely on the optimization of harvest conditions: early cell recovery in exponential growth phase (Louesdon *et al*. 2015) by microfiltration instead of centrifugation (Streit *et al*. 2011).

Modifying membrane fatty acid composition by inducing active cell responses thus appears as a powerful tool to act on LAB cryoresistance. However, the concomitant influence on other membrane properties (fluidity, flexibility) is often missing for the understanding of adaptation mechanisms.

2.1.2. Active cell responses influencing the proteome

The modification in the composition of the plasma membrane (and as a result, of its biophysical properties, *e.g.*, fluidity) originates from the upstream induction and/or repression of the synthesis of proteins involved in fatty acid metabolism. An increased UFA:SFA ratio is for instance the result of the induction of desaturases at sub-optimal growth temperatures (Shivaji and Prakash 2010).

The synthesis of many other proteins leading to increased cryoresistance has been evidenced. Depending on the technology employed for their analysis, some of them have been identified. According to **Table II.2-1**, these proteins appear to be involved in various cellular functions including stress response (Wang *et al*. 2005b; Streit *et al*. 2008; Song *et al*. 2014), but not fatty acid metabolism. This might be due to the two-dimensional gel electrophoresis (2DGE) method chosen by the authors to compare their experimental conditions; 2DGE relies on spot intensity differentiation, and may indeed lack sensitivity. Besides, the recovery of spots of interest for identification by mass spectrometry is not adapted for low molecular weight proteins (Streit *et al*. 2008), such as cold-shock proteins (CSPs) (Wouters *et al*. 2000; Keto-Timonen *et al*. 2016). CSPs act as RNA chaperones to maintain a single-stranded state of RNA and prevent the formation of hairpin structures that may provoke transcription termination at low temperatures. CSPs are therefore involved in the maintenance of efficient transcription and translation under cold environmental conditions (Keto-Timonen *et al*. 2016). A specific CSP, CspP, was interestingly identified in *L. plantarum* as presenting a cryoadaptive function (Derzelle *et al*. 2003). Its over-expression indeed resulted in an increased resistance to repeated freeze-thaw cycles.

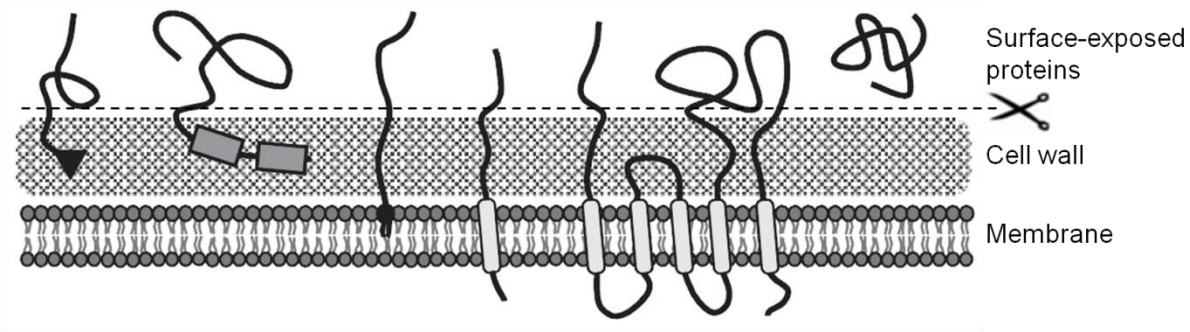

Figure II.2-1: Shaving the surface of bacteria to recover their surfaceome, or surface-exposed proteins (adapted from Barinov *et al.* 2009).

Submitting *L. bulgaricus* to a favourable acid stress for cryotolerance led to cellular proteomic modifications (Streit *et al*. 2008). In particular, the synthesis of a variety of stress proteins increased. Surprisingly, the synthesis of a Clp protease was found to be reduced, suggesting the non-essential character of this protein family in LAB cryoresistance.

There is a growing concern in high throughput proteomic approaches. Compared to 1- or 2DGE, they enable the identification of hundreds of differentially expressed proteins. These proteomic studies may also be combined to the analysis of specific proteome locations within the cell, by a partitioning of cytosolic (soluble), and envelope (insoluble) proteomes. From the latter, surface-exposed proteins may specifically be recovered by the technique of cell shaving (**Fig. II.2-1**). This protein fraction, also referred to as the surfaceome (or surfome), represents a potentially great source of answers for the understanding of cells' behaviour with their changing environment. The particular involvement of surface-exposed proteins in the adhesion and the interaction of probiotic bacteria with their host is indeed a significant field of research (Kleerebezem *et al*. 2010; van de Guchte *et al*. 2012; Zhu *et al*. 2016). Besides, the surfaceome of a permafrost-isolated bacterium (*Planococcus halocryophilus*) was recently studied to understand its adaptive response toward high salt and cryogenic temperatures (Ronholm *et al*. 2015). Notably, two proteins involved in peptidoglycan metabolism were identified under optimal conditions, and not upon exposure to subzero temperatures. Their absence pointed out the reduced cell wall biosynthesis at cryogenic temperatures. But to date, such approach remained rarely applied and none has yet been undertaken on LAB.

2.1.3. Accumulation of compatible solutes

During freezing, ice formation in the extracellular medium increases extracellular osmolarity leads to cell dehydration. An active response of Gram-positive bacteria can be observed under hyperosmotic conditions and provided that bacteria are in an active metabolic state. The cell will respond by importing so-called compatible solutes (solutes that do not interfere with cell metabolism even at high concentrations) from the extracellular environment to lower the osmotic gradient on both sides of the cell envelope. The compatible solutes accumulation restores the turgor pressure (the driving force for cell growth), limit water loss and stabilize proteins against freezing (Lippert and Galinski 1992; Poolman and Glaasker 1998; Romeo *et al*. 2001; Wood *et al*. 2001; van de Guchte *et al*. 2002).

Among the molecules identified as compatible solutes, the LAB *L. plantarum* and *Lc. lactis* seem to have a preference for the quaternary ammonium compounds glycine betaine and carnitine (Wood *et al*. 2001; van de Guchte *et al*. 2002). Their transport through the membrane uses the quaternary ammonium compounds transport system (QacT) in *L. plantarum* (Prasad *et al*. 2003) and the betaine uptake or osmoprotectant uptake system (BusA/OpuA) in *Lc. lactis* (Obis *et al*. 1999). Glaasker *et al*. 1998 and Robert *et al*. 2000 interestingly showed that the LAB *L. plantarum* and *Tetragenococcus halophila*, respectively, accumulate compatible solutes even under non-stressful conditions. This behaviour is probably shared by other LAB species. Besides, a variety of compatible solutes is naturally present in bovine whey (Le Marrec 2011), or beef and yeast extracts (Kets *et al*. 1994) that often supplement LAB growth media. Furthermore, the positive impact of compatible solutes such as betaine as LAB cryoprotectant was also evidenced (Fonseca *et al*. 2003).

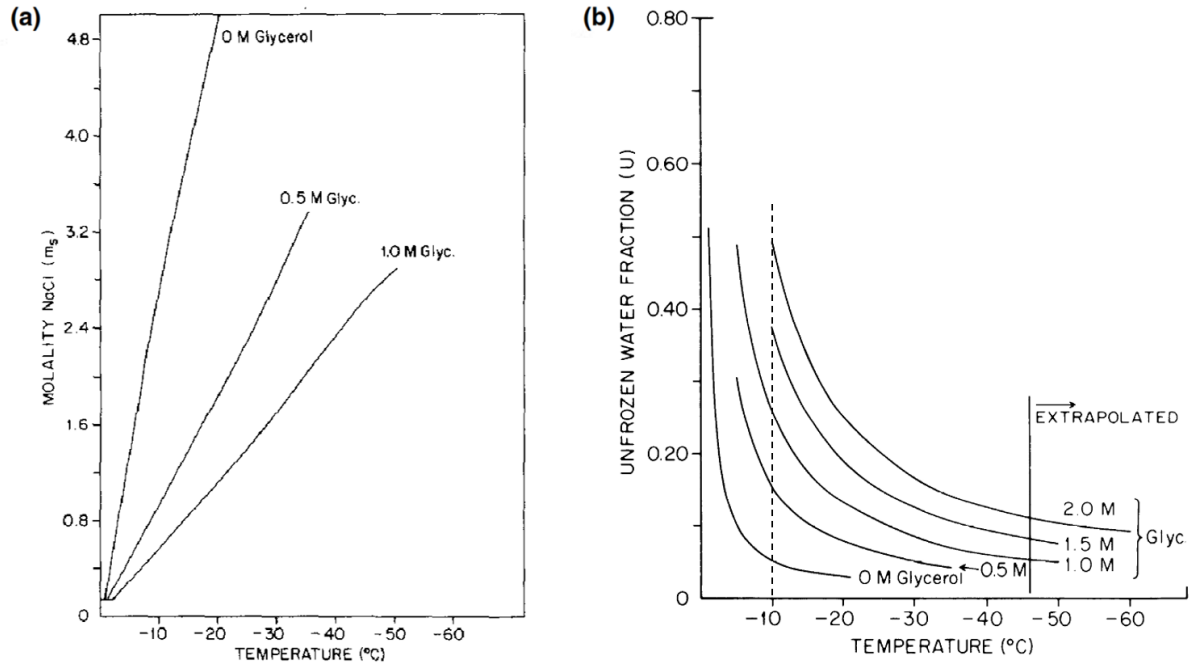

Figure II.2-2: General mechanisms of cryoprotection conferred by CPAs with the example of glycerol. At any temperature in the presence of ice, CPAs **(a)** diminish the concentration of electrolytes (*e.g.*, NaCl) in the unfrozen fraction, and **(b)** reduce the amount of ice formed. Both mechanisms are amplified with the initial concentration of the CPA (graphs were taken from Mazur and Rigopoulos, 1983).

Sum up of the improvement of LAB cryoresistance by triggering active cell responses:

Active responses of LAB that lead to an increased cryoresistance may be induced by modifying the fermentation and/or post-fermentation conditions. However, such strategies lead to **important cellular modifications** (membrane lipids, proteome, accumulation of solutes, …) **that are difficult to fully describe**. They also often rely on the application of suboptimal growth and post-harvesting conditions (*e.g.*, of temperature, pH). **The resulting improved cryoresistance is generally not sufficient to compensate for the detrimental effect on the initial biological state of cells**. In addition, such strategies are highly species and strain dependant and must be optimized for each LAB of interest. **First exploring their genomes to identify genes involved in cryo- or osmo-protection thus appears as a wise choice.**

In the following part, we will see how it is possible to increase LAB cryoresistance by triggering passive cell responses; that is to say in the absence of active metabolism.

2.2. Improvement of LAB cryoresistance by triggering passive cell responses

As quickly as possible following harvest, cellular metabolic activities are slowed down by chilling. The aim is to preserve the physiological state of cells upon harvest and limit the degradation following downstream processes. Despite a slowed down metabolism, it is still possible to limit cell cryoinjury by adding cryoprotective additives and controlling freeze-thawing and storage conditions.

2.2.1. Cryoprotection

The discovery by Polge, Smith and Parkes in 1949 that glycerol enabled spermatozoa to survive freezing caused the emergence of a new field of research and development: cryopreservation (Polge *et al*. 1949). Cryoprotective properties were allocated to numerous molecules, called cryoprotective agents (CPAs). The CPA itself and the conditions of its incorporation (temperature, time, and concentration) are important parameters that need to be optimized for a successful cryoprotection.

Cell cryoinjury is mainly due to solution effects caused by extracellular ice formation (or IIF depending at high cooling rates). The primary consequence of CPAs is to depress the freezing point of water. Because solutes are excluded from the ice fraction, their concentration in the unfrozen fraction is solely determined by temperature (at sufficiently slow cooling rates). In the presence of electrolytes such as NaCl, addition of CPAs increases the total solutes concentration and therefore lowers the concentration of NaCl at any temperature in the unfrozen fraction (Mazur and Rigopoulos (1983), **Fig. II.2-2a**). The initial CPA concentration thus influences the amount of ice formed at any time of the freezing process, and it is said that CPAs increase the unfrozen fraction (Mazur and Rigopoulos 1983; see the unfrozen fraction increment for increasing glycerol concentrations at -10 °C in **Fig. II.2-2b**). Cryoprotective agents also contribute to increase the viscosity of the solution, thereby reducing diffusion-driven processes (*e.g.*, ice growth and diffusion of molecules responsible for degradation reactions), and immobilizing cells in an extracellular matrix as it becomes glassy upon cryoconcentration.

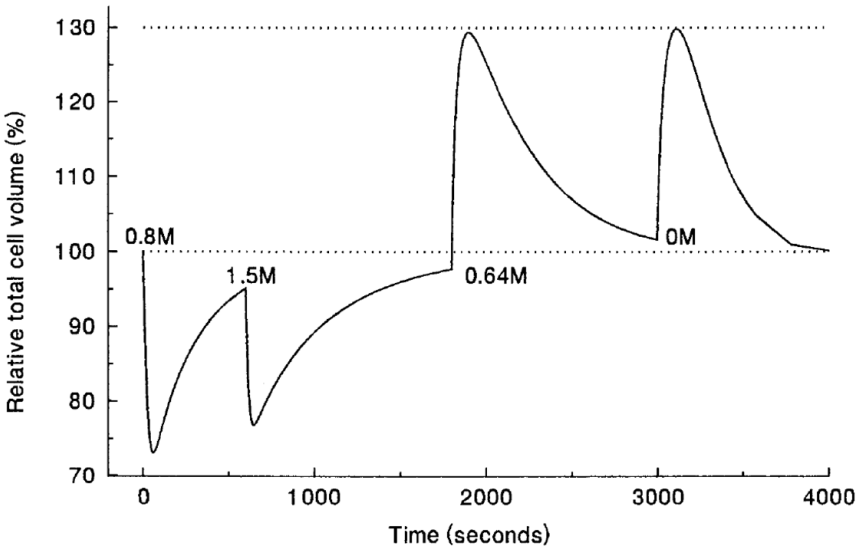

Figure II.2-3: Variations in cell volume of human oocytes exposed to increasing (0.8 and 1.5 M) and decreasing (0.64 and 0 M) concentrations of dimethylsulfoxide, a penetrating cryoprotectant (taken from Pegg, 2002).

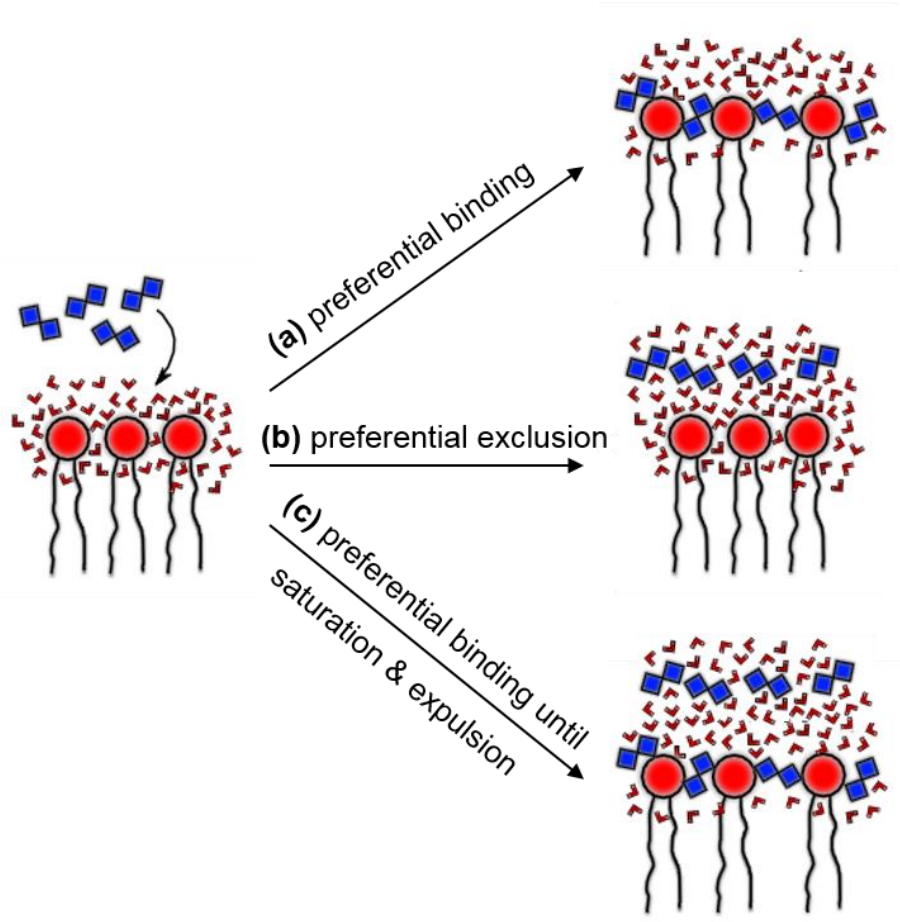

Figure II.2-4: Proposed mechanisms of membrane-sugar interactions following Andersen *et al*. (2011), based on the illustration of Kapla (2016).

Specific additional mechanisms exist, but they depend on the intrinsic characteristics of the CPA molecule, and most importantly their ability to penetrate cells or not.

i. Choice of the CPA, and protection mechanism

According to Hubalek (Hubálek 1996; Hubálek 2003), CPAs may be divided into three main categories depending on their molecular weight:

- Molecules that penetrate both the cell wall and the membrane, *e.g.*, dimethylsulfoxide (DMSO), glycerol
- Molecules that penetrate the cell wall but not the membrane, *e.g.*, disaccharides and low molecular weight polymers
- Molecules that do not penetrate any cell barrier, *e.g.*, high molecular weight polymers

Fonseca *et al*. (Fonseca *et al*. 2016) measured the intracellular glass transition temperatures (T_g'i) of *L. bulgaricus* in the presence of DMSO, glycerol or sucrose. The proposed categorization seems valid for this bacterium since T_g'i decreased to a large extent with DMSO and glycerol but not with sucrose, suggesting cell penetration of only the first two molecules. Besides, some proteins were identified in *L. bulgaricus* as facilitating the transport of glycerol (van de Guchte *et al*. 2006), but not sucrose.

Penetrating CPAs

Membranes permeability is greater to water than to permeable CPAs. Consequently, adding CPAs results in a transient outflow of water by osmosis. Cell volume is then restored as the CPA penetrates. This is illustrated in **Fig. II.2-3** with the example of consecutive additions and dilutions of DMSO to oocytes suspensions. Consequently, the osmotic stress imposed on cells by penetrating CPAs is transient.

By being inside the cell and on both sides of the membrane, permeable CPAs exert protective effects to the membrane and intracellular macromolecules. It has been proposed that stabilization is conferred by preferential interaction, a term gathering two types of interactions: preferential binding and preferential exclusion (both mechanisms are depicted for membrane lipids in **Fig. II.2-4a** and **Fig. II.2-4b**, respectively), the latter being the most likely scenario regarding proteins (Crowe *et al*. 1990; Lippert and Galinski 1992).

The most widely used CPA, DMSO, is a solvent and therefore not suitable for use in foods. Due to its toxicity, cryoprotection using DMSO is usually performed at low concentration (< 10 %, Hubalek, 2003) for a limited period of time (15 – 30 min) and at low temperature (0 – 5 °C) (Heylen *et al*. 2012). On the contrary, glycerol is much less toxic. Its permeability is also lower, and incubation periods are therefore usually longer (30 – 60 min) and performed at ambient temperatures (Heylen *et al*. 2012).

Non-penetrating CPAs

Because of their ability to diffuse through the peptidoglycan, disaccharides and low molecular weight polymers (molecular weight cut-off depending on the organism considered) may interact with the membrane lipid headgroups (Anchordoguy *et al*. 1987; Crowe *et al*. 1988; Crowe *et al*. 1990; Santivarangkna *et al*. 2008a), creating an external and surrounding viscous layer.

Under physiological conditions, membrane lipid headgroups are highly hydrated and several water molecules interact with lipids through hydrogen-bonding (Luzardo *et al*. 2000). During freezing, CPAs probably stabilize membranes throughout the whole freeze-thawing process, either by strengthening the

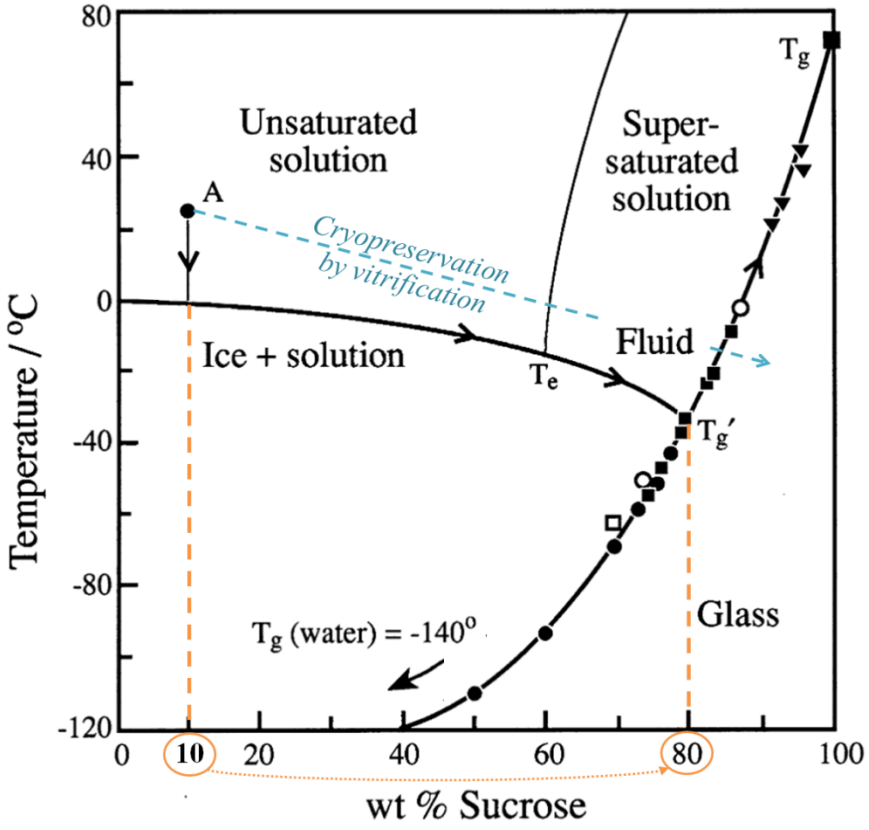

Figure II.2-5: State diagram of a water-sucrose binary mixture, showing the sucrose concentration increase of sample A during freezing at a slow rate (black arrows), and the cryopreservation method by vitrification (blue dashed arrow) (adapted from Franks, 1998).

existing water hydrogen bonds (preferential binding) or by replacing water molecules (preferential exclusion) (Crowe *et al*. 1990).

Some authors are in favour of preferential binding between disaccharides and membranes (Strauss and Hauser 1986; Anchordoguy *et al*. 1987). However, in such a case, the insertion of disaccharides between lipid headgroups should weaken the van der Waals forces between neighbouring fatty acyl chains. By means of FTIR spectroscopy, Crowe *et al*. (1990) argued that the opposite has been seen with trehalose. Andersen *et al*. (Andersen *et al*. 2011) tried to reconcile both theories by invoking a concentration dependency: if the sugar is present at low amounts, it would preferentially bind with lipids until saturation of the bilayer. Beyond a critical concentration, excess sugar molecules would be expelled and would stabilize the lipid hydration shell (**Fig. II.2-4c**). Yet, membrane-sugar interactions remain a current matter of debate (Crowe 2015).

Complex CPAs and mixtures

Microorganisms and particularly LAB have been successfully cryopreserved in the presence of complex CPAs such as yeast extracts, milk and its derivatives (Baumann and Reinbold 1966; Smittle *et al*. 1972; de Urraza and De Antoni 1997; Hubálek 2003). Also, combining different CPAs (penetrating and non-penetrating) in a cryoprotective mixture could be an alternative solution for the preservation of LAB. However, the protection mechanisms involved would not be easy to identify when using complex CPAs or mixtures of CPAs.

ii. Adverse effects of CPAs

Cryoprotective agents confer vital protection to cells during freezing. However, some CPAs are toxic for cells (*e.g.*, DMSO). Also, CPAs are used above isotonic concentrations and thus exert an osmotic stress on cells that increases during cryoconcentration of the extracellular medium. A certain paradox therefore characterises CPAs.

Practices of high concentrations of CPAs

Hubalek (2003) reported in a literature review an extensive variability in the CPA concentrations for the cryopreservation of microorganisms. For instance, the concentration of sucrose was indicated to range between 1 and 68 % (w/v). Besides, CPAs are very often solubilized in isotonic saline water (300 mOsm L^{-1}) (Morris *et al*. 2006; Morris *et al*. 2012; Fonseca *et al*. 2016). Any concentration of added CPA therefore exerts a more or less strong osmotic stress on cells. Formulation is usually simply performed by re-suspending freshly harvested cells in the cryoprotective solution, but step-by-step increments are sometimes preferred to limit the osmotic stress imposed on cells (**Fig. II.2-3**). During freezing, cryoconcentration reinforces this stress: freezing an isotonic sucrose solution (approximately 10 % wt) leads to an 8-fold concentration increase in the maximally freeze-concentrated matrix at T_g', as shown in the water-sucrose state diagram in **Fig. II.2-5**.

Besides, Pegg mentioned in his historical review of cryopreservation (Pegg 2002) that ideally, preservation by vitrification could be achieved by adding sufficiently high amounts of CPA to reach extreme viscosities

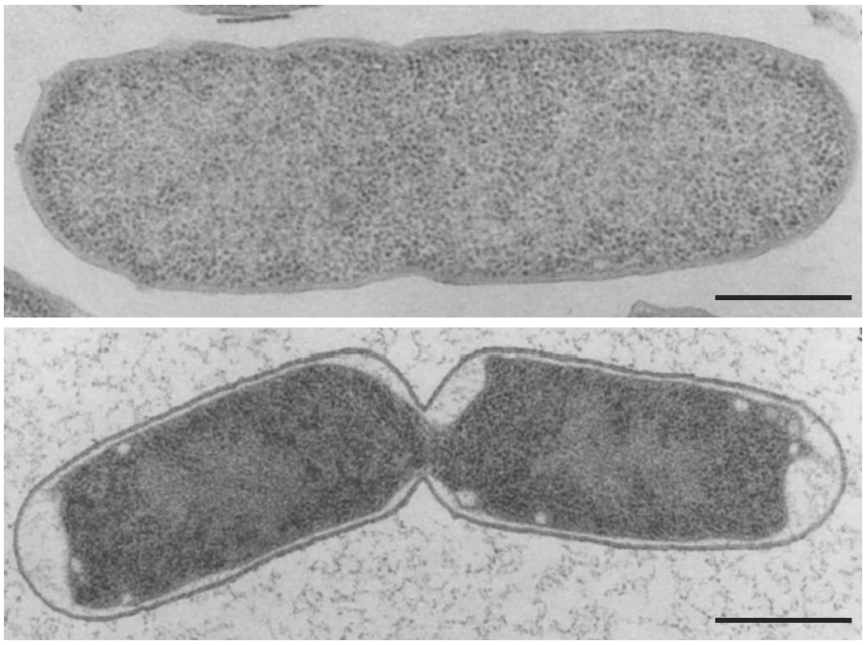

Figure II.2-6: Electron photomicrographs of *E. coli* under isotonic (above) and 16 % (w/v) sucrose conditions (below), showing plasmolysis and endocytotic vesiculation (scale bar: 0.5 µm; taken from Schwarz and Koch, 1995).

and a glassy state without any crystallization (**Fig. II.2-5**). While the complete absence of ice could be a solution for effective preservation, Pegg reminded that the required concentrations are by far exceeding the tolerable limits of living organisms to the osmotic and toxic damages (related to volume change and chemical toxicity, respectively) they can generate.

Effects of hyperosmotic concentrations of CPAs on prokaryotes

The osmotic stress caused by glycerol was studied on various microorganisms. As a membrane-penetrating CPA, glycerol addition to a cell suspension induces a transient hyperosmotic stress (**Fig. II.2-3**). Much higher concentrations of glycerol than non-penetrating CPAs of equivalent molar mass were therefore applied to study the consequences of its osmotic stress on bacteria. Mille *et al*. (2005) thus compared the resistance to glycerol-mediated hyperosmotic shocks (up to 133 MPa, *i.e.*, ~ 84 % (w/v) glycerol) of a variety of microorganisms: Gram-negative bacteria, LAB and yeasts. Their sensitivity was highly species specific. Consequently, a ranking among Gram-negative prokaryotes, Gram-positive prokaryotes and eukaryotes could not be established. In particular, *L. bulgaricus* appeared as the most sensitive organism tested (more than 90 % lethality under 14.5 MPa, *i.e.*, ~ 35 % (w/v) glycerol) compared to *L. plantarum*, the least sensitive. The authors assumed that membrane phospholipid composition, differing greatly among cell types and being rather close between both LAB for instance, could not explain the resistance behaviours observed, at least not only. Instead, they suggested that the conjunction of many factors could explain the different intra-species sensitivities, including intracellular solutes, ions and compatible solutes contents, as well as membrane proteins.

Ragoonanan *et al*. (Ragoonanan *et al*. 2008) reported the analysis of sucrose hyperosmotic stress on the viability of bacteria. They evidenced a proportional viability decrease of the proteobacterium *Geobacter sulfurreducens* (Gram-negative) to the intensity of the hyperosmotic stress conferred by sucrose above 500 mOsm L^{-1} (~ 7 % (w/v)). High sucrose concentrations (1100 mOsm L^{-1}, ~ 27 % (w/v)) also destabilized the membrane lipid acyl chains at low temperatures leading to lipid dissolution, according to the authors.

By observing *E. coli*, a model Gram-negative bacterium, under high glycerol concentrations by electron microscopy, Mille *et al*. (2003) and Beney *et al*. (2004) evidenced dramatic modifications of its envelope above osmotic pressures of 26 MPa (~ 47 % (w/v) glycerol): cell volume decrease, apparition of plasmolysis spaces and wrinkling of the membrane and wall surfaces, followed by endocytotic vesiculation above a certain hyperosmotic pressure threshold.

Plasmolysis and endocytotic vesiculation also occurred in *E. coli* in the presence of hyperosmotic concentrations of sucrose (16 % (w/v), (Koch 1995; Schwarz and Koch 1995), **Fig. II.2-6**). According to these authors, if membrane lipids were perfectly elastic, water loss would result in infinite cell shrinking. On the contrary, the low compressibility of lipids forces the membrane to wrinkle. Plasmolysis spaces predominantly formed at the poles by separation of the membrane from the cell wall, and endocytotic vesiculation occurred elsewhere to remove the excess of membrane.

No equivalent studies on Gram-positive bacteria have been reported, allowing only to speculate that similar mechanisms certainly apply. Overall, scientific works reporting on the osmotic stress generated by non-

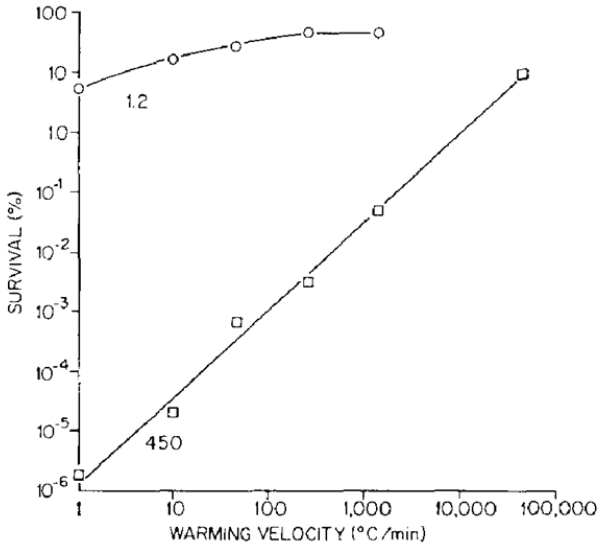

Figure II.2-7: Survival of *Saccharomyces cerevisiae* frozen slowly (at 1.2 °C min^{-1}, circles) or rapidly (at 450 °C min^{-1}, squares) depending on the warming rate applied (taken from Mazur, 1977).

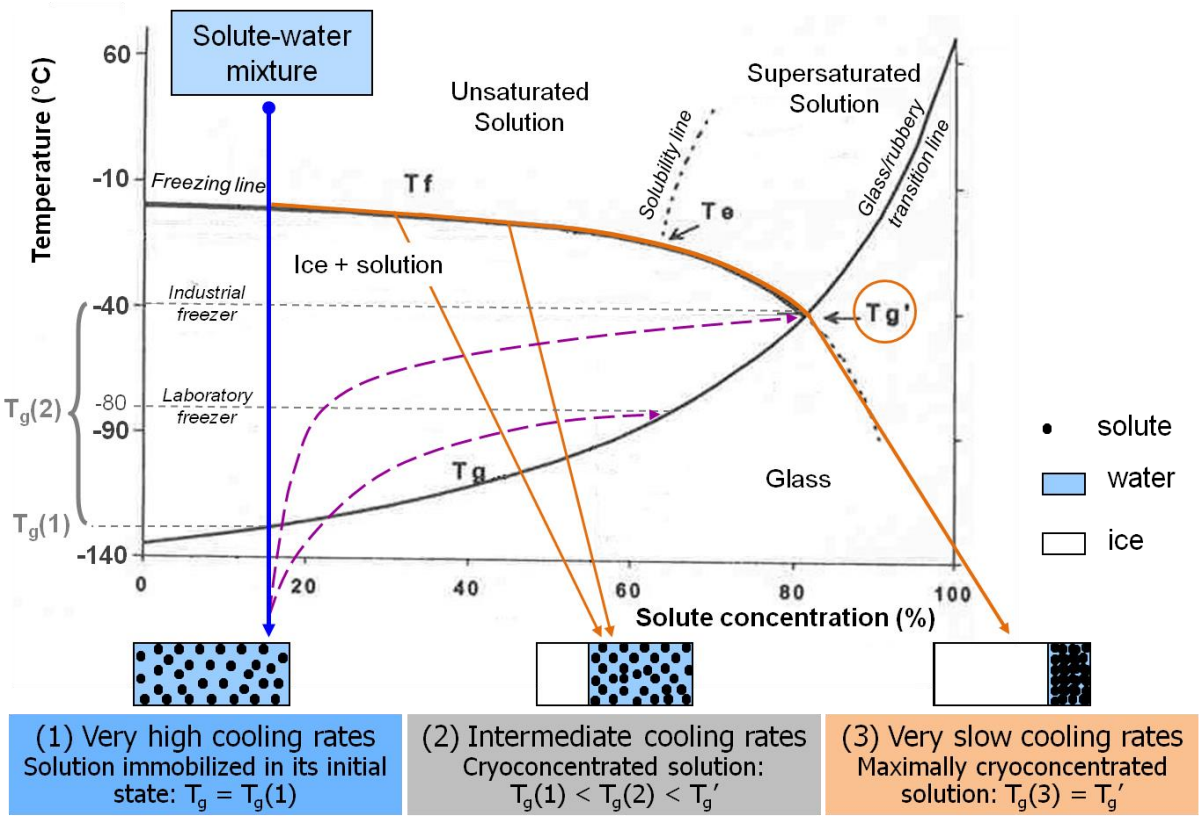

Figure II.2-8: State diagram of a solute-water mixture frozen at different cooling rates: (**1**) very high (*e.g.*, by immersion in liquid nitrogen), (**2**) intermediate and (**3**) very slow, leading to increasing ice fractions and solutes cryoconcentrations in the final product, as represented by the rectangles. If storage following very high cooling rates is performed at higher temperatures (-80 °C or -40 °C in laboratory or industrial freezers, respectively), instability and ice recrystallization occurs, as represented by the purple dotted arrows.

ionic CPAs such as sucrose seem scarce and even missing from LAB studies, despite their relevance for cryopreservation-related issues.

2.2.2. Controlling freeze-thawing and storage conditions

In order to maximally reduce the deleterious solution effects due to CPA cryoconcentration, the temperature profile of the freezing process must be optimized. Moreover, careful choice and control of the storage temperature and thawing conditions aim at avoiding ice recrystallization phenomena for conferring stability to the product.

i. Choice of the freeze-thawing rates

Optimal cooling rates are defined by the two-factor hypothesis (**§I.1.2**). However, the relationship between cooling and warming velocities has also to be considered. Mazur and Schmidt (1968) evidenced extensive lethality of the yeast *S. cerevisiae* when frozen at a high cooling rate followed by slow thawing (**Fig. II.2-7**). Whatever the cooling rate, the authors also showed that the faster the thawing procedure, the higher the survival for this microorganism. Thus, thawing by immersion of the frozen sample in a temperature-controlled water bath (at ~ 30 – 42 °C, depending on the microorganism considered) until no ice remains appears widely applied (De Paoli 2005; Smith *et al*. 2008; Prakash *et al*. 2013).

The physical explanation for such important cell damages upon slow warming is water recrystallization phenomena at subzero temperatures. When very high cooling rates are applied, water vitrifies in a glassy matrix without ice formation. Upon warming, this glass may recrystallize when the temperature becomes higher than the glass transition temperature of the matrix, and may form large ice crystals. The faster the cooling (typically obtained by immersion in liquid nitrogen) and the slower the thawing, the more extensive the recrystallization phenomenon is (Pegg 2002; Dumont *et al*. 2006). Consequently, slow freezing followed by rapid thawing rates were also recommended for the cryopreservation of LAB, as exemplified by Bâati *et al*. (2000) for *L. acidophilus*.

ii. Choice of the storage temperature

Applying optimized cryoprotection and freeze-thawing rates for a successful cropreservation of LAB is critical, but inappropriate storage conditions easily lead to dramatic deteriorations of cells and could ruin a well-performed freezing procedure. The choice of the storage temperature depends on the freezing rate applied and on the CPA used.

There are three major freezing/storage possible scenarii with respect to sample stability. They are illustrated in the state diagram presented in **Fig. II.2-8**, starting from a common state of solute fraction and temperature:

- Freezing and storage are performed in liquid nitrogen (LN_2, -196 °C, blue arrow) or in its vapor phase.
- Freezing is performed by immersion in LN_2 (blue arrow) followed by storage at higher temperatures in a laboratory (-80 °C) or industrial freezer (-40 °C), as represented by the purple dashed lines in **Fig. II.2-8**.
- Freezing is performed at a controlled slow rate until storage temperature is reached (orange arrows).

The first scenario is convenient, provided that thawing is fast enough to avoid ice recrystallization during thawing due to the large fraction of unfrozen water. In the second scenario, storage at higher temperatures,

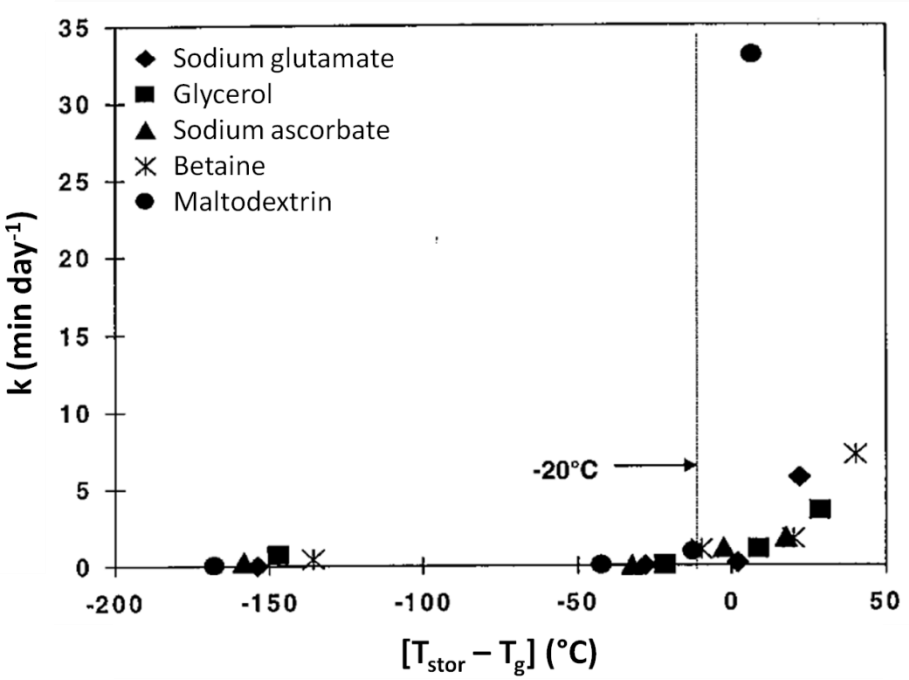

Figure II.2-9: Evolution of the degradation of the acidifying activity of LAB (**k**) as a function of the difference between storage ($\mathbf{T_{stor}}$) and glass transition temperature ($\mathbf{T_g}$) using various cryoprotective agents (adapted from Fonseca *et al.*, 2001).

i.e., above the glass transition temperature ($T_g(1)$ in **Fig. II.2-8**), leads to nucleation and ice recrystallization in the frozen state. Prolonged storage periods in such conditions is damaging for cells. Fonseca *et al*. (2001) showed that the rate at which the acidifying activity loss occurs in *L. bulgaricus* significantly increases for storage temperatures above a certain threshold, corresponding to T_g - 20 °C (**Fig. II.2-9**). In the third scenario, the slow freezing rate allows the sample to cryoconcentrate and to remain in an amorphous glassy state at higher temperatures; storage may thus be stable at -80 °C or -40 °C provided that $T_{stor} < T_g$ - 20 °C. The value of T_g depends on the solutes cryoconcentration and composition, *i.e.*, the CPA used. Glass transition of the maximally cryoconcentrated solutions of sucrose, glycerol and DMSO (T_g'e) occurs at -48 °C, -99 °C and -120 °C, respectively (Fonseca *et al*. 2016). Therefore, storage temperatures must be adapted accordingly. For instance, LAB suspensions protected in glycerol or DMSO will present a $T_g \leq$ -99 °C and ≤ -120 °C, respectively, and should be stored in LN_2. Furthermore, the authors have evidenced a link between intracellular T_g' (T_g'i; T_g'i > T_g'e) of *L. bulgaricus*, depending on growth conditions and on the CPA used, and the rate of loss of viability to freeze-thawing. CPAs leading to a low T_g'i appeared to be more protective than other CPAs, because of an increased since they allowed cells to osmotically equilibrate with the extracellular cryo-concentrating medium down to lower temperatures. This study also suggested the relevance of considering T_g'i in addition to T_g'e, in the determination of stable frozen storage temperatures, possibly allowing storage at higher subzero temperatures.

Anyhow, temperature variations must be avoided as much as possible. Bank and Mazur (1973) indeed showed that freezing *S. cerevisiae* in LN_2 and increasing the storage temperature to -20 °C for only 5 min had dramatic consequences on the shape of the cells, due to extensive ice recrystallization from nucleus formed intracellularly during the primary cooling to -196 °C. Considering LAB, no intracellular ice forms in the presence of CPAs, but extracellular recrystallization may also be very damaging (Fonseca *et al*. 2006).

Sum up of the improvement of LAB cryoresistance by triggering passive cell responses:

Cryoprotection of LAB limits the injurious effects of freeze-thawing. By being potentially present in different compartments (extracellular, intracellular, membrane interface), CPAs provide specific **stabilizing interactions with biomolecules** throughout the freezing process. Often, operational constraints impose the freeze-thawing protocol and storage temperature. In this case, the CPA should be carefully selected accordingly, in order to minimize cellular degradation rates.

Yet, **CPAs paradoxically exert an osmotic stress to cells during formulation and cooling**, **especially as they cryoconcentrate.** The damages may be different in nature and intensity from cell to cell within a bacterial population. Therefore, characterising the heterogeneity of cell responses to freezing and osmotic stress would be interesting to better understand the cellular damage mechanisms involved.

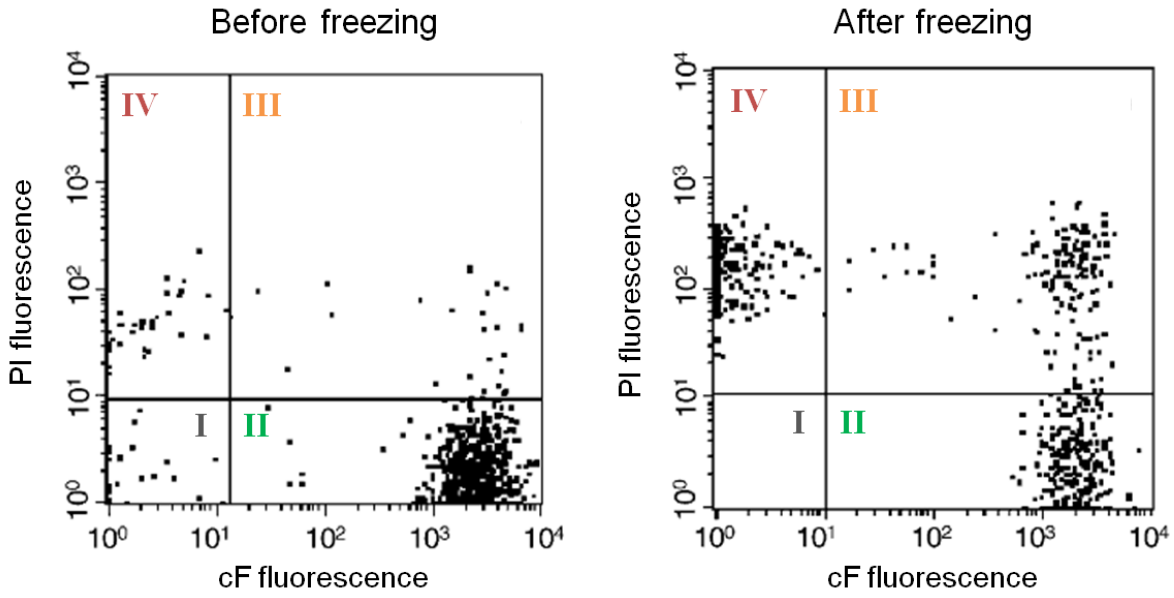

Figure II.2-10: Flow cytometry of *Lactobacillus delbrueckii* subsp. *bulgaricus* double stained with carboxyfluorescein (cF) and propidium iodide (PI). (**I**) unstained or lyzed cells; (**II**) cF-stained & PI-unstained viable cells; (**III**) cF-stained & PI-stained damaged cells; (**IV**) cF-unstained & PI-stained dead cells. Each point represents a bacterium. Note the decreased density of points in quadrant II in favour of quadrants III and IV after freezing (adapted from Rault *et al*. 2007).

2.3. Improvement of LAB cryoresistance by reducing population heterogeneity

When analysing bacterial populations, bulk information is often obtained, thus characterising an overall behaviour of the cells. For instance, the acidifying activity thus gives average information on the biological activity of the sample, and may hide subpopulations of bacteria with more or less active metabolisms. Analysing individual cells should allow to better understand degradation or preservation mechanisms, and to generate homogeneous populations of resistant cells by reverse engineering. However, it requires cutting edge technologies with extremely high resolution (at least one bacterium) and high throughput methods to deal with several orders of magnitude of micron-sized bacterial cells.

2.3.1. Heterogeneous biological responses to freeze-thawing

Assessing individual cell's physiological state is possible using specific fluorescent markers associated with flow cytometry. A flow cytometer exploits the properties of light to analyse the size, shape and fluorescence of individual cells as they are illuminated by a laser beam in a thin laminar flow. Flow cytometry counts cells in a defined volume and assigns one or more fluorescent characteristics to each counted event. By using the couple of dyes 'carboxyfluorescein (cF) and propidium iodide (PI)', Rault *et al*. (2007) could identify and quantify three subgroups within the population of *L. bulgaricus* and *L. delbrueckii* subsp. *lactis*: viable, dead and injured cells. With this technique, viable cells are characterised by a functional esterase activity and an intact membrane (cF-stained and non PI-stained); dead cells have lost any esterase activity and their membrane is damaged (non cF-stained and PI-stained); and injured cells are stained by both dyes, meaning that their membrane is damaged but that they retained a functional esterase activity. The authors monitored the evolution of the number of each subpopulation following freezing and frozen storage, and could thus attribute a cryorsensitive behaviour to *L. bulgaricus* strain CFL1 with a significant decrease in the proportion of viable cells, paralleled with an increase in the proportions of dead and injured cells (**Fig. II.2-10** and **Table II.1-4**), contrary to the other strains and subspecies tested. Flow cytometry has been associated to cell sorting for the analysis of the physiological state of *Bifidobacterium* cells following stressful treatments (Amor *et al*. 2002). Such approach, provided that cell sorting does not introduce further damage to cells, opens the way to strategies aiming at reducing population heterogeneity, thus increasing the proportion of viable and potentially more functional cells within a culture.

Rault *et al*. (2010) have then attempted to link the information obtained by flow cytometry (the stability of esterase activity and membrane integrity) to the technological properties of *L. bulgaricus* CFL1, such as culturability and acidifying activity after freezing and frozen storage. However, substantial losses in the technological properties of cells were not systematically correlated with a decrease in viability measured by flow cytometry. The authors concluded that the freezing conditions applied led to the apparition of VBNC that increased during frozen storage. Obtaining such information remains interesting per se, especially for probiotic applications since they do not need to be able to proliferate to exert their beneficial properties to the host, as pointed out by Lahtinen *et al*. (2006).

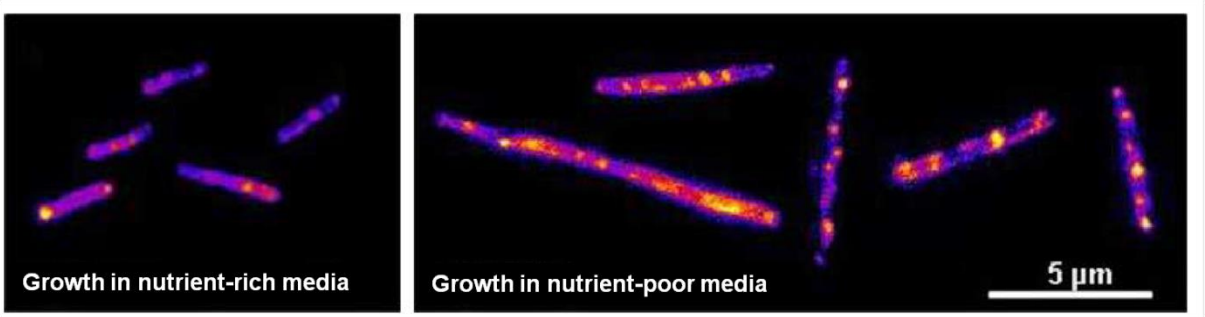

Figure II.2-11: Membrane fluorescence anisotropy in single *Lactobacillus delbrueckii* subsp. *bulgaricus* using Synchrotron UV microscopy depending on the growth media used. Colours are artificial and represent anisotropy grades from lowest (purple, fluid membrane domains) to highest values (yellow, rigid membrane domains) (adapted from Passot *et al*. 2014).

Associated flow cytometry with cell sorting – provided that it does not damage cells – and to traditional techniques for the evaluation of the biological activity of LAB would be interesting. It could enable to separate and characterise subpopulations (viable; damaged; dead cells) in terms of biological activity in response to environmental perturbations. However, such approach does not allow the identification of cellular stress markers with the same spatial resolution. This would be possible by the assessment of the subcellular biophysical properties.

2.3.2. Heterogeneous biophysical responses to freeze-thawing

To better understand the mechanisms of cell cryodamage, identifying cellular stress markers at a subcellular resolution could enable to characterise and quantify population heterogeneity in response to such environmental stresses. For that, associating analytical techniques for the evaluation of the biophysical response of cells (membrane fluidity, biochemical composition) to microscopy appears as a promising approach.

i. Heterogeneous membrane fluidity as evidenced by fluorescence anisotropy

Fluorescence anisotropy has thus been associated with microscopy in a setup using synchrotron radiation, for the analysis of membrane fluidity of single *L. bulgaricus* cells (Passot *et al*. 2014). This procedure made possible the dynamic quantification of membrane fluidity of individual cells with chilling. The authors evidenced for the first time that membrane fluidity was different from cell to cell, and that such heterogeneity was greater at low temperatures. By comparing two populations of *L. bulgaricus* grown in two different media, a nutrient-rich and a nutrient-poor medium, they also identified the existence of intra-cellular heterogeneity, especially in cells grown in the nutrient-poor medium, with co-existing fluid and rigid regions, as shown in **Fig. II.2-11**.

The lipophilic probe used to assess fluorescence anisotropy may also be used to evaluate membrane fluidity of LAB populations by flow cytometry (Velly *et al*. 2015). By combining such approach to a dual live/dead staining, a triple staining could potentially allow determining the membrane fluidity of each subpopulation: viable, damaged and dead cells.

ii. Heterogeneous biochemical composition as evidenced by vibrational spectroscopies

Vibrational spectroscopies exploit the transition of electrons to higher energy levels involving the vibration of molecular bonds. They include Raman and Fourier transform infrared (FTIR) spectroscopies, both providing a chemical analysis of the main molecules in biological samples (lipids, proteins, polysaccharides and nucleic acids), with sensitivity to their conformation and environment.

Raman spectroscopy detects the inelastic diffusion of light following excitation of the sample with a laser beam. Its combination with a confocal microscope (Raman micro-spectroscopy) using high magnification objectives lenses makes it possible to target individual bacterial cells with a spatial resolution of 1 µm (Schuster *et al*. 2000; Harz *et al*. 2009). Thanks to the highly specific Raman spectral fingerprints of bacteria, this technique is extensively used for identification purposes down to the strain and single-cell levels,

especially for clinical purposes on pathogenic bacteria (Chan *et al*. 2004; Xie *et al*. 2005; Stöckel *et al*. 2016). Optical tweezers were used to analyse and sort single-cells in aqueous media, and additionally enabled a dynamic analysis of cellular processes in individual cells, such as lysis (Chen *et al*. 2009) and trehalose uptake in Gram-negative bacteria (Avetisyan *et al*. 2013). However, Raman diffusion is a rare event (1 photon is inelastically diffused over 10 billion incident photons) and conventional Raman has long suffered from a lack of sensitivity. In parallel, the popularity of FTIR spectroscopy, the alternative vibrational spectroscopy technique, has resulted in a less active development field for Raman spectroscopy in the past decades. As a consequence, Raman spectra are less straightforward to interpret than FTIR ones, even still today. The utilization of Raman spectroscopy, associated with methods of cluster analysis, therefore seems preferentially dedicated to microbial identification and species or strain differentiation more than biochemical and structural analyses of bacteria.

On the other hand, FTIR spectroscopy is based on the vibrational excitation of molecular bonds caused by infrared absorption and is complementary to Raman spectroscopy. Developments of FTIR spectroscopy since its exploitation in synchrotron facilities have recently allowed its application to the analysis of single microbial cells (Saulou *et al*. 2010; Saulou *et al*. 2013; Passot *et al*. 2015). In combination with statistical multivariate analyses, it has thus been possible to relate population heterogeneity to stressful treatments, such as nanosilver stress in *S. cerevisiae* (Saulou *et al*. 2010), silver stress *E. coli* (Saulou *et al*. 2013), and freeze-thawing in *L. bulgaricus* (Passot *et al*. 2015). Cryoresistant *L. bulgaricus* cells grown in a nutrient-rich medium thus appeared to display slightly higher biochemical heterogeneity than cryosensitive cells grown in a nutrient-poor medium. This difference was evidenced from the analysis of two spectral regions, assigned to membrane lipids and to proteins, polysaccharides and nucleic acids in the fresh state (**Fig. II.2-12**) and was ascribed to a more diversified metabolism enabled by the availability of nutrients (Passot *et al*. 2015).

In summary, both techniques have their own advantages and limitations, depending on specific requirements. In particular, FTIR spectroscopy is less invasive than Raman spectroscopy (exploits less energetic radiations) and provides higher signal-to-noise ratios but is limited on several other aspects, such as spatial resolution and strong absorption by water.

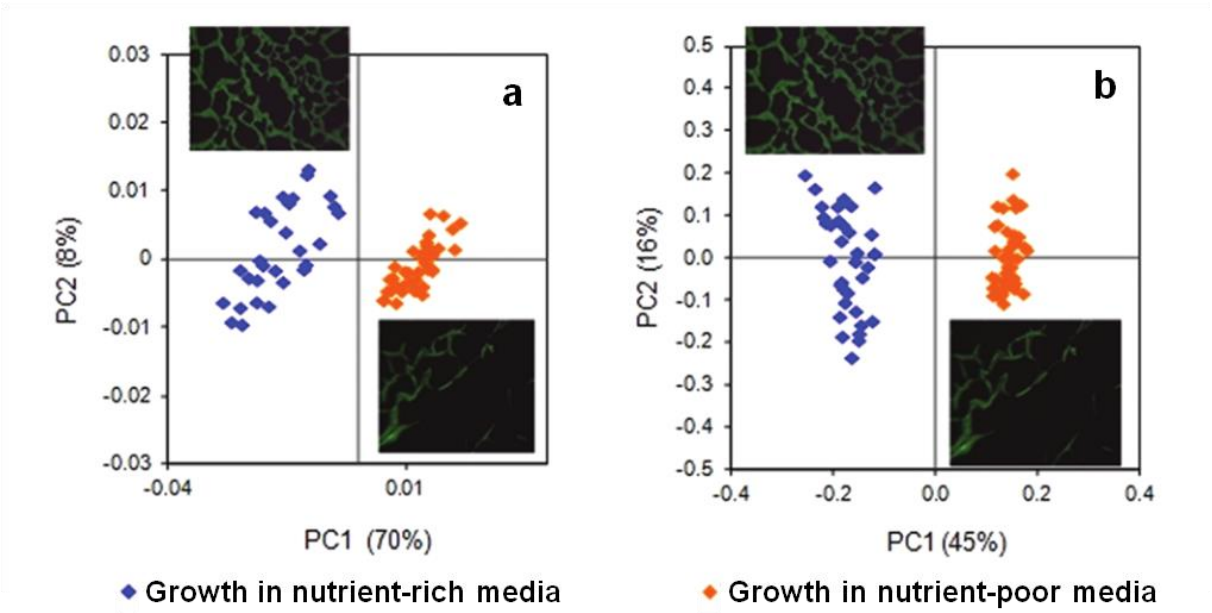

Figure II.2-12: Principal component analyses (PCA) of infrared spectra obtained on clusters of one to three fixed cells of *Lactobacillus delbrueckii* subsp. *bulgaricus* grown in two different media (nutrient-rich in blue, and nutrient-poor in orange) before freezing. The PCA were performed on (**a**) the lipid spectral region and (**b**) the proteins, polysaccharides and nucleic acids spectral region, and each point originates from an infrared spectra collected on a cluster of one to three bacterial cells. Inserts show that bacteria were viable before fixation through cF and PI staining (green fluorescence = cF-stained and non PI-stained). Cell fixation procedure: air-drying (adapted from Passot *et al*. 2015).

Sum up of the second part of the bibliographic review:

Many levers aiming at reinforcing the cryo-resistance of LAB are available. They are based on different cellular adaptation and protection mechanisms that can be combined for an optimal bacterial cryopreservation. It appeared, though, that protecting bacteria by adjunction of CPAs may have adverse side-effects during formulation and cryoconcentration that still needs to be investigated. Concentrates of LAB comprise billions of unique cells that may respond differently to cryopreservation. Assessing such heterogeneity is mandatory to provide a deeper insight into cellular mechanisms of cryoinjury and to make possible the delivery of homogeneous populations of active LAB following cryopreservation in the future. **By exploiting the properties of the synchrotron radiation in the ultraviolet and infrared regions, the analysis of single bacteria seems possible** for determining their membrane fluidity and biochemical composition, respectively. However, **the analysis of individual bacterial cells in solution remains a current technical challenge that requires further development**. In particular, synchrotron-based FTIR spectroscopy provides new opportunities and potentialities that will be developed in the following part.

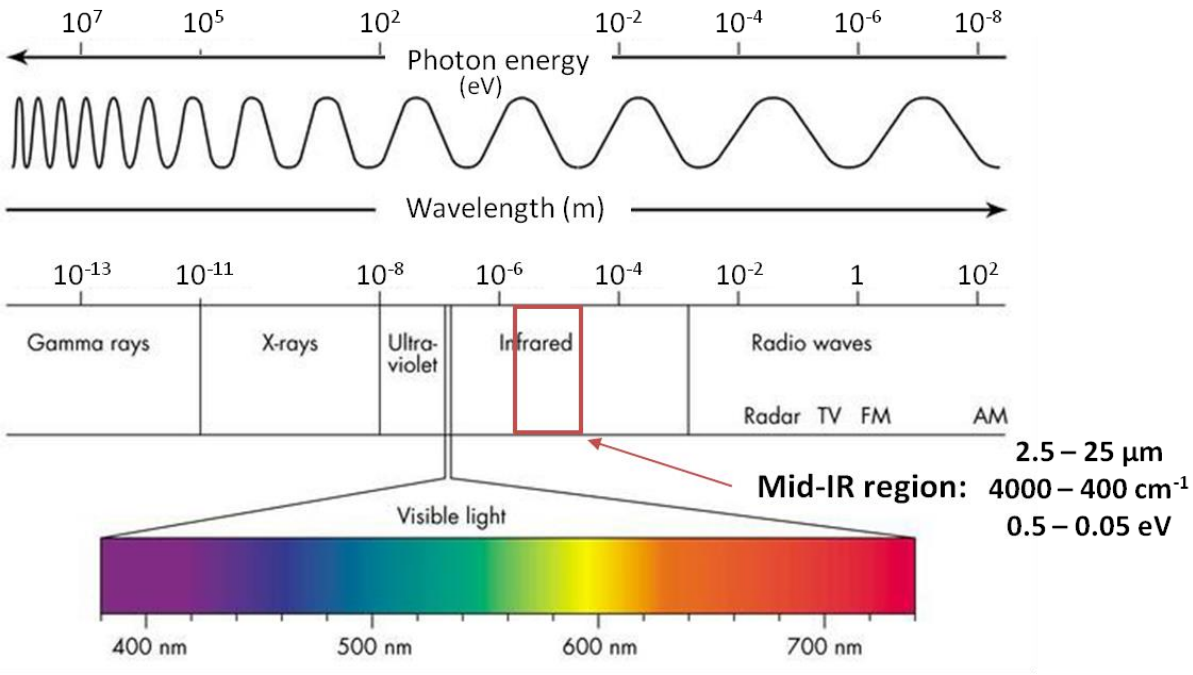

Figure II.3-1: Electromagnetic spectrum emphasizing on the mid-IR region with respect to visible light.

III. FTIR spectroscopy: a powerful vibrational approach to study LAB

Infrared spectroscopy exploits the absorption of infrared radiation by molecular vibrations of the probed samples. FTIR spectroscopy is the associated technique that records all IR active molecular motions, thus providing chemical information and composition of the sample and their interaction with the environment. Therefore, the study of LAB by infrared spectroscopy can shed light on the damages induced by freezing and freeze-associated stresses caused to the different biological building blocks (lipids, proteins, polysaccharides and nucleic acids). In addition, it does not require the introduction of exogenous dyes or probes and does not produce radiation damage to the sample, potentially allowing analysis of bacterial samples under native conditions.

Basics of FTIR spectroscopy and its potential development for the analysis of single bacterial cells are detailed in this last part of the bibliographic review.

3.1. FTIR spectroscopy of biological samples

3.1.1. Basics of FTIR spectroscopy

By interacting with the electron clouds of chemical bonds, energy quanta of IR light are absorbed by these electrons that move to higher vibrational energy states (owing to specific selection rules which state that infrared absorption takes place only if the electric dipole moment of the molecule changes). This absorption results in a decrease of the transmitted IR intensity at the vibrational resonance frequency (or wavelength). Therefore, measuring the transmitted IR light after interaction with a sample gives an IR spectrum over the wavelength (or frequency) range of interest.

For biological samples, the mid IR range (4000 – 400 cm^{-1}, or 2.5 – 25 µm; wavenumber = 1/wavelength; **Fig. II.3-1**) is of particular interest because it encompasses the vibrational energies of bonds that constitute biomolecules. Considering a simple diatomic molecule as a harmonic oscillator (two entities bound by a string), the vibration occurs at a particular wavenumber $\bar{\upsilon}$, which depends on the force constant of the bond, k, and on the mass of the atoms, m_1 and m_2. It may be predicted according to the following equation (**Eq. 1**):

$$\bar{\upsilon} = \frac{1}{2\,\pi\,c}\sqrt{\frac{k}{\mu}} \qquad \textbf{(Eq. 1)}$$

where c is the speed of light (3.10^8 m s^{-1}) and µ the reduced mass of both entities:

$$\mu = \frac{m_1 m_2}{m_1 + m_2} \qquad \textbf{(Eq. 2)}$$

In a non-linear polyatomic molecule composed of n atoms, a total of 3n – 6 vibration modes exist. By considering polyatomic molecules as an assembly of diatomic molecules, it is possible to extrapolate **Eq. 1** to more complex systems, including biological cells.

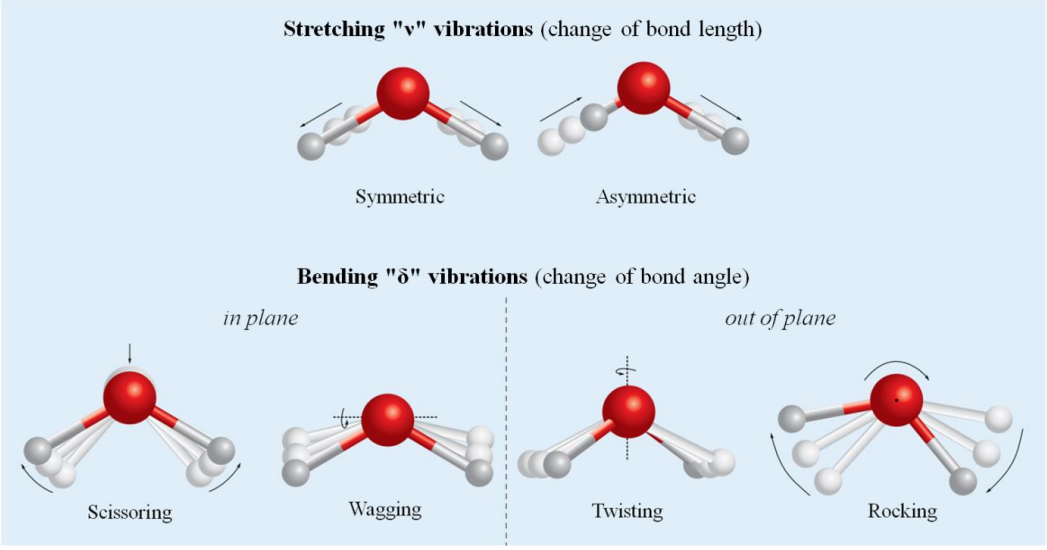

Figure II.3-2: Overview of the vibration modes causing IR absorption, illustrated with a water molecule (adapted from Chaplin, Martin, 2000, Water structure and science http://www1.lsbu.ac.uk/water/water_vibrational_spectrum.html, last updated on 29 March, 2017).

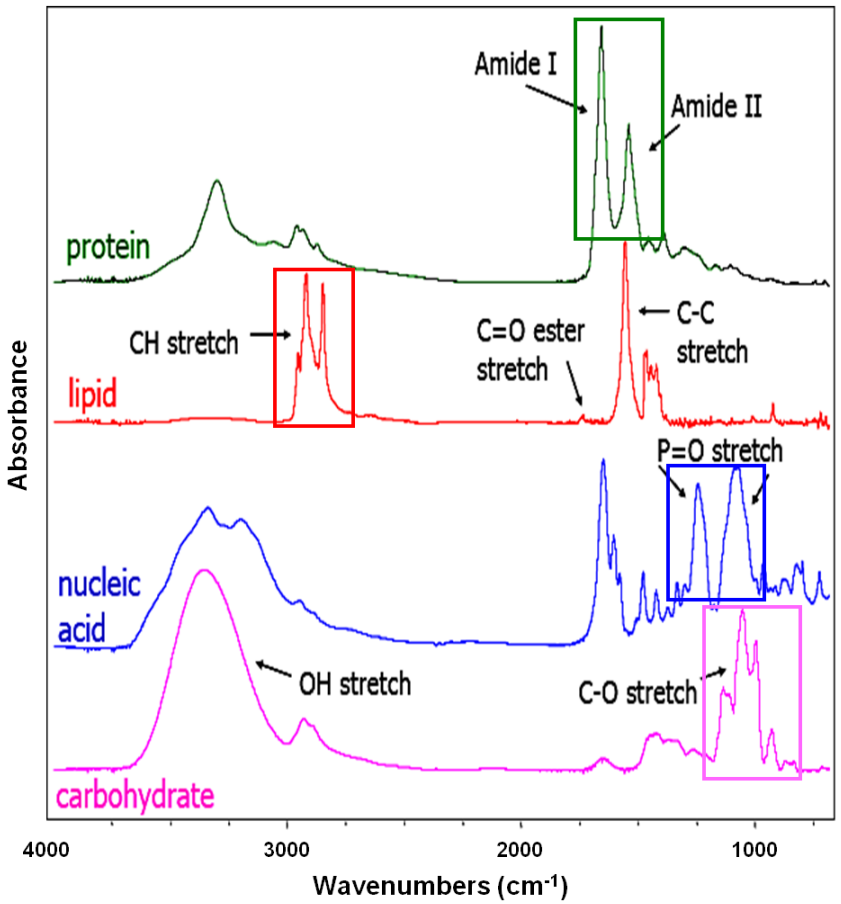

Figure II.3-3: Typical infrared spectra of a protein, a lipid, a nucleic acid, and a carbohydrate, whose primary features are indicated by boxes (adapted from Miller and Dumas, 2006).

Vibration modes include stretching and bending of the chemical bond, and are usually identified by the symbols ν and δ, respectively. Stretching modes involve a modification of the bond length in a symmetric or asymmetric way. Bending modes involve a modification of the bond angle (or torsion angle) occurring in-plane (scissoring and rocking) or out-of-plane (wagging and twisting). They are illustrated in **Fig. II.3-2**. Depending on the nature of the chemical bond (force constant and mass of the atoms, **Eq. 1**), each vibration mode gives rise to a specific absorption band at a specific wavenumber.

Cells are a mixture of proteins, lipids, nucleic acids and carbohydrates; this complexity is reflected in their infrared spectra (Miller *et al*. 2003; Tobin *et al*. 2004; Miller and Dumas 2006) and the same applies with lactic acid bacteria (LAB). Typical infrared spectra of the main biomolecules are shown in **Fig. II.3-3**, and boxes highlight their primary features:

- the Amide I and Amide II bands, located between 1700 – 1600 cm^{-1} and 1580 – 1510 cm^{-1}, respectively, mainly result from the C=O stretching vibration, and the N-H bending and C-N stretching vibrations of the protein backbone, respectively (cf. **Fig. II.1-10**). Amide I and II vibration modes are hardly affected by the nature of the protein side-chain, but are sensitive to protein secondary structures, especially the Amide I (Miller *et al*. 2003; Barth 2007);
- the CH_2 and CH_3 stretching vibrations, which are the dominant features arising from the hydrocarbon chains of lipids between 3000 and 2850 cm^{-1} (Lewis and McElhaney 2013);
- the symmetric and anti-symmetric stretching of PO_2^- near 1080 and 1225 cm^{-1}, respectively, that could be attributed to phospholipid headgroups, phosphorus-containing carbohydrates (teichoic and lipoteichoic acids) and nucleic acids (Naumann 2000).
- various carbohydrate vibrations, comprising C-O-C, C-O and C-O-P stretching vibrations, occur in the complex region between 1200 and 900 cm^{-1} (Naumann 2000).

Detailed vibration bands of interest that have been identified within bacterial samples are listed in **Table II.3-1**. The frequency ranges of these vibration bands are indicated, knowing that precise frequencies depend on the sample environment (*e.g.*, temperature, water activity) but also on intramolecular effects (*e.g.*, spatial arrangement of secondary structures in proteins). The shifts and intensity variations of these vibrations thus give important indications about the state alteration of macromolecules (Tobin *et al*. 2004; Miller and Dumas 2006).

3.1.2. Description of the FTIR micro-spectroscopy equipment and technology

i. The FTIR spectrometer

A FTIR spectrometer is composed of an IR light source, an interferometer, a sample compartment and a detector (**Fig. II.3-4**).

The IR light source

Internal infrared sources of FTIR spectrometers are thermal sources, often made of a silicon carbide rod that is heated up to 1,000 to 1,650 °C. Such IR source is often named a Globar (for “glow-bar”). More recently, it was discovered that synchrotron radiation also emits infrared photons, which is 100 to 1000 times brighter

Table II.3-1: Infrared band assignments from spectra of lactic acid bacteria

Frequency (cm^{-1})	Assignment		References
	Vibration mode	Biomolecule	
3050-00	νC = C	Phospholipid fatty acyl chains	Naumann, 2000*; Santivarangkna *et al*. 2007; Dianawati *et al*. 2012; Gautier *et al*. 2013; Passot *et al*. 2015
2983-59	ν_{as} – CH_3		
2925-17	ν_{as} > CH_2		
2894-72	ν_s – CH_3		
2856-49	ν_s > CH_2		
1740-45	νC = O		
~ 1468	δC-H in CH_2 (scissoring)		
~ 720	δC-H in CH_2 (rocking)		
~ 1715	νC = O	Nucleic acids	Naumann, 2000*; Santivarangkna *et al*. 2007
1700 – 1600	Amide I: νC = O, νC-N	Proteins	Naumann, 2000*; Oldenhof *et al*. 2005; Passot *et al*. 2015
1695-85	β-sheet structures		
~ 1675	β-turn structures		
1657-48	α-helical structures		
1641-23	β-sheet structures		
1580 – 1510	Amide II: δN-H, νC-N		
1545	α-helical structures		
1530	β-sheet structures		
~ 1516	Tyrosyl side-chain		
1230 – 1330	Amide III		
1250-1215	ν_{as} PO_2^-	Phospholipid headgroups / Nucleic acids	Dianawati *et al*. 2012
1090-1077	ν_s PO_2^-		
1200 – 900	δC-O, δC-C, δC-O-H, δC-O-C	Cell wall carbohydrates	Naumann, 2000*; Dianawati *et al*. 2012
900 – 600	"Fingerprint region"		Naumann, 2000*

ν: stretching vibrations, δ: bending vibrations, s: symmetric vibrations, as: asymmetric vibrations
* Major reference for infrared band assignments in microorganisms

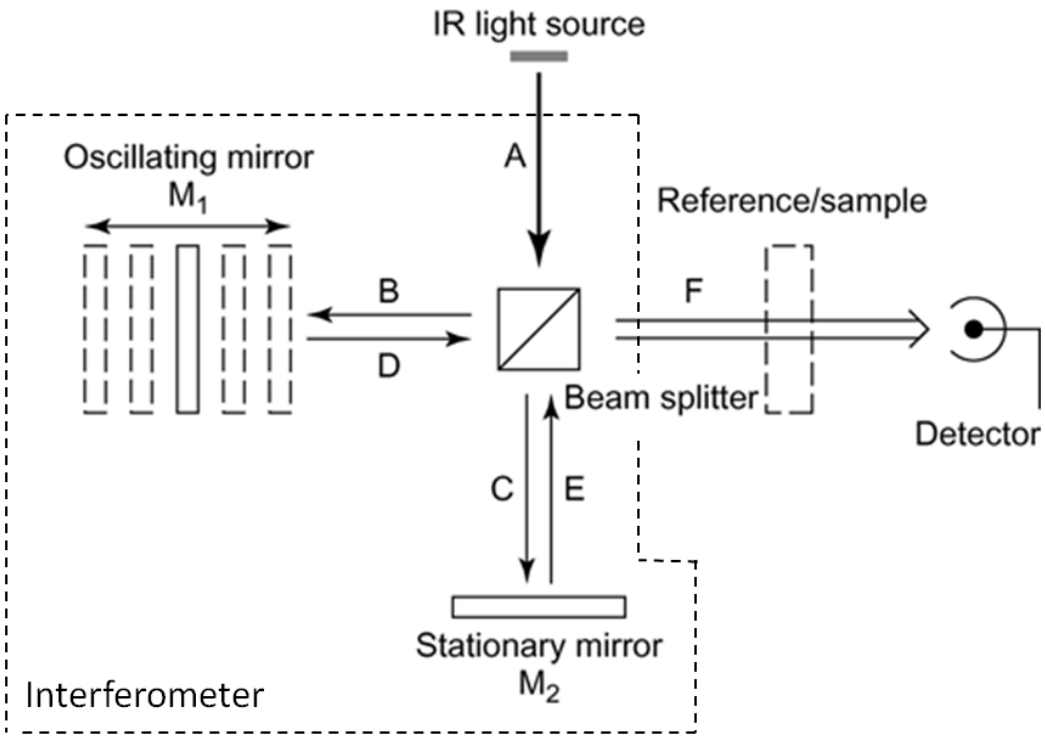

Figure II.3-4: Block diagram of a FTIR spectrometer.

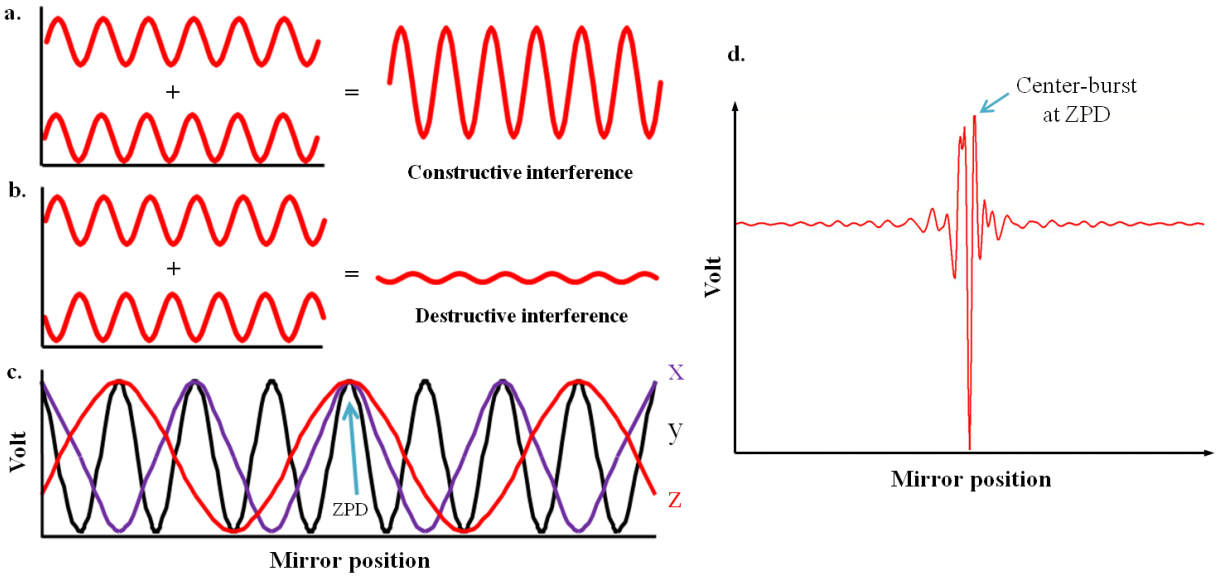

Figure II.3-5: The construction of the interferogram: (**a**) two signals in phase create a constructive interference; (**b**) two signals out of phase create a destructive interference and (**c**) the combination of all signals (here: x, y and z), giving a constructive interference at the zero path difference (ZPD), results in (**d**) the interferogram with the characteristic centre-burst at ZPD.

(the brilliance of a radiation is the number of photons per unit area and per solid angle) than conventional IR sources (Miller and Dumas 2006). The experimental advantages and applications of synchrotron radiation will be described later in this chapter (**§3.2.2**).

The interferometer

The particularly important component of a FTIR spectrometer is the Michelson-type interferometer. By contrast with the technology of dispersive IR spectrometers (preceding the FTIR technology), all frequencies are recorded simultaneously. This advantage, known as the *Folgett advantage*, considerably reduces the acquisition time of IR spectra. The available frequency domain depends on the nature of the beam splitter and of the response of the detector, but typically encompasses the 4000 – 400 cm^{-1} range.
The interferometer is composed of a beam splitter that reflects half of the incident IR beam to an oscillating mirror (B, **Fig. II.3-4**) and transmits the other half to a stationary mirror (C, **Fig. II.3-4**) (or vice-versa). Both are reflected back to the beam splitter (D and E, **Figs. II.3-4**) where they combine and interfere according to the path difference generated by the oscillating mirror's position.
The influence of the path difference on the resulting intensity of the interference is illustrated in **Figs. II.3-5a** and **II.3-5b**. Thus, if beams are in phase or out of phase, constructive or destructive interferences will be produced, respectively. The combination of all signals resulting from all mirror's positions produces the interferogram, which is the signal generated by a FTIR spectrometer recorded at the detector level after each scan of the moving mirror (**Figs. II.3-5c** and **II.3-5d**). Because all wavelengths have constructive interferences at zero path difference (ZPD; when the oscillating and fixed mirrors are at the same distance from the beamsplitter), a sharp high intensity spike, known as centre-burst, occurs there.
The time-domain interferogram has to be mathematically decoded with a technique termed Fourier transformation into a frequency-domain spectrum. A Fast Fourier Transform (FFT) algorithm is computed and displays the resulting single beam IR spectrum. The specific spectrum related to the sample under study ("dual beam" sample spectrum) results from the ratio of a single beam IR spectrum recorded with the sample, to a single beam IR spectrum recorded without it (often called "reference spectrum"). This process gets rid of all the aside absorptions due to the atmospheric environment, beamsplitter and mirror coatings:

$$dual\ beam\ sample\ spectrum\ = \frac{single\ beam\ sample\ spectrum}{single\ beam\ reference\ spectrum} \qquad \textbf{(Eq. 3)}$$

The detector

There are two commonly used detectors: thermal and photon-sensitive semiconductor. The DTGS detector (for deuterated triglycine sulphate) is the typical thermal detector. It works at room temperature but it suffers from slower response and lower sensitivity than photon-sensitive semiconductors (Robinson *et al*. 2005). Among the latter, MCT detectors (for mercury cadmium telluride) are either of broad band or narrow band nature. The broad band MCT detectors (cooled to liquid nitrogen temperature) are less sensitive than narrow band MCT detectors, but still sufficiently to allow detecting the main components of a biological sample, even at single cell level, in an extended frequency domain.

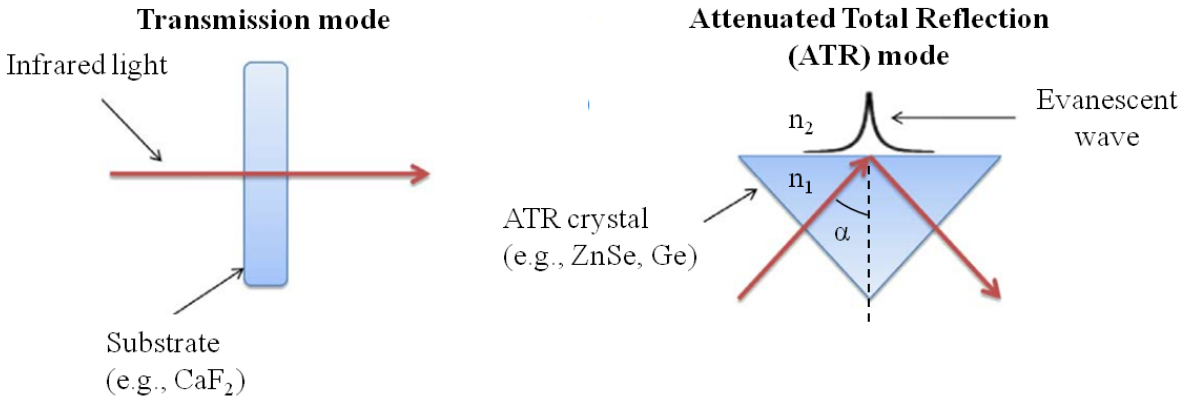

Figure II.3-6: Schematic illustration of the two main sampling modes utilized for FTIR spectroscopy in this work, suitable for biological applications (adapted from Baker *et al*. 2014).

Table II.3-2: Specifications of some IR materials and their use in transmission (Tr) and/or attenuated total reflection (ATR) modes; ranking according to decreasing water solubility (source: www.piketech.com):

Material	Water solubility (g/100g)	Hardness (kg mm^{-2})	RI at 1000 cm^{-1}	pH range	Use
KBr	53	6	1.52	NA	Tr
BaF_2	0.17	82	1.45	5-8	Tr
CaF_2	0.0017	158	1.4	5-8	Tr
ZnS	0	240	2.2	5-9	Tr/ATR
ZnSe	0	120	2.4	5-9	Tr/ATR
Ge	0	555	4.0	1-14	Tr/ATR
Si	0	1.150	3.4	1-12	Tr/ATR
Diamond	0	5.700	2.4	1-14	Tr/ATR

RI: refractive index; KBr: potassium bromide; BaF_2: barium fluoride; CaF_2: calcium fluoride; ZnS: zinc sulfide; ZnSe: zinc selenide; Ge: germanium; Si: silicon; Tr: transmission sampling mode; ATR: attenuated total reflection sampling mode.

ii. Infrared microscopy

Infrared microscopy is the coupling of a microscope with a FTIR spectrometer. The setup is similar to the conventional visible light microscope, with a few modifications in the optics to accommodate both visible and infrared lights. Mirrors and focusing elements are all metallic to avoid chromatic aberrations(Levin and Bhargava 2005). The IR light follows the same path as the sample illumination light, so that IR micro-spectroscopy can be performed on the sample at the centre of the viewing field. The IR microscope has been developed as a multifunctional accessory suitable for a wide variety of measurements like reflection, grazing angle, transmission, and attenuated total reflection (ATR) modes (Dumas and Miller 2003).

Aperture dimensions are defined to confine the infrared beam to smaller areas at the sample level (projected aperture sizes), but are limited in size by diffraction (according to the Rayleigh criterion). However, the limits are not reached with low brightness thermal sources because of the reduced number of photons passing through apertures of projected size smaller than 25 µm. This decrease is linear with aperture size reduction, leading to extremely poor spectral quality and signal-to-noise properties when approaching the diffraction limit (Miller and Dumas 2006).

3.1.3. Sampling modes frequently used to study biological samples

Two acquisition modes suitable for the analysis of biological samples have been utilized in this thesis work: transmission and attenuated total reflection (ATR) modes (**Fig. II.3-6**).

i. Transmission mode

In transmission mode, the IR beam passes through the sample that is deposited on an IR transparent material such as, for example, calcium fluoride (CaF_2), barium fluoride (BaF_2), zinc selenide (ZnSe), zinc sulfide (ZnS) Silicon (Si) or germanium (Ge). The choice of the material is based on its resistance depending on the sample characteristics (*e.g.*, presence of water, pH, temperature), its IR domain of transmission, and its transparency in the visible spectral region. Some characteristics of these IR materials are given in **Table II.3-2**.

ii. Attenuated Total Reflection (ATR) mode

In ATR mode, the sample is placed on a high refractive index crystal (ZnSe, Ge, Si, diamond). The IR beam is directed towards the crystal surface with a particular angle of incidence (above the critical angle α) and is completely reflected. At this bounce location, an evanescent wave is created and penetrates the sample. Its penetration depth (d_p) is very small and depends on the wavelength λ, according to **Eq. 4**:

$$d_p = \frac{\lambda}{2\pi n_1}\sqrt{\sin^2\alpha - \left(\frac{RI_1}{RI_2}\right)^2} \qquad \textbf{(Eq. 4)}$$

with RI_1 and RI_2 the refractive indexes of the crystal and sample, respectively, and α the angle of incidence. For example, an optical configuration with an angle of incidence of 30° using a Ge ATR crystal ($RI_1 = 4.0$) and considering $RI_2 = 1.5$, the penetration depth ranges from ~ 0.5 µm to ~ 1.6 µm in the mid-IR spectral region of interest (3000 – 900 cm^{-1}). Due to this small penetration depth of the evanescent wave into the sample, especially for high refractive-index crystals, an intimate contact between the sample and ATR

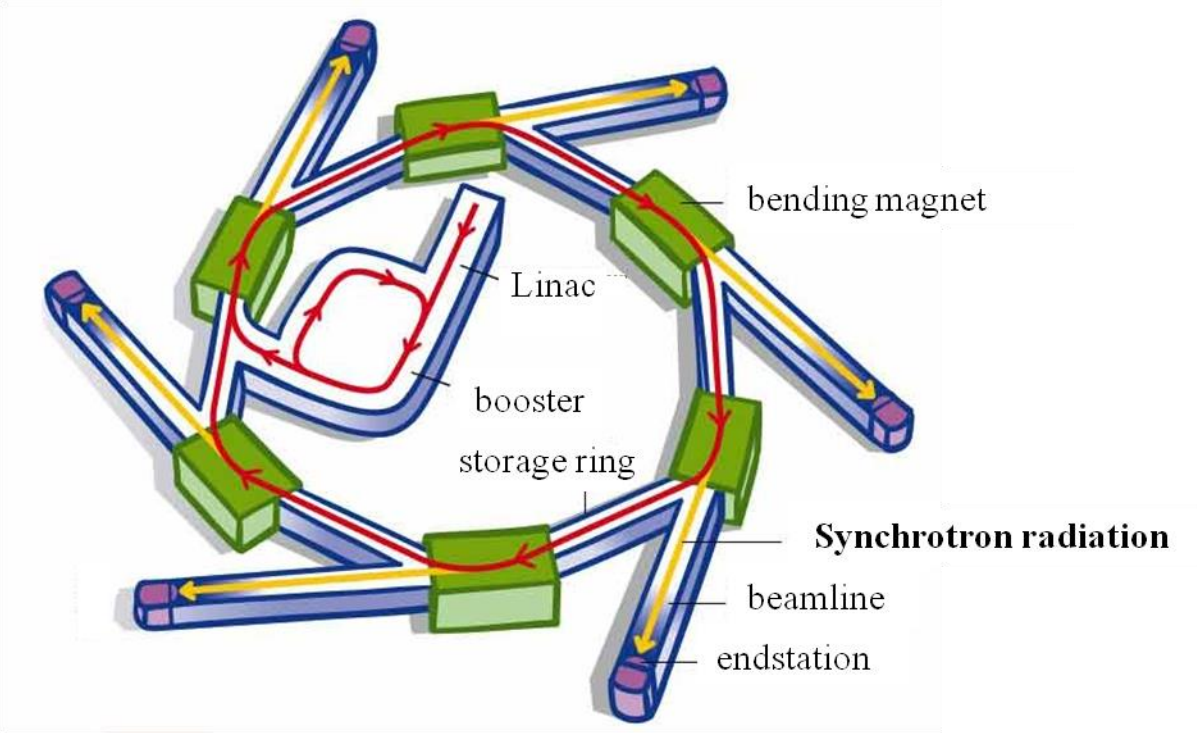

Figure II.3-7: Schematic representation of the production of Synchrotron radiation in a typical synchrotron facility (Source: RC2C ©).

crystal is required. Levin and Bhargava (2005) recommend immersing the sample into a liquid over the use of pressure that may distort the sample's microstructure.

Sum up of the analysis of biological samples by FTIR spectroscopy:

FTIR spectroscopy is an interesting analytical tool for LAB in providing a **complete biochemical analysis of all major biomolecules** constituting bacterial cells. The choice between several sampling modes makes FTIR spectroscopy a versatile technique potentially applicable to a variety of samples in a variety of environments. In the next paragraph we will introduce some of the limits of the techniques as well as solutions for overcoming them.

3.2. Overcoming the limits of the method for biological applications

FTIR spectroscopy has been used for the study of biological samples since the 1950s (Naumann 2001). It is a method with great analytical and discriminating potential presenting many advantages, among which:

- low running costs;
- short acquisition times;
- low requirements for sample quantities and preparation;
- no destruction of the sample after analysis and no need for exogenous probes (non invasiveness).

The development of interferometry paralleled with computing technologies and the introduction of the fast Fourier transform considerably shortened the acquisition, treatment and spectral analysis time. The generalization of its use also enabled the growth of spectral libraries useful for band assignment and sample identification. Classical FTIR spectroscopy is however limited to the analysis of dried bulk samples. This limitation is due to:

- The low signal-to-noise (S/N) ratio with conventional thermal IR light sources, preventing the size reduction of the focused IR beam projected on the sample (Miller and Dumas 2006);
- The somewhat low spatial resolution due to IR wavelengths (2.5 – 25 μm);
- The high contribution of water to the IR spectra, particularly in the amide I region.

Fortunately, technological developments have been made to overcome each of these three hurdles and are described thereafter.

3.2.1. Improved signal-to-noise (S/N) ratio by synchrotron radiation (SR)

The brightness of thermal IR sources is limited (**§3.1.2**). In contrast, the brightness of the infrared radiation emitted by a synchrotron source is hundreds of times greater (Holman *et al*. 2003). Synchrotron radiation is exploited in large scale facilities, in which specific beamlines are adapted to the collection and exploitation of a specific range of wavelengths, from IR to X-rays (**Fig. II.3-7**). Additional details about the synchrotron source and the application to microscopy are reported by Carr *et al*. (2001). Briefly, the small source size of the synchrotron emission allows the analysis of restricted biological sample areas or micron-sized samples by SR-FTIR spectromicroscopy, with still a good S/N ratio (Miller and Dumas 2006).
Besides, the high photon flux density of SR does not induce significant temperature increase of the sample

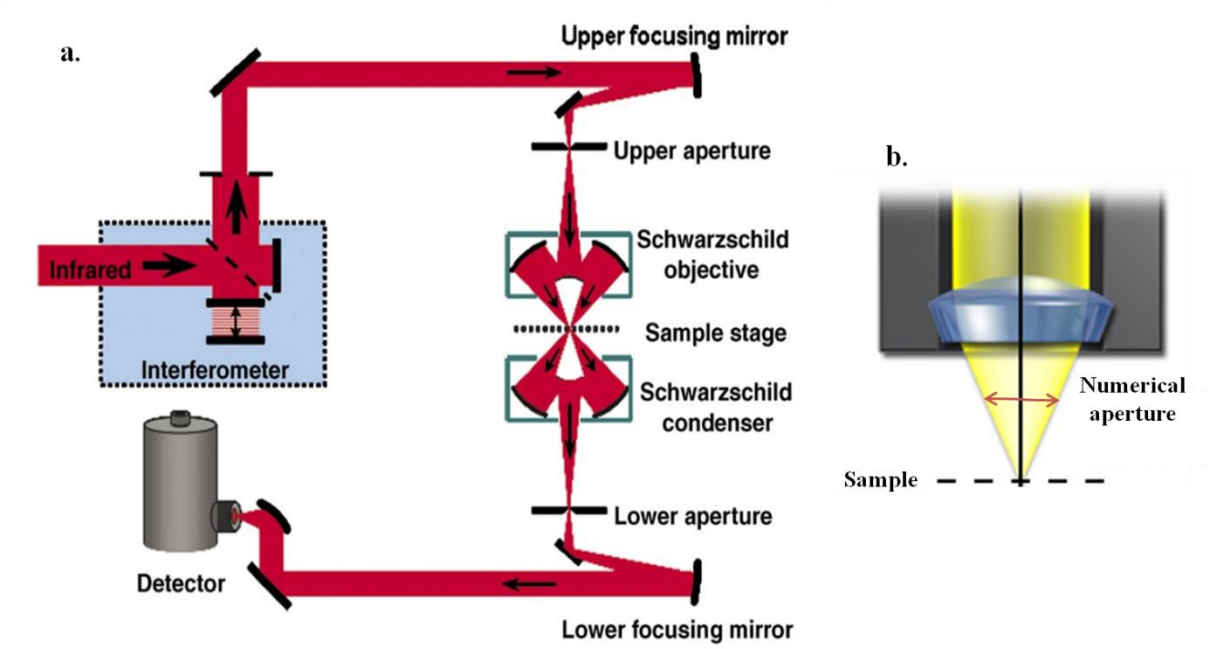

Figure II.3-8: Schematic representations of (**a**) the configuration of a FTIR micro-spectroscopy device using a confocal Schwartzschild confocal objective (taken from Miller and Dumas, 2006), and (**b**) numerical aperture of a microscope objective.

(less than 1 °C) (Miller and Dumas 2006) and the energy brought by mid-IR radiation is low: 0.05 eV (~ 400 cm^{-1}) to 0.5 eV (~ 4000 cm^{-1}) (**Fig. II.3-1**). A demonstration of the lack of any cytotoxic effects or sample heating of the SR IR radiation to living kidney cells was given by Holmann *et al*. (2003), after 30 min of constant exposure of ~ 1 mW at the focused sample position. It can therefore be safely concluded that SR-FTIR spectroscopy enables the non invasive analysis of living biological samples, including bacteria.

3.2.2. Improved spatial resolution by ATR-FTIR microscopy

The desired spatial resolution is achieved either by restricting the illuminated sample area by projecting apertures on the optical path before and/or after the sample (Carr 2001), as shown in **Fig. II.3-8a**. The upper aperture constrains the sample area being illuminated, while the lower aperture, only present in confocal microscopes, constrains the sample area being detected.

SR radiation is typically required when using apertures smaller than approximately 25 µm so as to preserve high spectral signal-to-noise properties (Miller and Dumas 2006). This was first evidenced by Jamin *et al*. (1998) in their pioneering highly resolved chemical imaging of single living eukaryotic cells in 1998.

Spatial resolution (d) is diffraction-limited according to the Rayleigh criterion at a value that depends on wavelength.

$$d = \frac{0.41 \times \lambda}{\mathrm{NA}} \qquad \textbf{(Eq. 5)}$$

where λ is the wavelength and NA is the numerical aperture of the objective (**Fig. II.3-8b**).

This optical limit may be circumvented and spatial resolution enhanced by using high refractive index materials as additional condensing units in an ATR-FTIR sampling mode (Levin and Bhargava 2005; Kazarian and Chan 2013). For instance, a germanium hemisphere thus condenses the beam by a factor of 4 (Sommer *et al*. 2001).

Summarizing, relying only on apertures to reduce the IR beam down to the desired size is quickly limited by diffraction. Combining IR spectroscopy to microscopy plus the use of high refractive index hemispheres to focus the IR beam allows to go beyond the diffraction limit and to achieve higher spatial resolutions than theoretically possible. Therefore, spectra could be assigned to specific small sample areas or small samples such as individual bacteria. Recently, the analysis of small clusters of one to three bacteria in the dried state was thus achieved by Saulou *et al*. (2013) on *E. coli* and Passot *et al*. (2015) on *L. bulgaricus* by SR ATR-FTIR spectroscopy using ZnSe as ATR crystal, who achieved a spatial resolution of 4.1 µm and 3.3 µm, respectively using upper apertures set at 10 x 10 μm^2 and 8 x 8 μm^2, respectively.

3.2.3. Minimizing the spectral contribution of water

Water is a strong IR light absorber whose vibration modes occur in different regions of the mid IR domain (**Table II.3-3** and **Fig. II.3-9**). In particular, the H-O-H bending frequency, centred at 1650 cm^{-1} occurs at the same position as the Amide I and thus interferes with the analysis of proteins in aqueous or hydrated samples.

Table II.3-3: Vibration modes of water in the mid-IR range and their interferences with the vibration modes of other cell components.

Frequency (cm^{-1})	Vibration mode	Potential interference
3400 – 3300	νO-H	/
2200	Combination of libration and bending modes	/
1650	δO-H (scissoring)	Amide I

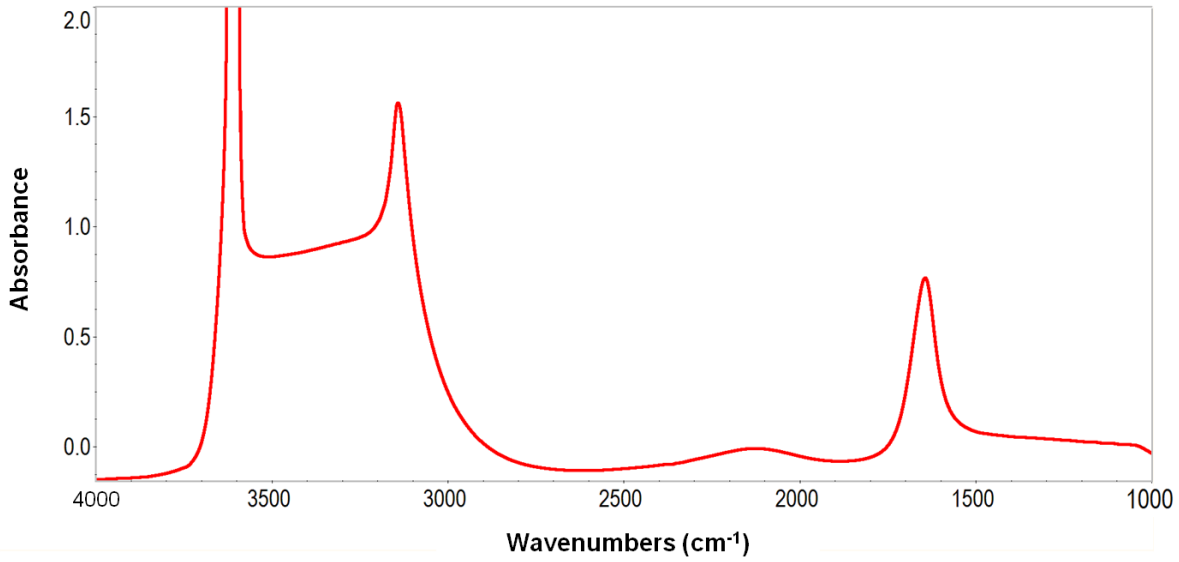

Figure II.3-9: Infrared spectrum of liquid water at 25 °C, recorded with a Nicolet Magna 750 FTIR spectrometer in transmission mode (Thermo Fisher Scientific). Note the detector saturation.

When spatial resolution is not an issue, *i.e.*, when working in Globar mode, water subtraction from sample spectra appeared to be feasible. Haris, Bischof, Wolkers and their co-workers could indeed analyse the protein secondary structure of rhodopsin (Haris *et al*. 1989) and the evolution of the protein secondary structure of eukaryotic cells with temperature under native conditions (Bischof *et al*. 2002; Wolkers *et al*. 2007) from their Amide I band. Their sample preparation was similar and consisted in sandwiching a dense concentration of sample after centrifugation between two IR-transparent windows separated by a 6 µm Mylar spacer for a controlled optical path. However, in these conditions, cell populations are analysed in a "hydrated state" rather than "in solution".

In solution, *i.e.*, when cell density is lower, a possible way to get rid of the superimposition between the H-O-H bending mode of water and the vibration mode of Amide I is to use deuterated water since the bending mode of heavy water is shifted to approximately 1200 cm^{-1}. Adverse effects of deuterated water enrichments on the growth of *E. coli* were clearly noticed for enrichment levels > 0.5% (Xie and Zubarev 2014). Nevertheless, the authors advised to perform enrichment levels of 0.03% since the incidence of deuterated water on bacteria is still unclear.
Limiting the quantity of water interacting with the IR beam is another clue, which was successfully performed to analyse single eukaryotic cells in solution. There are two ways to achieve sampled water reduction: using of microfluidics devices or ATR sampling mode.

i. Reducing water interferences with microfluidics

It was demonstrated that reducing the path length to or below 10 µm in a transmission-mode FTIR experiment can be sufficient to allow the analysis of live eukaryotic cells. For instance, Tobin *et al*. (2010) achieved path length reduction by using demountable liquid cells and 9 µm Mylar spacers, whereas Birarda *et al*. (2010a, 2010b) and Vaccari *et al*. (2012a, 2012b) used microfluidics devices with channels of < 9 µm height. Because the cell thickness was similar to the path length, the contribution of water to the spectra was low enough to be removed, either by division (Munro *et al*. 2010; Tobin *et al*. 2010) or subtraction (Birarda *et al*. 2010; Vaccari *et al*. 2012b; Vaccari *et al*. 2012a). Spectral division consists in taking the medium surrounding cells as the reference spectrum, while subtraction of the diluent spectrum from the 'cells + diluent' spectra requires their previous division with a reference recorded in the absence of cells and diluent, as shown in **Eq. 6**:

$$\text{spectrum}_{\text{after water subtraction}} = \frac{\text{spectrum}_{(\text{cells+diluent})}}{\text{spectrum}_{\text{reference}}} - \frac{\text{spectrum}_{\text{diluent}}}{\text{spectrum}_{\text{reference}}} \qquad \textbf{(Eq. 6)}$$

Note that spectral division led to incomplete water contribution removal since the resulting spectra showed a lower Amide I absorbance with respect to the Amide II than what is commonly observed in the dried state (Munro *et al*. 2010; Tobin *et al*. 2010). Water subtraction, on the other hand, resulted in satisfactory subtracted spectra with a higher Amide I intensity compared to Amide II, consistent with their particular shape in dried samples (Vaccari *et al*. 2012b; Vaccari *et al*. 2012a). The criterion for accurate subtraction as defined by the authors was the optimization of the subtraction coefficient applied to the diluent spectrum

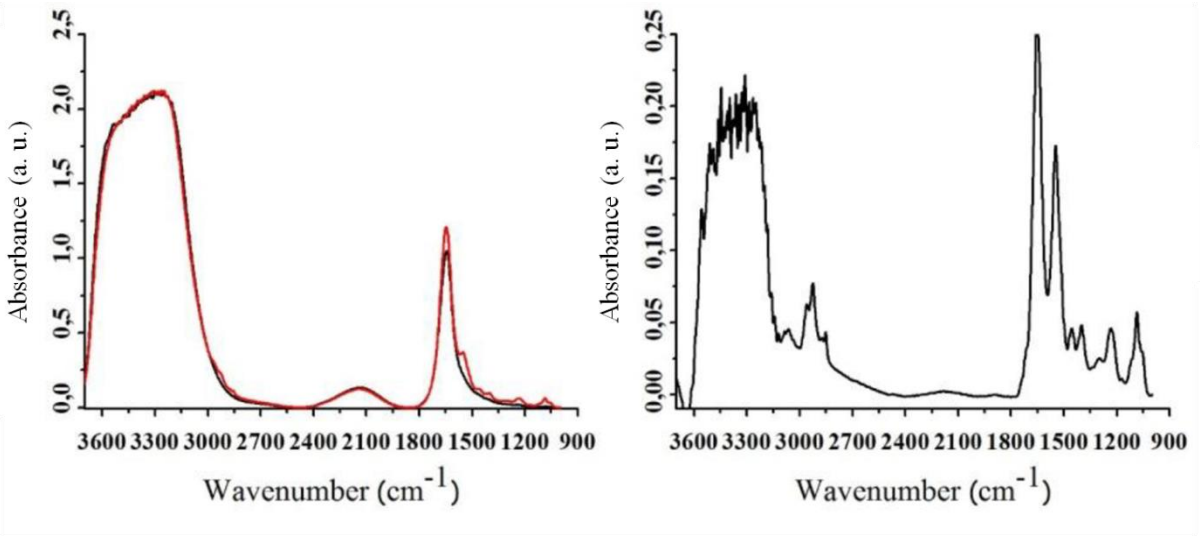

Figure II.3-10: FTIR experiment performed in transmission mode using a 8.5 µm microfluidic device showing a spectrum of a group of eukaryotic cells in a diluent (red), the corresponding diluent spectrum (black, left pannel), and the resulting subtraction with a coefficient 0.914 (right panel). Note the saturation induced by water in the O-H stretching mode region (3400 – 3300 cm^{-1}), and the features resolved after subtraction, especially the shape of the Amide I and II bands (taken from Vaccari *et al*. 2012a).

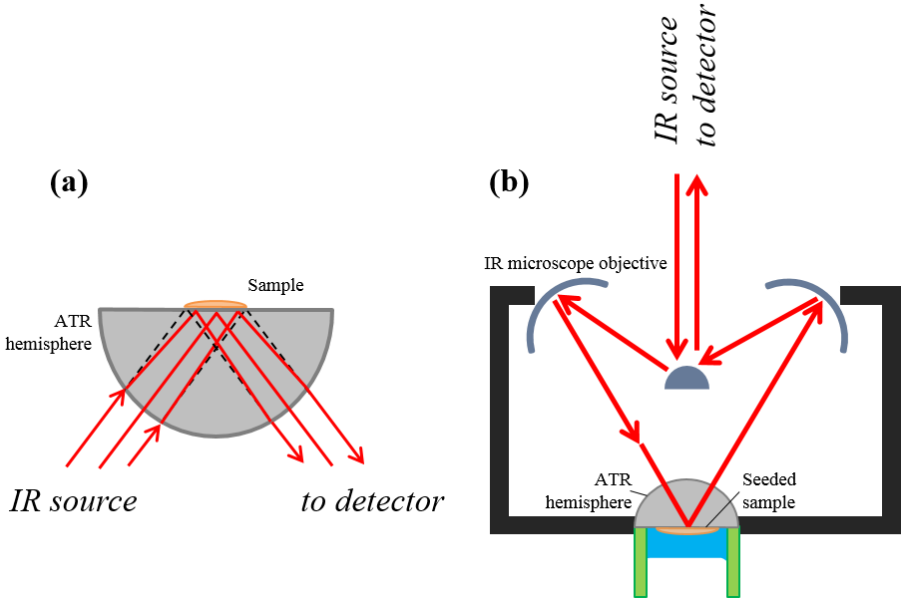

Figure II.3-11: Schematic representations of (**a**) a classical ATR-FTIR spectroscopy experiment, (**b**) an ATR-FTIR microscopy experiment with a Schwartzschild-type microscope objective with a liquid sample chamber turned upside-down containing seeded cells (adapted from Kazarian and Chan, 2013).

prior to subtraction. The optimized coefficient shall lead to the minimization of the spectral region between 2500 and 1850 cm^{-1} corresponding to the combination of bending and libration modes of water molecules (**Fig. II.3-9**), while remaining in the range 0.8 – 1.0. This leads to the modification of **Eq. 6** as follows:

$$\text{spectrum}_{\text{after water subtraction}} = \frac{\text{spectrum}_{(\text{cells+diluent})}}{\text{spectrum}_{\text{reference}}} - \text{Coeff} \times \frac{\text{spectrum}_{\text{diluent}}}{\text{spectrum}_{\text{reference}}} \qquad (\textbf{Eq. 7})$$

To illustrate the swamping effect of water on the FTIR spectra of biological samples, a FTIR spectrum of eukaryotic cells is shown before and after water subtraction in **Fig. II.3-10** (Vaccari *et al*. 2012a).
However, for small bacterial cells as LAB (few µm-long and approx. one µm-thick) the challenge is to reduce the path length further, down to the height of one bacteria. Thinner demountable liquid cells or lithographically defined channels in microfluidics devices have thus to be used. While demountable cells enable only static investigations in transmission mode, the fabrication of micron-sized channels in microfluidics devices is more challenging and tedious. Aside from requiring microfluidics expertise for lithographic microfabrication, bio-compatible materials with excellent resistance properties and appropriate adhesion to the IR transparent windows are to be used. In addition, spatial resolution in transmission mode is poorer than in ATR mode and does not allow single bacterial cells analysis.

ii. Reducing water interferences with ATR sampling mode

In contrast, in ATR configuration, the spectral information arises from the thin layer at the crystal interface and water absorption does not saturate the detector anymore (Kazarian and Chan, 2013). By analysing the biofilms of *Streptococcus mutans* grown over a trapezoidal ZnSe ATR crystal, Marcotte *et al*. (2010) could follow the diffusion of various solutes through the biofilm after water subtraction (**Fig. II.3-11a**).
Combining ATR-FTIR to microscopy is possible, but sample holding becomes tricky. Since the IR beam is delivered from the microscope objective standing over the sample, the ATR crystal must be turned upside-down compared to a classical ATR-FTIR setup. This is problematic with liquid samples, but Kazarian and Chan (2013) have described a procedure that circumvents this issue when dealing with adherent cells. By seeding cells over the ATR crystal until their attachment in a small volume of liquid, it is possible to maintain the aqueous solution in place by capillary forces once the system is turned over (**Fig. II.3-11b**). This solution is yet limited to adherent cells and to our knowledge, not directly applicable to planktonic bacterial cells in solution.

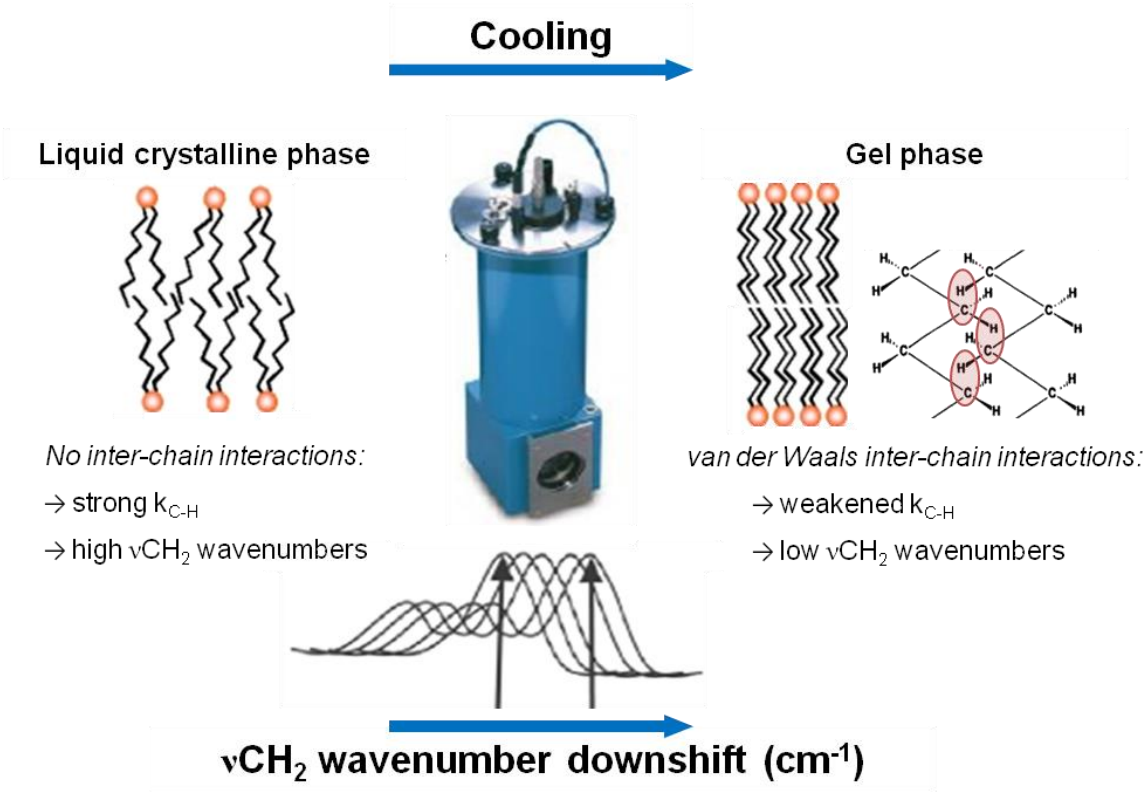

Figure II.3-12: Schematic representation of the membrane lipid phase transition as monitored by FTIR spectroscopy. Cooling favours van der Waals inter-chain interactions (represented by the red circles) which results in the weakening in the force constant of the aliphatic C-H bonds (k_{C-H}) and thus a shift of the CH_2 stretching bands (νCH_2) to lower wavenumbers. The insert is a picture of a variable temperature cell holder required to perform such experiments, handling temperature variations from -190 to +250 °C (Specac Ltd.; Orpington, Kent, UK).

Sum up of overcoming the limits of FTIR spectroscopy:

Many advantages are afforded by FTIR spectroscopy including, in particular, **analysis of biological samples in a completely non-invasive manner**. However, limitations preventing *a priori* the study of single live bacteria do exist: signal-to-noise ratios achieved by conventional thermal IR sources, diffraction-limited spatial resolution, and significant water contribution to the sample spectra. **Combining synchrotron IR radiation with specific optical methods** (IR microscopy in ATR mode using high refractive index hemispheres) **and advanced spectral processing techniques for successful water subtraction makes possible the investigation of single cells in solution, currently limited to large eukaryotic cells.** Different combinations of optical methods enabling a wide range of biological analyses are presented thereafter.

3.3. A wide range of biological analyses: under native conditions, in dynamic, cell-by-cell

The recording time for a FTIR spectrum depends on the desired spectral quality and resolution but it ranges between a few seconds to a few minutes. As a consequence, time-evolved or dynamic processes can be studied under native conditions (in an aqueous environment). Cellular biochemical processes occurring on such times-scales have therefore been assessed by FTIR spectroscopy. Examples in microbiology include the works of Holman *et al*. (2009) and Marcotte *et al*. (2004) that followed in real-time the intake of different solutes by bacteria organized in biofilms. In both cases, the chemical alterations of different biofilm areas induced by tested solutes revealed that a significant part of the biofilm was not accessible to the solutes. This highlighted issues for their elimination with antibiotics (Holman *et al*. 2009) or detergents (Marcotte *et al*. 2004). FTIR spectroscopy may also be used as a tool to select efficient microorganisms for performing a desired bioprocess in a rapid and cost-effective way. Ami *et al*. (2014) thus followed the accumulation of lipids in oleaginous yeasts and emphasized on the increased accuracy provided by FTIR spectroscopy over traditional evaluation methods that rely upon lipid extraction and may provoke lipid degradation.
Furthermore, investigating individual cells by high-resolution FTIR spectroscopy enables to characterise population heterogeneity for a deeper insight into cell biochemistry.

3.3.1. Freeze-related structural changes in cells as probed by FTIR spectroscopy

Dynamic physical modifications of the environment, such as those relevant to cryopreservation, can be assessed. Availability of variable temperature cell holders enables to reproduce a freezing procedure. Analyses of cellular biochemical changes during freeze-thawing have therefore been performed using such devices.

i. Focus on the membrane

Probing the membrane lipid phase transition

As introduced in **§1.1.1**, cooling leads to the transition of membrane fatty acyl residues from a disordered liquid-crystalline phase characterised by trans-gauche rotamers to an ordered all-trans gel phase. In the

Table II.3-4: Lipid transition temperatures reported for different bacterial species, phenotypes (thermophilic, mesophilic and psychrophilic bacteria), culture and post-harvest conditions. Values were determined during cooling (lipid solidification, $T_{s\,lip}$) or warming (lipid melting, $T_{m\,lip}$) by FTIR spectroscopy in intact cells or by DSC in bacterial phospholipids.

Microorganism	Phenotype	Conditions	$T_{s\,lip}$ (°C)	$T_{m\,lip}$ (°C)	Reference
Lactobacillus delbrueckii subsp. *bulgaricus*	Thermophilic	Growth in a nutrient-poor medium	-	35	Oldenhof *et al.* 2005
			22 ± 5	33 ± 5	Gautier *et al.* 2013
		Growth in a nutrient-rich medium	-8 ± 4	-2 ± 5	Gautier *et al.* 2013
Lactococcus lactis	Mesophilic	Growth at 30 °C Growth at 22 °C (harvest: early stationary growth phase)	- -	13 ± 1 10 ± 0.2	Velly *et al.* 2015
Lactococcus lactis	Mesophilic	Cell suspension in milk buffer containing: no additive 0.5 M sucrose 4 M NaCl	 - - -	 21.4 16.8 16.6	Molina-Höppner *et al.* 2004
Lactobacillus plantarum	Mesophilic	Growth: at 37 °C at 30 °C + 5 % ethanol at 30 °C at 15 °C	 - - - -	 20.1 19.3 17.4 12.6	Ulmer *et al.* 2002
Escherichia coli	Mesophilic	Optimal growth conditions	-	10	Leslie *et al.* 1995
Bacillus thuringiensis	Mesophilic	Optimal growth conditions	-	5	Leslie *et al.* 1995
Geobacter sulfurreducens	Mesophilic	Cell suspension containing sucrose (% w/v) upon harvest: 0 % 6.75 % 13.5 % 27 %	 - - - -	 23 ± 1 24 24 28 ± 1	Ragoonanan *et al.* 2008
Micrococcus cryophilus	Psychrophilic	Extracted phospholipids	-30	-	McGibbon *et al.* 1985

liquid-crystalline phase, few van der Waals interactions exist between neighbouring fatty acyl chains. On the contrary, the straight acyl chain conformation induced by all-trans rotamers compresses the membrane in the gel phase. This ordered and close arrangement of hydrocarbon chains favours interchain van der Waals interactions (London dispersion forces), thereby weakening the C-H bonds of successive CH_2 groups in each fatty acyl chain. This weakening in the C-H force constant ("k" in **Eq. 1**) results in a decrease in the wavenumber of the corresponding IR vibration, and therefore a progressive shift of the νCH_2 sym. and νCH_2 asym. vibrations to lower wavenumbers upon cooling, as shown in **Fig. II.3-12**. The midpoint of the transition is referred to as the membrane lipid phase transition temperature ($T_{s\ lip}$ for solidification upon cooling, and $T_{m\ lip}$ for melting upon warming). The thermotropic behaviour of the νCH_2 sym. (~ 2850 cm^{-1}) and the νCH_2 asym. (~ 2920 cm^{-1}) are equivalent, but the latter is rarely used to follow membrane lipid phase transition because of interferences with overlapping CH_3 vibration modes (Lewis and McElhaney, 2013).

Monitoring the exact position of the νCH_2 sym. upon cooling by FTIR spectroscopy allows the detection of the membrane lipid phase transition and provides dynamic structural information about the membrane fatty acyl chains (Crowe *et al*. 1989; Lewis and McElhaney, 2013). By relating this monitoring to chilling and freeze-thaw resistance, the advantage of cell membranes to remain in a liquid-crystalline phase at low temperatures could be established in plants (Crowe *et al*. 1989) and LAB (Gautier *et al*. 2013), respectively. Also, the less ordered state of the cryoresistant cells membrane in the gel phase (identified by the higher νCH_2 sym. positions below 0 °C) denoted the maintenance of higher membrane fluidity in the frozen state. Lipid phase transition temperature was measured in a variety of microorganisms, and some of them are reported in **Table II.3-4**. Membrane lipid melting ($T_{m\ lip}$) is often reported in comparison to membrane solidification ($T_{s\ lip}$) because few works have focused on membrane lipid behaviour upon cooling or freezing (McGibbon *et al*. 1985; Gautier *et al*. 2013).

Probing the effects of cryoprotectants

During freezing, some cryoprotective agents (CPAs) may interact with membrane lipids, especially as the medium cryoconcentrates (**§2.2.1**). This can be assessed by FTIR spectroscopy by studying the characteristic vibration modes of membrane lipids. Ragoonanan *et al*. (2008) thus analysed the effect of sucrose on the thermotropic behaviour of the membrane of *Geobacter suflurreducens* by monitoring the vibrational mode of νCH_2 sym. during chilling. They observed an increased $T_{m\ lip}$ with hyperosmolarity at high sucrose concentration. In addition, the lower fatty acyl chains ordering in the gel phase, lower cooperativity (slope) of the phase transition and bacterial mortality were, according to the authors, signs of a deleterious effect of high sucrose concentrations on the bacterial membrane structure. In a following study, the authors analysed the effect of other CPAs (DMSO and glycerol) on the membrane behaviour of eukaryotic cells (human fibroblasts) during freezing. These CPAs exerted their cryoprotective action by decreasing the extent of the νCH_2 sym. downshift in the frozen gel state, and thereby the packing degree of cell membrane lipids (Ragoonanan *et al*. 2010).

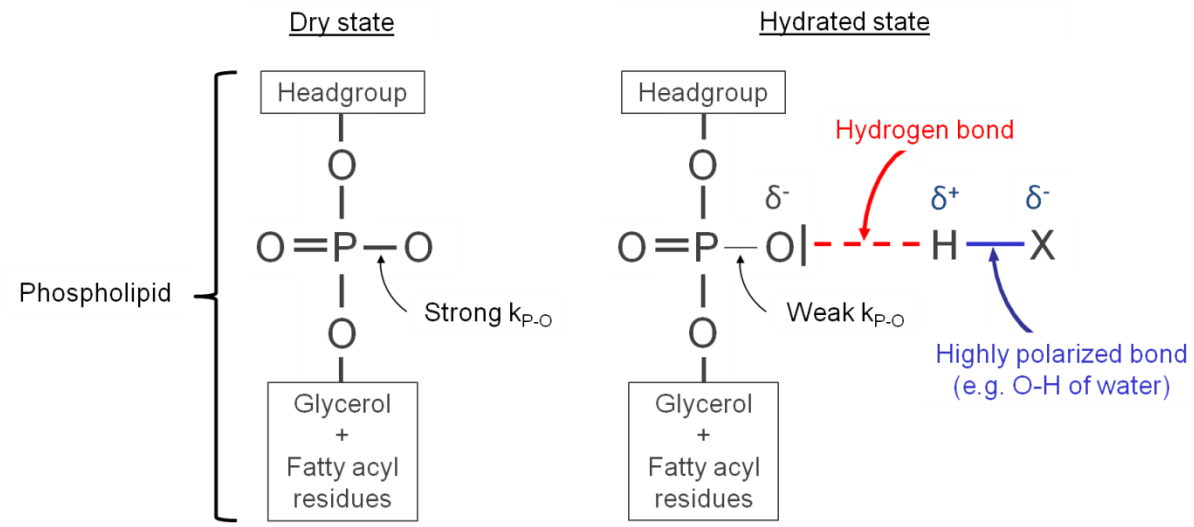

Figure II.3-13: Schematic illustration of the weakening of the force constant of the P-O covalent bond (k_{P-O}) of the phosphate moiety of membrane phospholipids when the oxygen atom is involved in a hydrogen bond. The oxygen atom carries a lone pair (*i.e.*, very electronegative element) and the hydrogen atom is covalently linked to an electronegative element (*e.g.*, O-H of water or other solutes).

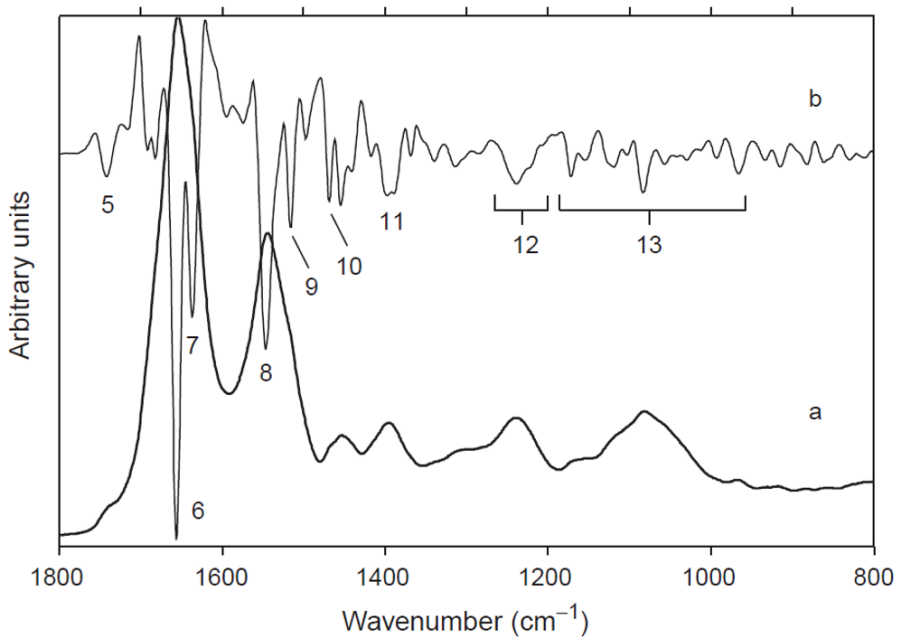

Figure II.3-14: Example of a FTIR spectrum of dehydrated *Staphylococcus aureus* sample (thick line) and its second derivative (thin line) in the 1800 – 800 cm^{-1} spectral region, revealing protein secondary structures (Naumann, 2000).

Membrane lipids are constituted of two FA chains, but also a polar headgroup. In phospholipids, this headgroup contains a phosphate moiety (**§1.2.1**) whose PO_2^- asymmetric stretching mode (νPO_2^- asym.) is sensitive to hydrogen-bonding (Goñi and Arrondo 1986; Lewis and McElhaney 1998; Arrondo and Goñi 1998). In the dry state, the covalent bond P-O is not involved in any interaction with the environment. The force constant of the νPO_2^- asym. (k_{P-O}) is therefore strong and was found to vibrate at around 1260 cm^{-1} (Lewis and McElhaney 1998). In the hydrated state, phospholipid headgroups are normally involved in hydrogen bonding with several water molecules (Luzardo *et al*. 2000) via, for instance, the oxygen atom of the P-O bond that carries a lone pair. This makes the P–O bond weaker, as illustrated in **Fig. II.3-13**. The νPO_2^- asym. was reported to be located between 1215 and 1240 cm^{-1} in various hydrated lipid vesicles (Goñi and Arrondo 1986; Linders *et al*. 1997; Lewis and McElhaney 1998; Arrondo and Goñi 1998) and a Gram-positive bacterium in the fresh state (Dianawati *et al*. 2012).

Downshifts of the νPO_2^- asym. have been identified in hydrated lipid vesicles in the presence of solutes (sucrose, trehalose, cysteine derivative), indicating a weakening of the covalent force constant (Díaz *et al*. 2003; Arias *et al*. 2015). In this case, two hypotheses emerge. Either the solute replaces the hydrating water and creates stronger hydrogen bonds with phospholipid headgroups through a preferential binding mechanism, or the solute strengthens the existing interactions of water with phosphate groups by preferential exclusion (as illustrated in **Fig. II.2-4**). Very often, these studies are performed on model lipid vesicles, but Dianawati *et al*. (2012) successfully applied it to the analysis of the protection mechanisms conferred by microencapsulation formulations to the freeze-dried probiotic *Bifidobacterium*. Analysing the νPO_2^- asym. by FTIR spectroscopy can contribute to better understanding the interactions between CPAs and the membrane of LAB during freezing.

ii. Focus on proteins

The amide bands in a FTIR spectrum carry information about protein secondary structures that can be revealed by deconvolution or calculating the inverted second-derivative of the spectrum (Bandekar 1992). The second method is illustrated in **Fig. II.3-14**. Typical secondary structures are the α–helix and β-sheet structures (**Table II.3-1**), and are the result of hydrogen bonding in the protein backbone, as illustrated in **Fig. II.1-10**. Shifts and variations in the intensity of the constitutive peaks of the inverted second derivatives are the sign of an alteration in the protein secondary structure. Due to the close relationship between protein structure and functionality (**§1.2.1**), a treatment inducing irreversible protein secondary structure alteration might therefore result in the inactivation of proteins.

For instance, Bischof *et al*. (2002) studied the effect of freezing eukaryotic cells (prostate cancer cells) to -20 and -80 °C on the secondary structure of cell proteins. They evidenced by the analysis of heat denaturation profile of the amide bands by FTIR spectroscopy that freezing to -80 °C led to irreversible modifications of protein secondary structures, whereas freezing to -20 °C either had no impact or the putative modifications were reversible. The identified irreversible secondary structures modifications included a great reduction of the α–helical structures (centred at 1655 cm^{-1}) paralleled with an increase in the content of extended β-sheets (1625 cm^{-1}). However, the method used to subtract the contribution of water

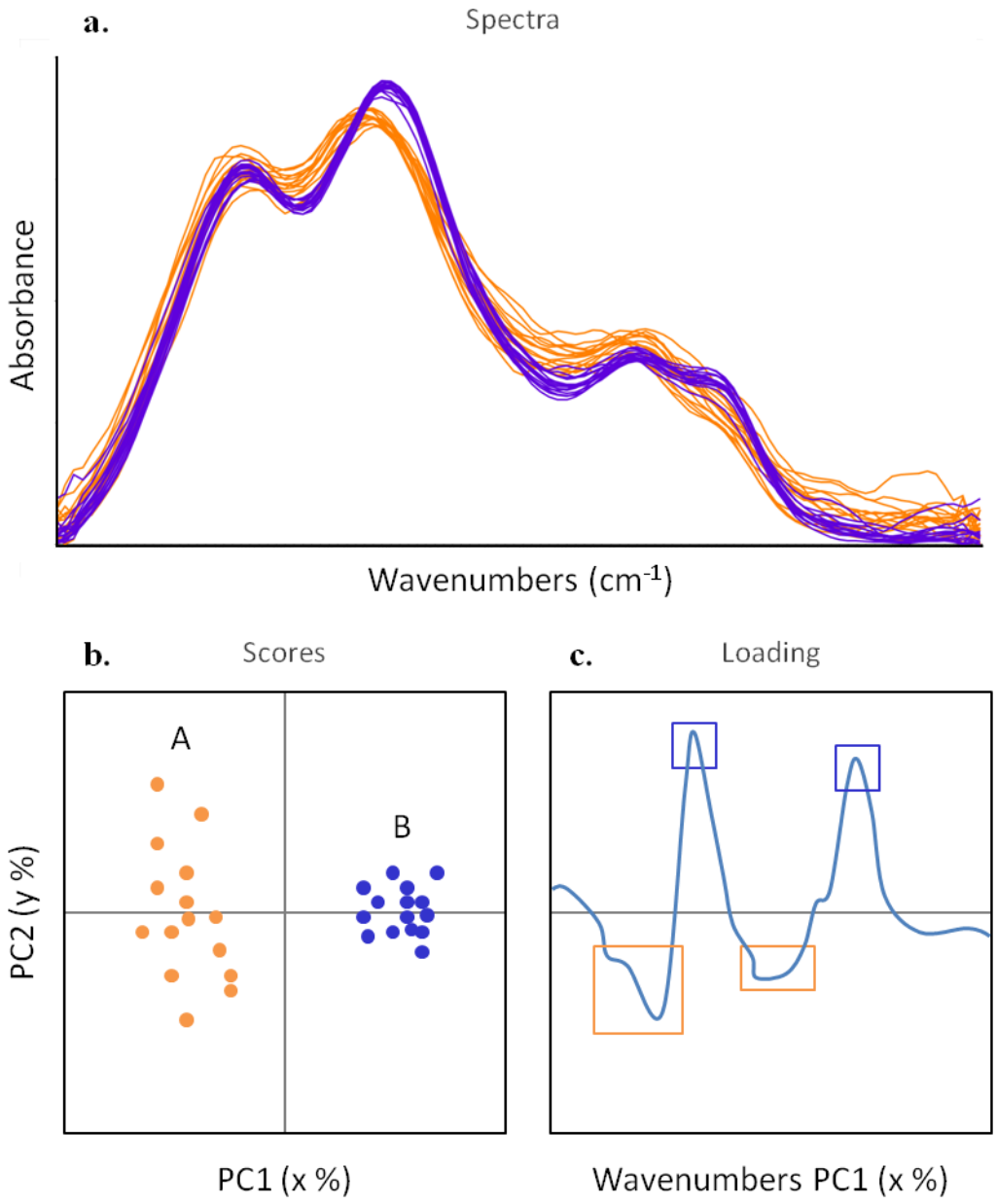

Figure II.3-15: Principle of a principal component analysis (PCA) on the IR spectra of two samples (A, in orange; B, in purple). (**a**) Overview of the spectra to be analysed on the spectral range of interest, (**b**) score plots along the principal components PC1 and PC2 explaining x % and y % of the variance, respectively, and (**c**) loading plot of PC1, in which the coloured squares highlight the wavenumbers that are positively correlated to the corresponding sample. In this example, sample A presents a heterogeneous biochemical composition over this wavenumber range, whereas sample B is more homogeneous (adapted from Passot *et al*. 2015).

to the spectra is questionable. Due to the interference between the Amide I band and water in a FTIR spectrum of hydrated cells, there is a lack of studies on cell protein structure under native conditions.
As a consequence, for studying proteins structural changes upon freezing, some authors have compared FTIR spectra of air-dried microorganisms on an adequate support before and after the freeze-thawing process. For instance, Pénicaud *et al*. (2014) analysed the yeast *Yarrowia lipolytica* and did not identify any change in their global protein conformation after freeze-thawing. In contrast, Passot *et al*. (2015) pointed out a transition from α–helical to β-sheets dominant structures in the LAB *L. bulgaricus* following freezing in the presence of glycerol as CPA, although this was not accompanied by cell lethality. It is not excluded that the conformational transition observed was due, at least partly, to the cell fixation method used: air drying.

3.3.2. Evaluation of microbial population heterogeneity by FTIR spectroscopy

The information provided in a FTIR spectrum is averaged over the whole illuminated sample area. This means for instance, that the Amide bands result from the vibration modes of all cellular proteins constitutive of all the cells probed by the IR beam. Restricting the IR beam to the size of individual cells thus gives more specificity to the measurement.

i. Population heterogeneity in microbiology: pioneering works

Due to their extremely small size, probing single bacteria by FTIR spectroscopy requires the exploitation of a synchrotron radiation source (**§3.2.3**), and such studies therefore remain extremely scarce. Saulou *et al*. pioneered in this field by analysing the response to silver stress exposure of single cells of the yeast *S. cerevisiae* (Saulou *et al*. 2010) and small clusters of *E. coli* cells (Saulou *et al*. 2013). Shortly afterwards, Passot *et al*. (2015) investigated the impacts of freeze-thawing on small clusters of *L. bulgaricus*. These three studies were achieved after drying the cell samples over the surface of ZnSe ATR hemispheres.

ii. Visualizing population heterogeneity requires multivariate data analysis

Multivariate data analysis procedures are essential to reduce the number of variables composing a FTIR spectrum (each wavenumber is considered as a variable; in the range 4000 – 900 cm^{-1} acquired at a spectral resolution of 4 cm^{-1} corresponding to a frequency of data acquisition every 2 cm^{-1}, this corresponds to 1550 variables) and to extract the most relevant and discriminating wavenumbers. By using principal component analysis (PCA), Saulou *et al*. (2010, 2013) and Passot *et al*. (2015) have represented individual cell's spectral variance along two principal components (PC), each PC representing the most relevant variables or wavenumbers (as depicted in the corresponding loading plots, and in **Fig. II.3-15b**). They evidenced dispersion in the spectral response of cells within populations, highlighting the diversity of cell-by-cell damages and/or adaptive responses to the changing environmental conditions by differentially expressing a common genome.
In particular, the work of Saulou *et al*. (2013) has evidenced the higher heterogeneity of the biochemical composition of *E. coli* cells after exposure to silver stress. Moreover, they have highlighted the existence of a heterogeneous biochemical composition between different cells, even in 100 % viable populations. In the

Table II.3-5: Summary of the evolution of FTIR spectroscopy analyses performed on biological samples. Their observation scale depending on the size of the cells and their hydration state is given, with special emphasis on microorganisms, single-cell analyses, and performed in an aqueous environment:

Category	Organism	Scale	State	Analysis mode	Study	Reference
Microbial populations; Dried / hydrated state	*Geobacter sulfurreducens*	Population	Hydrated & air-dried	GR, Transmission, CaF_2 sandwich	Lipid structure & phase transition behavior (νCH_2, $T_{m\,lip}$, ξ)	Ragoonanan *et al.* 2008
	Lactobacillus delbrueckii subsp. *bulgaricus*	Population	Air-dried	GR, Transmission, CaF_2	Effect of protectants on protein secondary structure + thermophysical properties of dried cells	Oldenhof *et al.* 2005
	Lactobacillus delbrueckii subsp. *bulgaricus*	Population	Hydrated	GR, Transmission, CaF_2 sandwich	Effect of growth medium on $T_{s\,lip}$, $T_{m\,lip}$	Gautier *et al.* 2013
	Lactococcus lactis	Population	Hydrated	GR, Transmission, CaF_2 sandwich	Effect of growth temperature and growth phase on $T_{m\,lip}$	Velly *et al.* 2014
	Escherichia coli & *Bacillus thuringiensis*	Population	Hydrated & Dried	GR, Transmission, CaF_2 sandwich	Protective effect of trehalose & sucrose on proteins and membrane lipids to drying	Leslie *et al.* 1995
	Lactobacillus plantarum	Population	Hydrated & Dried	GR, Transmission, CaF_2 sandwich	Protective effect of carbohydrates on membrane phase behavior T_{Lm}	Linders *et al.* 1997
Individual microbial cells or small clusters of cells; Dried state	*Saccharomyces cerevisiae*	Single cells	Air-dried	µSR, trans-reflection on low-e slides	Effect of silver nanoparticles on proteins & nucleic acids	Saulou *et al.* 2010
	Escherichia coli	1 to 3 cells (4.1 µm sp. reso)	Air-dried	µSR, ATR, ZnSe hemisphere	Effect of ionic silver on lipids and protein secondary structure	Saulou *et al.* 2013
	Lactobacillus delbrueckii subsp. *bulgaricus*	1 to 3 cells (3.3 µm sp. reso)	Air-dried	µSR, ATR, ZnSe hemisphere	Effect of growth medium on protein secondary structure, lipid conformation and their evolution after freeze-thawing	Passot *et al.* 2015
Microbial biofilms; Aqueous envt.	Biofilm of *E. coli*	Population	Aqueous envt.	µSR, open channel microfluidic device	Diffusion and effects of the addition of an antibiotic to bacteria organized in a biofilm	Holmann *et al.* 2009
	Biofilm of *Streptococcus mutans*	Population	Aqueous envt.	ATR, ZnSe trapezoidal crystal	Diffusion of the addition of solutes inside a bacterial biofilm	Marcotte *et al.* 2010

work of Passot *et al*. (2015), a more important spectral heterogeneity was observed in the cryoresistant population of *L. bulgaricus* cells compared to the cryosensitive population before freezing (**Fig. II.3-15b**). It was ascribed to the variety of available substrates in the corresponding nutrient-rich growth medium, allowing individual cells to express their metabolism in various ways. Heterogeneity in the protein secondary structures was found to increase further following freeze-thawing in the cryosensitive cells. In parallel, the PCA allowed the differentiation of two cryoprotective agents based on their capacity to preserve protein conformation: sucrose was found more efficient than glycerol.

It is presumed that cellular heterogeneity arises from a stochastic genes expression and protein synthesis (Schmid *et al*. 2010; Wang and Bodovitz 2010), but the work of Passot *et al*. (2015) has revealed the importance of selecting the cell cultivation conditions to act on the resulting population biochemical heterogeneity. Identifying the production conditions leading to homogeneous populations of resistant cells to industrial processes, including cryopreservation, appears promising.

Sum up of the third part of the bibliographic review:

Since the cellular impacts of cryopreservation are multi-targeted (membrane lipids, proteins), FTIR spectroscopy appears as a promising tool for their investigation. It makes possible their simultaneous characterisation in a dynamic and non-invasive way – critical considering biological samples.

In particular, FTIR spectroscopy provides information in a rather straightforward manner on the **global composition and conformational state of membrane lipids and proteins**. Its application to the analysis of single bacteria confers an additional interest to this technique in **characterising population heterogeneity**. Yet, studies on dry samples are only reported to date, because dealing with water in FTIR spectroscopy requires some delicate experimental conditions, especially for single-cell experiments.

Nevertheless, the application of FTIR spectroscopy is clearly moving towards the analysis of smaller biological samples under fully native conditions, as non-exhaustively presented in **Table II.3-5**. In this context, **the challenging step further thus emerges to be the analysis of single bacterial cells in solution**, and to apply it to the understanding of LAB cryopreservation issues.

Table II.3-5 (continued): Summary of the evolution of FTIR spectroscopy analyses performed on biological samples. Their observation scale depending on the size of the cells and their hydration state is given, with special emphasis on microorganisms, single-cell analyses and performed in an aqueous environment:

Category	Organism	Scale	State	Analysis mode	Study	Reference
Monolayers of eukaryotic cells; Aqueous envt. Broadband analysis	Human lung fibroblasts	Densely packed monolayers, 50x50 µm	Aqueous envt. (cells attached to a gold surface)	SR, gold-coated glass + ZnSe lid	Cell cycle; changes in the IR spectral features at different points of the cell cycle (especially in the Amide bands)	Holman *et al*. 2000
	U937 monocytic cell line	-	Aqueous envt.	SR, transmission CaF_2; microfab. fluidic devices	Fabrication of the microfluidic device using photoresist XARP 3100/10	Birarda *et al*. 2010
	Human breast adenocarcinoma cell line	-	Aqueous envt.	SR, transmission CaF_2; microfab. fluidic devices	Cell spectral features monitoring for a long time; cells remain viable.	Grenci *et al*. 2012
	U937 monocytes, round shaped cells of 8−10 µm dia.	densely packed monolayers, 50x50 µm	Aqueous envt.	Globar, transmission, CaF_2 microfluidics device of 8.5 µm pathlength	Effect of various cell fixation methods on the biochemical alteration of lipid composition, and structure of proteins & nucleic acids.	Vaccari *et al*. 2012a
Single eukaryotic cells; Hydrated state	Mouse cells	Single cells	Cytospun on BaF_2 slides	SR, transmission, BaF_2 slide	Mapping functional groups inside single living and necrotic cells	Jamin *et al*. 1998
Single eukaryotic cells; Aqueous envt.	Various human cells (colorectal cancer cells, fibroblasts, endothelial cells)	Single cells grown on CaF_2 windows	Aqueous envt.	SR, transmission, CaF_2 cuvette of 11-12 µm pathlength	The possibility of performing IR spectroscopy of single cells under aqueous media	Moss *et al*. 2005
	Micrasterias hardyi (~300µm dia., 12µm thick) & leukaemia cells	Single cells	Aqueous envt.	SR, transmission, CaF_2; microfabricated device	Obtaining high quality mid-IR spectral information from live eukaryotic cells using in-house microfabricated devices of 7.6 or 12.7 µm pathlength	Tobin *et al*. 2010
	U937 monocytes, round shaped cells of 8−10 µm dia.	Single cells, 10x10 µm	Aqueous envt.	SR, transmission, CaF_2 microfluidics device of 8.5 µm pathlength	Proof of principle for the analysis of the 3000-2800 cm^{-1}, 1760-1480 cm^{-1} and 1350-1000 cm^{-1} spectral regions arising from individual monocytes in an aqueous environment	Vaccari *et al*. 2012b

sp. reso: spectral resolution; GR: globar radiation; SR (µSR): synchrotron radiation (combined with microscopy); νCH_2: stretching vibration mode of CH_2 bonds in lipids; $T_{m\,lip}$: membrane lipid melting; $T_{s\,lip}$,: membrane lipid solidification; ξ: lipid transition cooperativity; dia.: diameter; microfab.: microfabricated.

EXPERIMENTAL APPROACH

EXPERIMENTAL APPROACH

This work aimed at investigating the cryopreservation-induced biochemical modifications in *Lactobacillus delbrueckii* subsp. *bulgaricus* which leads to the degradation of its biological response. The plasma membrane is a highly functional molecular assembly involved in signal transduction, transport mechanisms, cell elongation, division and maintenance of the cell's physical integrity. As the membrane serves as the only barrier between the exterior and all intra-cellular materials, it is often considered as the primary target of injuries following the modification of environmental conditions, especially in unicellular organisms. A particular focus was thus given to the characterisation of the cell membrane of *L. bulgaricus* at a biochemical and a biophysical level. A schematic overview of the experimental approach adopted throughout this PhD thesis is presented in **Fig. III.1-1**. The approach was composed of 4 main phases (noted "**a**" to "**d**" in the following).

Freeze-thaw resistance comparison (**Fig. III.1-1a**)

A preliminary comparison of the freeze-thaw resistance of three *L. bulgaricus* strains was initiated: *L. bulgaricus* CFL1, ATCC BAA-365 and ATCC 11842. The former is a model strain that has been studied for more than 15 years at the GMPA laboratory (INRA Grignon), known for its sensitivity to preservation processes (Fonseca *et al*. 2000, 2006; Oldenhof *et al*. 2005; Rault *et al*. 2007; Streit *et al*. 2008; Gautier *et al*. 2013; Passot *et al*. 2015). On the contrary, the two other strains have been selected due to their putative higher resistance to production and preservation processes compared to *L. bulgaricus* CFL1 because of their commercial use, and also due to the availability of their genomes (Makarova *et al*. 2006a; van de Guchte *et al*. 2006, respectively).

The loss of technological properties of bacterial cells following freeze-thawing was evaluated by assessing their culturability and acidifying activity both before and after freeze-thawing. The cryopreservation method applied was a slow cooling rate (-2 °C min^{-1} until -80 °C in an EF600 controlled-rate freezer, Asymptote, Cambridge, UK) and a high thawing rate (by immersion in a 42 °C water bath for 5 min) in the presence of sucrose as cryoprotective agent to ensure controlled and reproducible cryopreservation conditions. Sucrose was chosen because it is an extracellular CPA (Hubàlek 2003) and because it provides relatively good protection of *L. bulgaricus* (Gautier *et al*. 2013, Passot *et al*. 2015, Fonseca *et al*. 2016).

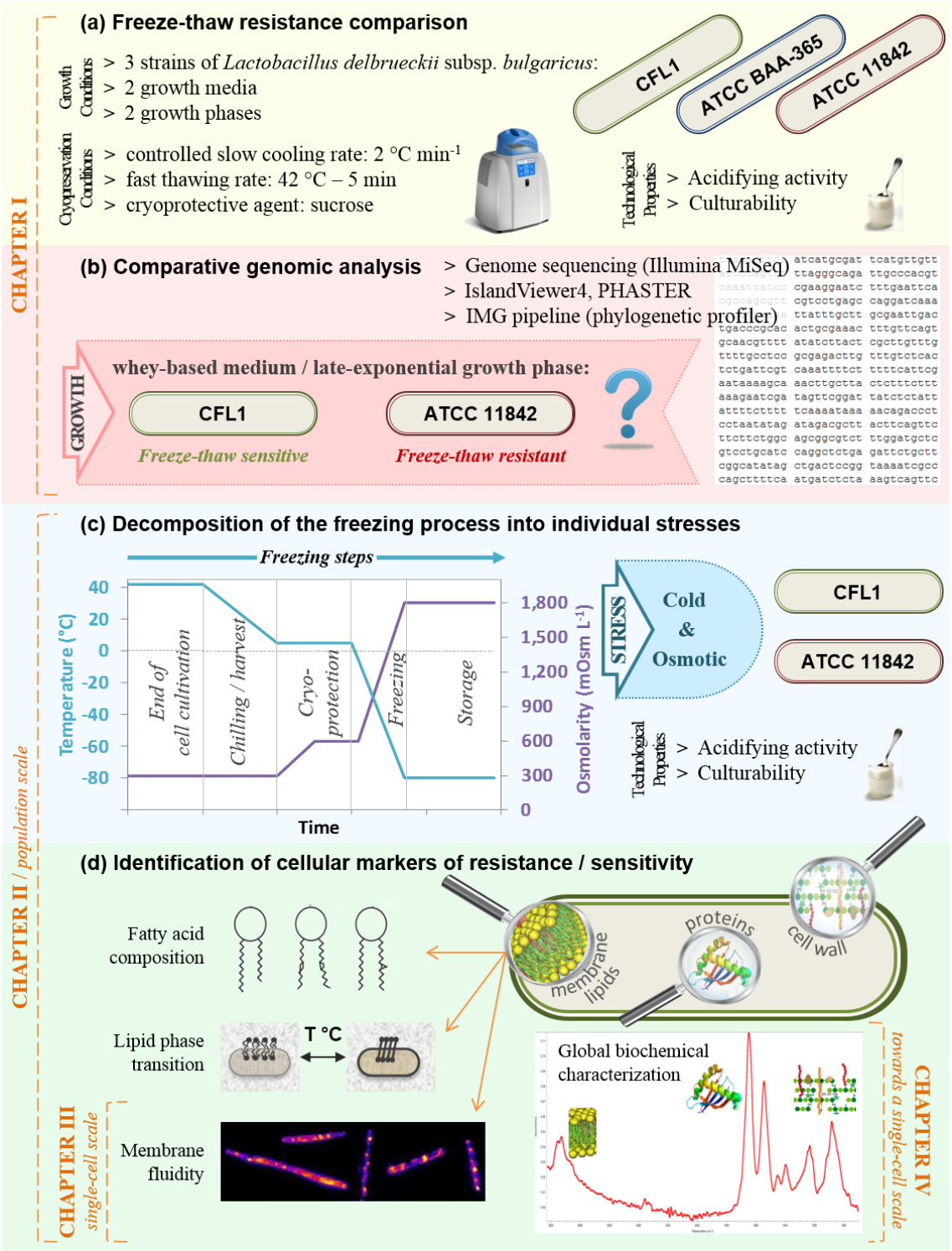

Figure III.1-1: Schematic overview of the experimental approach of the present work. It is divided into four main phases ("**a**" to "**d**"), each referring to at least one of the four different chapters of the Results & Discussion section ("**CHAPTER I**" to "**CHAPTER IV**"). *L. bulgaricus* is represented as a rod-shaped bacillus with a membrane bilayer (thin surrounding lines) and a cell wall (thick surrounding lines), and the magnifying glasses highlight the major biomolecules examined (from left to right: membrane lipids, proteins and the cell wall).

The influence of some growth conditions on the resulting bacterial cryoresistance was also investigated. Two growth media were tested, namely MRS broth and whey-based medium, because of their significant influence on the cryoresistance of *L. bulgaricus* (Gautier *et al*. 2013; Passot *et al*. 2015), and cells harvest was performed either at the late exponential or early stationary growth phase.

Comparative genomic analysis (Fig. III.1-1b)

In a second phase, a comparative genomic analysis of the three strains was undertaken as an attempt to explain their different cryoresistances. Before that, the genome of *L. bulgaricus* CFL1 was sequenced by Illumina MiSeq technology. It was then automatically annotated and announced in a brief report (*Genome Announc*, 2016, 4:e00052-16). The acquisition of novel genes and functionalities in bacteria may occur through horizontal gene transfer (HGT). Genomic islands and prophage indicate the occurrence of HGT, and both were looked for thanks to the IslandViewer4 and PHASTER tools, respectively. Genome comparison was subsequently performed using the tools available on the Integrated Microbial Genomes (IMG) pipeline. The phylogenetic profiler tool was thus used to identify strain-specific genes, and to reveal the presence of orthologous genes between any of the three *L. bulgaricus* strains and cold-adapted bacteria. Finally, assignment of function to genes of interest coding for hypothetical proteins was attempted by means of Basic Local Alignment Search Tool (BLAST, NCBI).

The work corresponding to phases ***a*** and ***b*** is detailed in the first chapter of the Results & Discussion section (**CHAPTER I**). It enabled to identify the growth conditions resulting in significantly different freeze-thaw resistances for two of the three strains that were further studied in the rest of the work:

L. bulgaricus CFL1 and *L. bulgaricus* ATCC 11842
Whey-based growth medium
Cell harvest at late exponential growth phase

Decomposition of the freezing process into individual stresses (Fig. III.1-1c)

From the end of cell cultivation to the frozen state, environmental conditions evolve, making bacterial cells suffer different kinds of stress. The graph in **Fig. III.1-1c** illustrates the temperature decrease and osmolarity increase during the sequential steps of this process. In particular, cells were chilled from 42 °C to approximately 5 °C upon harvest. Then, the addition of cryoprotective additives increased the osmolarity of the cell mixture from isotonicity (300 mOsm L^{-1}) to a mild hypertonic condition (600 mOsm L^{-1} with the 20 % wt. sucrose solution in saline water added to a 1:1 ratio as cryoprotective solution in this work). During the subsequent slow cooling rate of 2 °C min^{-1} until -80 °C, at some point below 0 °C, ice nucleates. This led to the cryo-concentration of the extracellular medium, and cells remained in solution in a strongly hypertonic unfrozen fraction (1800 mOsm L^{-1} could be expected). Cold and osmotic stresses thus appeared as the main stresses that bacteria may encounter during freezing in the presence of cryoprotective agents.

To better understand the mechanisms of freeze injury, the freezing process was split into individual stresses. The relative impact of cold and osmotic stresses on the technological properties of *L. bulgaricus* CFL1 and *L. bulgaricus* ATCC 11842 was thus investigated.

Identification of cellular markers of resistance / sensitivity (Fig. III.1-1d)

In addition to the biological characterisation, a cautious analysis of the membrane properties of both strains was undertaken. It involved the assessment of: (i) fatty acyl residues composition by gas chromatography-mass spectrometry (GC-MS) following accelerated solvent extraction (ASE), (ii) membrane lipid phase transition and other lipid conformational order characteristics by FTIR spectroscopy, and (iii) fluidity by spectrofluorimetric fluorescence anisotropy. These results (the biological characterisation plus the biochemical and biophysical analysis of the membrane) were published in a peer-reviewed scientific journal (*Appl Microbiol Biotechnol*, 2017, 101:1427-1441) and are presented in the second chapter of the Results & Discussion section (**CHAPTER II**).

This study provided information about bulk membrane properties. To go further in the characterisation of bacterial populations, the high brilliance of the synchrotron radiation in the ultraviolet and infrared regions was exploited to assess bacterial membrane fluidity and biochemical composition of single cells, respectively. Fluorescence anisotropy mapping of single cells was thus performed by combining the use of polarized deep UV-synchrotron radiation and fluorescence anisotropy microscopy on the DISCO beamline of synchrotron SOLEIL. The membrane fluidity of individual cells from both strains was analysed under cold and osmotic stress and allowed the quantification of inter-cellular (= population) heterogeneity, and the high spatial resolution of the technique also provided an insight into intra-cellular heterogeneity. This work was accepted for publication (*Appl Microbiol Biotechnol*, 2017, 101, 6907-6917) and is presented in the third chapter of the Results & Discussion section (**CHAPTER III**).

Vibrational spectroscopies, namely synchrotron FTIR and Raman, were also developed to analyse single bacterial cells. The high analytical potential of these tools allows the inspection of the global biochemical composition of *L. bulgaricus*.
A methodological development was thus undertaken to apply synchrotron FTIR spectroscopy to the analysis of single bacteria in an aqueous environment. It involved (i) the modification of the optics of a FTIR spectrometer to design an inverted attenuated total reflection (ATR) mode connected to microscopy, using Germanium as high refractive index material (ii) the setting up of a dedicated sampling chamber receiving liquid samples and (iii) the development of an in-house water subtraction program to allow spectra analysis in the protein IR fingerprint (amides I and II), otherwise swamped by water spectral features.
The same aqueous samples were analysed in parallel by transmission FTIR micro-spectroscopy (without synchrotron) in a static micro-chamber. By using the same water subtraction program, the global secondary structures of proteins and cell envelope carbohydrates and phosphorylated molecules could be analysed from a few thousands of bacteria in an aqueous environment.

This work is presented in the fourth chapter of the Results & Discussion section (**CHAPTER IV**) in the format of a scientific article that will be submitted to *Analyst* or *Analytical and Bioanalytical Chemistry* for publication, and the vibrational description of both strains was completed by Raman micro-spectroscopy with respect to proteins conformation.

In summary, an overview of the analytical methods employed in this work is presented in **Fig. III.1-2**. It emphasizes on the attempts made: (i) for a global analysis of the stress response of *L. bulgaricus* by combining various techniques providing information on different cellular biomolecules (ii) through a multi-scale approach from the population down to the single cell level to investigate the input of exploring cell's response heterogeneity, and (iii) as much as possible in a non-invasive and non-perturbing way (green font, **Fig. III.1-2**).

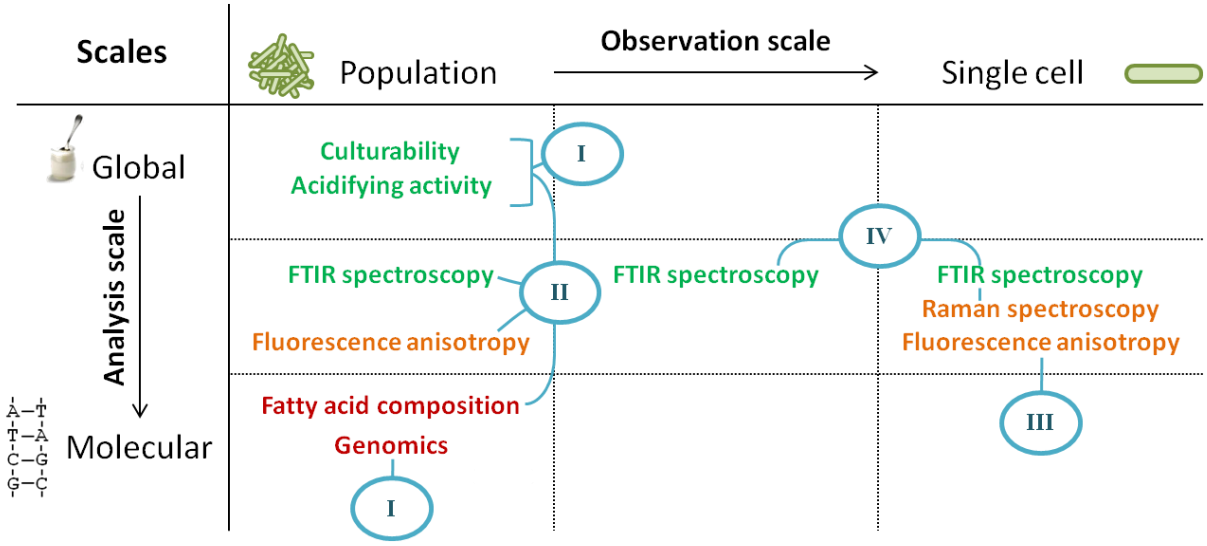

Figure III.1-2: Schematic representation of the multi-scale aspects of the experimental approach through the different analytical methods employed: (i) from top to bottom, the multi-scale analyses span from a global characterisation of the physiological cellular state (resulting from the expression of many genes and activity of many proteins, *e.g.*, by the measurement of the cells' culturability and acidifying activity), to a characterisation of specific categories of biomolecules (cellular proteins, lipids and carbohydrates *e.g.*, by FTIR spectroscopy; membrane lipids fluidity by fluorescence anisotropy), to a determination of the primary structure of specific molecules (including phospholipids' fatty acid composition and DNA sequencing), and (ii) from left to right, the multi-scale observation spanning from a bacterial population comprising trillions of cells, to a few thousands of cells, and down to individual cells. Traffic-light colours represent the degree of invasiveness of each technique, from non invasive (in green), slightly invasive (requiring labeling or drying; in orange), to extremely invasive (cell degradation using thermal, pressure and/or solvents treatments; in red). Numbers in blue ("**I**" to "**IV**") refer to the chapter of the Results & Discussion section in which the corresponding technique(s) was (were) employed.

RESULTS & DISCUSSION

RESULTS & DISCUSSION

CONTENTS

I. Comparative cryoresistance and genomic analyses of three strains of *Lactobacillus delbrueckii* subsp. *bulgaricus*

1.1. Context and objectives

According to the literature review, the cryoresistance of *L. bulgaricus* appears to depend on several factors, including the strain considered, as well as growth and cryopreservation conditions. Numerous studies have investigated the cryoresistance of different genera and species of LAB under various conditions of cryoprotection and freezing protocols. Comparing different LAB and experimental conditions makes difficult the elucidation of mechanisms of cryoinjury and the identification of cellular markers of stress. To reduce the number of experimental factors having an impact on bacterial cryoresistance, and therefore enable a deep study of cryoinjury mechanisms in *L. bulgaricus*, we compared the cryoresistance of three *L. bulgaricus* strains cultivated in different conditions (two growth media and two growth phases upon harvest), while keeping standard and reproducible conditions of concentration, protection and cryopreservation. This work made it possible to identify the cell production conditions leading to markedly different cell cryoresistances of two strains, to be applied for the rest of the work. Moreover, the aim was to provide some clues for the explanation of the different growth kinetics and cryoresistances observed at a genomic level through a comparative analysis of the strains' genome.

The cryosensitive *L. bulgaricus* CFL1 and two commercial strains with suspected higher cryoresistance and available genomes sequences, *L. bulgaricus* ATCC BAA-365 and *L. bulgaricus* ATCC 11842 were thus tested. Bacterial growth kinetics were monitored in MRS broth and whey-based medium, and their cryoresistance was evaluated as a function of the growth medium and growth phase upon harvest, by quantifying their culturability and acidifying activity losses following freeze-thawing by the plate count method and the CinAc system, respectively. The genome of *L. bulgaricus* CFL1 was sequenced, and online tools were subsequently used for the comparative genomic analysis. The webservers PHASTER and IslandViewer4 enabled to predict prophages and genomic islands, respectively, and the Integrated Microbial Genomes (IMG) database and comparative analysis system was used to search for orthologous genes between the three *L. bulgaricus* strains, but also with the genome of a cold-adapted lactic acid bacterium, *Carnobacterium pleistocenium* FTR1.

Genome sequencing of *L. bulgaricus* CFL1 was announced and published in a brief report (*Genome Announcement*, 2016, 4:e00052-16), and the results of the biological activity and genomic comparisons are presented thereafter in the form of a scientific article to be submitted for publication to *Journal of Dairy Science*.

1.2. Article

Authors
Julie Meneghel[1] • Séverine Layec[1] • Stéphanie Passot[1] • Fernanda Fonseca[1]

Title
Comparative cryoresistance and genomic analyses of three strains of *Lactobacillus delbrueckii* subsp. *bulgaricus*

Affiliations
[1] UMR GMPA, AgroParisTech, INRA, Université Paris-Saclay, 78850 Thiverval-Grignon, France
Address all correspondence to Fernanda Fonseca. Email: fernanda.fonseca@inra.fr; Phone: +33 (0)1 30 81 59 40; Fax: +33 (0)1 30 81 55 97

Abstract
Lactobacillus delbrueckii subsp. *bulgaricus* is a lactic acid bacterium (LAB) and a dairy starter used to produce yogurt and some varieties of cheese. Growth kinetics and cryoresistance of *L. bulgaricus* vary according to culture conditions and strains, and this work aimed at better characterising these parameters. For that, three strains of *L. bulgaricus* – CFL1, ATCC BAA-365 and ATCC 11842 – were cultivated in two different growth media (MRS broth and whey-based medium) and harvested in late exponential and early stationary growth phases. Their culturability and acidifying activity losses following freezing (at 2 °C min^{-1} until -80 °C for 24 h) and thawing (at 42 °C for 5 min) were evaluated by the plate count method and the time necessary to reach maximum acidification rate in milk using the CinAc system, respectively. Higher growth rates were obtained from cultivation of *L. bulgaricus* strains in whey-based medium compared to MRS broth. *L. bulgaricus* CFL1 presented the highest growth rates, regardless of the growth medium, although this result was not significant. On the other hand, this strain was the most sensitive to freeze-thawing when grown in whey-based medium. A comparative genomic analysis was subsequently performed to explain the results of biological activity thanks to the Integrated Microbial Genome (IMG) database. A total of 87 and 81 putative genes specific for the cryosensitive and cryoresistant strains were identified. The presence in the genome of *L. bulgaricus* CFL1 of additional genes encoding a carbohydrate transporter, riboflavin biosynthesis enzymes and proteases, could explain its higher growth rates compared to the other two strains. Besides, the higher cryoresistance of *L. bulgaricus* ATCC BAA-365 and ATCC 11842 could be attributed to three genes that had orthologs in the permafrost-isolated LAB *Carnobacterium pleistocenium* FTR1 but not in *L. bulgaricus* CFL1. These genes encoded a cold-shock protein and two ribosomal subunits. Also, differences in the *espII* loci and in other transporters suggest a different composition and biophysical properties of the cell envelope between the strains, potentially involved in the differential cryoresistance of *L. bulgaricus*.

Keywords
Lactobacillus delbrueckii subsp. *bulgaricus* • cryoresistance • comparative genomic analysis

Introduction

Food industries, pharmaceutical industries and culture collections rely on cryopreservation and freeze-drying to store and maintain bacterial strains alive in order to reactivate them whenever required. The availability of bacterial starters with high and constant quality (viability and functional properties of cells) is critical, especially for the fermentation industries to ensure more reproducible fermentation processes and thus deliver qualitative end products. The fermentation of many raw materials (mainly dairy products, but also meat, fish, vegetables and cereals) involve lactic acid bacteria (LAB). *Lactobacillus delbrueckii* subsp. *bulgaricus* is a homofermentative member of the LAB group which is mainly used in protocooperation with *St. thermophilus* to produce yogurt. It plays an important role in this manufacturing process by contributing to the development of organoleptic properties and to its safety. The accumulation of lactic acid from the consumption of lactose by *L. bulgaricus* thus has an influence on taste, texture and shelf-life extension of yogurt. *L. bulgaricus* also produces flavour compounds, exopolysaccharides (EPS) and bacteriocins (Beshkova *et al*. 1998; Hati *et al*. 2013) that reinforce these three characteristics, respectively. In addition, by assisting with lactose digestion, *L. bulgaricus* contributes to the consumption of dairy products by lactose-intolerant people (Gilliland and Kim 1984; Savaiano 2014). Probiotic properties of *L. bulgaricus* (probiotics being "live microorganisms which when administered in adequate amounts confer a health benefit on the host") also include its suspected implication in immune modulation (Mercenier *et al*. 2003; Zanni *et al*. 2017).

The quality of LAB starters is usually evaluated by the concentration of viable cells and their acidifying activity (Champagne and Gélinas 1998; Monnet *et al*. 2008). The ready-to-use concentrated frozen form of LAB starters is usually preferred over the freeze-dried form for costs and practicality reasons (rehydration of freeze-dried products constitutes an additional step in the process) and due to the generally higher sensitivity of LAB to drying (Wright and Klaenhammer 1983; Teixeira *et al*. 1996; Broadbent and Lin 1999; Strasser *et al*. 2009; Velly *et al*. 2014; Bravo-Ferrada *et al*. 2015). However, freezing may also lead to significant lethality within LAB, especially in some strains of *L. bulgaricus* (Smittle *et al*. 1972; Fonseca *et al*. 2000; Gomez Zavaglia *et al*. 2000; Rault *et al*. 2007).

Improving the cryotolerance of LAB is possible by activating specific mechanisms involved in their cold response. Applying mild stressful conditions might thus induce such cold response *via* homologous or heterologous adaptation, leading to an improved cryotolerance. For instance, cold shocking *St. thermophilus* (Wouters *et al*. 1999), *Lactobacillus acidophilus* (Lorca and Font de Valdez 1999; Wang *et al*. 2005b), cold or heat shocking *Lactococcus lactis* ssp. (*Lc. lactis*) (Broadbent and Lin 1999) or acid shocking *L. bulgaricus* (Streit *et al*. 2008) before freezing had a positive impact on post-thaw survival and/or acidifying activity. Playing on cell growth conditions has also proved to be efficient in the modulation of the cryotolerance of LAB, such as the choice and formulation of the culture medium (Smittle *et al*. 1972; Beal *et al*. 2001; Gautier *et al*. 2013), growth temperature and pH (de Urraza and De Antoni 1997; Fernández Murga *et al*. 2000; Wang *et al*. 2005a). Among active cell responses associated with improved cryotolerance, the

modulation of membrane fatty acid composition has frequently been reported (Broadbent and Lin 1999; Fernández Murga *et al*. 2000; Wang *et al*. 2005a; Wang *et al*. 2005b; Streit *et al*. 2008; Gautier *et al*. 2013). The modification in the synthesis of proteins also suggests their involvement in cryotolerance (Lorca and Font de Valdez 1999; Wouters *et al*. 1999; Wang *et al*. 2005b; Streit *et al*. 2008), with the particular implication of cold shock proteins (Derzelle *et al*. 2003). By reaching negative temperatures quickly, cell response to freezing is yet mostly passive and can be improved through the optimization of the cryopreservation process of LAB by carefully selecting the cryoprotective agent (Baumann and Reinbold 1966; Tsvetkov and Brankova 1983; Chavarri *et al*. 1988; Cárcoba and Rodríguez 2000; Péter and Reichart 2001; Fonseca *et al*. 2003; Bravo-Ferrada *et al*. 2015; Fonseca *et al*. 2016), freezing rates (Baumann and Reinbold 1966; De Valdéz and De Giori 1993; Bâati *et al*. 2000; Péter and Reichart 2001; Fonseca *et al*. 2001; Dumont *et al*. 2004; Fonseca *et al*. 2006) and storage conditions (Baumann and Reinbold 1966; Chavarri *et al*. 1988; Fonseca *et al*. 2000; Fonseca *et al*. 2001; Fonseca *et al*. 2003; Bravo-Ferrada *et al*. 2015). In this work, the cryopreservation procedure was fixed and some growth conditions (medium and duration) were screened to evaluate their incidence on the cryotolerance of several strains of *L. bulgaricus*. In the literature, *L. bulgaricus* was reported to develop a strain-dependant cryotolerance response (Smittle *et al*. 1972; Gomez Zavaglia *et al*. 2000; Rault *et al*. 2007). Nevertheless, the identification of genetic factors potentially involved in the cryotolerance of this LAB member remains scarce. In fact, two studies have investigated on the cryoresistance of mutants of *L. bulgaricus* strain CFL1 (Monnet *et al*. 2003; Rivals *et al*. 2007). In the work of Rivals *et al*. (2007), the acquisition of resistance to specific antibiotics (ATB) in *L. bulgaricus* strain CFL1 could be paralleled with an enhanced cryoresistance. Thus, mutations supposedly leading to the inactivation of genes involved in DNA replication, RNA translation and cell wall biosynthesis, seemed to be implicated in the resistance of the bacterium to freeze-thawing. In the work of Monnet *et al*. (2003), natural mutants with a higher cryoresistance were generated by repetitive cycles of transfers through milk followed by freeze-thawing. The authors did not perform the identification of the mutated genes in the cryoresistant cultures of *L. bulgaricus* but both studies suggest that few genes could significantly influence the cryotolerance of *L. bulgaricus*.

The aim of this work was first to identify the cultivation conditions leading to markedly different cell cryoresistances of three *L. bulgaricus* strains by evaluating and comparing their viability and acidifying activity losses following freeze-thawing. In a second part, a comparative genomic analysis between cryosensitive and cryoresistant strains was performed to identify putative genes involved in the cold stress response and adaptive mechanisms to freeze-thawing.

Material and methods

Bacterial strains and culture conditions

The freeze-thaw resistance of three strains of *Lactobacillus delbrueckii* subsp. *bulgaricus* was compared in this study: *L. bulgaricus* CFL1 (CIRM-BIA; Rennes, France), *L. bulgaricus* ATCC BAA-365 (Chr. Hansen; Copenhagen, Denmark) and *L. bulgaricus* ATCC 11842 (Manassas, VA, USA).

Table IV.1-1: Composition of the growth media used to cultivate *Lactobacillus delbrueckii* subsp. *bulgaricus i.e.*, MRS broth and whey-based medium.

MRS broth		Whey-based medium	
Composition	**Concentration (g L^{-1})**	**Composition**	**Concentration (g L^{-1})**
Glucose	20	Lactose	43.2
Polypeptone	10	Whey proteins	6.6
Meat extract	10	Whey mineral salts	5.1
Yeast extract	5	Yeast extract	5
Tween 80	1.08		
Dipotassium phosphate	2		
Sodium acetate	5		
Ammonium citrate	2		
Magnesium sulfate	0.2		
Manganese sulfate	0.05		

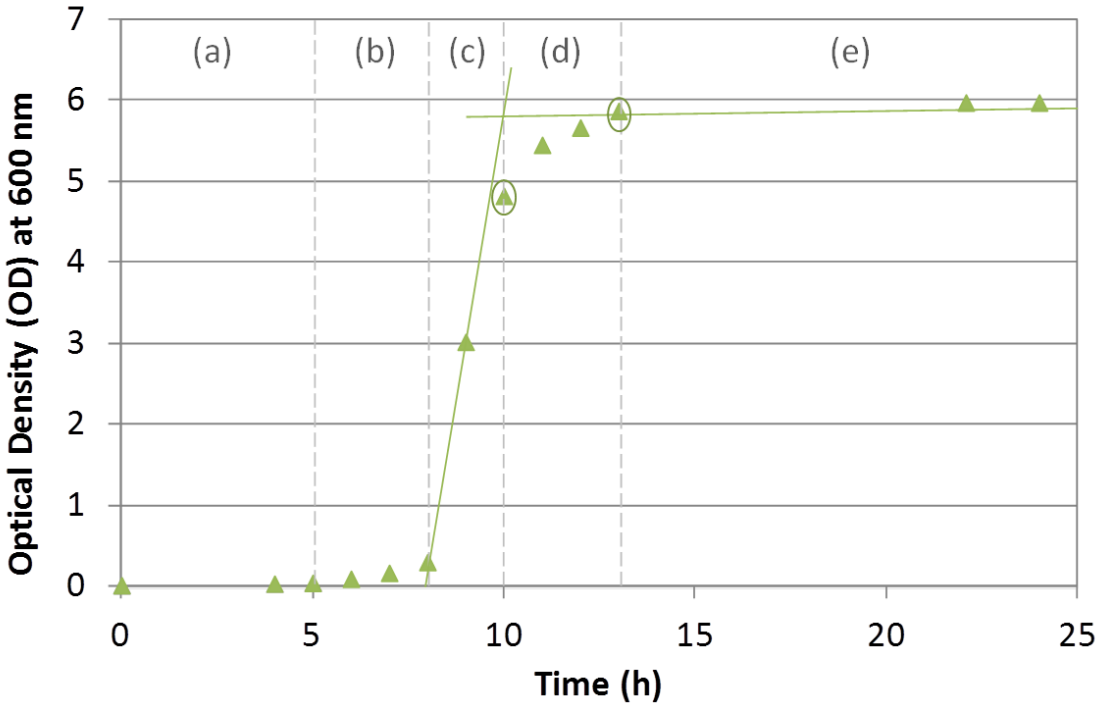

Figure IV.1-1: Illustration of the method applied to determine harvesting points based on the growth kinetics of *Lactobacillus delbrueckii* subsp. *bulgaricus*. Here, the growth kinetic of *L. bulgaricus* CFL1 in whey-based medium at 42 °C for 25 hours measured by optical density measurements at 600 nm is presented. Successive growth phases are separated by dashed lines: (**a**) lag, (**b**) positive acceleration, (**c**) exponential, (**d**) negative acceleration, (**e**) and stationary growth phases. The tangents to the exponential and stationary growth phases are drawn in green, and their intercept was considered as the end of exponential growth phase. The beginning of the stationary growth phase was fixed three hours afterwards and both time points (circled) corresponded to cell harvesting points (see **Table 3** for harvesting time details).

Two growth media were used to cultivate cells, namely MRS broth (de Man, Rogosa, Sharpe) as a nutrient-rich medium designed for the laboratory cultivation of fastidious lactobacilli (De Man *et al*. 1960) and a whey-based medium, closer in composition to industrial cultivation media. Their composition is given in **Table IV.1-1**. The MRS broth (Biokar Diagnostics; Beauvais, France) was reconstituted according to the manufacturer's instructions (55 g L^{-1} in deionized water) and sterilized at 120 °C for 15 min. The whey-based medium consisted of 60 g L^{-1} mild whey powder (Euroserum; Port-sur-Saône, France) that was heated at 110 °C for 20 min. The supernatant obtained after centrifugation (17,000 x *g* for 30 min at 4 °C) and filtration was supplemented with 5 g L^{-1} yeast extract (Organotechnie SAS; La Courneuve, France) and sterilized at 110 °C for 20 min.

Inocula were stored at -80 °C and were thawed at 42 °C for 5 min before inoculation in 30 mL of MRS broth (the experimental procedure for inocula preparation is detailed in **Appendix I**). Pre-culture was carried out at 42 °C up to the early stationary growth phase (corresponding to a cell density of approximately 1.10^8 CFU mL^{-1}). Growth of *L. bulgaricus* being faster in whey-based medium than in MRS broth, a different inoculation rate was performed in each medium to reduce the resulting growth duration difference. Approximately 1.5 mL or 150 µL of the pre-culture was thus used to inoculate 300 mL of MRS broth or whey-based medium, respectively and the cultures were incubated at 42 °C until the end of the exponential or early stationary growth phase.

Growth kinetics were monitored by measuring the optical density (OD) at 600 nm of bacterial suspensions during pre-culture and culture in both media until the stationary growth phase was reached (typically for 25 hours, corresponding to $OD_{600\ nm} \geq 4.0$). The corresponding sterile medium was used as blank. Bacterial suspensions and the blank were diluted by a factor 10 in sterile saline water (0.9 % w/v NaCl) to remain in the linear range of the optical system. Maximum growth rates were calculated from the slope of the growth kinetics in the exponential growth phase (μ_{max}, h^{-1}). The intercept of the tangents to the curves in the exponential and stationary growth phases was considered as the end of the exponential growth phase (Fencl *et al*. 1966), as illustrated in **Fig. IV.1-1**. Early stationary growth phase was arbitrarily established three hours later. Both characteristic times were thereby determined for each strain and each growth medium and were used as harvesting times, further adjusted by OD measurements at 600 nm.

Cell harvest was performed by centrifugation on pre-cooled bacterial suspensions at 5 °C (11,000 x *g* for 10 min at 5 °C). Cell pellets were then washed in Tris-HCl buffer (50 mM, pH 8.8, Bio-Rad; Hercules, CA, USA) in order to remove growth medium constituents and excreted microbial metabolites that might negatively interfere with further analysis procedures. Such washing procedure was repeated two additional times for cells cultivated in whey-based medium.

Freezing and thawing protocols

Washed cell pellets were resuspended in the same weight (1:1 ratio) of a sucrose solution (20 % wt. sucrose in saline water). Cryotubes were filled with 500 µL of cryoprotected bacterial suspension and inserted into a controlled rate freezer (EF600-103, Asymptote; Cambridge, UK) pre-cooled to 5 °C. The sample temperature was monitored by inserting a thermocouple (K type) into one cryotube. After a holding step of

10 min at 5 °C, the freezer was programmed to cool the sample device at 2 °C min^{-1}, from 5 °C to -80 °C. Frozen samples were stored at least 24 h at -80 °C and thawed for 5 min at 42 °C before evaluating the biological activity of bacterial cells.

Biological activity measurements

Two properties were measured to describe the biological activity of *L. bulgaricus* before and immediately after freeze-thawing: cell culturability and acidifying activity.

Culturability measurement

Bacterial cell concentration was determined using the agar plate count method. Serial decimal dilutions of samples were prepared in saline water and the appropriate dilutions were inoculated in the bulk of MRS agar (Biokar Diagnostics; Beauvais, France) plates in triplicate. Colonies were enumerated after incubating the plates for 48 h at 42 °C in anaerobic conditions (GENbox anaer, bioMerieux; Marcy l'Etoile, France). Plates containing between 30 and 300 colonies were kept for cell concentration calculation (in CFU mL^{-1}). Culturability loss after freezing (in log (CFU mL^{-1})) was calculated using the following equation (**Eq. 1**):

$$\text{Culturability loss} = log\ \frac{[\text{CFU mL}^{-1}]_{\text{after freezing}}}{[\text{CFU mL}^{-1}]_{\text{before freezing}}} \quad (1)$$

Acidifying activity measurement

The CinAc system (AMS; Frepillon, France) was used to evaluate the acidifying activity of the bacterial suspensions according to Fonseca *et al*. (2000), with minor modifications. Briefly, 150 mL of skim milk was reconstituted from dry powder at 100 g L^{-1} (EPI Ingredients; Ancenis, France), distributed in flasks, sterilized (at 110 °C for 20 min) and pre-warmed to 42 °C in a temperature-controlled bath. Following the inoculation of three flasks with 100 µL of the bacterial suspensions, their pH was continuously monitored every 3 min until the end of the acidification. The minimum of the first-order derivative of the acidification curves represents the time required for the bacterial suspension to reach its maximum acidification rate in milk and was used as a discriminating descriptor between experimental conditions (tm, in min). The higher the tm value was, the longer the latency phase and the lower the acidifying activity were.
The acidifying activity loss (dtm, in min) after freezing was quantified as follows (**Eq. 2**):

$$\text{dtm} = \text{tm}_{\text{after freezing}} - \text{tm}_{\text{before freezing}} \quad (2)$$

Statistical analysis

Statistical analyses of maximum growth rates and culturability and acidifying activity losses of bacterial populations according to experimental conditions (growth medium; growth phase upon harvest; strain) were performed in R 3.4.1 using the R Commander package (Fox 2005) from at least three independent productions. After testing the homogeneity of variances at a 95 % confidence interval, pairwise comparisons of means were performed through Tukey-Kramer tests assuming normality of distributions.

Comparative genomic analysis

The genomes of *L. bulgaricus* CFL1 (Meneghel *et al*. 2016), *L. bulgaricus* ATCC BAA-365 (Makarova *et al*. 2006a) and *L. bulgaricus* ATCC 11842 (van de Guchte *et al*. 2006) were taken into consideration for the comparative genomic analysis. They are available in the NCBI (under the GenBank assembly accession numbers GCA_001510975.1, GCA_000014405.1 and GCA_000056065.1, respectively; https://www.ncbi.nlm.nih.gov/genome/genomes/514) and IMG databases (under the IMG genome IDs 2600255386, 639633029 and 637000139, respectively). The web servers PHASTER (Arndt *et al*. 2016) and IslandViewer 4 (Bertelli *et al*. 2017) were used to predict prophages and genomic islands, respectively. Orthologous genes were searched for *via* the phylogenetic profiler tool of the Integrated Microbial Genomes (IMG) database and comparative analysis system (Markowitz *et al*. 2012), as described in the corresponding operating procedure (MGAP v.4; https://img.jgi.doe.gov/er/doc/MGAandDI_SOP.pdf) using maximum E-value of 10^{-5} and a minimum percent identity of 70 % as cut-off parameters. Genes of interest were also searched for orthologs in the Alaskan permafrost-isolated LAB *Carnobacterium pleistocenium* (*C. pleistocenium*) FTR1 (Pikuta *et al*. 2005) using the same parameters.

Results and discussion

Growth kinetics and cryoresistance of the three strains of *L. bulgaricus*

The monitoring of the growth kinetics of *L. bulgaricus* was performed for each of the three strains (CFL1, ATCC BAA-365 and ATCC 11842) cultured at 42 °C in MRS broth and in whey-based medium. From these growth kinetics, several parameters could be calculated and determined: maximum growth rates, lag times, and harvesting time points.

Maximum growth rates are given in **Table IV.1-2**; a strong medium dependency was observed with significantly higher values in whey-based medium compared to MRS broth with for instance 1.34 ± 0.04 h^{-1} and 0.55 ± 0.05 h^{-1} for *L. bulgaricus* CFL1, respectively (p values < 0.01). This could suggest the existence among the three *L. bulgaricus* strains considered of a common preference for lactose catabolism compared to glucose, as main carbohydrate sources in whey-based medium and MRS broth, respectively (**Table IV.1-1**). The general preference of some LAB for the carbohydrate source of their ecological niche (*e.g.*,

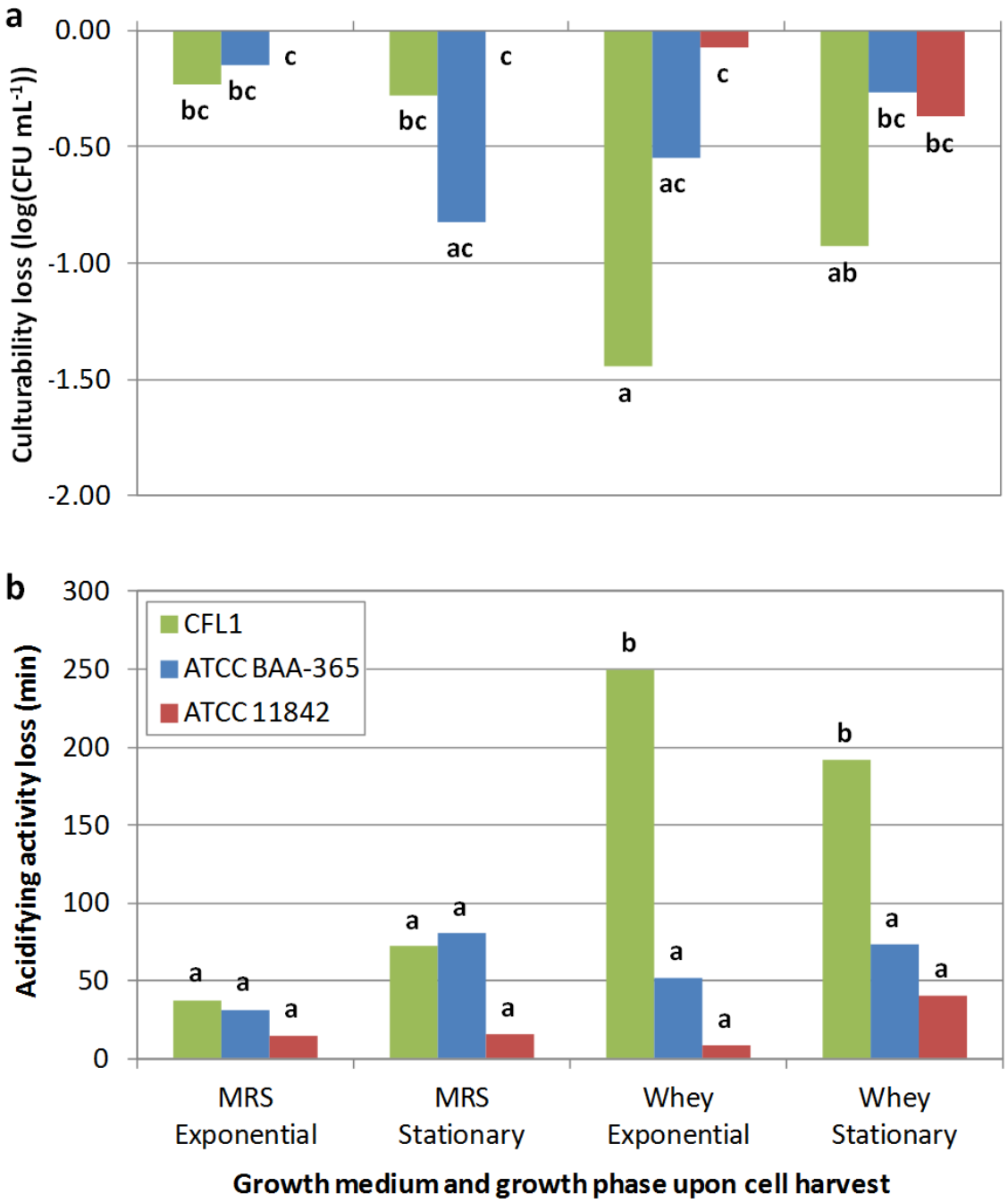

Figure IV.1-2: Comparative resistance of three *Lactobacillus delbrueckii* subsp. *bulgaricus* strains to freeze-thawing. Mean (**a**) culturability and (**b**) acidifying activity losses depending on the growth medium (MRS broth or whey-based medium) and growth phase upon harvest (late exponential or early stationary) of *L. bulgaricus* CFL1 (green), ATCC BAA-365 (blue) and ATCC 11842 (red). Letters represent statistical contrasts between means (p value < 0.05).

Table IV.1-2: Maximum growth rates (μ_{max}, h^{-1}) of different strains of *Lactobacillus delbrueckii* subsp. *bulgaricus* cultivated in MRS broth and whey-based medium.

	Maximum growth rate (μ_{max}, h^{-1})	
Strain	MRS broth	Whey-based medium
CFL1	0.55 ± 0.05^{b}	1.34 ± 0.04^{d}
ATCC BAA-365	0.47 ± 0.06^{ab}	1.11 ± 0.03^{c}
ATCC 11842	0.34 ± 0.03^{a}	0.94 ± 0.15^{c}

Mean values (n = 3) ± standard deviations are indicated. Superscript letters indicate statistical contrasts (*p* values < 0.01).

Table IV.1-3: Approximate harvesting time (hours) for the recovery of different strains of *Lactobacillus delbrueckii* subsp. *bulgaricus* in the late exponential and early stationary growth phases following cultivation in MRS broth and whey-based medium at 42 °C.

		Pre-culture	***Culture***			
	Growth medium	**MRS broth**	**MRS broth**		**Whey-based medium**	
	growth phase	Early stationary	Late exponential	Early stationary	Late exponential	Early stationary
***L. bulgaricus* strain**	CFL1	13	12	15	10	13
	ATCC BAA-365	24	22	25	14	17
	ATCC 11842	24	25	28	13	16

Table IV.1-4: Raw data for culturability loss (log(CFU mL^{-1})) following freeze-thawing of three strains of *Lactobacillus delbrueckii* subsp. *bulgaricus* according to various growth conditions.

Strain	Growth medium and growth phase upon harvest			
	MRS Late exponential	MRS Late stationary	Whey-based End exponential	Whey-based Early stationary
CFL1	-0.2 ± 0.1^{bc}	-0.3 ± 0.1^{bc}	-1.4 ± 0.1^{a}	-0.9 ± 0.4^{ab}
ATCC BAA-365	-0.2 ± 0.1^{bc}	-0.8 ± 0.3^{ac}	-0.5 ± 0.5^{ac}	-0.3 ± 0.5^{bc}
ATCC 11842	0 ± 0.1^{c}	0 ± 0.1^{c}	-0.1 ± 0.2^{c}	-0.4 ± 0.5^{bc}

Mean values (n = 3) ± standard deviations are indicated, and superscript letters represent statistical contrasts between means (*p* value < 0.05).

Table IV.1-5: Raw data for acidification activity loss (min) following freeze-thawing of three strains of *Lactobacillus delbrueckii* subsp. *bulgaricus* according to various growth conditions.

Strain	Growth medium and growth phase upon harvest			
	MRS Late exponential	MRS Late stationary	Whey-based End exponential	Whey-based Early stationary
CFL1	37 ± 12^{a}	72 ± 16^{a}	250 ± 10^{b}	192 ± 42^{b}
ATCC BAA-365	31 ± 34^{a}	81 ± 45^{a}	52 ± 14^{a}	73 ± 63^{a}
ATCC 11842	14 ± 16^{a}	16 ± 3^{a}	9 ± 11^{a}	40 ± 21^{a}

Mean values (n = 3) ± standard deviations are indicated, and superscript letters represent statistical contrasts between means (*p* value < 0.05).

lactose for dairy LAB; maltose for sourdough LAB) has been reported (Endo and Dicks 2014), as well as the specific preference of *L. bulgaricus* for lactose compared to glucose (Chervaux *et al*. 2000). In addition, De Urraza and De Antony (1997) showed that upon early stationary growth phase, *L. bulgaricus* produced more ATP from lactose than from glucose (approximately 35%). Lactose fermentation seems therefore energetically more favourable than glucose fermentation for *L. bulgaricus*. Furthermore, as suggested by a recent metabolomic analysis of *Lactobacillus delbrueckii* subspecies *bulgaricus* and *lactis*, the metabolism of the *bulgaricus* subspecies appeared importantly sustained from a protein-based source (Zanni *et al*. 2017). The nitrogen sources of MRS broth and whey-based medium have yeast extract in common but differ by the presence of polypeptone (protein-based digests) plus meat extract in the former and whey proteins in the latter (**Table IV.1-1**). These different nitrogen sources also certainly participate in the preference of *L. bulgaricus* for the whey-based medium over MRS broth. From **Table IV.1-2**, it also appeared that *L. bulgaricus* CFL1 presented higher maximum growth rates compared to the two other strains (ATCC BAA-365 and ATCC 11842) regardless of the growth media. However, these differences were significant in whey-based medium (p values < 0.05) but not in MRS broth (p values > 0.05).
The 10-times lower inoculation rates performed in whey-based medium compared to MRS broth led to longer lag times of *L. bulgaricus* of approximately 2 hours, regardless of the strain considered (**Fig. S1**, **Appendix II**). Harvesting time points were determined according to the procedure illustrated in **Fig. IV.1-1** and are presented in **Table IV.1-3**. In the end, the different cell productions could be performed altogether (*i.e.*, under the same conditions of incubation for each biological replicate) while remaining compatible with working hour constraints.

Bacterial cryoresistance was determined as culturability and acidifying activity losses between the fresh and frozen-thawed states. The results are presented in the histograms of **Fig. IV.1-2a** and **IV.1-2b**, and the corresponding values may be found in **Tables IV.1-4** and **IV.1-5**, respectively. Both parameters were evaluated as a function of strain (*L. bulgaricus* CFL1, ATCC BAA-365 or ATCC 11842), growth medium (MRS broth or whey-based medium) and growth phase (late exponential or early stationary).
From these results, the general following characterisation of the three strains may be proposed with respect to their cryoresistance: *L. bulgaricus* ATCC BAA-365 and ATCC 11842 appeared as cryoresistant strains regardless of the growth conditions tested (growth medium and phase upon harvest) with a slightly higher cryoresistance of *L. bulgaricus* ATCC 11842. On the contrary, *L. bulgaricus* CFL1 presented a medium-dependent cryoresistance with the recovery of cryosensitive cells from their cultivation in the whey-based medium, especially when cells were harvested in the late exponential growth phase.
Cultivating *L. bulgaricus* ATCC BAA-365 and ATCC 11842 in MRS broth or in whey-based medium thus had no significant influence on their cryoresistance. On the other hand, cultivating *L. bulgaricus* CFL1 in whey-based medium was associated to increased culturability and acidifying activity losses following freeze-thawing compared to growth in MRS broth. This observation confirms that of the work of Gautier *et al*. (2013), who identified medium-dependant cryoresistances in *L. bulgaricus* CFL1, associated with different membrane fatty acid composition and lipid phase transition temperature. In their study, cryoresistance was associated with higher levels of unsaturated and cyclic fatty acyl residues, and to a lower

lipid phase transition temperature. The authors suggested that these membrane biophysical properties facilitated water fluxes during freezing and therefore limited the concomitant membrane damage of bacteria. Different membrane fatty acid composition and biophysical properties may thus also be associated to the cryoresistant and cryosentitive strains of the present study, that it could be interesting to investigate.

No significant influence of the growth phase on both culturability and acidifying activity losses could be identified from any of the three strains. The absence of significant growth phase effect could be due to the proximity of both harvesting time points. Nevertheless, Rault *et al*. (2010) also came to this conclusion when analysing the cryoresistance of *L. bulgaricus* CFL1 harvested in late exponential, early and late stationary phases. Although not significant, *L. bulgaricus* CFL1 grown in whey-based medium showed a slightly higher cryoresistance when harvested in the early stationary growth phase compared to the late exponential growth phase. A higher resistance was indeed expected from cells in stationary growth phase since the upregulation of stress response proteins is the common observation of Cohen *et al*. (2006), Wu *et al*. (2009) and Yap *et al*. (2014) from their growth phase-dependant proteomics studies on the LAB *Lactobacillus plantarum*, *Lactobacillus casei* and *Lactococcus lactis*, respectively.

Finally, both parameters (culturability and acidifying activity losses) showed similar general tendencies, although statistical clustering was clearer when considering acidifying activity loss than culturability loss (**Fig. IV.1-2b**). The coefficient of variation (CV) of the CinAc method is indeed 8 to 10 times higher than the CV of the plate count method (average CV of 2.0 % versus 16.1 %, and median CV of 1.5 % versus 14.5 %, respectively, when considering 38 different measurements performed in triplicate). A couple of reasons may explain this difference: measuring the acidifying activity requires fewer steps in the experimental procedure (no serial decimal dilutions) and because of its independency on cell arrangement into chains of varying number of cells. A lower tendency for experimental error and variability therefore resulted from the assessment of acidifying activity loss compared to culturability loss.

Growth rate differences could be explained at a genomic level by strain-dependant metabolic pathways for the utilization of the nutrients contained in each growth medium. The strain-dependent and medium-dependent cryoresistances could be explained by different factors including membrane properties (Beney and Gervais, 2001), interaction between cryoprotective agents and membrane phospholipids and other cellular components (Anchordoguy *et al*. 1987; Santivarangkna *et al*. 2008a), and the cold stress response of cells. The mechanisms of cell adaptation to glacial environments were recently reviewed and include the synthesis of antifreeze proteins, cold-shock proteins, exopolysaccharides (EPS), polyunsaturated fatty acids, compatible solutes, and modification to RNA transcription and protein folding (Jansson and Taş 2014; Boetius *et al*. 2015; Bar Dolev *et al*. 2016). The ability of cells to synthesize the proteins implicated in such cold stress response and potentially conferring cryoresistance to cells could be identified at a genomic level. We addressed this issue by further comparing the genomes of *L. bulgaricus* CFL1, ATCC BAA-365 and ATCC 11842.

Comparative genomic analysis

Global genomic comparison and most striking differences

The genome of *L. bulgaricus* CFL1 was published as a permanent draft with 44 largest contigs of > 1000 bp (Meneghel *et al*. 2016), whereas the genomes of *L. bulgaricus* ATCC BAA-365 and *L. bulgaricus* ATCC 11842 have been completely sequenced (Makarova *et al*. 2006a; van de Guchte *et al*. 2006). The genomic characteristics of all three *L. bulgaricus* strains, presented in **Table IV.1-6,** revealed general consistency (genome size, overall G+C content, number of genes). The apparently lower number of rRNA and tRNA genes in *L. bulgaricus* CFL1 may be explained by the consideration of only the 44 largest contigs of the draft sequencing status of its genome (Meneghel *et al*. 2016). However, a particularity regarding the detected clustered regularly interspaced short palindromic repeats (CRISPRs) was emphasized by Meneghel *et al*. (2016) in *L. bulgaricus* CFL1. CRISPRs are hypervariable genetic loci widely distributed in bacteria and archaea, notably among LAB. They represent a family of DNA repeats which typically consist of short and highly conserved repeats, interspaced by variable sequences called spacers (both constituting the CRISPR array), often found adjacent to Cas (CRISPR-associated) genes (Makarova *et al*. 2006b; Sorek *et al*. 2008). The biological function of CRISPR-Cas systems is defensive against plasmid and phage invasions. As such, they constitute an emerging technology to combat phage attacks in the dairy industry, and have also been broadly used for gene editing purposes, as exemplified by the exponential number of patents deposited in the past decade on both technologies (Egelie *et al*. 2016). CRISPR-Cas systems thus play a critical role in adaptation and persistence of a eukaryotic host in a particular ecosystem and environmental niches where phages are present. They are classified into three major groups (type I, II, and III), as reviewed by Bhaya *et al*. (2011). In *L. bulgaricus* CFL1, two CRISPR-Cas systems were present, belonging to types II and III and including the famous Cas9 protein (**Table IV.1-7**). In contrast, none or only one CRISPR-Cas system appeared to be regularly present in other *L. bulgaricus* strains (33 unsequenced strains tested; Urshev and Ishlimova, 2015) as well as in *L. bulgaricus* ATCC BAA-365 and *L. bulgaricus* ATCC 11842 (**Table IV.1-6**). Besides, these two strains possessed the same CRISPR-Cas system type I (**Table IV.1-7**). By expanding this comparison to the eight other *L. bulgaricus* genomes available on the IMG database, it could be confirmed that most strains possessed a single CRISPR-Cas system, except *L. bulgaricus* CNCM I-1632, CRL871 and VIB44 that possessed two of them (**Table IV.1-8**). However, the couple of CRISPR-Cas system types of *L. bulgaricus* CNCM I-1632 and VIB44 (types I and III) differed from those of *L. bulgaricus* CRL871 and CFL1 (types II and III), and those present in *L. bulgaricus* CRL871 seemed incomplete considering the number of constitutive genes and/or the lack of CRISPR array (**Table IV.1-8**). Overall, the diversity of CRISPR loci in *L. bulgaricus* likely reflects their lateral origin and their rapid evolution due to environmental pressure, notably linked to phage predation.

This suggests the possible presence of different prophages within the genomes of the three strains studied. A prophage is a genetic sequence of phage origin incorporated into the genome of a bacterium, potentially providing the host with additional genes and properties including the adaptation to specific environments (Arndt *et al*. 2016). Therefore, the presence of prophages was looked for in *L. bulgaricus* CFL1, ATCC

Table IV.1-6: Overview of the main characteristics of the genomes of *Lactobacillus delbrueckii* subsp. *bulgaricus* CFL1, ATCC BAA-365 and ATCC 11842.

Strain	**CFL1**	**ATCC BAA-365**	**ATCC 11842**
Origin	French handcrafted fermented milk	French starter	Bulgarian yoghurt
Genome sequencing status	Permanent draft	Finished	Finished
Scaffolds	44	1	1
Genome size (bp)	1,757,917	1,856,951	1,864,998
Overall G+C content (%)	49.8	49.7	49.7
Total predicted genes	1882	1865	2234
Coding DNA sequences	1794	1721	2094
Number of rRNA genes	20	27	27
Number of tRNA genes	68	98	95
Number of CRISPR-Cas systems	2	1	1
Genes with predicted function (%)	75.04	67.77	47.22
Reference	Meneghel *et al*. 2016	Makarova *et al*. 2006a	van de Guchte *et al*. 2006

Table IV.1-7: Comparison of genes coding for clustered regularly interspaced short palindromic repeats associated proteins (CRISPR-Cas) in the three strains of *Lactobacillus delbrueckii* subsp. *bulgaricus*.

Strain	Locus Tag §	Protein name	Protein size †	Protein accession number
CFL1	Ga0063702_01158 / CFL1_RS05530	Type II-A CRISPR-associated protein Csn2	222	WP_059217097
	Ga0063702_01159 / CFL1_RS05535	CRISPR-associated endonuclease Cas2	101	WP_059217132
	Ga0063702_01160 / CFL1_RS005540	Type II CRISPR-associated endonuclease Cas1	303	WP_059217099
	Ga0063702_01161 / CFL1_RS05545	Type II CRISPR RNA-guided endonuclease Cas9	1420	WP_059217133
	Ga0063702_01581 / CFL1_RS07565	CRISPR-associated endonuclease Cas2	101	WP_003618136
	Ga0063702_01582 / CFL1_RS07570	Subtype II CRISPR-associated endonuclease Cas1	304	WP_003618133
	Ga0063702_01583 / CFL1_RS07575	Type III-A CRISPR associated RAMP Csm5	350	WP_003618131
	Ga0063702_01584 / CFL1_RS07580	Hypothetical protein	292	WP_003618129
	Ga0063702_01585 / CFL1_RS07585	Type III-A CRISPR-associated RAMP protein Csm3	222	WP_003618127
	Ga0063702_01586 / CFL1_RS07590	Type III-A CRISPR-associated protein Csm2	163	WP_003618125
	Ga0063702_01587 / CFL1_RS07595	Type III-A CRISPR-associated protein Cas10/Csm1	659	WP_080582648
	Ga0063702_01588 / CFL1_RS07600	Hypothetical protein	121	WP_050980883
	Ga0063702_01589 / CFL1_RS07605	CRISPR-associated endoribonuclease Cas6	250	WP_003618119
ATCC BAA-365	LBUL_0793	CRISPR-associated helicase/endonuclease Cas3	921	WP_011678175
	LBUL_0794	CRISPR-associated protein	574	WP_011678176
	LBUL_0795	Type I-E CRISPR-associated protein Cse2/CasB	205	WP_011678177
	LBUL_0796	Type I-E CRISPR-associated protein Cas7/Cse4/CasC	358	WP_011543823
	LBUL_0797	Type I-E CRISPR-associated protein Cas5/CasD	233	WP_003619876
	LBUL_0798	Type I-E CRISPR-associated protein Cas6/Cse3/CasE	207	WP_003619878
	LBUL_0799	Subtype I-E CRISPR-associated endonuclease Cas1	316	WP_003619879
	LBUL_0800	Type I-E CRISPR-associated endoribonuclease Cas2	290	WP_011678179
ATCC 11842	Ldb0868	CRISPR-associated helicase/endonuclease Cas3	921	WP_011543820
	Ldb0869	CRISPR-associated protein	574	WP_011543821
	Ldb0870	Type I-E CRISPR-associated protein Cse2/CasB	205	WP_050899093
	Ldb0871	Type I-E CRISPR-associated protein Cas7/Cse4/CasC	358	WP_011543823
	Ldb0872	Type I-E CRISPR-associated protein Cas5/CasD	233	WP_011543824
	Ldb0873	Type I-E CRISPR-associated protein Cas6/Cse3/CasE	207	WP_003619878
	Ldb0874	Subtype I-E CRISPR-associated endonuclease Cas1	316	WP_003619879
	Ldb0875	Type I-E CRISPR-associated endoribonuclease Cas2	290	WP_011543825

§ Locus tags available on IMG / NCBI databases for *L. bulgaricus* CFL1 as: "Ga0063702_xxx / CFL1_xxx"; locus tags for *L. bulgaricus* ATCC BAA-365 as: "LBUL_xxx" and for *L. bulgaricus* ATCC 11842 as: "Ldbxxx".
† Amino acid sequence length.
The proteins may be searched for *via* their protein accession numbers on: https://www.ncbi.nlm.nih.gov/protein.

Table IV.1-8: Comparison of the distribution of CRISPR-Cas system types among the *Lactobacillus delbrueckii* subsp. *bulgaricus* strains available on the IMG database (https://img.jgi.doe.gov/cgi-bin/mer/main.cgi).

CRISPR-Cas system types	*L. bulgaricus* strains	Presence of a CRISPR array	Number of genes
Type I	ATCC 11842	Yes	8
	ATCC BAA-365	Yes	8
	CNCM I-1519	Yes	8
	CNCM I-1632	Yes	8
	PB2003/044-T3-4	Yes	8
	VIB27	Yes	8
	VIB44	Yes	9
Type II	CFL1	Yes	4
	CRL871	No	3
	MN-BM-F01	No	4
Type III	CFL1	Yes	9
	CNCM I-1632	No	9
	CRL871	No	9
	VIB44	Yes	9
Unknown	2038	Yes	1

A CRISPR array consists of unique spacers interspaced between repeats.

Table IV.1-9: Relevant genes specifically identified in *Lactobacillus delbrueckii* subsp. *bulgaricus* CFL1, and in both *L. bulgaricus* ATCC BAA-365 and ATCC 11842.

Strain	Locus tag §	Protein name (additional details)	Metabolic pathway	Protein size †	Protein accession number
CFL1	Ga0063702_00980 / CFL1_RS04665	PTS system, cellobiose-specific IIA component (cytosolic phosphorylation site)	Carbohydrate transport and metabolism	107	WP_059217066
	Ga0063702_00981 / CFL1_RS04670	PTS system, cellobiose-specific IIB component (cytosolic phosphorylation site)		107	WP_059217068
	Ga0063702_00982 / CFL1_RS04675	PTS system, cellobiose-specific IIC component (transmembrane channel)		443	WP_059217070
	Ga0063702_00969 / CFL1_RS04595 to Ga0063702_00977 / CFL1_RS04635	part of *epsI* gene cluster involved in exopolysaccharide biosynthesis	Glycan metabolism	323 to 590	WP_059217043 to WP_059217059
	Ga0063702_01886	riboflavin synthase alpha chain	Vitamin and cofactor metabolism (riboflavin)	70	-
	Ga0063702_01887	3,4-dihydroxy 2-butanone 4-phosphate synthase/GTP cyclohydrolase II		370	-
	Ga0063702_01888	6,7-dimethyl-8-ribityllumazine synthase		84	-
	Ga0063702_01889	6,7-dimethyl-8-ribityllumazine synthase		64	-
	Ga0063702_00563 / CFL1_RS02830	Peptidase family M13 (metalloendopeptidase)	Protein metabolism	114	WP_035174734
	Ga0063702_01926	Peptidase family M13 (metalloendopeptidase)		49	
	Ga0063702_01927	Peptidase family M13 (metalloendopeptidase)		124	
ATCC BAA-365 & ATCC 11842	**LBUL_1957 & Ldb2117**	**CspA, cold shock protein (RNA chaperone)**	**Stress response**	**65**	WP_003616492
	LBUL_0363 & Ldb0409	**Small subunit ribosomal protein S14P**	**Translation**	**61**	WP_002878192
	LBUL_0373 & Ldb0419	**Large subunit ribosomal protein L36P**		**38**	WP_002878160
	LBUL_0980; LBUL_1029 & Ldb1076; Ldb1131	Putative MerR family transcriptional regulators		91	WP_011678265
	LBUL_0987; LBUL_1021 & Ldb1086; Ldb1121.	Arsenate reductases ArsC (protein-tyrosine-phosphatases)		132	WP_003623434; WP_011543903
	LBUL_0989; LBUL_1019 & Ldb1088; Ldb1119.	FtsE, ATPase components (regulators of the cell division peptidoglycan hydrolase)	Regulatory functions	250	WP_003623437
	LBUL_0990; LBUL_1018 & Ldb1089; Ldb1118.	FtsX, permease components (regulators of the cell division peptidoglycan hydrolase)		194	WP_077299801
	LBUL_0992; LBUL_1016 & Ldb1115*	LysR family transcriptional regulator (helix-turn-helix domain containing proteins)		624	WP_011543905

§ Locus tags available on IMG / NCBI databases for *L. bulgaricus* CFL1 as: "Ga0063702_xxx / CFL1_RS0xxx"; locus tags for *L. bulgaricus* ATCC BAA-365 as: "LBUL_xxx" and for *L. bulgaricus* ATCC 11842 as: "Ldbxxx"; † amino acid sequence length; * pseudogene.
Due to probable informatic errors, the locus tags of the genes of *L. bulgaricus* CFL1 involved in riboflavin biosynthesis could not be found on the NCBI website, but were part of a contig > 5000 bp. On the contrary, the genes of *L. bulgaricus* CFL1 encoding the second and third peptidases were located on contigs < 1000 bp and were not listed on the NCBI website; they were identified from the IMG database. The proteins may be searched for *via* their protein accession numbers on: https://www.ncbi.nlm.nih.gov/protein. Genes with sequence homology to the psychrophilic permafrost-isolated *Carnobacterium pleistocenium* FTR1 are bold-typed. Cut-off parameters: maximum E-value of 10^{-5} and minimum percent identity of 70 %.

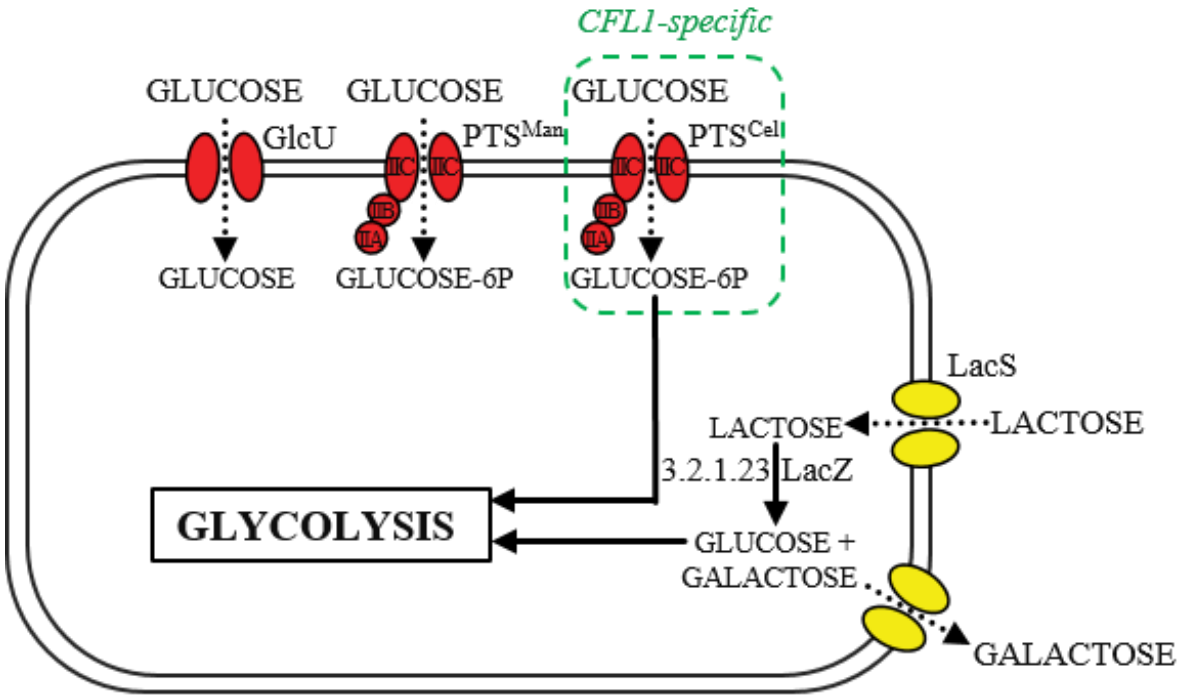

Figure IV.1-3: Utilization of the carbohydrates glucose and lactose in *Lactobacillus delbrueckii* subsp. *bulgaricus*. Import of glucose is mediated through the glucose uptake symporter, the mannose or the cellobiose phosphotransferase systems with a concomitant phosphorylation of the molecule before entry in the glycolysis pathway (GlcU, PTS^{Man} and PTS^{Cel}, respectively, in red). Import of lactose is mediated through the lactose symporter (LacS, yellow) and intracellular lactose is hydrolyzed into galactose and glucose *via* the enzyme β-galactosidase (LacZ). Galactose is excreted *via* the LacS and glucose enters the glycosysis pathway **(**adapted from Barrangou *et al*. 2006 and Castro *et al*. 2009). After comparing the genomes of *L. bulgaricus* CFL1, ATCC BAA-365 and ATCC 11842, it appeared that the genes coding for PTS^{Cel} were only present in the genome of *L. bulgaricus* CFL1 (green dashed rectangle).

11842 and ATCC BAA-365 using the PHASTER web server. Six different incomplete prophages were identified in total, among which four of them were identified in the genome of *L. bulgaricus* CFL1, three in *L. bulgaricus* ATCC BAA-365 and in ATCC 11842, including one prophage common to all three strains (prophage #1, **Table S1**, **Appendix II**) and two prophages common to *L. bulgaricus* CFL1 and ATCC BAA-365 (prophages #2 and #3, **Table S1**, **Appendix II**). *L. bulgaricus* CFL1 and ATCC 11842 presented one and two specific prophages, respectively (prophage #4 and prophages #5 and #6, **Table S1**, **Appendix II**, respectively). Despite apparent inter-strain differences, orthologs of the genes belonging to these prophages were consistently found in the other strains and could not be linked to the observed strain-dependant growth rates or cryoresistances. Strain-specific genes acquired by another means than phage DNA integration might still exist and genomic islands were looked for thereafter. The IMG phylogenetic profiler tool was thus used to identify the genes of *L. bulgaricus* CFL1 that had no homologs in *L. bulgaricus* ATCC BAA-365 and ATCC 11842 (*i.e*., the "CFL1-specific" genes), and the homologous genes between *L. bulgaricus* ATCC BAA-365 and *L. bulgaricus* ATCC 11842 without homologs in *L. bulgaricus* CFL1 (*i.e.,* the "ATCC-specific" genes). A total of 87 "CFL1-specific" genes and 81 "ATCC-specific" genes were thus identified, of which 67 and 44 genes could be assigned a putative function, respectively. As expected, almost all of them were part of genomic islands, as predicted by IslandViewer 4. The relevant genes are presented in **Table IV.1-9**.

Transport and metabolism of carbohydrates

Preference for the utilization of the carbohydrate lactose over glucose was identified in all three strains, with slightly higher growth rates in both media for *L. bulgaricus* CFL1 compared to *L. bulgaricus* ATCC BAA-365 and ATCC 11842. Lactose is the main carbohydrate source of dairy products and the preference of LAB for lactose utilization arising from their ecological niche, may be explained by differences in the functioning of lactose and glucose transporters and/or in affinity with their substrates. In the LAB *Lc. lactis* employed in cheese manufacturing, Castro *et al*. 2009 showed that glucose may indeed be transported either through the glucose/H^+ symporter (GlcU) which is proton-motive force dependent or actively through the phosphoenolpyruvate (PEP) dependant phosphotransferase systems (PTS) for the transport of mannose (PTS^{Man}) or cellobiose (PTS^{Cel}) (**Fig. IV.1-3**). PTS are major prokaryotic carbohydrate transporters consisting of a phosphoenolpyruvate-protein phosphotransferase (denominated enzyme I) and a substrate specific permease (denominated enzyme II) consisting of at least three subunits: IIA, IIB, two cytosolic phosphorylation sites, and IIC, a transmembrane channel. In contrast, lactose is internalized in LAB *via* a permease (LacS), which is probably an antiporter. Lactose is then further hydrolyzed by the enzyme β-galactosidase (LacZ) into glucose and galactose before glucose catabolism and galactose excretion through the LacS (Hickey *et al*. 1986; Chervaux *et al*. 2000; van de Guchte *et al*. 2006), as shown in **Fig. IV.1-3**. This carbohydrates antiport occurs according to their concentration gradients (Hickey *et al*. 1986; Chervaux *et al*. 2000; van de Guchte *et al*. 2006).

Interestingly, the genomic comparison revealed the presence of three genes coding for the IIA, IIB and IIC subunits of PTS^{Cel} in *L. bulgaricus* CFL1 (locus tags: Ga0063702_00980, Ga0063702_00981 and

Ga0063702_00982, respectively, **Table IV.1-9**), but not in the two other strains. Even though cellobiose is a disaccharide and glucose a monosaccharide, Castro *et al*. (2009) showed that the PTS^{Cel} could also serve as glucose transporter in *Lc. lactis*, although with a lower affinity. Besides, Carvalho *et al*. (2013) further showed that in *Lc. lactis*, maximal glucose uptake *via* the high affinity PTS^{Man} decreased linearly with pH. *L. bulgaricus* CFL1 could thus benefit from a supplementary transport system for glucose in addition to the GlcU and PTS^{Man} shared by all three strains, conferring a metabolic advantage especially under acid stress. Since glucose is the sole carbon source in MRS broth and cultures were performed without pH regulation, this could explain the observed faster metabolism of *L. bulgaricus* CFL1 compared to the other two strains when cultivated in MRS broth.

In addition, the genomic comparison revealed the exclusive presence in *L. bulgaricus* CFL1 of three genes encoding metalloendopeptidases (Ga0063702_00563, Ga0063702_01926 and Ga0063702_01927, **Table IV.1-9**) and a cluster of five genes involved in the biosynthesis of riboflavin (Ga0063702_01886 to Ga0063702_01890, **Table IV.1-9**). The peptidases, belonging to the M13 family, may be used for the digestion of milk proteins, as suggested by Rawlings and Barrett (1995) and Janer *et al*. (2005). They could thus also contribute to the slightly higher maximum growth rates of *L. bulgaricus* CFL1 compared to *L. bulgaricus* ATCC BAA-365 and ATCC 11842 in the whey-based medium. Finally, the gene cluster involved in the biosynthesis of riboflavin could account for the higher growth rate of *L. bulgaricus* CFL1, regardless of the growth medium. In fact, riboflavin is a precursor of important cofactors – the coenzymes flavin mononucleotide (FMN) and flavin adenine dinucleotide (FAD) – involved in many metabolic reactions, especially redox reactions (Burgess *et al*. 2006).

Genetic determinants potentially involved in the cold stress response

The cryoresistance comparison indicated that *L. bulgaricus* ATCC BAA-365 and ATCC 11842 were resistant regardless of the cultivation conditions tested and that *L. bulgaricus* CFL1 was sensitive when grown in the whey-based medium. As an attempt to explain this discrepancy, genes specifically present in both *L. bulgaricus* ATCC BAA-365 and ATCC 11842 without orthologs in *L. bulgaricus* CFL1, the "ATCC-specific" genes, were looked for. Out of the 44 "ATCC-specific" genes that could be assigned a putative function, 11 were considered particularly relevant. They are presented in **Table IV.1-9** and are involved in the cold stress response, translation and regulatory functions.

In this study, the gene coding for the cold-shock protein CspA was thus specifically found in *L. bulgaricus* ATCC BAA-365 and ATCC 11842 (locus tags: LBUL_1957 and Ldb2117, respectively). The cold stress alleviation mechanism of CSPs occurs through binding to mRNA, which results in the destabilization of the mRNA structure for translation activity maintenance at low temperature (Chattopadhyay 2006; Keto-Timonen *et al*. 2016). In the LAB *Lc. lactis*, the overproduction of a cold shock protein (CspB or CspE) improved its resistance to freeze-thawing up to a factor 10 (Wouters *et al*. 2000). The ability of *L. bulgaricus* ATCC BAA-365 and ATCC 11842 to synthesize the CspA protein could thus also participate in their cryoresistance.

The two ribosomal proteins that were identified (the small subunit S14P: LBUL_0363 and Ldb0409, and the large subunit L36P: LBUL_0373 and Ldb0419) could also play a role in the cold shock response of *L. bulgaricus* ATCC BAA-365 and ATCC 11842. The overproduction of some ribosomal proteins in *Escherichia coli* (Jones *et al*. 1992), *Bacillus subtilis* (Graumann *et al*. 1996) and *Lc. lactis* (Wouters *et al*. 2000) during cold shock was indeed suggested to help correct assembly of rRNA under such conditions. Besides, ribosomes were attributed a role of thermostat, by activating the synthesis of heat- or cold-shock proteins depending on the environmental temperature (VanBogelen and Neidhardt 1990).
Alternatively, eight genes coding for proteins involved in regulatory functions were also found to be "ATCC-specific": two regulators of the cell division peptidoglycan hydrolase, known as the FtsEX complex (Bajaj *et al*. 2016) (LBUL_0989, LBUL_0990, LBUL_1018, LBUL_1019 and Ldb1088, Ldb1089, Ldb1118, Ldb1119), two protein tyrosine phosphatases (LBUL_0987, LBUL_1021 and Ldb1086, Ldb1121) and two putative transcriptional regulators of the MerR family (activators). Regulation of gene expression and protein activity is involved in correct cell functioning in response to the environment (Hoopes 2008) and could have an indirect implication in the cryoresistance of both strains.

Interestingly, two gene clusters coding for the four subunits of polyamine ABC transporters appeared present in *L. bulgaricus* ATCC 11842 (Ldb0647 to Ldb0650 and Ldb2178 to Ldb2181), while orthologs of only one of them were found in *L. bulgaricus* ATCC BAA-365 and *L. bulgaricus* CFL1 (LBUL_0578 to LBUL_0581, and Ga0063702_00151 to Ga0063702_00154, respectively) (**Table S2**, **Appendix II**). ABC transporters indeed usually consist of two nucleotide-binding domains and two transmembrane domains (Davidson and Maloney 2007). One polyamine ABC transporter is therefore likely shared by all three strains, and *L. bulgaricus* ATCC 11842 seemed to possess an additional one. Polyamines, such as spermidine or putrescine, are the products of amino-acid decarboxylation. They are probably present in low amounts in the whey-based medium since they are minor constituents of milk (Sanguansermsri *et al*. 1974). Although their detection seems not to have been performed in MRS broth, polyamines might also be present in this medium because it is a rich source of meat-based amino-acids (**Table IV.1-1**). Polyamines are being attributed many roles including the regulation of gene expression and the induction of stress responses in bacteria and plants (Rhee *et al*. 2007). In particular, their involvement in response to freezing was demonstrated in higher plants (Cuevas *et al*. 2008; Gill and Tuteja 2010) but also to osmotic stress in the cyanobacteria *Synechocystis* and *Synechococcus* (Jantaro *et al*. 2003; Raksajit *et al*. 2009; Pothipongsa *et al*. 2016) and in *E. coli* (Schiller *et al*. 2000). During freezing, extracellular ice formation leads to solutes cryoconcentration which exerts an osmotic stress on cells. Polyamines uptake from the growth media by *L. bulgaricus* may thus occur and be more efficient in *L. bulgaricus* ATCC 11842 compared to the other two strains with its additional dedicated transport system. This could thereby potentially contribute to increase its cryoresistance. But to our knowledge, no work has reported their implication in the resistance of LAB to any kind of stress.

In addition, slight inter-strain differences in the gene composition of two clusters for the biosynthesis of exopolysaccharides (EPS) were noticed. These loci are designated *epsI* (Ga0063702_00962 to

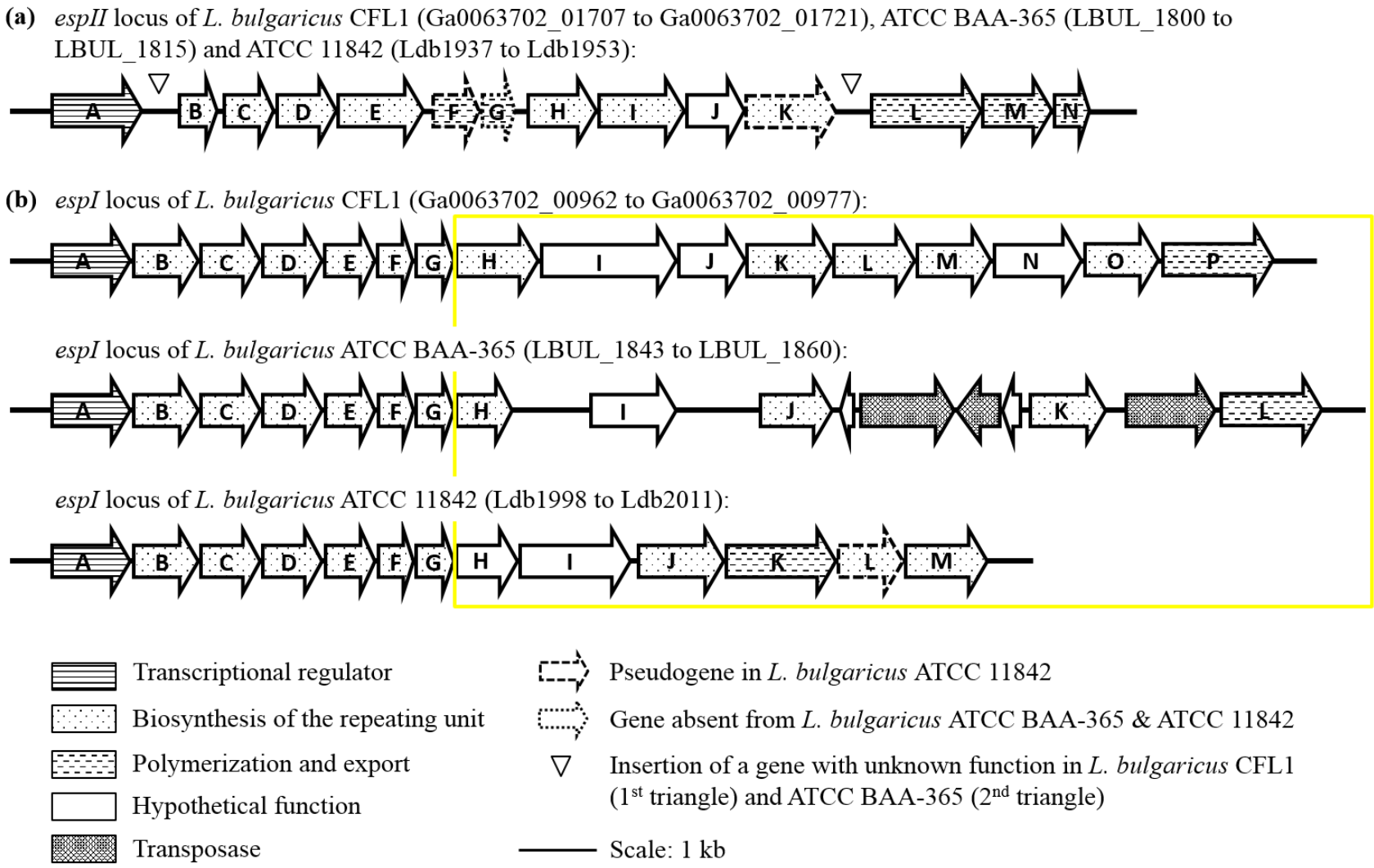

Figure IV.1-4: Comparative genetic organization of the *epsI* and *epsII* loci of *Lactobacillus delbrueckii* subsp. *bulgaricus* CFL1, ATCC BAA-365 and ATCC 11842, the yellow box highlighting a variable genetic region between the three strains.

Ga0063702_00977, LBUL_1843 to LBUL_1860, and Ldb1998 to Ldb2011) and *epsII* (Ga0063702_01707 to Ga0063702_01721, LBUL_1800 to LBUL_1815, and Ldb1937 to Ldb1953). Their global arrangement is similar to the *eps* locus of *L. bulgaricus* Lfi5 (14 genes: *epsA* to *epsN*) described by Lamothe *et al*. (2002), with genes involved in transcription regulation (transcriptional regulator of the LytR family), biosynthesis of the repeating unit (mainly glycosyltransferases), and export (flippases) (**Fig. IV.1-4**). The *epsII* locus appeared almost identical between the three strains with orthologous genes (**Fig. IV.1-4a**). The same hold true for the seven first genes of the *epsI* locus (named "A" to "G" in **Fig. IV.1-4b**). However, a cluster of nine genes within the *epsI* of *L. bulgaricus* CFL1 was found specific to this strain (Ga0063702_00969 to Ga0063702_00977, named "H" to "P" in **Fig. IV.1-4b**), among which some showed orthology with gut bacteria (such as other *Lactobacillus* species, *Bifidobacterium longum*, *Faecalibacterium prausnitzii*, *Clostridium bolteae*). Regarding *L. bulgaricus* ATCC BAA-365, transposases of the IS110 and IS 285 families were revealed at the level of the three last genes of the *epsI* locus (named "J" to "L" in **Fig. IV.1-4b**). This insertion has largely altered the structure of the *epsI* locus that could have compromised the transcription of the downstream genes (Berg *et al*. 1980). Exopolysaccharides, as envelope constituents harbouring an extracellular portion, may modify the physico-chemical properties of the envelope and interaction of the cell with its environment. They are also believed to contribute to cell survival in cold environments as anti-freeze agents (Boetius *et al*. 2015), and structural inter-strain differences may hence participate in the observed different cryoresistance of *L. bulgaricus*.

Based on works reporting on the cold stress response, other genes than those described above could have been expected. For instance, fatty acid desaturases (for membrane fluidity maintenance at low temperature), transporters or biosynthetic enzymes for the accumulation of compatible solutes (to alleviate the osmotic stress resulting from freezing), antifreeze proteins or DNA repair enzymes were reported in the genomes of cold-adapted microorganisms (Jansson and Taş 2014; Meadows and Wargo 2015; Bar Dolev *et al*. 2016). They were looked for in the three strains of *L. bulgaricus*, but without success.
Furthermore, no gene that could help understanding why *L. bulgaricus* CFL1 presented a cryoresistant profile when cultivated in MRS broth and a cryosensitive profile in whey-based medium was identified. Nevertheless, by comparing the transcriptome of *Lactobacillus helveticus* cultivated in milk and MRS broth, Smeianov *et al*. (2007) identified from the MRS broth cultivated cells the induction of genes coding for the GroESL chaperonin system involved in the maintenance of protein folding and stress-related clippases (proteases). For the three *L. bulgaricus* strains studied in this work, no difference was observed in terms of the genes encoding GroEL and GroES. They were indeed consistently present in their genome, as well as five genes coding for different clippases (**Table S2**, **Appendix II**). Because these proteins play a role in bacterial adaptation to low temperatures (Chattopadhyay 2006; Jansson and Taş 2014), they could account for the higher cryoresistance of *L. bulgaricus* CFL1 if such induction also occurred when cultivated in MRS broth compared to whey-based medium (whose composition is close to milk). To investigate deeper into this hypothesis, the proteome of *L. bulgaricus* CFL1 after cultivation in either of both media was extracted from fresh and frozen-thawed cells. Cytoplasmic and envelope proteomes were further separated and a quantitative proteomic analysis is underway to identify proteins involved in cryoresistance.

Finally, the "CFL1-specific" and "ATCC-specific" genes identified by the comparative genomic analysis were then searched for orthologs in the genome of the Alaskan permafrost-isolated LAB *C. pleistocenium* FTR1. No gene among the "CFL1-specific" was positive. By contrast, three genes were found to be orthologous between the "ATCC-specific" genes and *C. pleistocenium*: those coding for the CspA and both ribosomal proteins (bold-typed in **Table IV.1-9**). Their orthology with the genes of a bacterium that is adapted to cope with repetitive cycles of freeze-thawing and cold environments reinforces their putative role in the cryoresistance of *L. bulgaricus* ATCC BAA 365 and ATCC 11842. The effective production of the corresponding proteins in the cryoresistant strains remains to be confirmed by a proteomic study, and their effective role in increasing the cryoresistance of *L. bulgaricus* to be ascertained by mutagenesis. Inactivating them from *L. bulgaricus* ATCC BAA-365 and ATCC 11842 by homologous recombination, and/or to introducing and expressing them in *L. bulgaricus* CFL1 and analysing the cryoresistance of the resulting mutants are ways for future investigations.

Conclusions

When grown in whey-based, *L. bulgaricus* CFL1 appeared sensitive to freeze-thawing, while *L. bulgaricus* ATCC BAA-365 and ATCC 11842 were resistant. The investigation of the CRISPR-Cas systems in the three strains revealed a notable specificity of *L. bulgaricus* CFL1 over the cryoresistant strains, suggesting genomic evolution of strains and possible significant gene differences acquired through horizontal gene transfer. Genomic islands were thus found to harbour some genes that could be involved in the cold-stress response of *L. bulgaricus* ATCC BAA-365 and ATCC 11842. In particular, the presence in their genomes of genes encoding a cold-shock protein and two ribosomal proteins with probable roles in cold stress response and sequence orthology to a psychrophilic LAB could participate in the explanation of their higher cryoresistance compared to *L. bulgaricus* CFL1. Yet, further experiments are needed to confirm these hypotheses. Moreover, *L. bulgaricus* CFL1 presented a medium-dependant cryoresistance profile that the genomic comparison could not elucidate. Gene regulation occurring at the transcriptional and post-translational levels seems reasonable to speculate. Moreover, the genomes still currently hide indecipherable information with many hypothetical protein coding genes that could explain further the strain-dependant cryoresistances and growth kinetics.

Probable differences in terms of composition of the bacterial envelope between strains were also revealed with different biosynthetic enzymes for EPS production and transporters (PTS^{Cel} in *L. bulgaricus* CFL1; additional regulators of cell wall hydrolase in the cryoresistant strains; one additional ABC transporter for spermidine/putrescine in *L. bulgaricus* ATCC 11842). As the envelope is at the interface between the environment and intracellular contents, investigating deeper the cell envelope could provide interesting further information. In particular, comparing the biophysical properties of the membrane (fatty acid composition, phase transition temperature, conformational order and fluidity) between cryosensitive and cryoresistant cells under stressful conditions could help identifying the injuries leading to the degradation of the viability and functional activity of the cryosensitive cells. Cultivating *L. bulgaricus* CFL1 and ATCC

11842 in the whey-based medium until late exponential growth phase will ensure the recovery of such markedly different cell profiles, respectively, for the subsequent investigation of their membrane properties. This is the subject of the next chapter.

Acknowledgements

This work was supported by the National Institute for Agricultural Research (INRA) and the French National Research Agency (ANR) under the Investing in the Future Program, Grant n°ANR-10-IDEX-0003-02. We are grateful to Maarten van de Guchte for his advices, to Jiawei Xu for the experimental help with assessments of biological activities, and to Christophe Monnet for introduction to the use of IMG database.

1.3. Key points

- Important genetic differences suggested by the presence of two different CRISPR-Cas system types in *L. bulgaricus* CFL1, and only one and identical in *L. bulgaricus* ATCC BAA-365 and *L. bulgaricus* ATCC 11842;
- Higher growth rates of all *L. bulgaricus* strains in whey-based medium compared to MRS broth; confirmation of the reported preference of LAB for the utilisation of the disaccharide of their ecological niche: lactose;
- Tendency for higher growth rates of *L. bulgaricus* CFL1 compared to the other two strains, regardless of the growth medium; genes encoding a probable supplementary transporter for glucose (PTS^{Cel}), peptidases for the digestion of milk proteins and proteins for the biosynthesis of the vitamin and cofactor riboflavin;
- Cryosensitivity of *L. bulgaricus* CFL1 grown in whey-based medium, especially when harvested in late exponential growth phase; cryoresistance of *L. bulgaricus* ATCC BAA-365 and *L. bulgaricus* ATCC 11842, especially *L. bulgaricus* ATCC 11842;
- Possible explanation of the cryoresistance of *L. bulgaricus* ATCC BAA-365 and *L. bulgaricus* ATCC 11842 by the presence of three genes with orthology to a cold-adapted LAB encoding a cold-shock protein (*cspA*) and two ribosomal protein subunits, as well as the higher representation of genes involved in regulatory functions compared to *L. bulgaricus* CFL1;
- Evidence of possible differences in the composition of the cell surface of all three *L. bulgaricus* strains with putative implication in the cold response: large genomic differences in the *epsI* loci involved in the biosynthesis of exopolysaccharides; presence of genes coding for an additional ABC transporter (for the transport of polyamines such as putrescine/spermidine) in *L. bulgaricus* ATCC 11842;
- The acquisition of strain-specific genes occurred by horizontal gene transfer through genomic islands but not prophages;
- Parameters selected for the rest of the work: *L. bulgaricus* CFL1 and *L. bulgaricus* ATCC 11842; whey-based medium; late exponential growth phase.

II. Biophysical characterisation of the *Lactobacillus delbrueckii* subsp. *bulgaricus* membrane during cold and osmotic stress and its relevance for cryopreservation

2.1. Context and objectives

The cell membrane has been recognized as one of the main targets of cryoinjury. Previous works have characterised *L. bulgaricus* CFL1 membranes (fatty acid composition, lipid phase transitions, fluidity) and relationships to cryoresistance have been proposed. To further investigate the mechanisms underlying cell cryoinjury, the cryopreservation process was decomposed into major environmental stresses suffered by bacterial cells, namely cold and osmotic (an increased environmental osmolarity indeed occurs during freezing, which results from solutes cryoconcentration following ice nucleation) without ice formation. This work made it possible to evaluate the relative impact of both stresses on the biological activity and membrane characteristics of *L. bulgaricus*. Moreover, decoupling freezing in cold and osmotic stress allows obtaining valuable data by performing complementary analytical techniques that would not be feasible with ice formation. Different analytical techniques were thus employed for an in-depth characterisation of the membrane fatty acid composition and biophysical properties of *L. bulgaricus* under cold and osmotic stresses. Such characterisation should indeed allow to identify markers of cryoinjury and to better understand the underlying mechanisms of cell degradation.

The incidence of both environmental stresses on the biological activity of *L. bulgaricus* under the experimental conditions defined in the previous chapter (*L. bulgaricus* CFL1 and *L. bulgaricus* ATCC 11842 cultivated in whey-based medium until late exponential growth phase) was quantified through culturability and acidification activity losses by the plate count method and the CinAc system, respectively. The cold stress was performed by incubating cell suspensions at subzero temperature without nucleation of ice and the osmotic stress by incubating them in solutions of increasing concentrations of sucrose. In parallel, some membrane properties of both strains were assessed: membrane fatty acid composition was determined by gas chromatography-mass spectrometry (GC-MS) following extraction by means of accelerated solvent extraction (ASE); membrane fluidity was measured by steady state fluorescence anisotropy (spectrofluorimetry), that provide fluidity information of the membrane core (DPH) and surface (TMA-DPH); membrane lipids organization was characterised by FTIR spectroscopy by assessing the membrane acyl chains (νCH_2 *sym.*, at ~ 2850 cm^{-1}) and the membrane phospholipid headgroups (νPO_2^- *asym.* , at ~ 1220 cm^{-1}), informing on membrane core and surface, respectively. Fluidity and lipid organization were monitored upon cooling and at different osmolarities to identify the impact of both cryopreservation-related stresses on these membrane biophysical properties.

The results of this study have been published: *Applied Microbiology and Biotechnology,* 2017, 101:1427-1441.

2.2. Article

Authors
Julie Meneghel[1] • Stéphanie Passot[1] • Sébastien Dupont[2] • Fernanda Fonseca[1]

Title
Biophysical characterisation of the *Lactobacillus delbrueckii* subsp. *bulgaricus* membrane during cold and osmotic stress and its relevance for cryopreservation

Affiliations
[1] UMR GMPA, AgroParisTech, INRA, Université Paris-Saclay, 78850 Thiverval-Grignon, France
[2] Univ. Bourgogne Franche-Comté, AgroSup Dijon, PAM UMR A 02.102, 21000 Dijon, France
Address all correspondence to Fernanda Fonseca. Email: fonseca@grignon.inra.fr; Phone: +33 (0)1 30 81 59 40; Fax: +33 (0)1 30 81 55 97

Abstract
Freezing lactic acid bacteria often leads to cell death and loss of technological properties. Our objective was to provide an in-depth characterisation of the biophysical properties of the *Lactobacillus delbrueckii* subsp. *bulgaricus* membrane in relation to its cryoresistance. Freezing was represented as a combination of cold and osmotic stress. This work investigated the relative incidence of increasing sucrose concentrations coupled or not with subzero temperatures without ice nucleation on the biological and biophysical responses of two strains with different membrane fatty acid compositions and cryoresistances. Following exposure of bacterial cells to the highest sucrose concentration, the sensitive strain exhibited a survival rate of less than 10 % and 5 h of acidifying activity loss. Similar biological activity losses were observed upon freeze-thawing and after osmotic treatment for each strain, thus highlighting osmotic stress as the main source of cryoinjury. The direct measurement of membrane fluidity by fluorescence anisotropy was linked to membrane lipid organization characterised by FTIR spectroscopy. Both approaches made it possible to investigate the specific contributions of the membrane core and the bilayer external surface to cell degradation caused by cold and osmotic stress. Cold-induced membrane rigidification had no significant implication on bacterial freeze-thaw resistance. Interactions between extracellular sucrose and membrane phospholipid headgroups under osmotic stress were also observed. Such interactions were more evident in the sensitive strain and when increasing sucrose concentration, thus suggesting membrane permeabilization. The relevance of biophysical properties for elucidating mechanisms of cryoinjury and cryoprotection is discussed.

Keywords
Lactic acid bacteria • Freezing • FTIR spectroscopy • Membrane fluidity and organization • Phospholipid headgroups

Introduction

Lactic Acid Bacteria (LAB) are widely used as starters for manufacturing fermented foods and probiotic products, as well as in green chemistry applications. LAB are delivered to food companies in the form of highly concentrated, ready-to-use products. The commercialization of starters requires production and preservation techniques that maximize the technological properties and shelf life of bacterial cells. Freezing is a widely used preservation technique, and very fast cooling rates (immersion in liquid nitrogen) are currently applied in industry. However, fast freezing requires low storage temperatures (~ -50 °C for industrial application, ≤ -80 °C for culture collection) and often leads to a degradation of the viability and acidifying activity upon thawing (Smittle *et al*. 1972; Fonseca *et al*. 2006). Bacterial resistance to freezing and to frozen storage depends on many parameters including the bacterial species, growth conditions, protective additives, freezing rate and final storage temperature (Gomez Zavaglia *et al*. 2000; Fonseca *et al*. 2001). Applying slow cooling rates allows reproducible freezing protocols, but the biological response of LAB during freezing still needs to be characterised and linked to bacterial freezing tolerance.

The major physical events that take place during slow freezing are well documented (Mazur *et al*. 1972; Fonseca *et al*. 2016). Firstly, during the chilling step applied after fermentation, membrane lipid phase transition may occur. Upon cooling, the phospholipid bilayer changes from a fluid and disordered liquid-crystalline phase, to a rigid and ordered gel phase. This membrane solidification occurs at a temperature that mainly depends on cell type and growth conditions (Molina-Höppner *et al*. 2004; Ragoonanan *et al*. 2008; Gautier *et al*. 2013; Velly *et al*. 2014). Shortly thereafter or at the same time as the membrane lipid phase transition, water crystallizes and ice gradually forms in the extracellular matrix. No formation of intracellular ice was reported following LAB freezing in the presence of additives (Fonseca *et al*. 2006). The extracellular matrix becomes more and more concentrated and exerts an increasing osmotic pressure on the supercooled intracellular compartment. This osmotic gradient draws water out from the cells, leading to intracellular solute concentration. Cell dehydration and volume reduction proceed until the intracellular compartment reaches the maximal freeze-concentration and forms a glassy state. Cells thus become osmotically irresponsive to the extracellular matrix (Fonseca *et al*. 2016). During the subsequent reduction in temperature, the extracellular matrix continues to evolve with the formation of ice and freeze-concentration until it becomes a glass. After subsequent storage at low temperature, all these physical events are reversed during thawing before using LAB in industrial process.

The cell membrane is the primary target of damage following the sequential physical events previously described. Loss of membrane integrity, membrane permeabilization and leakage of intracellular contents were reported following freezing at slow cooling rates (Fernández Murga *et al*. 2001; Rault *et al*. 2007; Moussa *et al*. 2008; Simonin *et al*. 2015). The severity of membrane damage is dependent on the temperature value at which these physical transitions occur during freezing. Gautier *et al*. (2013) reported that the membrane of LAB with low lipid transition temperature exhibited no loss of membrane integrity following freezing and thawing. This membrane property is strongly related to fatty acid (FA) composition, which could be modulated by modifying LAB culture conditions (Fernández Murga *et al*. 2000; Beal *et al*. 2001; Wang *et al*. 2005a; Streit *et al*. 2008; Gautier *et al*. 2013). Furthermore, Fonseca *et al*. (2016) recently

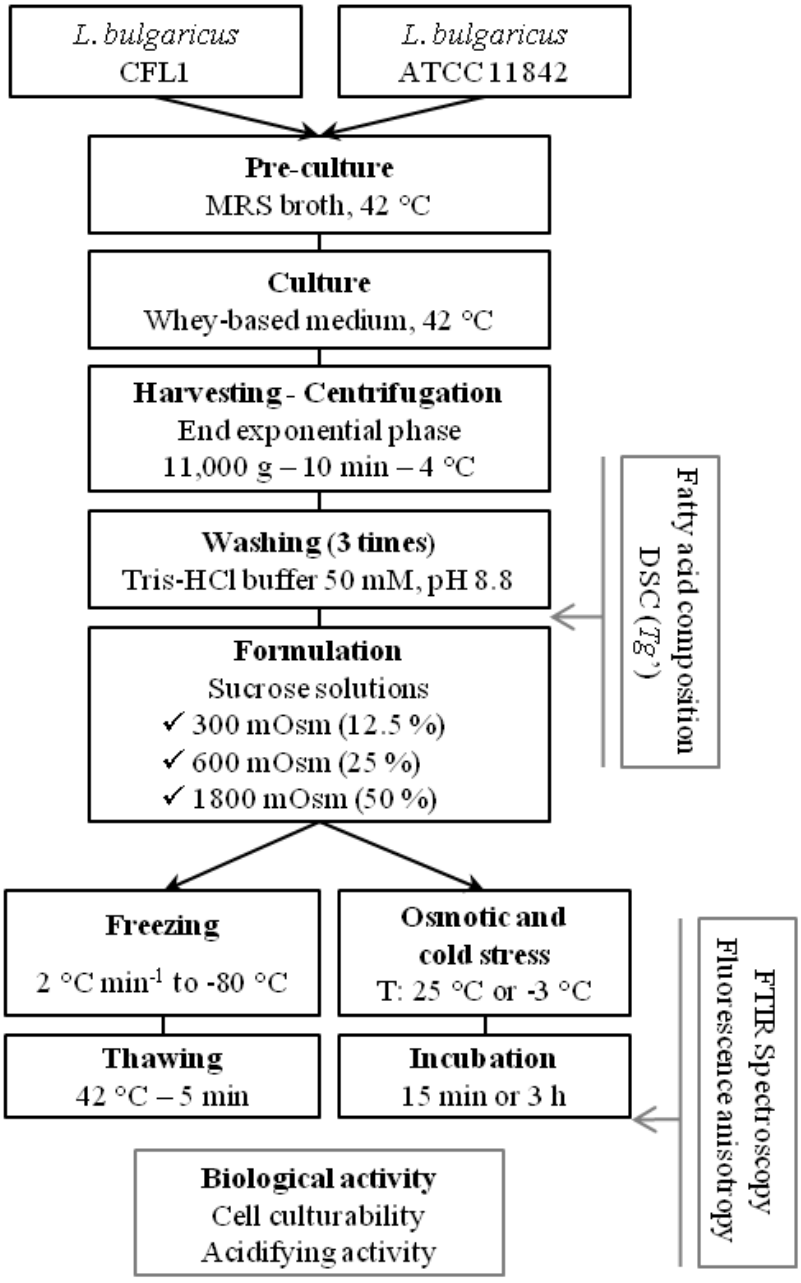

Figure IV.2-1: Diagram of the experimental approach used in the study and the main parameters investigated.

demonstrated that the freezing resistance of LAB could be improved by decreasing the glass transition temperature of the intracellular compartment by adding specific cryoprotective agents.

To limit freeze-thaw cellular damage, LAB concentrates are suspended in cryoprotective solutions. Disaccharides are non-penetrating cryoprotective agents (CPA) usually used for LAB preservation (Hubálek 2003). Sugars are known for their contribution to cell stabilization. Cells are immobilized in a sugar glassy matrix that strongly reduces the chemical and physical degradation reactions. Moreover, it has been reported that sugars exert a direct protective effect on membrane phospholipids and proteins (Crowe *et al*. 1988; Crowe *et al*. 1990; Santivarangkna *et al*. 2008a). Although the exact interaction mechanism between sugars and membranes is still unclear, two principal theories have emerged: preferential exclusion and water replacement. In physiological conditions, phospholipid hydrophilic head groups are involved in hydrogen bonding with several water molecules (Luzardo *et al*. 2000). The first theory hypothesizes that CPA are preferentially excluded from this hydration shell, thus reinforcing water hydrogen bonding to phospholipids. The second theory assumes a direct interaction between sugars and the membrane. According to this theory, sugars establish hydrogen bonds with phospholipid headgroups, thereby displacing the hydrating water molecules. Paradoxically, the addition of CPA also represents a source of osmotic stress for cells, especially as the extracellular medium cryoconcentrates. The freezing process may therefore be considered as a source of two major stresses for bacterial cells: cold and osmotic (Moussa *et al*. 2008; Simonin *et al*. 2015). To our knowledge, no study has yet focused on the individual contribution of exposure to cold temperatures and to increasing solute concentrations on the biological activity of LAB.

The aim of the present study was to better understand LAB cryoinjuries by analysing the relative incidence of cold and osmotic stresses on the biological response and on the membrane properties of two strains of *L. bulgaricus* with different cryoresistances. Membrane biophysical properties were dynamically assessed during cooling and at incremental solute concentrations to mimic a freezing procedure. Membrane fluidity and lipid organization were investigated at the centre and external surface of the phospholipid bilayers using spectrofluorimetry and FTIR spectroscopy, respectively.

Materials and Methods

Figure IV.2-1 presents the experimental approach used in this study as well as the main parameters investigated. Unless otherwise specified, all measurements were performed from three independent bacterial cultures.

Bacterial strains and culture conditions

Two strains of *Lactobacillus delbrueckii* subsp. *bulgaricus* were used in this study: *L. bulgaricus* CFL1 (CIRM-BIA; Rennes, France) and *L. bulgaricus* ATCC 11842 (Manassas, VA, USA).

Inocula were stored at -80 °C and were thawed at 42 °C for 5 min before inoculation in 30 mL of MRS broth (Biokar Diagnostics; Beauvais, France). Pre-culture was carried out at 42 °C up to the stationary

growth phase. Approximately 150 µL of the pre-culture was then used to inoculate 300 mL of whey-based medium and the culture was incubated at 42 °C until the end of the exponential growth phase (10 h for *L. bulgaricus* CFL1; 13 h for *L. bulgaricus* ATCC 11842) according to the procedure detailed by Gautier *et al*. (2013).

The whey-based medium consisted of 60 g L^{-1} mild whey powder (Euroserum; Port-sur-Saône, France) that was heated at 110 °C for 20 min. The supernatant obtained after centrifugation (17,000 x *g* for 30 min at 4 °C) and filtration was supplemented with 5 g L^{-1} yeast extract (Organotechnie SAS; La Courneuve, France) and sterilized at 110 °C for 20 min.

Absorbance measurements at 600 nm were regularly performed to adjust the culture time and the inoculation rate to guarantee harvest at the end of the exponential growth phase.

Cell cultures were cooled at 5 °C and harvested by centrifugation (11,000 x *g* for 10 min at 5 °C). Cell pellets were then washed three times in Tris-HCl buffer (50 mM, pH 8.8, Bio-Rad; Hercules, CA, USA) in order to remove growth medium constituents and excreted microbial metabolites that might negatively interfere with further analysis procedures.

Freezing and thawing protocol

Washed cell pellets were resuspended in the same weight (1:1 ratio) of a sucrose solution (20 % wt. sucrose in saline water, corresponding to a value of osmolarity of 600 mOsm L^{-1}, further referred to as mOsm). Cryotubes with a capacity of 2 mL were filled with 500 µL of cryoprotected bacterial suspension and inserted into a controlled rate freezer (EF600-103, Asymptote; Cambridge, UK) pre-cooled to 5 °C. The sample temperature was monitored by inserting a thermocouple (K type) into one cryotube. After a holding step of 10 min at 5 °C, the freezer was programmed to cool the sample device at 2 °C min^{-1}, from 5 °C to -80 °C. Frozen samples were stored at least 24 h at -80 °C and thawed for 5 min at 42 °C before evaluating the biological activity of bacterial cells.

Cold and osmotic stress treatments

The washed cell pellets were resuspended in the same weight of sucrose solutions of different concentrations (12.5, 25 and 50 % wt) to mimic their exposure to increasing cryoconcentrations. The final osmolarity of bacterial suspensions was: (i) isotonic (300 mOsm; 12.5 %), corresponding to the osmolarity of the fermentation medium; (ii) moderately hypertonic (600 mOsm; 25 %), corresponding to the osmolarity of the cryoprotective medium; or (iii) strongly hypertonic (1800 mOsm; 50 %), corresponding to an extreme cryoconcentration, which could be expected in the case of slow freezing rates. Osmolarities were determined using a Roebling osmometer (Type 13, Löser Messtechnik; Berlin, Germany).

The sucrose-cell suspensions were incubated either at room temperature (25 °C) or at -3 °C by immersion of the cryotubes in a Hyperion calibration liquid bath (AOIP; Ris Orangis, France) filled with silicone oil (Kryo 51, Lauda; Lauda-Königshofen, Germany) for 15 min and 3 h. The subzero temperature value applied for cold stress experiments was chosen from the liquidus curve of sucrose (between the melting point of 25

% and 50 % sucrose solutions: -2 °C and -6 °C, respectively) (Blond *et al*. 1997). The absence of ice formation during stress exposure was visually verified.
Previous tests were carried out to define the stress time that would ensure complete osmotic dehydration and significant degradation of the biological activity of the sensitive strain, *L. bulgaricus* CFL1 (Passot *et al*., personal communication; *Cryobiology*, Bristol, UK, 2010). The maximal cell volume reduction (16 %) was observed between 1 and 3 h of incubation under hypertonic conditions at 25 °C. No loss of biological activity was reported after incubation for 3 h under isotonic conditions at 25 °C.

Biological activity measurement

Two properties were measured to describe the biological activity of *L. bulgaricus*: cell culturability (CFU mL^{-1}) and acidifying activity (tm). The measurements were carried out: (i) before and after freezing; and (ii) 15 min and 3 h after exposure to cold and osmotic stress treatments. The biological activity of the frozen samples was determined immediately after thawing (5 min at 42 °C).

Culturability measurement

Bacterial cell concentration was determined using the agar plate count method. Samples were serially diluted in saline water and the appropriate dilutions were inoculated in the bulk of MRS agar (Biokar Diagnostics; Beauvais, France) plates in triplicate. Colonies were enumerated after incubating the plates for 48 h at 42 °C in anaerobic conditions (GENbox anaer, bioMerieux; Marcy l'Etoile, France). Plates containing between 30 and 300 colonies were kept for cell concentration calculation (in CFU mL^{-1}).
Culturability loss after freezing or stress treatments (in log (CFU mL^{-1})) was calculated using the following equation (Eq. 1):

$$\text{Culturability loss} = log\ \frac{[\text{CFU mL}^{-1}]_{\text{after treatment}}}{[\text{CFU mL}^{-1}]_{\text{reference}}} \quad (1)$$

where $[\text{CFU mL}^{-1}]_{\text{reference}}$ refers to cell concentration obtained before freezing or immediately after (15 min) resuspending cells in isotonic sucrose solution at 25 °C, and $[\text{CFU mL}^{-1}]_{\text{after treatment}}$ refers to cell concentration determined after freezing, or after a 15-min exposure to moderate and strong sucrose concentrations, or after a 3- h exposure to all osmotic conditions.

Acidifying activity measurement

The CinAc system (AMS; Frepillon, France) was used to evaluate the acidifying activity of the bacterial suspensions according to Fonseca *et al*. (2000), with minor modifications. Briefly, 150 mL of skim milk was reconstituted from dry powder at 100 g L^{-1} (EPI Ingredients; Ancenis, France), distributed in flasks, sterilized (at 110 °C for 20 min) and pre-warmed to 42 °C in a temperature-controlled bath. Following the inoculation of three flasks with 100 µL of the bacterial suspensions, their pH was continuously monitored

every 3 min until the end of the acidification. The minimum of the first-order derivative of the acidification curves represents the time required for the bacterial suspension to reach its maximum acidification rate in milk and was used as a discriminating descriptor between experimental conditions (tm, in min). The higher the tm value was, the longer the latency phase and the lower the acidifying activity were.
The acidifying activity loss ($dtm_{treatment}$, in min) after freezing or stress treatments was quantified as follows (Eq. 2):

$$dtm = tm_{\text{after treatment}} - tm_{\text{reference}} \quad (2)$$

where $tm_{reference}$ refers to the tm obtained before freezing or immediately after (15 min) resuspending cells in isotonic sucrose solution at 25 °C, and $tm_{after\text{-}treatment}$ refers to the tm determined after freezing, or after a 15-min exposure to moderate and strong sucrose concentrations, or after a 3-h exposure to all osmotic conditions. An increase of the dtm value corresponds to an increased loss of acidification activity during the considered treatment.

Differential scanning calorimetry (DSC): intracellular glass transition temperature

The intracellular glass transition temperature was determined with a differential scanning calorimeter (Diamond, Perkin Elmer LLC; Norwalk, CT, USA) equipped with a liquid nitrogen cooling accessory (CryoFill; Perkin Elmer) as previously described (Clarke *et al*. 2013; Fonseca *et al*. 2016). Cell pellets obtained after the washing steps with Tris-HCl buffer (**Fig. IV.2-1**) were additionally washed with peptone water (1 g L^{-1}) prior to DSC scanning. About 20 mg of cell pellets were sealed in an aluminum pan and samples were cooled to -100 °C and then heated to 20 °C at 10 °C min^{-1}. Cell pellets obtained from centrifuged cells resuspended in sucrose cryoprotective solution (20 % in saline water) as well as a sample of the sucrose solution (corresponding to the extracellular matrix) were also analysed for comparison. The glass transition temperatures of the intracellular contents and the sucrose solution, T_g'i and T_g'e (°C), respectively, were calculated from the first derivative of the heat flow recorded during warming (Fonseca *et al*. 2016).

Fatty acid (FA) composition

Membrane FA composition was determined on cell pellets obtained after the washing steps with Tris-HCl buffer (**Fig. IV.2-1**), according to the method fully described by Gautier *et al*. (2013) with minor modifications. Briefly, lipid extraction from washed cell pellets was performed by means of accelerated solvent extraction (ASE 350, Dionex; Sunnyvale, CA, USA) using three chloroform/methanol solvent ratios: 2:1, 1:1 and 1:2 (vol) under pressure at 100 °C. FA standards (Larodan; Solna, Sweden) including the cyclic FA cycC19:0 standard as well as freshly extracted phospholipid fatty acyl residues were methylated with trimethylsulfonium hydroxide (TMSH, Sigma-Aldrich; St. Louis, MO, USA), and analysed by gas chromatography-mass spectrometry (GC-MS) for their identification and quantification. A Hewlett-Packard 6890 gas chromatograph (GMI; Ramsey, MI, USA) was used. It was equipped with a capillary column packed with 70 % cyanopropyl polysilphenylene-siloxane BPX70 (60 m × 0.25 mm, with a film

thickness of 0.25 µm; SGE Analytical Science Pty Ltd.; Victoria, Australia), coupled to a mass spectrometer (5973, Agilent Technologies; Avondale, PA, USA). Results were expressed as FA percentages.

Steady state fluorescence anisotropy: membrane fluidity measurement

Membrane fluidity of bacterial cells was assessed by measuring the degree of polarization of two fluorescent probes, 1,6-diphenyl-1,3,5-hexatriene (DPH) and 1-[4 (trimethylamino) phenyl]-6-phenyl-1,3,5-hexatriene (TMA-DPH). These probes have strong lipophilic properties that allow them to be inserted into lipid bilayers of models and also complex cellular systems such as Gram-positive bacteria (Tourdot-Maréchal *et al*. 2000; Tymczyszyn *et al*. 2005; Chu-Ky *et al*. 2005; Martos *et al*. 2007; Passot *et al*. 2014), Gram-negative bacteria (Chadeau *et al*. 2012), yeasts (Simonin *et al*. 2008; Abe and Hiraki 2009) or plant cells endospores (Dubas *et al*. 2013). Since *L. bulgaricus* does not accumulate lipids in the intracellular compartment, both probes will exclusively locate in the only available cellular lipid reservoir, the cytoplasmic membrane: (i) within the hydrocarbon core for DPH, fully apolar; and (ii) at the water/lipid interface for its cationic derivative TMA-DPH (Ben-Yashar and Barenholz 1991; Kaiser and London 1998).

Stock solutions of DPH (0.6 mM, Sigma-Aldrich; St. Louis, MO, USA) and TMA-DPH (2 mM, Molecular Probes; Eugene, OR, USA) were prepared in dimethylsulfoxide (DMSO, Sigma-Aldrich; St. Louis, MO, USA). The method described by Chu-Ky *et al*. (2005) with minor modifications was applied. Briefly, bacterial samples incubated for 3 h at 25 °C in sucrose solutions of different concentrations were diluted in MES-KOH buffer (50 mM, pH 5.5, Sigma-Aldrich; St. Louis, MO, USA) supplemented with 10 mM glucose to obtain an OD600 nm of 0.5. DPH or TMA-DPH from stock solutions was then added to obtain a final probe concentration of 3 µM or 2 µM, respectively. Staining of bacterial solutions was performed for 3 min in darkness at 25 °C prior to centrifugation (18,500 x *g* for 2 min). The pellets were resuspended in the same volume of the corresponding sucrose solution to maintain osmotic condition during the measurement, and 3 mL were loaded into a stirred quartz cuvette. Fluorescence anisotropy was measured on a Fluorolog-3 spectrofluorometer (Jobin-Yvon Horiba; Longjumeau, France) as previously described (de Sarrau *et al*. 2013). The excitation wavelength was set at 360 nm and the emission wavelength at 430 nm. Polarizers were located on the excitation source and on the two photomultiplier tubes to measure anisotropy. Steady state anisotropy (***r***) was calculated according to the following equation (Eq. 3):

$$\boldsymbol{r} = \frac{I_{vv} - G \times I_{vh}}{I_{vv} + 2G \times I_{vh}} \quad (3)$$

where I_{vv} and I_{vh} represent the fluorescence intensity obtained with the vertical and horizontal orientations of the excitation and emission polarizers (*e.g.*, I_{vv} is the vertical excitation and vertical emission) and $G = I_{hv}/I_{hh}$ is a correction factor accounting for the polarization bias in the detection system.

Fluorescence anisotropy is inversely proportional to membrane fluidity: the higher the anisotropy (***r***) is, the more rigid the membrane will be. Anisotropy values were obtained at different sample temperatures ranging from 42 °C to 0 °C using a Peltier module (LFI-3751, Wavelength electronics; Bozeman, MT, USA). Temperature dynamics were performed from two independent bacterial cultures.

Fourier Transform InfraRed (FTIR) spectroscopy: phospholipid organization

Phospholipid organization in biological membranes can be evaluated by FTIR spectroscopy by measuring the vibrational energy of specific chemical functional groups relevant to the lipid bilayer. The study was focused on the position of: (i) the symmetric CH_2 stretching vibration band (*νCH_2 sym.*) located at approximately 2,850 cm^{-1} and arising from hydrocarbon chains of phospholipids (Crowe *et al*. 1989; Gautier *et al*. 2013; Wolkers and Oldenhof 2015); (ii) the asymmetric PO_2^- stretching vibration band (*νPO_2^- asym.*) located at approximately 1,220 cm^{-1} and arising from the phosphate moiety of phospholipid headgroups (Goñi and Arrondo 1986; Linders *et al*. 1997; Arrondo and Goñi 1998; Lewis and McElhaney 1998; Díaz *et al*. 2003; Wolkers *et al*. 2010; Dianawati *et al*. 2012).

Measurements were carried out on a Nicolet Magna 750 FTIR spectrometer (Thermo Fisher Scientific; Madison, WI, USA) equipped with a mercury/cadmium/telluride (MCT) detector and a variable temperature cell holder (Specac Ltd.; Orpington, Kent, UK), as described by Gautier *et al*. (2013). A thermocouple inserted as close as possible to the sample made it possible to accurately cool it at a rate of 2 °C min^{-1} by continuously pouring liquid nitrogen into the cell holder. The optical bench was continuously purged with dry air (Balston; Haverhill, MA, USA) to remove any spectral contribution from water vapor. Omnic software (version 7.1, Thermo Fisher Scientific; Madison, WI, USA) was used for spectra acquisition: 32 co-added scans were collected every 45 s with a resolution of 4 cm^{-1} in the mid-IR region from 4,000 to 900 cm^{-1}.

Bacterial samples incubated for 3 h at 25°C in sucrose solutions of different concentrations were centrifuged (16,100 x *g* for 5 min) and the cell pellet was tightly sandwiched between two calcium fluoride windows (ISP Optics; Riga, Latvia). The windows were inserted into the cell holder and infrared absorption spectra were recorded during cooling from 50 °C to -50 °C at 2 °C min^{-1}.

Spectra analysis (determination of peak location and lipid phase transition temperature) was performed using ASpIR software (Infrared Spectra Acquisition and Processing, INRA; Thiverval-Grignon, France). To determine specific peak locations from each spectrum, second-order derivatives were calculated, smoothed following a 7-point Savitzky-Golay algorithm and multiplied by -1. Wavenumbers (or frequencies) of the *νCH_2 sym.* and *νPO_2^- asym.* peaks were plotted as a function of temperature. The *νCH_2 sym.* plots were fitted with a curve based on an asymmetric sigmoid transition function, and the first-order derivative was calculated. Its maxima was taken as the lipid phase transition following freezing ($T_{s\ lip}$). Ice nucleation was also determined following the upshift of the combination band of OH libration and bending modes of water (*νH_2O*) from approx. 2,150 cm^{-1} to 2,220 cm^{-1} (Gautier *et al*. 2013).

Statistical analyses

Statistical analyses were performed in R 3.2.3 using the R Commander package. Sample means were compared after verifying the normality of their distribution at a 95 % confidence interval. The significance of results was assessed at a 90 % confidence level (p value < 0.1).

Results

Cryoresistance, membrane fatty acid composition and intracellular glass transition temperature of *L. bulgaricus* CFL1 and ATCC 11842 grown in whey-based medium

Following freezing and thawing, *L. bulgaricus* ATCC 11842 exhibited no loss of culturability or acidifying activity and thus appeared to be highly resistant to freezing. Conversely, large losses of culturability (-1.4 log units, corresponding to a survival rate of 4 %) and acidifying activity (dtm = 250 min, corresponding to a 4.2 h increase in the acidifying time) were observed for *L. bulgaricus* CFL1 (data reported in **Table S1**, **Appendix III**).

Membrane fatty acid compositions of the resistant and sensitive strains are summarized in **Table IV.2-1**. Regardless of the strain, the bacterial membrane was composed of four main fatty acids (FA), accounting for more than 80 % of the total FA: C14:0, C16:0, C16:1 and C18:1. A total of 14 FA were detected (low levels of C13:0, C15:0, C17:0, C19:0, C20:0 and C22:0 were detected and quantified; since they represented less than 1 % of the total FA, they were not included in **Table IV.2-1**). These results are in agreement with the membrane FA composition of different strains of *L. bulgaricus* reported in the literature (Veerkamp 1971; Gomez Zavaglia *et al*. 2000; Tymczyszyn *et al*. 2005; Gautier *et al*. 2013).

Table IV.2-1: Membrane fatty acid composition (relative percentages) of *L. bulgaricus* ATCC 11842 and *L. bulgaricus* CFL1 grown in a Whey-based medium and harvested at the exponential growth phase. Data presented are means of three independent replicates ± standard deviation.

Fatty Acids (FA)	ATCC 11842	CFL1
C12:0	3.6 ± 0.7	1.9 ± 0.3
C14:0	7.9 ± 1.7	10.2 ± 1.5
C16:0	27.4 ± 2.7	36.9 ± 4.2
C16:1	21.3 ± 1.9	22.5 ± 1.6
C18:0	6.9 ± 1.1	7.2 ± 2.9
C18:1	25.3 ± 4.0	15.1 ± 4.3
C18:2	2.0 ± 0.6	1.4 ± 0.3
C19:0cyc	3.9 ± 0.9	3.3 ± 0.5
Total SFA[a]	47.5 ± 6.2	57.7 ± 6.0
Total UFA[a,b]	48.6 ± 5.3	39.0 ± 5.7
UFA:SFA	1.04 ± 0.24	0.69 ± 0.16
Long chain FA[a,c]	38.6 ± 3.3	27.7 ± 1.9

SFA: Saturated FA, UFA: Unsaturated FA

[a] Total SFA, total UFA and long chain FA include FA from the table plus FA representing less than 1 % of total FA and not shown in the table

[b] Total UFA does not comprise C19:0cyc

[c] Long chain FA comprise FA with 18 carbon atoms or more

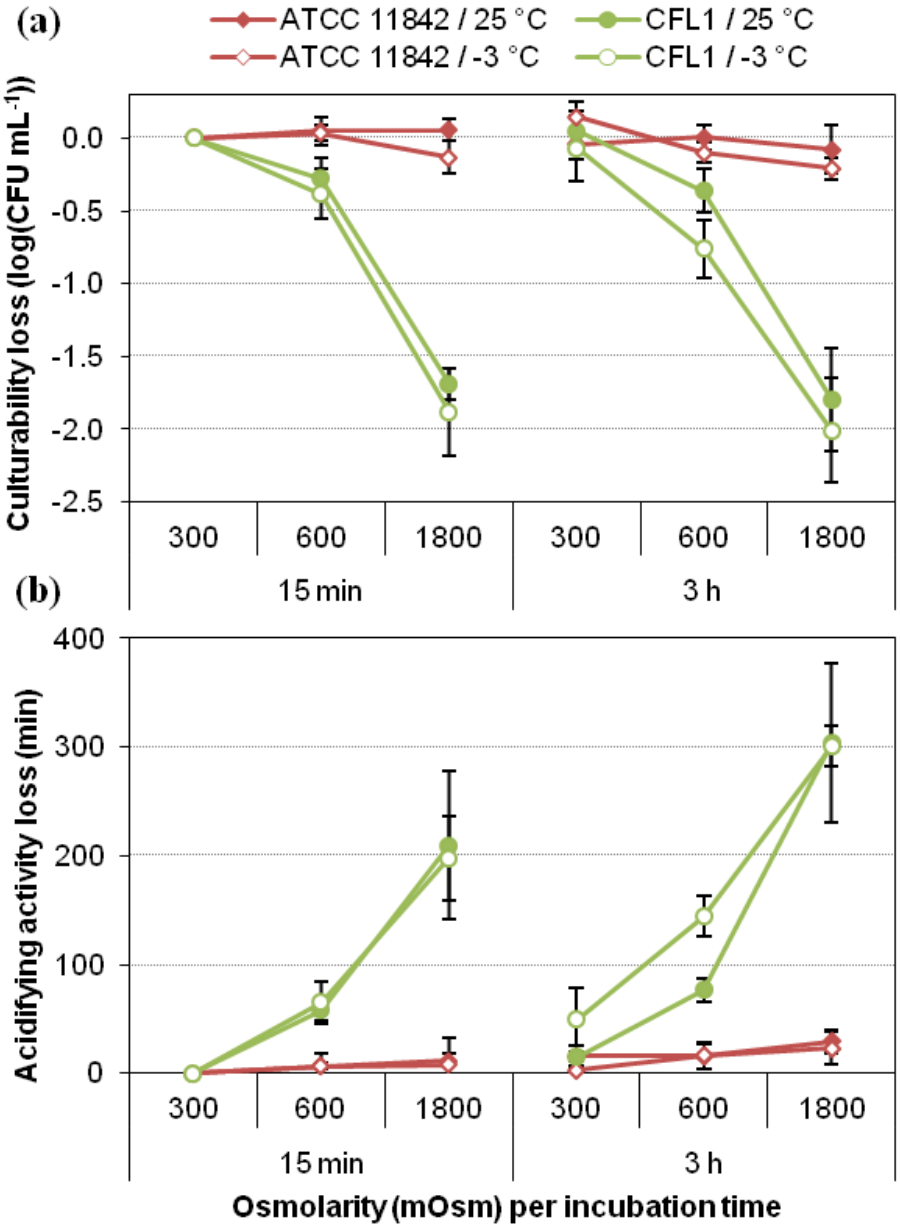

Figure IV.2-2: Biological activity losses of *L. bulgaricus* ATCC 11842 (in red) and *L. bulgaricus* CFL1 (in green) submitted to an osmotic stress at 25 °C (filled symbols) or -3 °C (open symbols) for 15 min (left side) and 3 h (right side) **(a)** Loss of culturability (in log (CFU mL^{-1}) and **(b)** loss of acidifying activity (in min). Values measured after 15 min of exposure at 25 °C at isotonic condition were considered as the reference condition for the calculation of losses.

Both strains exhibited different relative contents of C16:0 and C18:1. The membrane of *L. bulgaricus* ATCC 11842 was richer in C18:1 and, thus, in unsaturated fatty acid (UFA) than the membrane of *L. bulgaricus* CFL1 (p value = 0.04). This resulted in different ratios of unsaturated to saturated fatty acids (UFA:SFA): 1.0 for *L. bulgaricus* ATCC 11842 and 0.7 for *L. bulgaricus* CFL1 (p value = 0.1) and in a higher proportion of long chain FA (number of carbons ≥ 18) for *L. bulgaricus* ATCC 11842 (38.6 ± 3.3 %) compared to *L. bulgaricus* CFL1 (27.7 ± 1.9 %) (p value = 0.01).
Furthermore, both strains exhibited slightly different values of intracellular glass transition temperature: -19.2 °C for the washed *L. bulgaricus* ATCC 11842 (± 1.2 °C) and -17.4 °C for the washed *L. bulgaricus* CFL1 (± 0.9 °C). Adding the cryoprotective solution led to a T_g'i decrease in both strains with -27.6 °C (± 1.1 °C) and -25.5 (± 1.6 °C), respectively. The values reported for *L. bulgaricus* CFL1 were consistent with the recent work of Fonseca *et al*. (2016).

Influence of cold and osmotic stress treatments on the biological activity of *L. bulgaricus* (culturability and acidifying activity)

Regardless of the stress condition, *L. bulgaricus* ATCC 11842 exhibited no degradation of culturability and acidifying activity (**Fig. IV.2-2**, data reported in **Table S1**, **Appendix III**). Only a minor loss of acidifying activity (less than 30 min) was observed when cells were incubated for 3 h at -3 °C under the strongly hypertonic condition (1800 mOsm, p value = 0.4). Conversely, the biological activity of *L. bulgaricus* CFL1 was strongly affected by osmotic stress treatments. When considering incubation at 25 °C, loss of culturability progressively increased with increasing osmolarity: no loss at 300 mOsm (p value = 0.5), and losses of 0.4 and 1.8 log units at 600 and 1800 mOsm, respectively (p values = 0.1 and 0.001, respectively). No difference in culturability loss was observed in terms of incubation time (p values > 0.1). The same incremental trend was observed for the loss of acidifying activity but with an impact of the incubation time, especially for the strong hypertonic stress condition (1800 mOsm). Exposure of *L. bulgaricus* CFL1 cells to a mild hypertonic stress (600 mOsm) resulted in an increase of the acidifying time of 85 min, reaching 200 min (or 300 min after 3 h) under strong hypertonic conditions (1800 mOsm) at 25 °C. An incremental decrease of viability following gradual hyperosmotic stresses with sucrose was also observed by Ragoonanan *et al*. (2008) on *Geobacter sulfurreducens*.
The sensitivity of *L. bulgaricus* CFL1 to cold stress appeared quite weak. When considering incubation at -3 °C, no degradation of the biological activity was observed for the isotonic condition after 3 h of incubation (p values > 0.1). The impact of the incubation temperature appeared to be significant only for the moderate hypertonic condition performed for 3 h and resulted in a doubling of the culturability and acidifying activity losses compared to the same treatment performed at 25 °C (p values < 0.05). Degradation of biological activity observed following freezing and thawing of *L. bulgaricus* CFL1 could thus be ascribed to a strong osmotic stress.

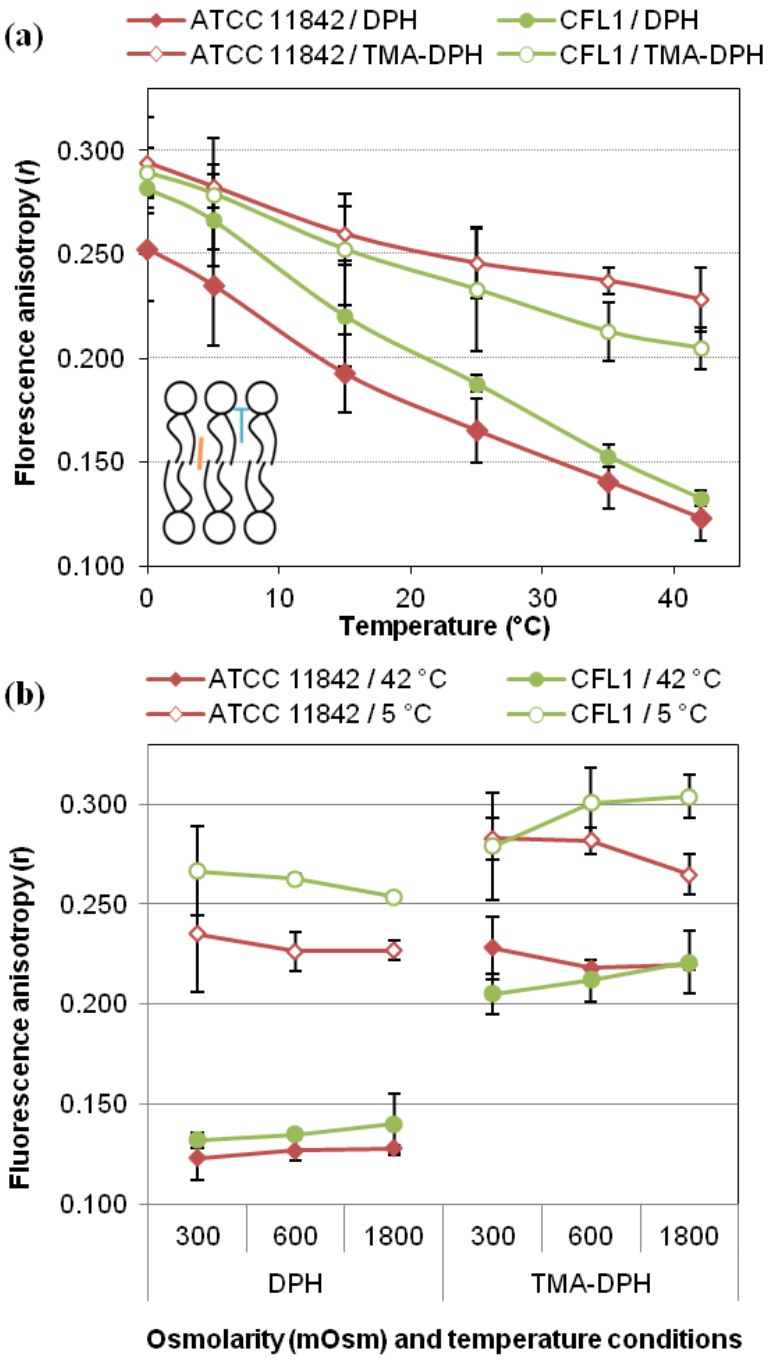

Figure IV.2-3: Membrane fluorescence anisotropy (***r***) of *L. bulgaricus* ATCC 11842 (in red) and *L. bulgaricus* CFL1 (in green) **(a)** upon cooling under isotonic conditions and **(b)** as a function of osmotic strength for selected temperatures (42 °C and 5 °C). Filled symbols represent **(a)** DPH anisotropy or **(b)** 42 °C and open symbols represent **(a)** TMA-DPH anisotropy or **(b)** 5 °C. The diagram inserted in **(a)** illustrates the position of the DPH (orange bar) and the TMA-DPH probes (blue "T") within the lipid bilayer.

Influence of cold and osmotic stress treatments on membrane fluidity evaluated by fluorescence anisotropy

The fluorescence anisotropy (***r***) of DPH and TMA-DPH probes is negatively related to membrane fluidity (*i.e.*, positively related to membrane rigidity). A schematic drawing was inserted in **Fig. IV.2-3a** to illustrate the commonly reported location of these fluorescent probes within a lipid bilayer.

Cold stress

When considering the LAB production process, the fermentation step is followed by chilling from 42 °C to 5 °C to stop any metabolic activity, and some changes in membrane fluidity are expected. **Figure IV.2-3a** illustrates the evolution of membrane fluidity under isotonic conditions following cooling for both *L. bulgaricus* strains (data reported in **Table S2**, **Appendix III**).

Regardless of the strain and probe, decreasing temperatures resulted in an increase in fluorescence anisotropy and, as a result, in membrane rigidification (p values < 0.02 for DPH and p values < 0.07 for TMA-DPH). Furthermore, this rigidification appeared to be more pronounced at the centre of the membrane (DPH) than at the periphery (TMA-DPH), with an increase of anisotropy of approximately 100 % and 30 %, respectively.

When comparing both strains, some differences can also be observed in membrane fluidity. At 42 °C (LAB growth temperature), membrane fluidity at the centre was similar for both strains (p value = 0.4), whereas the external membrane surface tended to be more rigid in *L. bulgaricus* ATCC 11842 than in *L. bulgaricus* CFL1 (p value = 0.2). At 0 °C (close to the formation of ice), the membrane core of *L. bulgaricus* ATCC 11842 became more fluid than *L. bulgaricus* CFL1, but the external surface of both strains reached similar rigidity levels. Furthermore, the membrane core and external surface of *L. bulgaricus* CFL1 were characterised by similar anisotropy values at 0 °C (0.285 ± 0.011, p value = 0.6).

Osmotic stress

Figure IV.2-3b illustrates the influence of osmotic stress on membrane fluidity of both strains for two values of temperature representative of our experimental approach: 42 °C for the growth temperature and 5 °C for the temperature applied during harvesting and formulation steps (data reported in **Table S2**, **Appendix III**). Exposing cells to hypertonic conditions did not seem to affect membrane core fluidity (DPH). A slight change in membrane fluidity was detected at 5 °C for the external membrane surface (TMA-DPH) but was not significant; increasing sucrose concentrations tended to increase anisotropy values (*i.e.*, increased membrane rigidity) for *L. bulgaricus* CFL1 (p value = 0.3), and to decrease anisotropy values (*i.e.*, increased membrane fluidity) for *L. bulgaricus* ATCC 11842 (p value = 0.2).

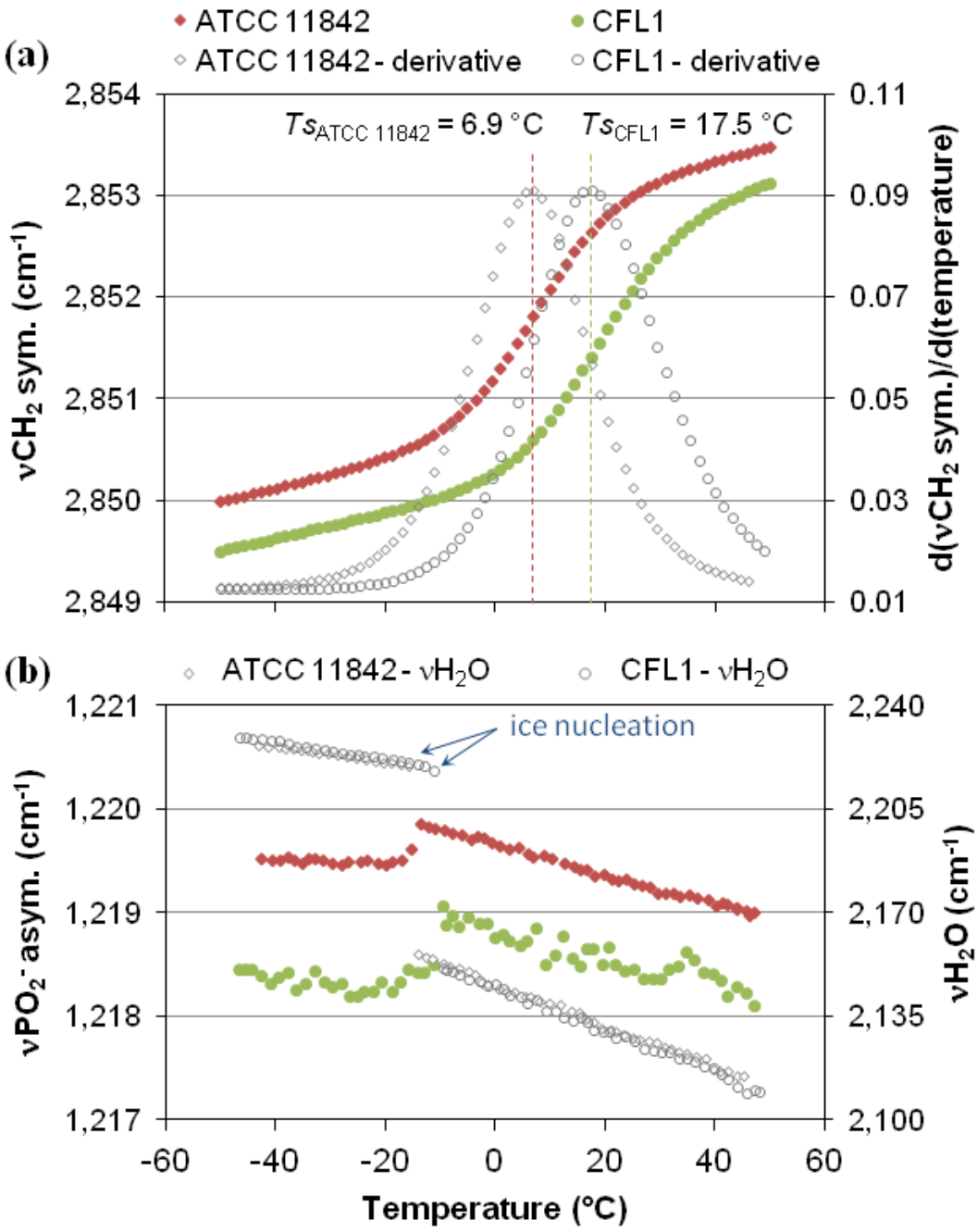

Figure IV.2-4: Peak position of the **(a)** symmetric CH_2 stretching (*νCH_2 sym.*) and **(b)** asymmetric PO_2^- stretching (*νPO_2^- asym.*) vibration bands arising from *L. bulgaricus* ATCC 11842 (in red) and *L. bulgaricus* CFL1 (in green) upon cooling under isotonic conditions. In panel **(a)**, lipid solidification temperatures (*Ts*) are highlighted by the maximum of the first derivatives of the curves (open symbols). In panel **(b)**, ice nucleation corresponds to the shift in the H_2O libration and bending band (νH_2O, open symbols) from approx. 2,150 cm-1 to 2,220 cm-1. For the sake of clarity, standard deviations were not included.

Influence of cold and osmotic stress treatments on membrane phospholipid organization evaluated by FTIR spectroscopy

FTIR spectroscopy was used to characterise changes in membrane phospholipid organization by tracking the vibration band position of two specific chemical groups during freezing: (i) the *νCH_2 sym.* arising from phospholipid acyl chains (*i.e.*, related to the central part of the bilayer); and (ii) the *νPO_2^- asym.* involving phosphate groups of the external surface of the bilayer.

Cold stress

Figures IV.2-4a and **IV.2-4b** display the evolution of the band position of *νCH_2 sym.* and *νPO_2^- asym.* following cooling from 50 °C to -50 °C for both strains under isotonic conditions, respectively. In **Fig. IV.2-4b**, the νH_2O was also plotted with temperature to identify the ice nucleation event (data reported in **Table S2**, **Appendix III**). Ice formation was visible during cooling as an abrupt increase in wavenumber, which occurred spontaneously at around -10 °C.

When considering the *νCH_2 sym.* (**Fig. IV.2-4a**), decreasing temperatures resulted in a shift of the band position to lower wavenumber values. This is known to reflect membrane lipid phase transition from a relatively disordered fluid lipid state, referred to as the liquid crystalline phase, to an ordered rigid lipid state, referred to as the gel phase (Crowe *et al*. 1989; Wolkers and Oldenhof 2015).

The first derivative of the *νCH_2 sym.* vs. the temperature curve was plotted to determine the lipid phase transition during freezing ($T_{s\ lip}$), reported in **Fig. IV.2-4a**. *L. bulgaricus* ATCC 11842 exhibited a significantly lower $T_{s\ lip}$ value (6.9 ± 1.3 °C) than *L. bulgaricus* CFL1 (17.5 ± 1.8 °C) (*p* value = 0.001). In addition, *L. bulgaricus* ATCC 11842 cells showed higher *νCH_2 sym.* wavenumbers regardless of the temperature, and especially in the frozen state (*p* value = 0.01 at -48 °C). This suggests that membrane of *L. bulgaricus* ATCC 11842 exhibited less ordered lipid acyl chains than membrane of *L. bulgaricus* CFL1.

When considering PO_2^- groups (**Fig. IV.2-4b**), decreasing temperature resulted in a linear elevation of the band position until ice nucleation occurred, at which point an abrupt wavenumber downshift was observed. The peak position remained at quite constant values with further temperature decrease. Regardless of the temperature, *L. bulgaricus* ATCC 11842 cells exhibited higher PO_2^- wavenumber positions than *L. bulgaricus* CFL1 cells (*p* values < 0.07). Moreover, the downshift observed upon ice nucleation was less extensive for strain ATCC 11842 compared to strain CFL1.

Since the thermotropic behaviour of the *νPO_2^- asym.* was directly affected by ice nucleation, the vibration of PO_2^- moieties could be attributed to bacterial macromolecules that are directly in contact with the extracellular medium, such as the external leaflet of the phospholipid bilayer and not nucleic acids or intracellular phosphorylated molecules (Dianawati *et al*. 2012).

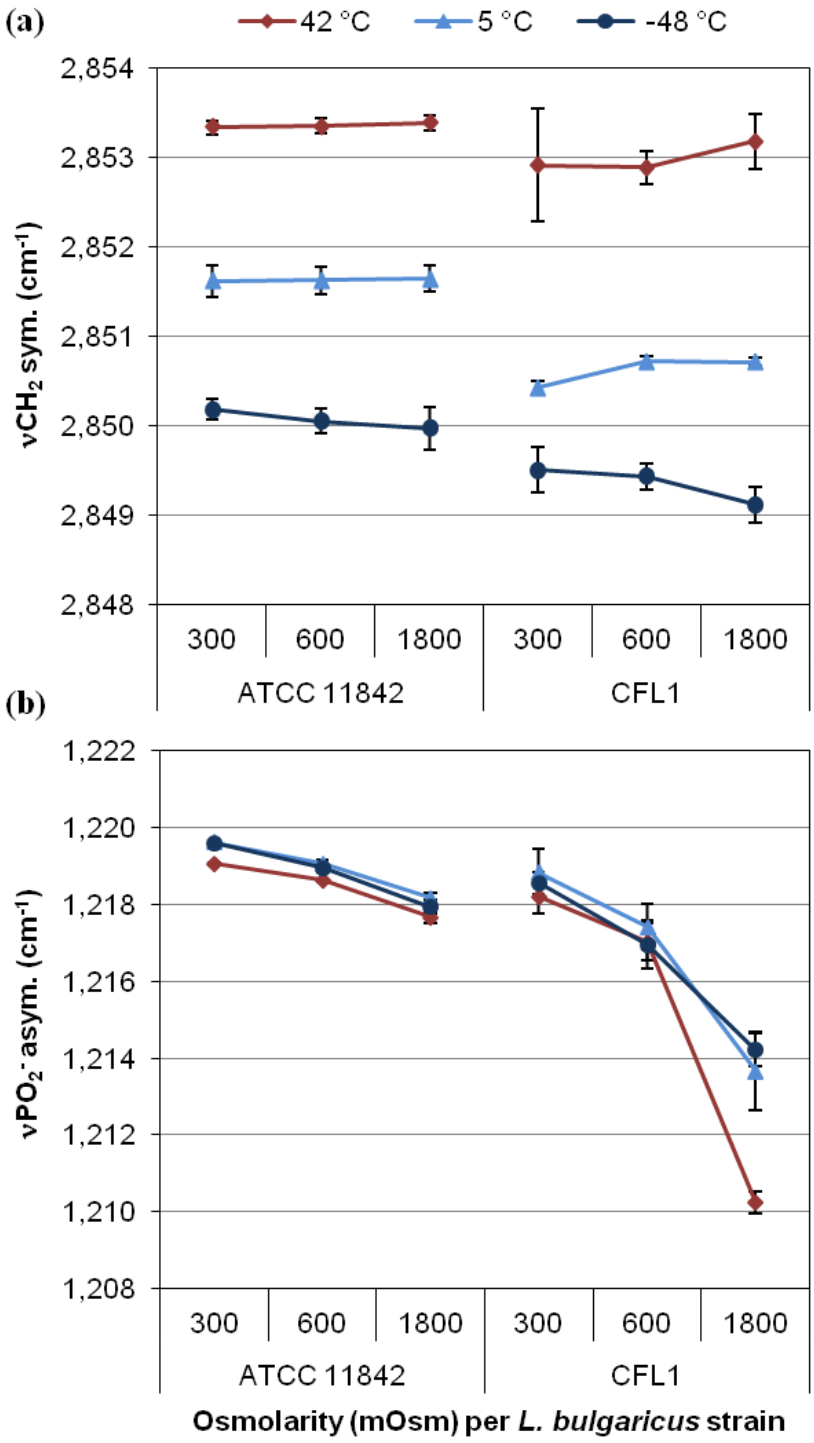

Figure IV.2-5: Peak position of the **(a)** symmetric CH_2 stretching (*vCH_2 sym.*) and **(b)** asymmetric PO_2^- stretching (*vPO_2^- asym.*) vibration bands arising from *L. bulgaricus* ATCC 11842 (left) and *L. bulgaricus* CFL1 (right) as a function of osmotic strength for selected temperatures.

Osmotic stress

Applying osmotic stress to cells did not modify the lipid phase transition temperature ($T_{s\ lip}$) for *L. bulgaricus* ATCC 11842 (*p* values > 0.2) but resulted in a 4 °C decrease of the $T_{s\ lip}$ value for *L. bulgaricus* CFL1 under strong hypertonic conditions (13.6 °C ± 2.2 °C) (*p* value = 0.08). **Figures IV.2-5a** and **IV.2-5b** illustrate the influence of osmotic stress on the position of the vCH_2 *sym.* and vPO_2^- *asym.* for selected values of temperatures, respectively (data reported in **Table S2**, **Appendix III**). The value of -48 °C corresponds to the extracellular glass transition temperature (T_g'e).

When considering *L. bulgaricus* ATCC 11842 (**Fig. IV.2-5a**), no change in the peak position of the vCH_2 *sym.* (related to the membrane core; **Fig. IV.2-5a**) with osmolarity was observed, regardless of the temperature values (*p* values > 0.2) (consistent with the DPH fluidity invariability with osmolarity increase in **Fig. IV.2-2b**). However, for the vPO_2^- *asym.*, a slight shift to lower wavenumbers when increasing osmolarity was observed. Consequently, for strain ATCC 11842, osmotic stress would not affect membrane core conformational order. It would, however, affect the conformational order of phospholipid headgroups, but only to a slight extent.

When considering *L. bulgaricus* CFL1, cell exposure to hypertonic conditions extensively modified the lipid membrane organization (**Figs. IV.2-5a** and **IV.2-5b**). At 5 °C, the vCH_2 *sym.* slightly upshifted with increasing osmolarity, denoting a higher conformational disorder of the lipid acyl chains. However, the shift occurred to a lower wavenumber in the frozen state, indicative of a conformational ordering of the lipid acyl chains (*p* values < 0.2). The vPO_2^- *asym.* also shifted to lower wavenumbers in *L. bulgaricus* CFL1, but to a greater extent than *L. bulgaricus* ATCC 11842, especially under strong hypertonic conditions at 42 °C (*p* values < 0.03). The external surface of the membrane of *L. bulgaricus* CFL1 was therefore extensively affected by hypertonic stress.

Discussion

Even if the physical events that occur during the freezing of cells are well-known at this time, maintaining their biological activity still remains a challenge, especially for lactic acid bacteria (LAB). Freezing can be considered as a combination of different stresses applied to bacterial cells: exposure to cold temperatures, ice formation and high concentrations of solutes. When applying slow cooling rates, cells are densely packed in the cryoconcentrated matrix, sharply reducing the direct contact between ice crystals and cells (Fonseca *et al*. 2006). The present work thus focused on the study of the individual contribution of cold and osmotic stress on the biophysical properties of bacterial membranes in relationship to the degradation of biological activity for two strains of LAB with different cryoresistances. To our knowledge, only two studies have applied a similar approach to the Gram-negative bacterium *E. coli* (Moussa *et al*. 2008; Simonin *et al*. 2015). The authors reported that maintaining cell suspensions in the presence of glycerol in a supercooled state for several hours (-20 °C without the formation of ice) was more damaging for cell viability and membranes than cell exposure to high concentrations of glycerol. In the case of *L. bulgaricus* CFL1, a Gram-positive

bacterium, the detrimental effect of exposure to cold temperatures appeared quite limited and was detected only after 3 h at moderate hyperosmotic conditions. Conversely, high losses of culturability and acidifying activity were observed after only 15 min of exposure to strong hyperosmotic conditions, making osmotic stress the most cell-damaging event following freezing. Exposing *L. bulgaricus* cells to osmotic stress (*i.e.*, to high concentrations of sucrose, a non-permeating molecule) induces water transport from the intracellular medium of the cell to the extracellular medium, which, in turn, will result in cell dehydration and cell volume contraction. Depending on the flexibility of the membrane, cell volume reduction could easily occur (*L. bulgaricus* ATCC 11842, the resistant strain) or be associated with considerable mechanical constraints (*L. bulgaricus* CFL1, the sensitive strain), possibly leading to membrane leakage.

The analysis of membrane fatty acid (FA) composition, lipid phase transition ($T_{s\ lip}$) and fluidity determined by fluorescence anisotropy showed that both strains exhibited different cytoplasmic membrane properties. The membrane of the resistant strain (*L. bulgaricus* ATCC 11842) was characterised by a higher content of UFA (49 %), a lower lipid phase transition following cooling ($T_{s\ lip}$ = 6.9 °C) and higher membrane fluidity at the centre and external surface at 0 °C than the membrane of the sensitive one (*L. bulgaricus* CFL1: UFA = 39 %; $T_{s\ lip}$ = 17.5 °C). The relationship between membrane composition, in particular the presence of unsaturated fatty acids, and the improvement of cryoresistance of LAB is well established in literature (Beal *et al*. 2001; Streit *et al*. 2011; Gautier *et al*. 2013). The UFA:SFA ratio is sometimes used for evaluating membrane fluidity (Álvarez-Ordóñez *et al*. 2008). The higher the UFA:SFA ratio, the more fluid the membrane and the higher the cryoresistance are. When considering the growth temperature (42 °C), the membranes of both strains exhibited similar fluidity values, despite different UFA:SFA ratios. The higher proportion of long chain FA within the membrane of *L. bulgaricus* ATCC 11842 (38.6 %) compared to CFL1 (27.7 %) could compensate for the fluidifying effect from unsaturations (Denich *et al*. 2003). Membrane fluidity could therefore be correlated with a combination of different fatty acid structures, including unsaturations and chain length. However, membrane fluidity is also dependent on temperature and it is thus important to determine its evolution with a temperature profile relevant to the process studied. In previous works, we showed that by modifying growth culture conditions, the freezing resistance of *L bulgaricus* CFL1 could be improved (Gautier *et al*. 2013; Passot *et al*. 2014). By growing cells in MRS broth, the membrane became rich in cyclic and unsaturated fatty acids, which, in turn, was associated with a low lipid phase transition temperature ($T_{s\ lip}$ = -8 °C) and high membrane fluidity at subzero temperatures when approaching ice nucleation. Freezing resistance of *L. bulgaricus* ATCC 11842 could thus be ascribed to a cytoplasmic membrane in a more fluid and flexible state around ice nucleation, which facilitates water efflux from the intracellular medium and cell shrinkage following cryoconcentration. However, in these two previous studies, membrane biophysical properties were characterised following cooling in the absence of any protective agent. In the present work, the osmotic stress is expressly addressed by investigating the change of membrane properties as a function of the two main environmental changes induced by freezing: low temperature and high osmotic condition.

Bacterial membrane organization was characterised using two complementary approaches: fluorescence anisotropy providing a direct measurement of membrane fluidity and vibrational spectroscopy affording

molecular insight on lipid bilayer organization. Data were obtained at two different locations within the membrane: (i) at the lipid acyl chains region by the anisotropy of DPH probe or the position of the symmetric CH_2 stretching band at approximately 2,850 cm^{-1}; and (ii) at the polar headgroups region by the anisotropy of TMA-DPH probe or the position of the asymmetric PO_2^- stretching band at approximately 1,219 cm^{-1}. The frequency (or wavenumber) of the *vCH_2 sym.* peak is often reported as an indirect way for evaluating membrane fluidity by providing information related to the degree of conformational order or disorder of the lipid acyl chains (Beney and Gervais 2001; Alvarez-Ordóñez *et al*. 2011). However, in molecular terms, a frequency shift has to be interpreted as a change of the force constant of the bond considered in the FTIR spectrum. A shift to higher frequencies is related to an increase in the force constant, *i.e.*, a strengthening of the C-H, or P=O bonds in our case (Disalvo *et al*. 2013). Considering the *vCH_2 sym* vibration, decreasing the temperature results in a shift to lower frequencies. The transition of acyl chain rotamers from *gauche* to all-*trans* conformation following cooling leads to a straightening and packing of acyl chains (Borchman *et al*. 1991). This decrease in inter-chain distances reinforces inter-chain interactions thereby weakening the C-H bond. When considering the *vPO_2^- asym.* vibration, a shift to lower frequencies and thus a weakening of the P=O bonds could be related to the interaction of the phospholipid headgroups with other groups of the surrounding medium. The band position of the *vPO_2^- asym.* was frequently used to indicate the phospholipid headgroup hydrogen bonding state (Goñi and Arrondo 1986; Arrondo and Goñi 1998; Lewis and McElhaney 1998). The involvement of phosphate groups in hydrogen bonding with the environment decreases the frequency of this vibration. Conversely, a shift to higher frequencies reveals a decrease in hydrogen bonding and has been linked to an increased phosphate headgroups packing (Díaz *et al*. 2003; Frías *et al*. 2006).

To discuss the results and their relevance for explaining cryoresistance, a dynamic representation of the behaviour of bacterial cells and membrane properties following environmental changes induced by freezing is proposed in **Fig. IV.2-6**. **Figure IV.2-6a** illustrates the evolution of sample temperature and osmolarity from the end of cell culture to the thawing of frozen samples of *L. bulgaricus* ATCC 11842 and CFL1, according to the experimental approach applied in this study (**Fig. IV.2-1**). The main physical events occurring in the samples (lipid phase transition ($T_{s\ lip}$), nucleation ($T_{n\ ice}$) and glass transition (T_g'i and T_g'e) temperatures), as well as schematic drawings of the physical state of the cells are also reported in **Fig. IV.2-6a**. After fermentation (step 1), membranes of *L. bulgaricus* are in a fluid crystalline phase and change to a gel state following chilling at 5 °C (step 2). The addition of the cryoprotective agent (sucrose, step 3) results in an increase of osmolarity (600 mOsm) which in turn leads to water transport from the intracellular medium and cell dehydration. At approximately -10 °C ($T_{n\ ice}$), ice nucleation occurs and the formation of ice crystals in the extracellular medium begins (step 4). This is associated with increasing osmolarity and further cell dehydration due to the cryoconcentration of the extracellular matrix. Cell dehydration terminates at T_g'i (*i.e.*, in *L. bulgaricus* CFL1 first, and then in *L. bulgaricus* ATCC 11842) with vitrification of the intracellular matrix, and osmolarity reaches its maximal value when vitrification of the extracellular matrix occurs (T_g'e). The temperature continues to decrease until it reaches -80 °C.

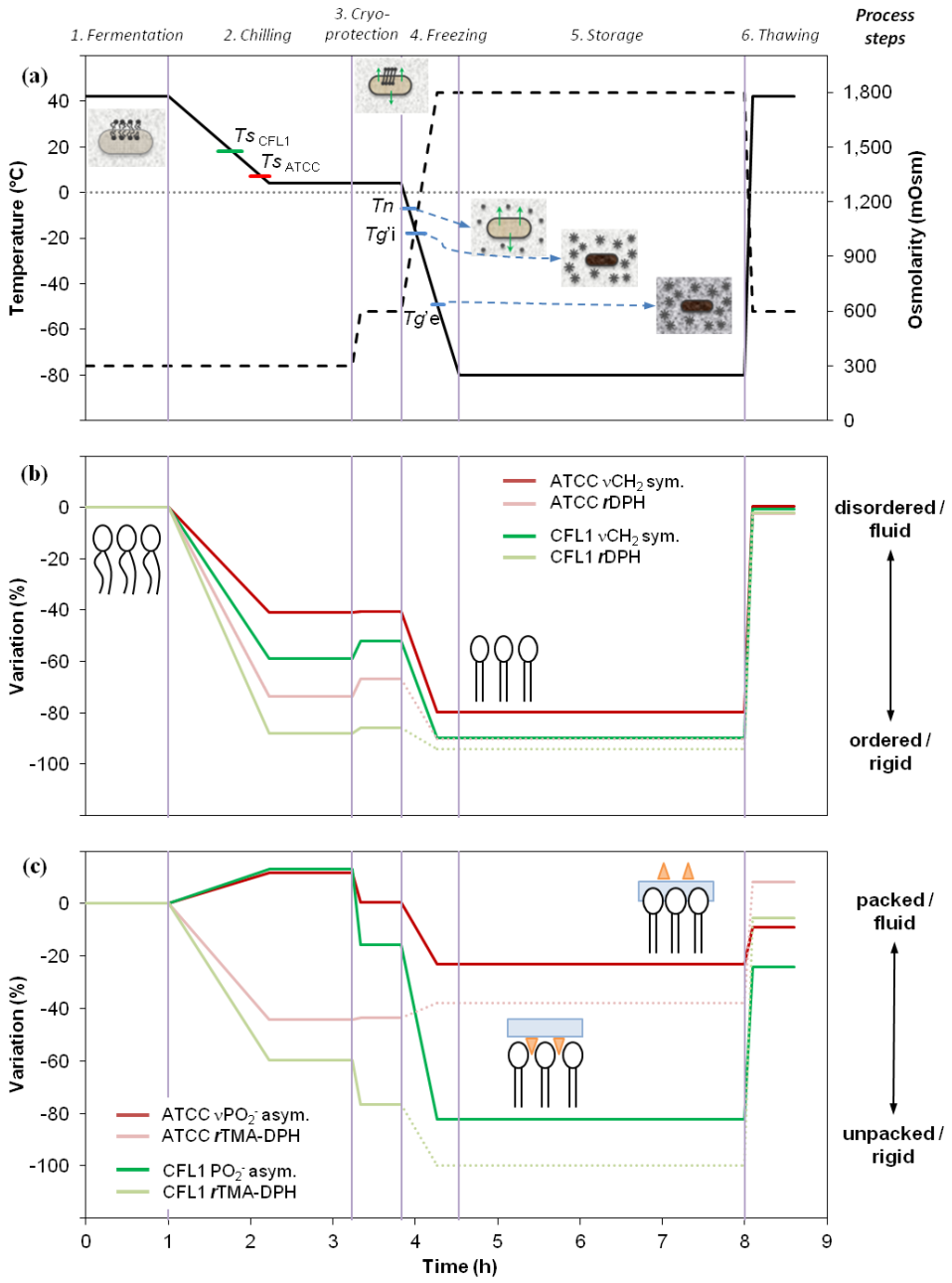

Figure IV.2-6: (a) Schematic overview of the main transitions (lipid: *Ts*; water: *Tn*; glass: *Tg*'i and *Tg*'e) occurring during cryopreservation of *L. bulgaricus* as a function of temperature (solid black line, °C) and osmolarity (dashed black line, mOsm), representative of 6 successive steps of the process. Membrane fluidity and organization variations of **(b)** the core and **(c)** external surface of the lipid bilayer are represented as percentage changes relative to the values corresponding to the end of fermentation: **(b)** DPH and **(c)** TMA-DPH anisotropy of *L. bulgaricus* ATCC 11842 (in light red) and *L. bulgaricus* CFL1 (in light green); **(b)** symmetric CH_2 stretching (*νCH_2 sym.*) and **(c)** asymmetric PO_2^- stretching (*νPO_2^- asym.*) of *L. bulgaricus* ATCC 11842 (in red) and *L. bulgaricus* CFL1 (in green). Cell diagrams in **(a)** were adapted from Fonseca *et al*. (2016). Diagrams in **(c)** illustrate the putative interaction of sucrose (orange triangles) and water (blue boxes) with membrane phospholipids of *L. bulgaricus* ATCC 11842 (top right; preferential exclusion) and CFL1 (bottom; preferential interaction). *L. bulgaricus* ATCC 11842 was abbreviated ATCC for the sake of clarity.

The evolution of the properties of the central part of membrane is represented in **Fig. IV.2-6b** by plotting the variation of DPH anisotropy values and *vCH_2 sym.* positions with time. The variation of TMA-DPH anisotropy values and the *vPO_2^- asym.* position are used to describe the evolution of the external surface part of the membrane and are plotted in **Fig. IV.2-6c**. The evolution of membrane properties was expressed as percentage changes relative to the values corresponding to the end of fermentation (42 °C, 300 mOsm; step 1). Negative variations of anisotropy indicate a decrease of membrane fluidity (*i.e.*, membrane rigidification). Fluorescence anisotropy measurements were technically limited to 0 °C. The steps of the process performed below this temperature were therefore reconstructed using the lowest measurable membrane fluidity values, represented as dotted lines in Figs. 6b and 6c. Negative variations of *vCH_2 sym.* and *vPO_2^- asym.* indicate a shift to lower frequencies, which in turn describe lipid acyl chain packing and involvement of phospholipid headgroups in hydrogen bonding, respectively. The organization of the lipid acyl chains of phospholipids is strongly affected by temperature. Following cooling, the acyl chains becomes densely packed and ordered, which is related to an increase of membrane rigidity measured by the fluorescence probes (DPH and TMA-DPH). A moderate difference exists between both strains. Following chilling to 5 °C (step 2), membrane lipid phase transition is almost completed for *L. bulgaricus* CFL1 ($T_{s\ lip}$ = 17.5 °C and the variation reaches 60 %) and is still in progress in *L. bulgaricus* ATCC 11842 ($T_{s\ lip}$ = 6.9 °C and the variation reaches 40 %). Osmotic stress, the most damaging stress on *L. bulgaricus* has minor impact on lipid acyl chains but highly altered the organization of the polar headgroups, in particular for the cryorsensitive strain CFL1. The variation of the *vPO_2^- asym.* band position reached 80 % in *L. bulgaricus* CFL1 (corresponding to a downshift of 8.0 cm^{-1}), vs. 20 % in *L. bulgaricus* ATCC 11842.

The band position of the *vPO_2^- asym.* has frequently been used to estimate the protective effect of various solutes towards drying (Linders *et al*. 1997) but few studies have linked it to freezing or cold and osmotic stresses. Adding sucrose to dimyristoyl-phosphatidylcholine (DMPC) multilamellar liposome solutions under hydrated conditions resulted in a depression of the band position of 17 cm^{-1} (Díaz *et al*. 2003). The authors deduced that strong interactions existed between the solutes they used and the phosphate headgroups, leading to a displacement of water molecules in hydrated conditions. Hincha and Crowe (1998) reported that membrane leakages observed following freezing in the presence of sugars could be due to hydrogen bonding of sucrose and other sugars to phospholipid headgroups. The intense wavenumber downshift observed for *L. bulgaricus* CFL1 (the sensitive strain) under strong hypertonic conditions (8.0 cm^{-1}), associated with a degradation of its biological activity, could therefore be the result of a displacement of water molecules weakly bound to phospholipid headgroups by sucrose. The direct interactions between sucrose and phospholipid headgroups could thus result in an alteration of membrane integrity. Conversely, this band position was barely affected by osmolarity in *L. bulgaricus* ATCC 11842 (1.5 cm^{-1} downshift), suggesting less direct interactions between its membrane and the sugar. Moreover, the membrane acyl chain ordering degree and lipid phase transition ($T_{s\ lip}$) were equal under hypertonic and isotonic conditions. This strongly suggests that sucrose did not alter the membrane core structure of *L. bulgaricus* ATCC 11842. According to Wolkers *et al*. (2010), the maintenance of the hydrogen bonding level to phospholipid headgroups associated with that of hydrocarbon chain disordering level is the sign of preferential exclusion of the solute from the bilayer hydration shell. Preferential exclusion could thus be the preservation

mechanism exerted by sucrose on *L. bulgaricus* ATCC 11842. These putative interaction mechanisms between sucrose and the membrane phospholipids of *L. bulgaricus* CFL1 and ATCC 11842 are schematically illustrated on **Fig. IV.2-6c**.

In this work, freezing was considered as a combination of two distinct stresses by exposing cells to cold and/or osmotic treatments. For the first time, it was evidenced that the organization of the headgroups of membrane phospholipids and in particular its modification with osmotic stress, plays a key role in cryopreservation of lactic acid bacteria. Furthermore, monitoring the position of the asymmetric stretching vibration of PO_2^- groups with temperature appeared to be a simple and relevant tool to select the optimal cryoprotective agent or fermentation conditions making it possible to obtain cryoresistant cells.

Acknowledgements

This work was supported by the National Institute for Agronomic Research (INRA) and the French National Research Agency (ANR) under the Investing in the Future Program, Grant n°ANR-10-IDEX-0003-02. We are grateful to our colleague Caroline Pénicaud for providing help with fatty acid extraction and analysis, and to Jiawei Xu for experimental help with assessments of biological activities.

2.3. Key points

- Resistance of *L. bulgaricus* ATCC 11842 to cold and hyperosmotic stresses;
- Sensitivity of *L. bulgaricus* CFL1 to hyperosmotic stress; explanation of its cryosensitivity by its sensitivity to solutes cryoconcentration upon ice nucleation;
- Different membrane fatty acid composition between both strains with more UFA and long-chain FA in the cryoresistant *L. bulgaricus* ATCC 11842, and more SFA and short-chain FA in the cryosensitive *L. bulgaricus* CFL1;
- Membrane rigidification at the core and surface levels upon cooling to similar extents in both strains; this result was ascribed to a counterbalancing effect of their membrane fatty acid composition (fluidifying effect of UFA and short-chain FA; rigidifying effect of SFA and long-chain FA);
- Lower conformational order of the membrane fatty acids of *L. bulgaricus* ATCC 11842 upon cooling compared to *L. bulgaricus* CFL1, resulting in a lower membrane lipid phase transition temperature, and a higher membrane flexibility; consistent with the higher UFA/SFA ratio for *L. bulgaricus* ATCC 11842; no significant impact of the osmotic stress on this parameter;
- Significant impact of the osmotic stress on the conformational order of the membrane phospholipid headgroups of the cryosensitive *L. bulgaricus* CFL1; evidence for the existence of different interactions between the osmotic agent sucrose and the membrane phospholipids of both strains, suggesting preferential binding in *L. bulgaricus* CFL1 and preferential exclusion in *L. bulgaricus* ATCC 11842.

III. Subcellular membrane fluidity of *Lactobacillus delbrueckii* subsp. *bulgaricus* under cold and osmotic stress

3.1. Context and objectives

A recent methodological development has made possible the mapping of bacterial membrane fluidity at a single-cell resolution (Passot *et al*. 2014). This was achieved by combining microscopy to the exploitation of the high brilliance of the synchrotron radiation in the UV spectral range on the DISCO beamline of SOLEIL synchrotron (Gif-sur-Yvette). The authors could characterise the membrane fluidity of individual *L. bulgaricus* CFL1 cells during cooling, according to two growth media leading to different cell cryoresistances. Besides, the fluorescence anisotropy experiments performed by spectrofluorimetry and presented in previous chapter revealed the absence of significant differences in the membrane fluidity of both strains during cooling and under hypersomotic conditions. However, the high standard deviations obtained indicated that possible cell-to-cell differences could be masked by these bulk measurements.
In this context, the membrane fluidity of *L. bulgaricus* CFL1 and *L. bulgaricus* ATCC 11842 under conditions of cold and osmotic stresses was further characterised at a subcellular resolution by synchrotron UV fluorescence microscopy on the DISCO beamline of SOLEIL synchrotron. The work presented in the previous chapter revealed potential interactions between sucrose cell membranes at the level of their phospholipid headgroups. To preferentially target the membrane surface and investigate this potential interaction further, the use of the fluorescent dye TMA-DPH was preferred. Furthermore, to quantify population heterogeneity and allowed statistics to be performed, a high number of individual cells per experimental condition were analysed. A methodology to characterise the distribution of membrane fluidity and thus intra-cellular heterogeneity was also proposed.

The results of this study have been published: *Applied Microbiology and Biotechnology*, 2017, online:1-11.

3.1. Article

Authors

Julie Meneghel[1] • Stéphanie Passot[1] • Stéphanie Cénard[2] • Matthieu Réfrégiers[3] • Frédéric Jamme[3] • Fernanda Fonseca[1]

Title

Subcellular membrane fluidity of *Lactobacillus delbrueckii* subsp. *bulgaricus* under cold and osmotic stress

Affiliations

[1] UMR GMPA, AgroParisTech, INRA, Université Paris-Saclay, 78850 Thiverval-Grignon, France

[2] INRA, UMR792, Ingénierie des Systèmes Biologiques et des Procédés, 31400 Toulouse, France

[3] Synchrotron SOLEIL, DISCO beamline, Gif-sur-Yvette, France

Address all correspondence to Fernanda Fonseca. Email: fernanda.fonseca@inra.fr; Phone: +33 (0)1 30 81 59 40; Fax: +33 (0)1 30 81 55 97

Abstract

Cryopreservation of lactic acid bacteria may lead to undesirable cell death and functionality losses. The membrane is the first target for cell injury and plays a key role in bacterial cryotolerance. This work aimed at investigating at a subcellular resolution the membrane fluidity of two populations of *Lactobacillus delbrueckii* subsp. *bulgaricus* when subjected to cold and osmotic stresses associated to freezing. Cells were cultivated at 42 °C in whey-based medium and they were exposed to sucrose solutions of different osmolarities (300 mOsm L^{-1} and 1800 mOsm L^{-1}) after harvest. Synchrotron fluorescence microscopy was used to measure membrane fluidity of cells labeled with the cytoplasmic membrane probe 1-[4 (trimethylamino) phenyl]-6-phenyl-1,3,5-hexatriene (TMA-DPH). Images were acquired at 25 °C and 0 °C and more than a thousand cells were individually analysed. Results revealed that a bacterial population characterised by high membrane fluidity and a homogeneous distribution of fluidity values appeared to be positively related to freeze-thaw resistance. Furthermore, rigid domains with different anisotropy values were observed and the occurrence of these domains was more important in the cryorsensitive bacterial population. The cryosensitive cells exhibited a broadening of existing highly rigid lipid domains with osmotic stress. The enlargement of domains might be ascribed to the interaction of sucrose with membrane phospholipids, leading to membrane disorganization and cell degradation.

Keywords

Lactic acid bacteria • Synchrotron UV microscopy • Fluorescence anisotropy • Membrane fluidity • Heterogeneity • Rigid lipid domain

Introduction

The efficiency of lactic acid bacteria (LAB) cryopreservation is not consistent and leads to cell death and considerable functionality losses in some species such as *Lactobacillus delbrueckii* subsp. *bulgaricus* (Smittle *et al*. 1972; Fonseca *et al*. 2000; Gomez Zavaglia *et al*. 2000; Fonseca *et al*. 2001; Rault *et al*. 2007; Meneghel *et al*. 2017). During freezing, several physical events take place in the extra-cellular matrix (ice crystallization, solute concentration, glass transition) and within the cells (membrane lipid transition, solute concentration, cell dehydration, glass transition), directly affecting cell viability and activity recovery (Mazur *et al*. 1972; Fonseca *et al*. 2016). These physical events result from strong modifications of environmental conditions and induce passive responses of cells. Cold stress thus leads cell membranes to rigidify and to undergo a transition from a liquid-crystalline to a gel phase (Gautier *et al*. 2013). Osmotic stress caused by the extracellular ice crystallization, induces cell dehydration leading to volume reduction and intracellular solute concentration (Dumont *et al*. 2004). Mechanical stress may arise both from intracellular ice formation (in the absence of cryoprotective additives) and extracellular ice growth (Fonseca *et al*. 2006). Oxidative stress can also take place mainly during fermentation and storage at high subzero temperatures (Fonseca *et al*. 2003). Mechanical and oxidative stresses have minor contribution to LAB cryoinjury in usual cryopreservation conditions compared to cold and osmotic stress (Fonseca *et al*. 2003; Clarke *et al*. 2013; Meneghel *et al*. 2017). Cryoinjury could arise from the alteration of various cell components but the bacterial cell membrane remains the main site for cell injury due to its direct contact with the extracellular environment (Beney and Gervais 2001).

Two main strategies are generally reported to minimize the undesired cell injuries induced by freeze-related stresses. The first one is the addition of cryoprotective agents to harvested cell suspensions such as disaccharides, polysaccharides, amino acids, antioxidants. The major effects of these molecules are (i) to prevent the formation of intracellular ice in bacterial cells (Fonseca *et al*. 2006; Fonseca *et al*. 2016), (ii) to increase the viscosity of the unfrozen fraction and immobilize the cells in a glassy matrix (Hubálek 2003), thereby slowing down diffusion-driven degradation reactions during storage, (iii) to stabilize the conformation and organization of cell components (in particular the lipid bilayer and proteins) by maintaining hydrogen bonding between them and the unfrozen water, and (iv) to limit oxidation (Fonseca *et al*. 2003).

The second strategy is the adaptation of bacteria to freezing stresses by inducing active responses during the fermentation or post-fermentation steps. By modulating environmental conditions (temperature, pH, medium composition), specific metabolic pathways can be activated resulting in a modification of bacterial composition. Active responses of LAB, and particularly of lactobacilli, include the synthesis of cold shock proteins (Kim *et al*. 1998; Derzelle *et al*. 2003; Shao *et al*. 2014; Song *et al*. 2014) and the accumulation of compatible solutes (Kets *et al*. 1996; Glaasker *et al*. 1998). However, unlike other lactobacilli, *L. bulgaricus* URL-LB1 tested by Kets and co-workers does not accumulate compatible solutes under osmotic stress (Kets *et al*. 1996). Besides, several studies have evidenced a correlation between the cryotolerance of LAB and the modification of their membrane lipid composition. In particular, the enrichment of the membrane of lactobacilli, including *L. bulgaricus*, in cyclic fatty acid and/or unsaturated fatty acid was positively related

to cryotolerance (Smittle *et al*. 1974; Goldberg and Eschar 1977; Gomez Zavaglia *et al*. 2000; Wang *et al*. 2005b; Streit *et al*. 2011; Gautier *et al*. 2013). These modifications of membrane fatty acid composition were related to modifications of membrane biophysical properties, including lipid phase transition temperature and fluidity (Gautier *et al*. 2013; Passot *et al*. 2014). The maintenance of the membrane in a fluid state when approaching ice nucleation appeared as a critical parameter for limiting membrane damage. Recently, we have investigated the membrane biophysical properties of bacterial populations of two strains of *Lactobacillus delbrueckii* subsp. *bulgaricus* (ATCC 11842 and CFL1) when submitted to cold and osmotic stresses (Meneghel *et al*. 2017). Exposure of bacterial cells to a low temperature (without ice crystallization) induced a decrease of membrane fluidity and was not associated with bacterial lethality. Conversely, osmotic stress was responsible for a major degradation of cell culturability and functionality but no modification of membrane fluidity was observed. Membrane fluidity was assessed by measuring the polarization of a fluorescence probe inserted in the lipid bilayer of cells by spectrofluorimetry. This method allows a bulk measurement and provides global fluorescence anisotropy values over the entire cell population under investigation (tens of millions of cells). However, this characterisation remains incomplete since it does not evaluate membrane fluidity of individual cells and thus does not provide any information regarding inter- or intra-cellular distribution of this property. To solve this issue, Passot *et al*. (2014) recently proposed an original experimental device to map membrane fluidity in individual bacterial cells by coupling fluorescence microscopy to synchrotron UV radiation.

In the present study, synchrotron UV fluorescence microscopy was used to evaluate the effect of a cold and an osmotic stress on the membrane fluidity of the LAB *L. bulgaricus* at a single-cell scale by comparing a stress-resistant and a stress-sensitive strain. The objectives were to further characterise and quantify inter-cellular heterogeneity by analysing a sufficiently high number of individual bacteria and to consider intra-cellular heterogeneity in light of lipid domains, in order to contribute to a better understanding of bacterial cryoresistance mechanisms.

Materials and Methods

Bacterial strains and culture conditions

This study involved two strains of *Lactobacillus delbrueckii* subsp. *bulgaricus*: *L. bulgaricus* CFL1 (CIRM-BIA; Rennes, France) and *L. bulgaricus* ATCC 11842 (Manassas, VA, USA), previously characterised as being sensitive and resistant to freeze-thawing and osmotic stress, respectively (Meneghel *et al*. 2017). Inocula stored at -80 °C were used to inoculate MRS pre-cultures (Biokar Diagnostics, France). Cells from the preculture were then used to inoculate the culture medium composed of 60 g L^{-1} mild whey power (Euroserum, France) supplemented with 5 g L^{-1} yeast extract (Organotechnie SAS, France). Cell cultures were carried out at 42 °C. At the end of the exponential growth phase, cells were cooled down to 5 °C, harvested and subsequently washed three times in Tris-HCl buffer (50 mM, pH 8.8, Bio-Rad, USA) to remove any components (excreted metabolites, growth medium constituents) that could interfere with

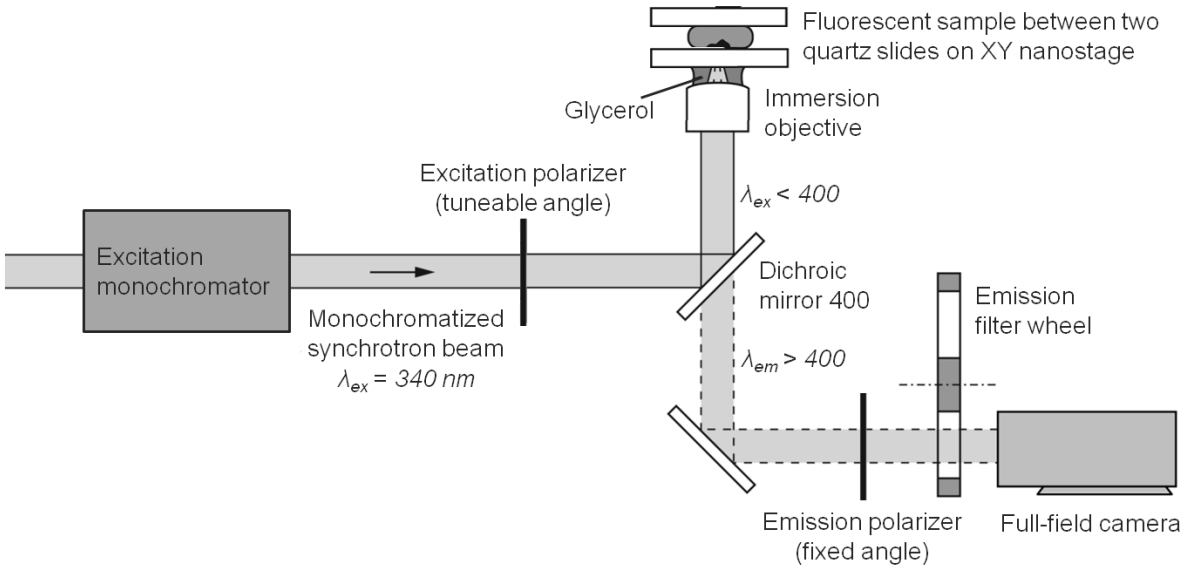

Figure IV.3-1: Schematic setup of the synchrotron UV fluorescence microscopy experiment, adapted from Thoury *et al*. (2011)**.**

further analysis. The detailed procedures for cell growth, harvest and washing were previously described by Meneghel *et al*. (2017).

Stressful treatments and labeling of cells

The washed cell pellets were resuspended in the same weight of 12.5 % and 50 % (wt) sucrose solutions, leading to isotonic (300 mOsm L^{-1}) and hypertonic (1800 mOsm L^{-1}) cell suspensions, respectively. This osmotic treatment was performed for 1 hour at 42 °C prior to cell labeling since it leads to significant degradation of cell biological activity for the sensitive strain (Meneghel *et al*. 2017).
The lipophilic and fluorescent probe 1-[4 (trimethylamino) phenyl]-6-phenyl-1,3,5-hexatriene (TMA-DPH) was used for labeling cell membranes (Passot *et al*. 2014). A stock solution of 2 mM TMA-DPH (Molecular Probes, USA) in dimethylsulfoxide (DMSO, Sigma-Aldrich, USA) was prepared. A volume of 2 µL of isotonic or hypertonic cell suspensions was washed in 1 mL of MES-KOH buffer (50 mM, pH 5.5, Sigma-Aldrich, USA) supplemented with 10 mM glucose. After centrifugation (17,000 x *g* for 1 min), the pellets were resuspended in 1 mL of MES-KOH buffer to obtain an approximate cell concentration of 10^{7-8} CFU mL^{-1}. A volume of 5 µL of thoroughly shaken TMA-DPH stock solution was then added to obtain a final probe concentration of 10 µM. After another thorough shaking of the samples (using a vortex for 1 min), a 5-min incubation at 42 °C was performed prior to centrifugation (17,000 x *g* for 1 min). The labeled cell pellets were then resuspended in 50 µL of either isotonic or hypertonic sucrose solution before fluorescence anisotropy analysis.

Fluorescence anisotropy imaging by synchrotron DUV microscopy

Fluorescence anisotropy of TMA-DPH was used to evaluate the membrane fluidity of *L. bulgaricus* by measuring its degrees of freedom within the lipid bilayer (Lentz 1989; Lentz 1993; Trevors 2003). Measurements were performed on the TELEMOS full field microscope of the DISCO beamline (Giuliani *et al*. 2009) at the SOLEIL synchrotron (Saint-Aubin, France).
The setup described by Jamme *et al*. (2010) and Passot *et al*. (2014) was used for the present study with some modifications (**Fig. IV.3-1**). Briefly, the labeled cell suspension (approximately 0.5 µL) was sandwiched between two quartz coverslips and placed in a closed temperature-controlled chamber (Okolab S.R.L, Italy). Bacterial cells were observed in brightfield mode under the microscope with a 100X magnification lens, NA 1.2 (Zeiss Ultrafluar, glycerin immersion). Excitation of TMA-DPH was performed at 340 nm. A 400-nm dichroic mirror and a 420-480-nm bandpass emission filter (OMEGA Optical, Inc., USA) were selected as pre-tests and showed that the emission spectrum of TMA-DPH was maximal at 450 nm. The closed chamber was connected to a Lauda ECO RE 415 cooling thermostat (Lauda, Germany) filled with a Kryo51 cryogenic fluid (Lauda, Germany) and its temperature was controlled using an Oko-Touch controller (Okolab S.R.L, Italy) and a thermocouple placed as close as possible to the sample in the closed chamber.
The orthogonal positions of the tunable excitation polarizer leading to minimum and maximum fluorescence

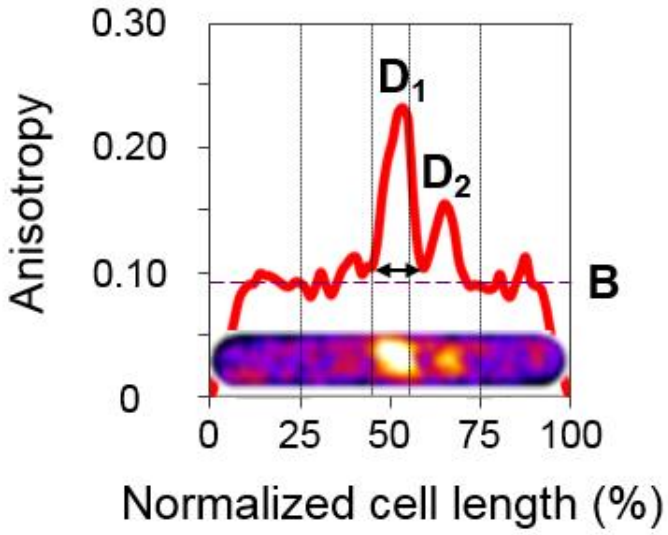

Figure IV.3-2: Illustration of the method applied for the identification and characterisation of rigid domains in one bacterial cell. The graph represents the distribution of anisotropy data along the normalized length of the cell image inserted. The dashed line B indicates the anisotropy value of the peaks baseline, and D_1 and D_2 the anisotropy values of the peaks associated with yellow and orange spots in the image, respectively. The double-headed arrow indicates the width at the base of the rigid domain associated with D_1, and the vertical dotted lines delineate the cell extremities (0-25 and 75-100 % of cell length), centre (40-60 % of cell length; containing D_1) and intermediate positions (remaining 30 % of cell length; containing D_2).

intensities were determined (I_{min} and I_{max}, respectively). This polarizer was first set to the minimum position and a fluorescence image was recorded after an exposure time of 100 seconds; the excitation polarizer was then automatically rotated 90° and the second image was recorded after the same exposure time. The microscope, stage, shutters and polarizer rotation were controlled using a universal interface developed under µManager (Stuurman *et al*. 2010).
In this study, approximately 100 cells were analysed under each temperature and osmolarity condition after a thermal equilibration of 10 min, thus allowing statistics to be collected and the notion of heterogeneity to be addressed.

Image processing

The software ImageJ (1.49v, NIH, USA) was used for image processing. Using both I_{min} and I_{max} images, a fluorescence anisotropy (***r***) image was calculated according to the following equation (Eq. 1) (Lakowicz 2006):

$$\boldsymbol{r} = \frac{I_{max} - I_{min}}{I_{max} + 2 \times I_{min}} \quad (1)$$

Fluorescence anisotropy and fluidity are inversely proportional. A low ***r*** therefore indicates that the membrane is fluid and vice-versa. To better visualize anisotropy distribution among different cells and within individual cells, the images were edited with the "fire" Look Up Table (LUT) from ImageJ, ranging from purple to yellow, as was done by Passot *et al*. (2014). Membrane regions with the lowest anisotropy (*i.e.*, fluid) thus appeared to be purple, whereas membrane regions with the highest anisotropy (*i.e.*, rigid) appeared to be yellow. The segmented line selection tool (line width: 4 pixels, corresponding to 0.34 µm) was used to obtain anisotropy data along each bacterial cell. This enabled to calculate an average value of anisotropy for each cell and to identify and characterise high anisotropy domains within individual cells, here called rigid domains (**Fig. IV.3-2**). Rigid domains were defined as membrane portions presenting an anisotropy ratio between peak values (D_1 and D_2, **Fig. IV.3-2**) and peak baseline (B, **Fig. IV.3-2**) higher than 1.5. The number of rigid domains per cell, as well as their width at the base and relative position were determined. Relative positions were obtained by normalizing the location of each domain on the length of the cell. For each cell, the percentages of domains located at the extremities (0-25 and 75-100 % of cell length), centre (40-60 % of cell length) and intermediate positions (remaining 30 % of cell length) were calculated.

Instrumental upgrades of the DISCO Imaging endstation were made since the work of Passot *et al*. (2014): different camera (EM-CCD C9100-14, Hamamatsu, Japan), homogenization of the beam, and new polarizers (MgF2 Rochon, Edmunds Optics SARL, France). These upgrades make it impossible to compare the numeric values of their dataset to the one presented in this work. The fitting coefficient to be applied to the current synchrotron experimental dataset is a factor of 3, and also allows relative comparisons with spectrofluorimetric measurements.

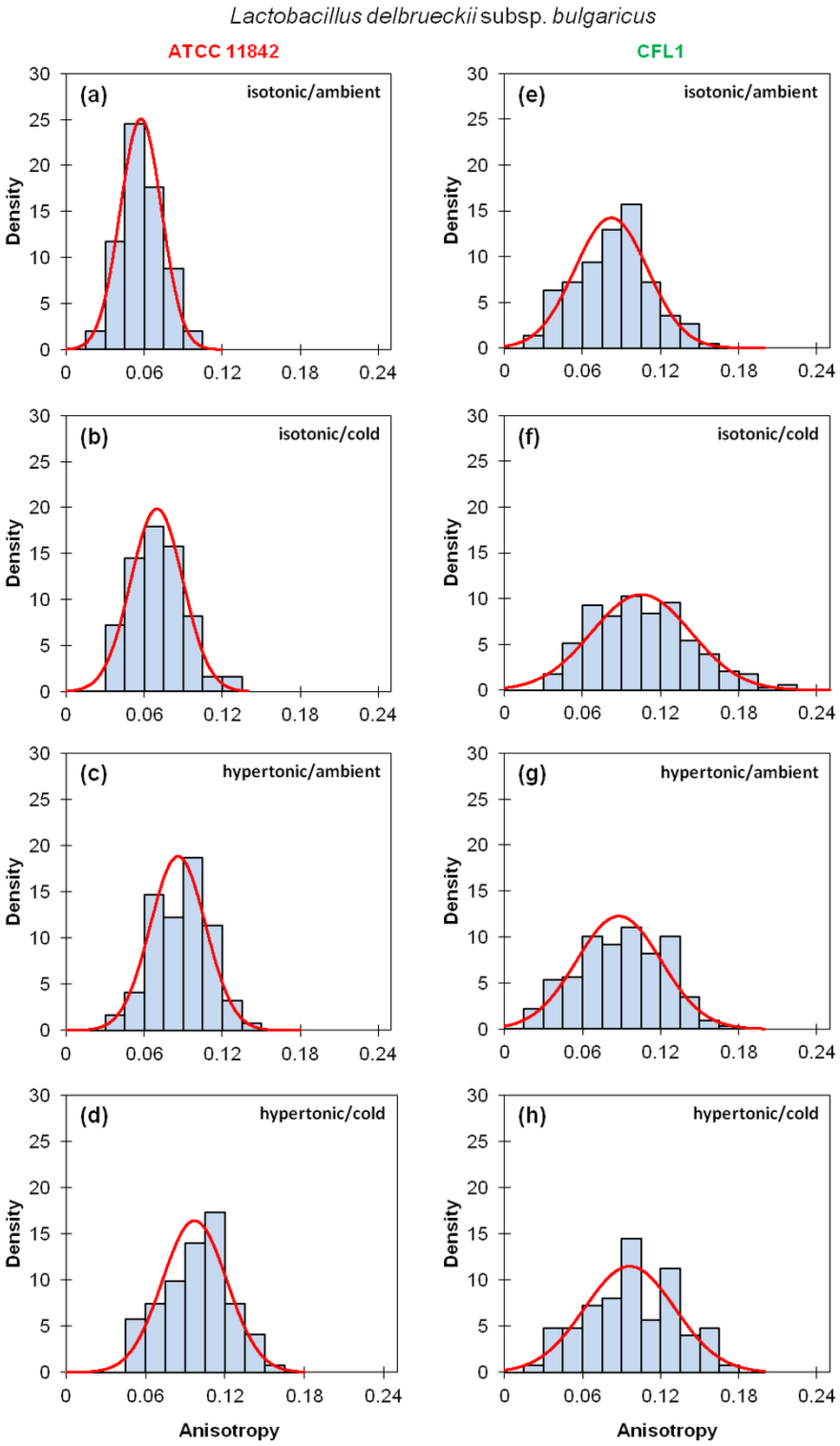

Figure IV.3-3: Density histograms of membrane fluorescence anisotropy values within bacterial populations (blue; intervals = 0.015 anisotropy units) and normal distributions (red) for *Lactobacillus delbrueckii* subsp. *bulgaricus* ATCC 11842 (left panels) and CFL1 (right panels) under **(a, e)** reference (ambient temperature: 25 °C; isotonic: 300 mOsm L^{-1} sucrose), **(b, f)** cold (0 °C), **(c, g)** hypertonic (1800 mOsm L^{-1} sucrose), and **(d, h)** cold and hypertonic conditions.

Statistical analyses

Normal distribution fitting of anisotropy data was assessed according to the Kolmogorov-Smirnov test. Parametric tests were performed for identifying differences between means and variances. Means were compared by t-tests for two independent samples and variances with Fisher's F-test. The variance of each normal distribution of anisotropy values was used as an indicator of the heterogeneity of the sample since it measures how far a set of values are spread out from their mean.
Data concerning the characterisation of rigid domains (anisotropy ratio, number, width and relative position in individual cells) were subjected to non-parametric analysis of variance through Dwass-Steel-Critchlow-Fligner multiple comparisons with Kruskal-Wallis tests. All tests were implemented at a significance level of 5% (XLSTAT Base, Addinsoft, Paris France).

Results

Membrane fluidity at a population-scale: inter-cellular heterogeneity

All conditions considered, more than a thousand individual cells were analysed using image processing, and for each cell, a mean value of anisotropy was calculated. The subsequent density distributions of cell anisotropy values within *L. bulgaricus* ATCC 11842 and *L. bulgaricus* CFL1 populations for the different conditions of temperature and osmolarity are presented in **Fig. IV.3-3**. All distributions followed a normal law represented by the red line. The corresponding mean and variance values are presented in **Table IV.3-1**, and the statistical differences between conditions are indicated (superscript letters; p values < 0.05). These data make it possible to compare different conditions and to assess sample heterogeneity through the corresponding variance values. The culturability and functionality losses of both strains following freezing, cold and osmotic stresses were established in our previous work: *L. bulgaricus* ATCC 11842 emerged as being resistant to all treatments and *L. bulgaricus* CFL1 as being sensitive to freeze-thawing and to hyperosmotic stress (Meneghel *et al*. 2017).
Under the reference condition (isotonic and ambient temperature; **Fig. IV.3-3a**), the anisotropy distribution of *L. bulgaricus* ATCC 11842 ranged from 0.024 to 0.096 for a mean anisotropy of 0.057 and a variance of 2.6×10^{-4}. The anisotropy distribution following exposure of cells to cold or osmotic stress shifted to higher values and broadened compared to the reference condition, thus indicating higher membrane rigidity and inter-cellular heterogeneity (**Figs. IV.3-3b** and **IV.3-3c**). The mean anisotropy and variance of *L. bulgaricus* ATCC 11842 incubated at 0 °C under isotonic conditions thus reached 0.070 (increase of 23 %) and 4.1×10^{-4}, respectively (**Fig. IV.3-3b** and **Table IV.3-1**). For cells incubated under hypertonic conditions at ambient temperature, the mean anisotropy and variance reached 0.086 (increase of 51 %) and 4.5×10^{-4}, respectively (**Fig. IV.3-3c** and **Table IV.3-1**). Both of these stresses presented a cumulative effect on the increase in both mean and variance values in this resistant strain by reaching 0.097 (+70 % increase compared to the reference condition) and 6.0×10^{-4}, respectively (**Fig. IV.3-3d**).

Table IV.3-1: Membrane fluorescence anisotropy mean and variance values (10^{-4}) of *Lactobacillus delbrueckii* subsp. *bulgaricus* ATCC 11842 and CFL1 populations for each experimental condition of osmolarity and temperature.

***Lactobacillus delbrueckii* subsp. *bulgaricus* strain**	**Experimental conditions**	**Mean**	**Variance (10^{-4})**
ATCC 11842	isotonic – ambient	0.057 ± 0.016^{a}	2.6^{a}
	isotonic – cold	0.070 ± 0.020^{b}	4.1^{b}
	hypertonic – ambient	0.086 ± 0.021^{c}	4.5^{c}
	hypertonic – cold	0.097 ± 0.024^{d}	$6.0^{c,d}$
CFL1	isotonic – ambient	0.082 ± 0.028^{c}	$7.9^{d,e}$
	isotonic – cold	0.105 ± 0.038^{d}	14.7^{f}
	hypertonic – ambient	0.088 ± 0.033^{c}	$10.6^{e,f}$
	hypertonic – cold	0.096 ± 0.035^{d}	12.2^{f}

Superscript letters represent statistical contrast between means (Student t-test) and between variances (Fisher test) at a 95% confidence level.

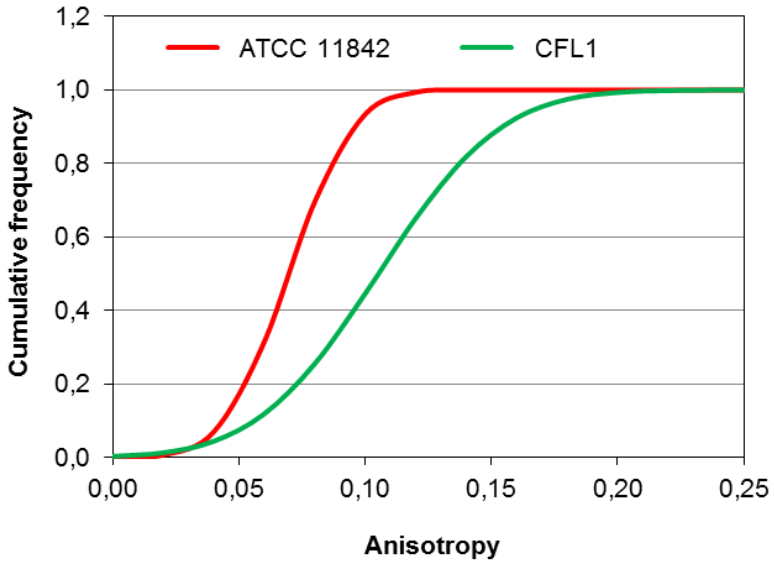

Figure IV.3-4: Cumulative frequencies of anisotropy values within the population of *Lactobacillus delbrueckii* subsp. *bulgaricus* CFL1 (green) and ATCC 11842 (red) under cold stress (0 °C; 300 mOsm L^{-1} sucrose).

With an anisotropy distribution ranging from 0.024 to 0.159 for a mean anisotropy of 0.082 and a variance of 7.9 x 10^{-4} (**Fig. IV.3-3e**) under the reference condition, the bacterial population of *L. bulgaricus* CFL1 exhibited a significantly more rigid membrane and a higher inter-cellular heterogeneity than the population of *L. bulgaricus* ATCC 11842 (p value < 0.05). Exposure of this sensitive strain to cold stress also led to increased membrane rigidity (mean anisotropy of 0.105, *i.e.*, +28 % compared to the ambient temperature; **Table IV.3-1**) and inter-cellular heterogeneity (14.7 x 10^{-4}; **Table IV.3-1**), thus shifting the anisotropy distribution to higher values and broadening it compared to the reference condition (**Figs. IV.3-3e** and **IV.3-3f**). On the contrary, membrane fluidity of *L. bulgaricus* CFL1 was not affected by osmotic stress (mean anisotropy of 0.088 and variance of 10.6 x 10^{-4}, p values > 0.5; **Fig. IV.3-3g** and **Table IV.3-1**).
Figure IV.3-4 illustrates the cumulative frequency curves of the anisotropy values of the two strain's populations under the cold and isotonic condition, corresponding to the environmental conditions just before ice crystallization. The slope of the cumulative frequency of *L. bulgaricus* ATCC 11842 appeared to be steeper than that of *L. bulgaricus* CFL1. The bacterial population of the cryoresistant strain thus exhibited a more fluid membrane and a higher inter-cellular homogeneity than the cryorsensitive bacterial population when approaching ice formation.

Membrane fluidity distribution in single-cells: intra-cellular heterogeneity

Since images of bacterial cells were acquired, it was possible to obtain a cellular map of membrane fluidity and to identify domains of different anisotropy values within the cell membrane (*i.e.*, to quantify intra-cellular heterogeneity). **Figure IV.3-5** illustrates (i) the membrane fluidity mapping of several individual cells representative of all the cells analysed under the reference, cold, and hyperosmotic conditions, (ii) the anisotropy value plots along the length of one representative cell per condition, and (iii) the cell morphology of both strains. The effect of cold stress and hyperosmotic stress is presented to evaluate their specific impact on the intracellular fluidity of both strains compared to the reference condition (25 °C, isotonic). The cumulative impact of both stresses did not provide further information and this condition is therefore not presented.
Rigid domains of different values of anisotropy, *i.e.*, orange to yellow spots in **Fig. IV.3-5**, were observed within bacterial membranes. Cells were individually analysed to statistically characterise these membrane domains (**Fig. IV.3-6**). The characterisation involved comparing for each condition mean values of: the number of domains per cell (**Fig. IV.3-6a**), the width of domains (**Fig. IV.3-6b**), their relative distribution within the cell (**Fig. IV.3-6c**) and the anisotropy ratio (data not shown). The anisotropy ratio was about 2 regardless the condition studied.
Under the reference conditions (isotonic and ambient temperature), *L. bulgaricus* ATCC 11842 exhibited about one domain per cell of 0.9 µm average width, while *L. bulgaricus* CFL1 revealed about 2.5 domains per cell of higher width (1 µm, **Fig. IV.3-6a** and **IV.3-6b**). For both strains, rigid domains were preferentially located at cell extremities (**Fig. IV.3-6c**).
Exposing *L. bulgaricus* ATCC 11842 to cold or osmotic stress led to an increased anisotropy of both the rigid domains and the more fluid membrane portions while maintaining a constant anisotropy ratio (left-

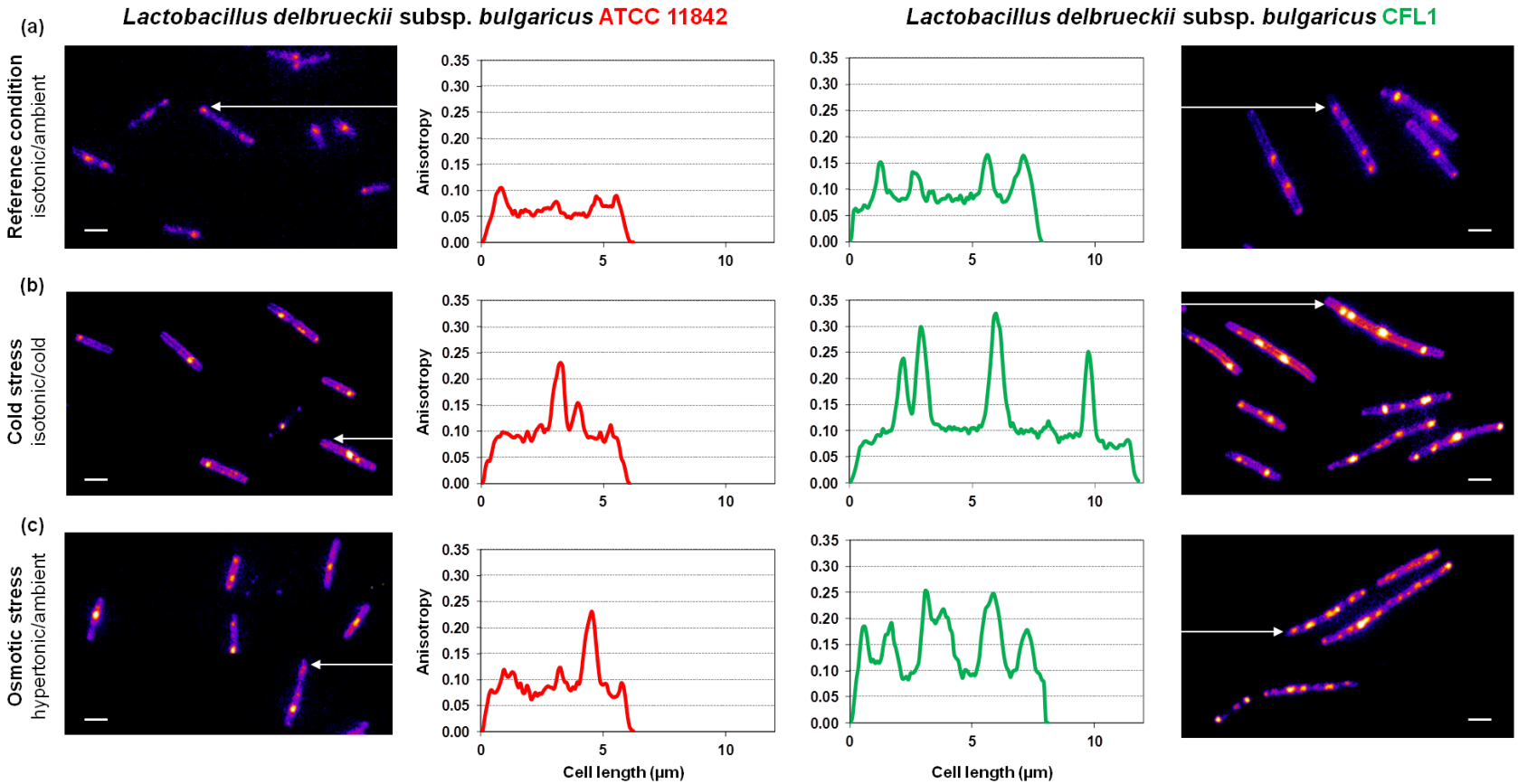

Figure IV.3-5: Fluorescence anisotropy images of *Lactobacillus delbrueckii* subsp. *bulgaricus* ATCC 11842 (left panels) and CFL1 (right panels) in pseudo colours under **(a)** reference (ambient temperature: 25 °C; isotonic: 300 mOsm L^{-1} sucrose), **(b)** cold (0 °C), and **(c)** hypertonic (1800 mOsm L^{-1} sucrose) conditions. Low anisotropy values appear to be blue to purple and reflect fluid membrane areas, whereas elevated anisotropy values appear to be orange to yellow and reflect domains of higher rigidity. The distribution of anisotropy values along one representative cell per experimental condition and strain is drawn. The arrow points to the first extremity of the cell considered; scale bar: 2 µm.

hand side of **Figs. IV.3-5b** and **IV.3-5c**). The average number of domains identified per cell and their mean width were not significantly different between conditions (**Figs. IV.3-6a** and **IV.3-6b**). However, an evolution of their position within cells could be noticed from Fig. **IV.3-**6c, with a preferential location at cell extremities under reference conditions and a similar distribution at cell extremities and centre under stressful conditions. Conversely, *L. bulgaricus* CFL1 exposed to both stresses exhibited a significant rise of the number of domains (higher than 3.3, **Fig. IV.3-6a**) and osmotic stress led to a significant increase of domain's mean width (1.2 µm, **Fig. IV.3-6b**). However, no modification of their distribution along the cell was noticed (**Fig. IV.3-6c**).

Considering cell size at reference conditions, *L. bulgaricus* CFL1 rods were approximately twice as long (6.4 µm ± 2.9 µm, n = 149 cells) as *L. bulgaricus* ATCC 11842 rods (3.0 µm ± 1.0 µm, n = 196 cells) for an equivalent thickness (p value < 0.05). Consequently, the surface area-to-volume ratio was higher for *L. bulgaricus* ATCC 11842 cells than for *L. bulgaricus* CFL1.

Discussion

Several strategies limiting the cryoinjury of LAB and lactobacilli in particular, have been reported in the literature. They include cell preadaptation during fermentation, addition of cryoprotective molecules, and selection of optimal cryopreservation conditions (cooling and thawing rates; storage temperature). The interrelationships between pre- and post-fermentation factors and the strain dependent response to different protocols generally make the development of highly active frozen LAB concentrates quite complex and time-consuming. Increasing knowledge of passive cell's behaviour and modifications following freezing appears essential to identify relevant cellular properties for optimizing bacterial survival.

Meneghel *et al*. (2017) have investigated the cryotolerance of two strains of *Lactobacillus delbrueckii* subsp. *bulgaricus* grown in the same culture medium (whey-based medium) representative of industrial practices. *L. bulgaricus* ATCC 11842 was resistant to freeze-thawing while *L. bulgaricus* CFL1 was strongly affected by freezing. Furthermore, in that study the impact of the individual freezing stresses (cold and osmotic) was quantified and the osmotic stress was reported as the main source of cryoinjury.

The passive response of lactobacilli exposed to high solute concentration undoubtedly affects bacterial survival following freezing. During cooling, ice forms outside the cell resulting in an increased solute concentration in the extracellular medium. This solute cryo-concentration triggers water efflux from cells, thus resulting in cell dehydration and cell volume reduction. Two bacterial characteristics can importantly influence the cellular damage induced by osmotic stress and will be discussed: (i) the bacterial morphology and (ii) the membrane fluidity.

Firstly, some studies have linked bacterial cryoresistance to cell size and shape, in particular to the surface area-to-volume ratio (Fonseca *et al*. 2000; Dumont *et al*. 2004). For instance, *St. thermophilus*, a cryoresistant species of LAB, exhibited a surface area-to-volume ratio four times higher than the cryorsensitive *L. bulgaricus* CFL1 (Fonseca *et al*. 2000). In the present study, the average surface area-to-volume ratio was higher for the cryoresistant *L. bulgaricus* ATCC 11842 cells than for *L. bulgaricus* CFL1.

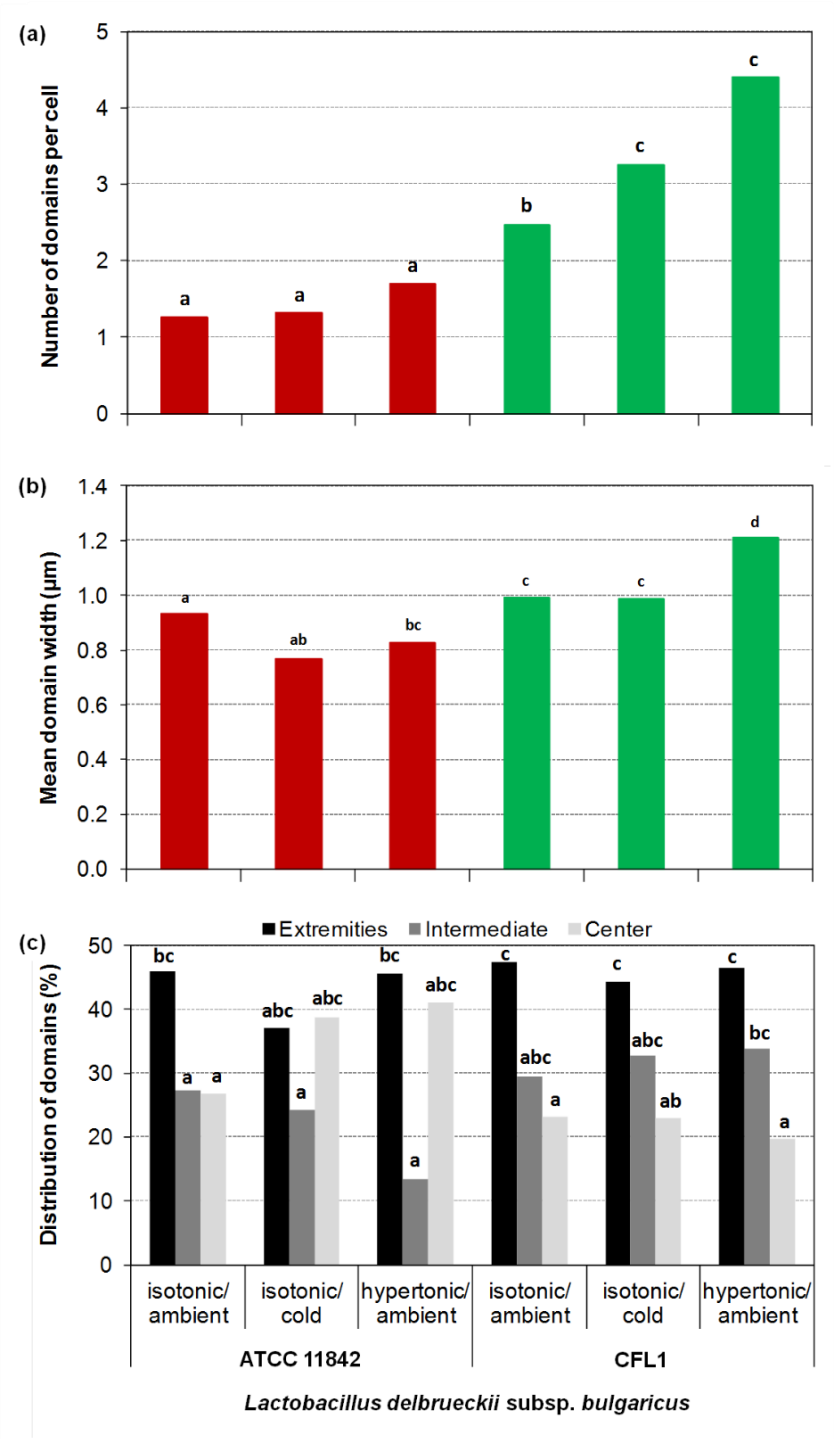

Figure IV.3-6: Statistical characterisation of rigid domains identified in individual *Lactobacillus delbrueckii* subsp. *bulgaricus* ATCC 11842 and CFL1 cells under reference (ambient temperature: 25 °C; isotonic: 300 mOsm L^{-1} sucrose), cold (0 °C) and hypertonic (1800 mOsm L^{-1} sucrose) conditions: **(a)** number of domains per cell, **(b)** width of domains and **(c)** distribution of domains according to their location within cells: extremities (0-25 and 75-100 % of cell length), centre (40-60 % of cell length) and intermediate positions (remaining 30 % of cell length). Letters represent statistical contrast between means (p value < 0.05).

This means that for the same cellular volume, the available membrane surface exchange of *L. bulgaricus* ATCC 11842 for water efflux induced by an osmotic stress is greater than *L. bulgaricus* CFL1.

Secondly, the cell membrane is a dynamic supramolecular assembly whose fluidity is a crucial parameter to be controlled for its functionality maintenance after exposure to environmental stress (Beney and Gervais 2001). Membrane fluidity governs cell membrane permeability to water and membrane flexibility to support mechanical stress induced by osmotic cell contraction. Gautier *et al*. (2013) and Passot *et al*. (2014) have investigated the influence of a modification of membrane composition of *L. bulgaricus* CFL1 on membrane properties in relation with freeze-tolerance. Cryoresistant bacteria exhibited a higher content of unsaturated and cyclic fatty acids that was related to a lower lipid phase transition temperature ($T_{s\ lip}$ = -8 °C, Gautier *et al*. 2013), a more fluid membrane and a higher homogeneity of intracellular membrane fluidity than the cryosensitive cells (Passot *et al*. 2014). The maintenance of the cell membrane in a relatively fluid state during freezing was thus proposed as a key parameter to facilitate water efflux from the cell and the concomitant volume reduction following cryoconcentration of the extracellular medium.

The membrane properties of *L. bulgaricus* ATCC 11842 and *L. bulgaricus* CFL1 were thoroughly characterised by Meneghel *et al*. (2017). The three main fatty acids produced by *L. bulgaricus* grown in whey-based medium were C16:0, C16:1 and C18:1 with different relative percentages for both strains (37 %, 23 % and 15 % for *L. bulgaricus* CFL1 and 27 %, 21 % and 25 % for *L. bulgaricus* ATCC 11842, respectively). A higher proportion of unsaturated fatty acyl (UFA) residues and a lower membrane lipid phase transition temperature ($T_{s\ lip}$) were detected for the cryoresistant *L. bulgaricus* ATCC 11842 (UFA = 49 % and $T_{s\ lip}$ = 6.9 °C) compared to *L. bulgaricus* CFL1 (UFA = 39 % and $T_{s\ lip}$ = 17.5 °C). Cooling induced a membrane rigidification in both strains, while osmotic stress did not. Furthermore, FTIR spectroscopy revealed that osmotic stress elicited a major disorganization of phospholipid headgroups in the sensitive *L. bulgaricus* CFL1. It was suggested that hydrogen bonds between phospholipid headgroups and the surrounding extracellular water, maintained when considering the resistant strain *L. bulgaricus* ATCC 11842, were replaced by sucrose during the applied sucrose osmotic stress in the case of the sensitive *L. bulgaricus* CFL1. In turn, it was assumed that such disorganization of the membrane surface led to membrane disruption.

Some studies reported a decrease of membrane fluidity (increase of membrane rigidity) of lactobacilli when applying cold stress (Gautier *et al*. 2013; Meneghel *et al*. 2017) while the incidence of an osmotic stress on the membrane fluidity of bacteria has rarely been reported and appears to depend on the species considered (Beney *et al*. 2004; Beney *et al*. 2007; Meneghel *et al*. 2017). Membrane fluidity is generally evaluated as a bulk property of the cell population by spectrofluorimetry whereas bacterial populations are reported to be heterogeneous (Passot *et al*. 2014). The quantification of membrane fluidity at a single-cell level is crucial for increasing knowledge on individual modifications according to membrane composition and environmental conditions. The cryoresistant population of *L. bulgaricus* ATCC 11842 cells was characterised by higher membrane fluidity with a more homogenous distribution compared to the cryorsensitive population of *L. bulgaricus* CFL1.

Besides, the cellular mapping of membrane fluidity revealed the occurrence of domains of high rigidity within cells. Higher number of domains and higher content of C16:0 fatty acyl residue were observed in the

membrane of *L. bulgaricus* CFL1 compared to *L. bulgaricus* ATCC 11842 cells, thus suggesting a high proportion of such fatty acyl residue in rigid domains. Domains of specific lipid composition have also recently been evidenced within prokaryotic membranes, making their membrane organization much more complex than formerly thought. For instance, membrane poles and septa of various bacilli including Gram-positive bacteria were reported to be enriched in anionic phospholipids, especially cardiolipin (CL) (Kawai *et al*. 2004; López *et al*. 2006; Bernal *et al*. 2007; Seydlová *et al*. 2013). Moreover, CL was reported to be responsible for the membrane rigidification of *B. subtilis* (Seydlová *et al*. 2013). Exterkate *et al*. (1971) evaluated the lipid composition of *L. bulgaricus* strain 9LB, which included 54 % of phophatidylglycerol (PG) and 7 % CL. However, to our knowledge, the relationships between CL concentrations, rigid domains and the cryoresistance in LAB still need to be investigated.

The cryosensitive *L. bulgaricus* CFL1 cells exhibited a higher number of rigid domains than the cryoresistant ones as well as a broadening of the domains with osmotic stress. This supports our recent hypothesis for the deleterious interaction between sucrose molecules and the phospholipid headgroups of *L. bulgaricus* CFL1, absent in the case of *L. bulgaricus* ATCC 11842 (Meneghel *et al*. 2017). By replacing hydrating water molecules at the membrane surface of *L. bulgaricus* CFL1, sucrose would lead to a high heterogeneity in membrane fluidity and broad lipid domains that could possibly prevent correct lipid reorganization and free movement, thus affecting membrane functioning. As reported by Lin and Weibel (2016), specific membrane lipids are required for bacterial processes, including cell division. Such membrane disruption could potentially lead to a reduced ability of cells to divide and to lethal leakages.

In conclusion, this work quantified for the first time membrane fluidity at a subcellular level as a key biophysical property of the bacterial membrane. Its modification with freeze-related environmental stresses was also investigated and associated to bacterial cryoresistance. Small cells, exhibiting high initial membrane fluidity and low degree of inter- and intra-cellular heterogeneities of this property appeared positively related to cryoresistance. The visualization of lipid domains of high rigidity within the membrane of lactobacilli raises several scientific questions and new fields of investigation, in particular the precise composition of lipid domains and their mechanisms of formation. Furthermore, the protective mechanism of sucrose molecules appears to be versatile and dependent on membrane composition. The presumed harmful interaction between sucrose and rigid domains needs further studies.

Acknowledgements

This work was supported by the French National Institute for Agricultural Research (INRA) and the French National Research Agency (ANR) under the Investing in the Future Program, Grant n°ANR-10-IDEX-0003-02. It was conducted on the DISCO beamline of the SOLEIL synchrotron (Gif-sur-Yvette, France) under the project 20140401, and we are grateful to the beamline staff for providing assistance on the experimental work.

3.2. Key points

- More homogeneous distribution of membrane fluidity in the cryoresistant *L. bulgaricus* ATCC 11842 compared to the cryosensitive *L. bulgaricus* CFL1;
- Significant membrane rigidification and inter-cellular heterogeneity increase in *L. bulgaricus* ATCC 11842 under cold and hyperosmotic conditions; idem for *L. bulgaricus* CFL1 but only under cold stress;
- Existence of high anisotropy domains within individual cells, preferentially located at cellular extremities; more numerous domains in *L. bulgaricus* CFL1 cells compared to *L. bulgaricus* ATCC 11842; increase of their number in *L. bulgaricus* CFL1 under stressful conditions, and increase of their mean width under hyperosmotic stress;
- Information supporting the existence of deleterious interactions between increasing concentrations of sucrose and the membrane of the cryosensitive strain.

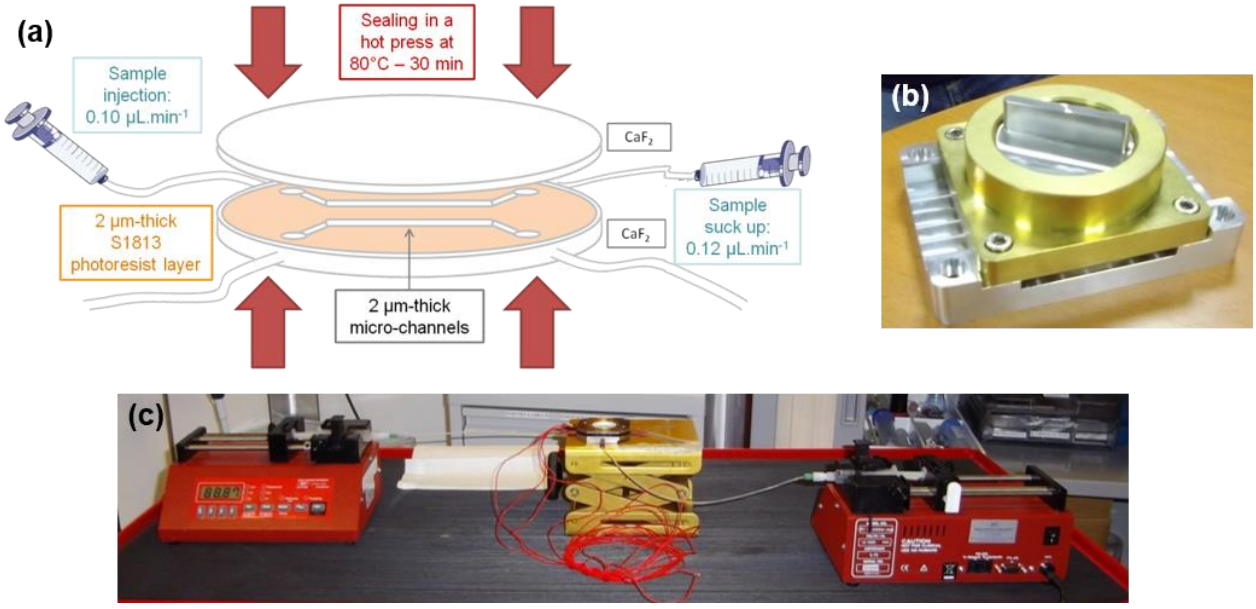

Figure IV.4-1: Microfluidics experimental set up: **(a)** schematic view of the microfluidic cell, **(b)** picture of the hot press, and **(c)** picture of the whole experimental set up, with syringes and pumps for sample injection on the left and for sample suck up on the right, and the microfluidic device in-between.

IV. Towards the analysis of single bacteria in an aqueous environment using synchrotron infrared micro-spectroscopy

4.1. Context and objectives

The interest for non-invasive *in situ* analytical techniques stands in the wish to probe matter as closely as possible to reality with minimum perturbation of the specimen, as well as allowing in real time monitoring of the effects of various environmental conditions. Another important requirement is to attain high resolution, thus enabling single cell analysis and heterogeneity assessment of the parameter under investigation. FTIR micro-spectroscopy gives a nonrestrictive chemical description of the major cellular components (lipids, proteins, etc.). Relating such information to cryoresistance would thus help identifying cellular stress markers and understanding cryodamage mechanisms. The broad IR spectrum of biological samples is usually analysed in the dry state, because of the intense IR absorption of water bond vibrations that masks, in particular, the spectral region carrying information on cell protein conformation (the amide I band). With the aim of using FTIR spectroscopy to analyse single bacterial cells in their aqueous environment and achieve deep biophysical characterisation, technological developments were undertaken and got into different stages.

Our first strategy was to design a microfluidic cell to perform transmission FTIR micro-spectroscopy from isolated bacteria in solution, after visually locating them by microscopy. The idea was to work with an extremely small channel height (2 µm) to reduce the quantity of sampled water and thus allow its subsequent spectral subtraction. Real-time monitoring of cell response to various kinds of stress in an aqueous solution were envisioned with such fluidic devices. The microfluidic cell comprised circular CaF_2 windows as substrate and lid. A layer of S1813 positive photoresist (Shipley; Marlborough, MA, USA) was deposited by spin-coating on the substrate window, and lithographed to define two micro-channels (**Fig. IV.4-1a**). Photolithography was kindly processed by William André (SMIS local contact). The lid was thermomechanically sealed on the top of the substrate using a newly acquired hot-press to ensure a strong adhesion of both windows (80°C, 30 min, **Fig. IV.4-1b**). A micro-channel was connected to two syringes pumping for fluid circulation with a slight depression to help guiding the fluid and prevent it from leaking out (inlet: 0.10 µL.min^{-1}, outlet: 0.12 µL.min^{-1}, **Fig. IV.4-1c**). Filling the microfluidic device with a liquid sample required a couple of hours because of the very low flow rate. Despite the use of a hot-press and cautiously implementing the microfluidic device, leakages could not be avoided. Besides, when the fluid circulation was momentarily stopped to acquire FTIR spectra on immobilized cells, the micro-channel dried in less than 5 minutes. These drawbacks were due to the excessively small thickness of the micro-channels, preventing leak-tightness.

A demountable CaF_2 micro-chamber (Hellma Analytics; Paris, France) was then used to perform transmission FTIR micro-spectroscopy on the Continµum II microscope coupled to a Nicolet 8700 FTIR

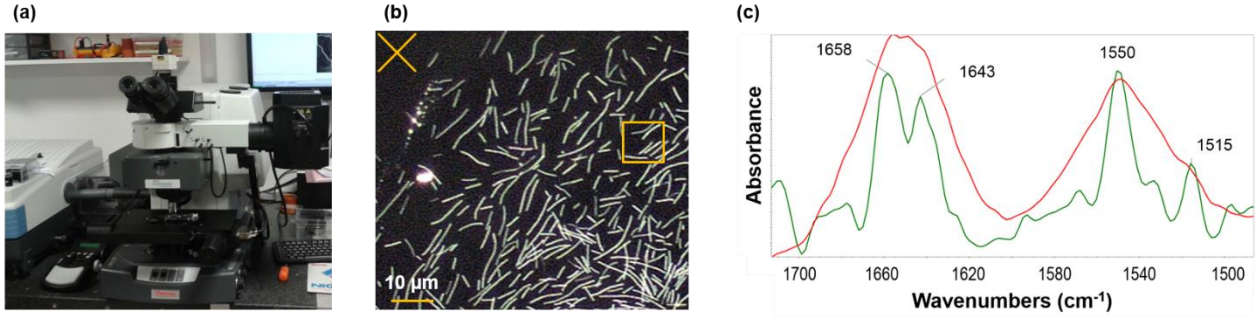

Figure IV.4-2: Illustration of the device combining transmission FTIR spectroscopy to the static micro-chamber for analysis of clusters of 5-6 bacterial cells in an aqueous environment using synchrotron radiation. **(a)** Picture of the Continuµm II microscope (Thermo Scientific; USA), **(b)** Microscopy field of view image showing an optimal sample deposit of *Lactobacillus delbrueckii* subsp. *bulgaricus* CFL1 cells in saline water (10x magnification factor), allowing the acquisition of background and sample FTIR spectra of 4-5 cells spatially close from each other (orange cross and square, respectively; scale-bar: 10 µm), and **(c)** example of a FTIR spectrum obtained in the amide region (in red) and its inverted second derivative (in green).

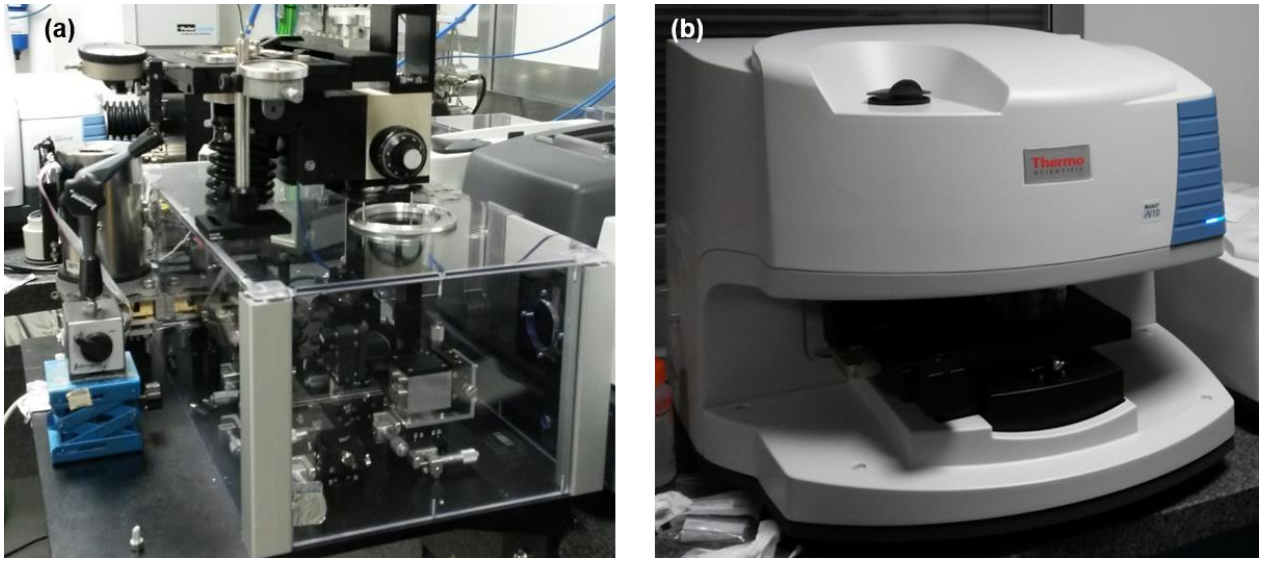

Figure IV.4-3: Images of **(a)** the custom-design inverted microscope for the analysis of individual bacterial cells in an aqueous environment, and **(b)** the Nicolet IN10 IR microscope for the analysis of a few thousands of bacterial cells in an aqueous environment.

spectrometer (Thermo Scientific; USA) equipped with MCT detector (**Fig. IV.4-2a**). The micro-chamber was filled with a bacterial solution of appropriate dilution to record spectra from clusters of 5-6 cells with a projected beam size on sample set at 10 x 10 µm². A suitable bacterial deposit required individualised cells close from an area devoid of bacteria, to enable the acquisition of sample and background spectra, respectively. A cell concentration gradient equivalent to those shown on the microscopy images (**Fig. IV.4-2b**) were considered ideal. The exact optical path of the micro-chamber was not controlled and local microvariations of the optical path between background and sample spectra indeed had important consequences on the resulting spectrum. Although adequate sample deposits were difficult to be obtained, we succeeded in recording some good quality FTIR spectra arising from clusters of 5-6 bacteria in solution (**Fig. IV.4-2c**).

In parallel, experimental tests were performed in Attenuated Total Reflexion (ATR) mode using a thermal source. They revealed the interest for developing an experimental setup for the exploitation of individual or small groups of bacteria in solution, by combining an inverted ATR configuration with synchrotron radiation to microscopy. Simple cell deposition over the ATR crystal under their own weight indeed ensured a sufficiently intimate contact with the ATR crystal for allowing the evanescent wave to interact with cells and only with some surrounding and underlying water.

From these results, the engineering of this "inverted microscope" device started. The work of conception, design, order of optical components and other equipment, setting up and alignment of the synchrotron radiation was performed by Paul Dumas and Stéphane Lefrançois from the SMIS beamline. This device, shown in **Fig. IV.4-3a**, was first tested using ATR hemispheres in ZnSe. Unfortunately, such material has a too low refractive index ($RI_{ZnSe} = 2.4$) to meet the critical angle of the ATR configuration and the resulting spectra combined ATR and external reflectance features. A second trial was operated later on with Germanium ATR hemispheres ($RI_{Ge} = 4.0$).

The aim of the work presented thereafter was thus to obtain IR spectra from individual *L. bulgaricus* CFL1 and ATCC 11842 cells in an aqueous environment by using the developed inverted microscope. Moreover, a transmission FTIR configuration using the CaF_2 demountable micro-chamber (Hellma Analytics; Paris, France) and the internal thermal source of a Nicolet IN10 IR microscope (Thermo Scientific; USA, **Fig. IV.4-3b**) was launched in parallel. This time, the micro-chamber was maintained tightly close using a dedicated sample holder (in-house device, Stéphane Lefrançois). Spectra could thus be obtained from a few thousands of *L. bulgaricus* CFL1 and ATCC 11842 cells in an aqueous environment. In both cases (individual and a few thousands of cells), water was subtracted from sample spectra using an in-house program (created by Frédéric Jamme). Sample spectra acquired with both configurations originated from the same cell productions, allowing their relative comparison for the identification of cellular stress markers and the evaluation of population heterogeneity.

The results are presented in the form of a scientific article to be submitted for publication to *Analyst* or *Journal of Synchrotron Radiation*.

4.2. Article

Authors

Julie Meneghel[1] • Stéphanie Passot[1] • Frédéric Jamme[2] • Stéphane Lefrançois[3] • Pascale Lieben[1] • Paul Dumas[3] • Fernanda Fonseca[1]

Title

Towards the analysis of single bacteria in an aqueous environment using synchrotron infrared micro-spectroscopy

Affiliations

[1] UMR GMPA, AgroParisTech, INRA, Université Paris-Saclay, 78850 Thiverval-Grignon, France

[2] Synchrotron SOLEIL, DISCO beamline, Gif-sur-Yvette, France

[3] Synchrotron SOLEIL, SMIS beamline, Gif-sur-Yvette, France

Address all correspondence to Fernanda Fonseca. Email: fernanda.fonseca@inra.fr; Phone: +33 (0)1 30 81 59 40; Fax: +33 (0)1 30 81 55 97

Abstract

Fourier transform infrared (FTIR) spectroscopy is a non-invasive probe for biological samples without the need for exogeneous dyes or probes. However, investigations of samples in their aqueous environment is limited by the high infrared absorption of water vibrational motions. Eukaryotic cells have been successfully studied at the single cell level and in aqueous environments, but for prokaryotic microorganisms this challenge has not been met so far. To reach this goal, a new optical set up was developed in this work for recording the FTIR spectra from individual *Lactobacillus delbrueckii* subsp. *bulgaricus* cells in physiological conditions (saline water). An inverted Attenuated Total Reflexion (ATR) configuration coupled with IR microscope objective was designed, and associated with the use of a high brightness infrared source from synchrotron radiation. High infrared refractive index Germanium ATR hemispheres were used in combination with small apertures to reduce the projected beam size on sample to 1 x 1 µm², and a sampling chamber adapted to receive liquid samples was designed. The FTIR spectra obtained from a cryosensitive and a cryoresistant *L. bulgaricus* strains were analysed and compared in the 1800 – 1300 cm^{-1} region. In parallel, the same samples were analysed down to 975 cm^{-1} with a lower spatial resolution (50 x 50 µm²) using demountable micro-chambers and the internal source of a FTIR microscope. In both cases, water subtraction was accurately and reproducibly performed using an in-house program. Both approaches suggested a relationship between cryoresistant cells and protein structures in β-sheets. Moreover, the lower resolution FTIR experiment indicated compositional and/or conformational differences in the cell envelope (carbohydrates and phosphorylated molecules) of both strains. The combined approaches provided information at different levels of population heterogeneity, and together highlighted a relationship between a homogeneous population of *L. bulgaricus* cells and cryoresistance.

Keywords

FTIR spectroscopy • native conditions • single bacteria • water subtraction • population heterogeneity

Introduction

Fourier transform infrared (FTIR) spectroscopy in the mid IR region (4000 - 400 cm^{-1}) is able to provide a wide range of chemical information on biomolecules and has thus revealed to be a powerful analytical technique for characterising complex biological samples. Molecular motions involving vibrations of chemical bonds are at the origin of infrared absorption. Infrared absorption is sensitive to the type of vibration and to the nature of the chemical bond involved (stretching or bending, its dynamic dipole moment, its force constant, the mass of its constitutive atoms) and to the environment. It is thus possible to identify vibrational motions from lipids, proteins, carbohydrates or nucleic acids, among others. As a mid-IR spectrum is composed of thousands of wavenumbers carrying information on the vibrational modes of the sample's components, a pure microbial sample has a very specific infrared signature, often referred to as infrared chemical fingerprint (Norris 1959; Naumann *et al*. 1991). Microbial species and strains have thus been distinguished and/or identified by FTIR spectroscopy using multivariate data analysis (Naumann *et al*. 1988; Helm *et al*. 1991; Sandt *et al*. 2006; Puzey *et al*. 2008; Wenning *et al*. 2014; Grangeteau *et al*. 2016; Johler *et al*. 2016), including lactic acid bacteria (LAB) (Amiel *et al*. 2000; Savić *et al*. 2008; Wenning *et al*. 2010). This makes FTIR spectroscopy a very sensitive analytical tool in particular for biological species. Besides, because vibrational modes are sensitive to the force constant of a chemical bond, any intra or inter-molecular effect modifying the electron density in the bond will induce a change in the resulting IR spectrum. As an example, one may consider the intramolecular effects in the fingerprint of protein secondary structures, named amide I band. This broad IR vibrational massif is centred at approximately 1660 cm^{-1}. It mainly involves the C=O stretching vibration ($\nu C{=}O$). This large massif is composed of subbands related to the various secondary structures of the proteins (α-helices, parallel and antiparallel β-sheets, turns, random coils…). Therefore, this vibration is not sensitive to the side chain amino acid residues, but to their spatial arrangement into secondary structures (Barth and Zscherp 2002). Because of the relationship between protein structure and function, the study of the amide I band is of particular interest for the characterisation of stressful treatments on microbial cells, including yeasts (Saulou *et al*. 2010; Pénicaud *et al*. 2014) Gram-negative (Saulou *et al*. 2013) and Gram-positive bacteria (Oldenhof *et al*. 2005; Passot *et al*. 2015).

Analytical advantages of FTIR spectroscopy also include the absence of required exogenous probes or contrast agents into the sample, and the absence of radiation damage to biological samples (Holman *et al*. 2003), making it a non-invasive analytical tool. The majority of FTIR analyses are however currently performed on concentrated cell pellets or dried samples because water absorbs strongly in the mid-IR region, causing problems in the exploitation of the weak spectral features superimposed in the intense water absorption bands. Water may be removed from samples by centrifugation or by drying. However, centrifugation does not remove water completely and drying constitutes a stressful process that may introduce modifications to the sample spectra (Vaccari *et al*. 2012a). In both cases, the interpretation of the shape of the Amide I band becomes doubtful. To circumvent the water issue, Vaccari *et al*. (2012a) used closed-channel microfluidic devices to probe live monocytes by transmission FTIR spectroscopy. In this

case, the volume of water surrounding the sample is reduced at minimum, and the resulting weaker signal from water allowed a subtraction procedure to be undertaken. The use of sample holders with a short pathlength associated with optimized procedures for water subtraction would be an interesting approach to be developed for the analysis of microbial samples in solution by transmission FTIR spectroscopy. Furthermore, Attenuated Total Reflectance (ATR) FTIR spectroscopy offers the possibility to investigate the formation and growth of bacterial biofilms under native conditions by growing them directly over ATR crystals (Marcotte *et al*. 2004; Delille *et al*. 2007; Comeau *et al*. 2009; Quilès *et al*. 2010; Humbert and Quilès 2011). In such a configuration, the evanescent wave produced at the ATR surface interacts with bacterial cells in intimate contact with the ATR crystal and not with the liquid flowing over the biofilm. FTIR spectroscopy thus enables real-time monitoring of biological processes in physiological conditions through different sampling modes. Besides, Kazarian and Chan (2013) proposed to associate liquid ATR spectroscopy to microscopy, and to seed adherent eukaryotic cells on the surface of removable ATR hemispheres for their mapping in an aqueous environment. They used a focal plane array detector (which simultaneously acquires an array of 64 by 64 or 128 by 128 spatially resolved spectra), and the liquid sample was held in place by capillary forces.

The next step forward into the exploitation of the high-resolution capabilities of FTIR spectroscopy is to analyse individual bacteria and address the population heterogeneity issues. By developing strategies aiming at reducing the IR pathlength, authors have achieved the dual challenge of analysing single cells and in solution. The closed-channel microfluidic devices developed by Vaccari *et al*. (Vaccari *et al*. 2012a) were thus used in combination with the high brightness of the synchrotron radiation (SR) to analyse individual living monocytes (~ 9 µm in diameter) in buffer (Vaccari *et al*. 2012b). Likewise, Tobin *et al*. (Tobin *et al*. 2010) pioneered in this field with demountable liquid cells and the analysis of the algae *Micrasterias hardyi* as well as individual leukaemia cells in an aqueous environment (projected beam size of 7 x 7 µm²), while Holman *et al*. (2009) used open-channel microfluidic devices to study biofilm dynamics at a high spatial resolution (with a projected beam size of about 10x10 µm²). These studies have in common the exploitation of small pathlengths (typically below 10 µm) along with the combination of synchrotron beam brightness and small apertures to reduce the IR beam size for spatial resolution increase. The use of the synchrotron radiation is indeed mandatory to provide sufficient photon flux, at diffraction-limited beam size, from single cells and to detect them.

Equivalent achievement on prokaryotes has not been performed yet. The challenge is indeed greater because of the smaller size of cells, but clusters of 4-5 *Escherichia coli* and *L. bulgaricus* cells (rods with projected areas of 2 µm² and 3-5 µm², respectively) have recently been analysed in the dry state by SR-ATR FTIR spectroscopy combined with microscopy (Saulou *et al*. 2013; Passot *et al*. 2015, respectively). For that, the authors used high refractive index ATR hemispheres (in ZnSe; refractive index = 2.40) coated with dried bacteria and achieved spatial resolutions (*i.e.*, projected beam size) of approximately 4.1 and 3.3 µm², respectively (Saulou *et al*. 2013; Passot *et al*. 2015, respectively). However, due to the upside-down position of the sample, this setup is hardly adaptable to the analysis of live cells in solution.

From this literature review, it appears that FTIR spectroscopy may be applied to the analysis of individual live eukaryotic cells on the one hand, and of dried bacterial cells with a high spatial resolution on the other hand. In the present work, an equivalent setup of liquid ATR micro-spectroscopy as that presented by Kazarian and Chan (2013) was further associated to synchrotron radiation. The aim was to address the dual challenge of analysing individual bacteria and in an aqueous environment, through the development of a new FTIR micro-spectroscopy equipment on the SMIS beamline of SOLEIL synchrotron. An SR-ATR FTIR spectroscopy experiment coupled to an inverted microscope designed for this purpose is described in the following, in which a liquid chamber standing over a Germanium hemisphere contained live *L. bulgaricus* cells. Populations of a few thousands of the same bacterial cells in solution were analysed in parallel by transmission FTIR using demountable liquid cells without SR and the spectral results from both FTIR approaches were compared. In both cases, an in-house program was used to subtract the contribution of water from sample spectra in an optimized manner.

Material and methods

Bacterial strains, growth conditions, freezing procedure and preparation of cell suspensions

Two strains of the lactic acid bacterium *Lactobacillus delbrueckii* subsp. *bulgaricus* were used in this study: CFL1 (CIRM-BIA; Rennes, France) and ATCC 11842 (Manassas, VA, USA). They were cultivated according to the procedure described by Meneghel *et al*. (2017), resulting in the recovery of cryosensitive *L. bulgaricus* CFL1 and cryoresistant *L. bulgaricus* ATCC 11842.
Briefly, cultivation of bacteria was performed at 42 °C in a whey-based medium consisting of 60 g L^{-1} whey powder (Eurosérum; Port-sur-Saône, France) supplemented with 5 g L^{-1} yeast extract (Organitechnie SAS; La Courneuve, France) until the end of exponential growth phase. Cells were then harvested by centrifugation (11,000 x *g* for 10 min at 5 °C) and washed twice with Tris-HCl buffer (50 mM, pH 8.8, Bio-Rad; Hercules, CA, USA) to remove growth residues and metabolites that may contribute to the vibrational spectra. Cells were additionally washed in saline water before analysis.

Freshly harvested and washed bacterial samples were analysed in solution by FTIR spectroscopy on two different devices to provide analysis at different spatial resolutions: (i) spectra of individual cells were acquired by ATR FTIR spectroscopy coupled to an inverted microscope using a liquid chamber and synchrotron radiation, and (ii) spectra of a few thousands of cells were acquired with a thermal source using a Nicolet IN10 IR microscope in transmission mode and a liquid micro-chamber and sample holder. All data were recorded with Omnic software (Version 8.1, Thermo Scientific, USA).

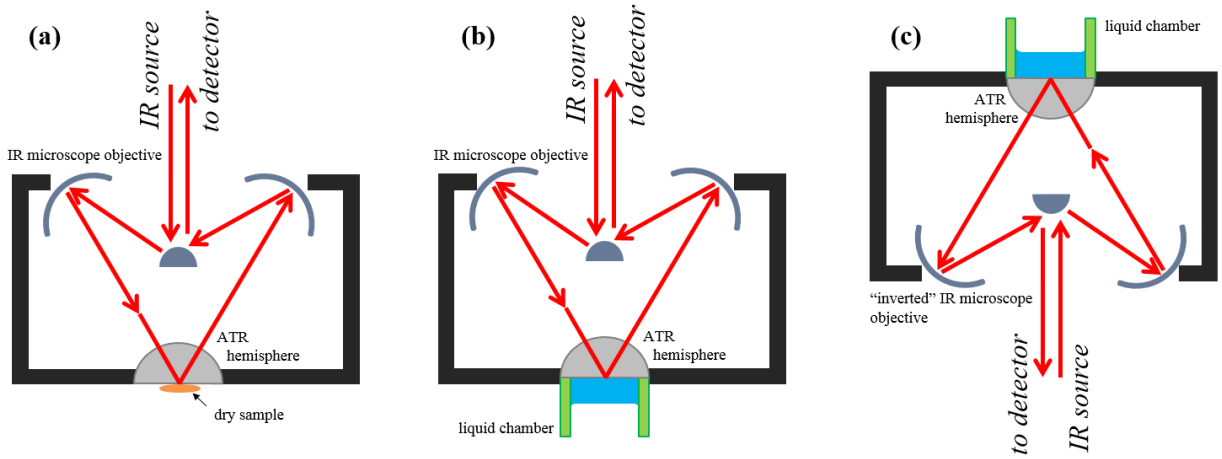

Figure IV.4-4: Schematic diagrams showing different ATR FTIR spectroscopy setups: **(a)** classical ATR FTIR micro-spectroscopy setup described by Saulou *et al*. (2013) and Passot *et al*. (2015), **(b)** liquid ATR FTIR micro-spectroscopy setup described by Kazarian and Chan (2013), and **(c)** "inverted" ATR FTIR micro-spectroscopy setup developed in this work.

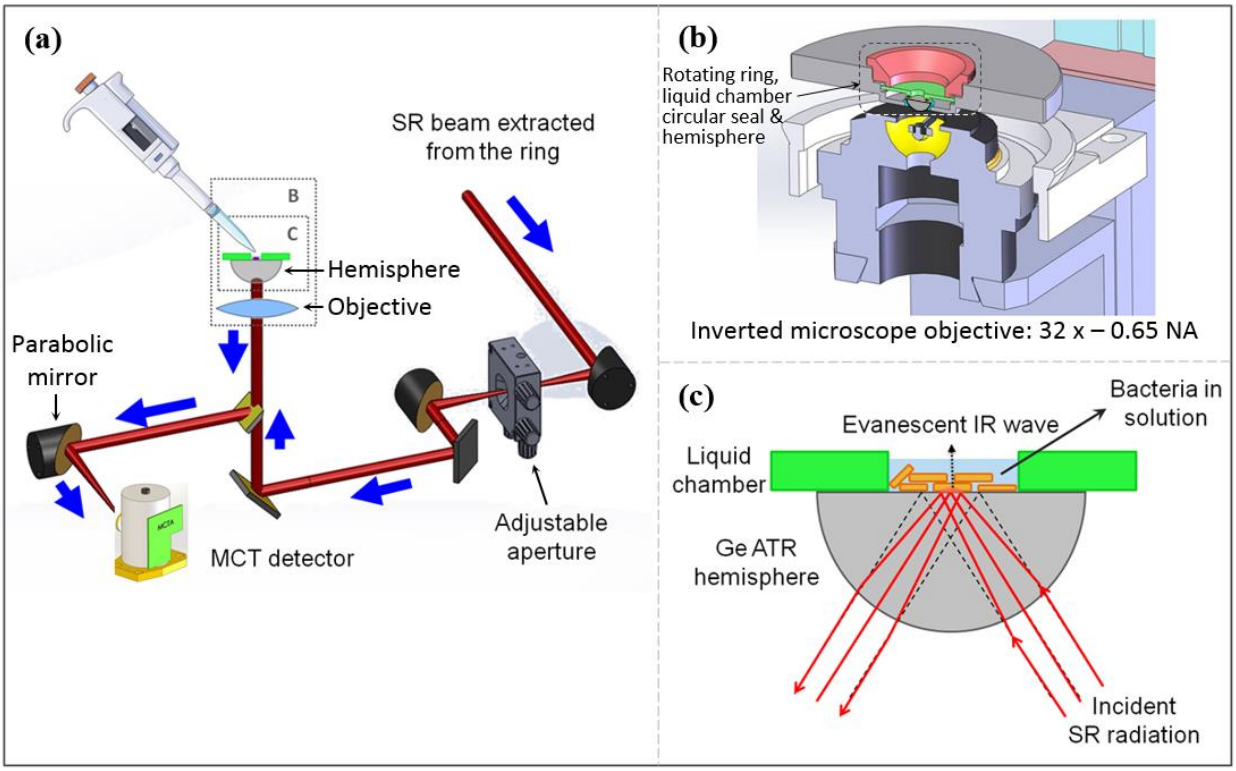

Figure IV.4-5: Scheme of the ATR FTIR micro-spectroscopy device developed for the analysis of individual bacterial cells in solution on the SMIS beamline of SOLEIL synchrotron (Gif-sur-Yvette) with **(a)** the overview of the optical path of the IR beam, **(b)** a cross-section view of the inverted microscope objective, hemisphere and liquid chamber, and **(c)** an enlargement diagram of the liquid sampling area showing the Attenuated Total Reflectance (ATR) principle.

ATR-FTIR micro-spectroscopy using synchrotron radiation in an aqueous environment (new inverted microscope)

In order to achieve the analysis of individual bacteria in an aqueous environment, a specific setup was developed on the SMIS beamline of SOLEIL synchrotron (Gif-sur-Yvette). The ATR FTIR micro-spectroscopy device described by Kazarian and Chan (2013) was thus modified. Usually, ATR-FTIR spectroscopy setups (without microscopy) consist in focusing the IR beam directly at the surface of the ATR crystal (a single-bounce hemisphere or a multi-bounce geometry) on which a sample is deposited. By placing an ATR hemisphere in upside-down position (**Fig. IV.4-4a**), it has been possible to combine such a set up for microscopic analysis, in which the IR (upright) microscope objective focused at the base of the ATR hemisphere surface. This type of setup was used by Saulou *et al*. (2013) and Passot *et al* (2015) for their analysis of dried bacterial samples. However, it becomes tricky for liquid samples, although Kazarian and Chan (2013) were able to maintain aqueous solutions in place by capillary forces, as shown in **Fig. IV.4-4b**. It has to be pointed out though, that such a configuration is delicate and adaptable only to adherent cells to ensure a permanent intimate contact with the ATR crystal. In the present work, we used an inverted ATR configuration, along which the bacteria will naturally deposit on the surface of the ATR crystal. As the hemisphere was maintained with its base in an upright position, liquid samples can be easily introduced, as illustrated in **Fig IV.4-4c**.

Because of the very small dimension of bacteria for analysis at a single cell level, a high photon flux was required and the device was thus connected to synchrotron radiation (SMIS beamline, SOLEIL synchrotron, Gif-sur-Yvette, France) which has approximately 1000 times higher brightness than conventional thermal sources (Dumas and Miller 2003). A schematic overview of the device and enlargements of the inverted optical configuration and sampling areas are presented in **Fig. IV.4-5**. The synchrotron source was extracted and focused by a parabolic mirror through an adjustable aperture, set at 128 x 128 µm² (**Fig. IV.4-5a**). The beam was then collimated and reduced by a factor of 32 through a Schwartzschild objective (32x – NA 0.65; **Fig. IV.4-5b**). Finally, focusing through a high refractive index (RI) ATR hemisphere in Germanium (RI_{Ge} ≈ 4.01 in the mid IR region) reduced the beam size by a factor equal to the refractive index. The flat face of the Ge hemisphere constituted the base of the liquid sampling chamber, as shown in **Fig. IV.4-5c**. The body of the chamber was appended to the base of the ATR hemisphere with a circular seal in between and water-tightness was guaranteed by pressing the assembly together thanks to a rotating ring. The liquid chamber could be closed during experiments thanks to a screw cap. Hemisphere and liquid chamber were supported by an X Y linear translation stage, and all optical components were insulated from humidity in a box constantly purged with dry air.

The performances of this setup were very satisfactory, and fulfilled our expectations regarding the potentiality of recording infrared spectra of individual bacteria (*i.e.*, the peak-to-peak voltage was higher than the signal-to-noise ratio). For example, a signal-to-noise ratio of 0.42 % transmittance unit has been achieved with a 1 x 1 µm² projected beam size, and with 100 co-added scans at 4 cm^{-1} resolution, for a peak-to-peak voltage of 2V.

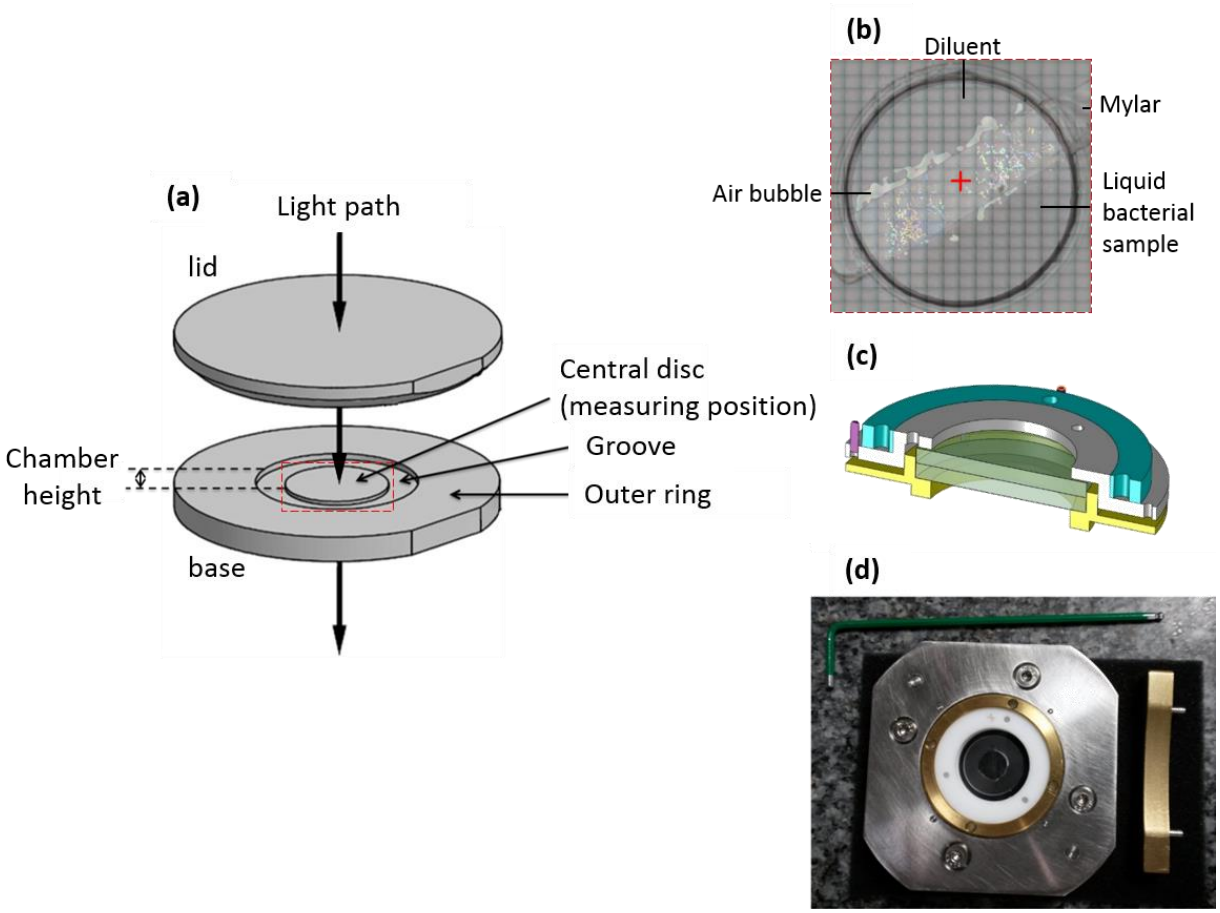

Figure IV.4-6: (a) Schematic view of a demountable CaF_2 micro-chamber (Hellma Analytics, Paris, France; adapted from www.hellma-analytics.com), **(b)** mosaic image of the sampling area (enlargement of the red dotted area in **(a)**) where the diluent and liquid sample are separated by a Mylar strip, **(c, d)** technical drawing and picture of the sample holder maintaining the micro-chamber tightly close, respectively.

A background spectrum was recorded at the centre of the hemisphere in the absence of sample (128 co-added scans, 4 cm^{-1} resolution). A volume of 10 µL of saline water (the diluent) was then poured in the chamber and spectra were acquired. Saline water was removed and dryness of the hemisphere was verified by checking the disappearance of the water O-H stretching vibration in preview mode (the broad band centred at ~3400 cm^{-1}). A volume of 10 µL of a bacterial suspension in saline water was then poured in the chamber. Spectral features of bacterial cells became more and more visible as cells dropped down on the bottom of the liquid chamber until contact with the hemisphere. Once the amide II band arising from cell proteins appeared (after typically 15 min), 50-100 spectra at different locations spread around the centre point of the hemisphere were recorded (128 co-added scans, 4 cm^{-1} resolution). The X Y stage had a translation step of 5 µm, which ensured probing different cells at each position. Sampling was performed up to 30 µm away from the centre point, while remaining at focus.

The projected beam size at the interface of the Ge hemisphere was theoretically 1 x 1 $µm^2$ (setting an intermediate aperture at 128 x 128 $µm^2$), and the penetration depth (d_p) of the evanescent wave was lower than 1.6 µm (effective d_p at 3000 cm^{-1} (lipids region) = 0.53 µm; 1650 cm^{-1} (proteins region) = 0.96 µm; 1000 cm^{-1} (carbohydrates region) = 1.59 µm). In such a configuration, and given the size of the rod-shaped bacteria under investigation (1 µm thick x 3 – 6 µm long) as determined in a previous study (Meneghel *et al*. 2017), the absorption of IR light essentially arose from single bacteria plus some surrounding or underlying water.

Transmission FTIR micro-spectroscopy in aqueous environment (Nicolet IN10 IR microscope)

Demountable CaF_2 micro-chambers were purchased from Hellma Analytics (Paris, France). They consist of two precisely polished circular windows of 22 mm diameter and 2 mm thickness. The upper window (lid) is plain, whereas the lower window (base) presents a groove separating a central disc for sample deposition from the outer ring. The central disc of 6.7 mm diameter is recessed with respect to the outer ring to form a small chamber when closing both windows (**Fig. IV.4-6a**). A thin strip of Mylar (polyethylene terephthalate film of 2.5 µm thickness from GoodFellow; Lille, France) was placed in the middle of the central disc of the lower window to separate the chamber into two parts. One µL of saline water (the diluent) was deposited over one side of the disc and 1 µL of bacterial solution over the other side (**Fig. IV.4-6b**). The lid was immediately appended to avoid sample drying and the chamber was maintained tightly close in a dedicated sample holder (**Figs. IV.4-6c** and **IV.4-6d**). Chamber height (or light path) was accurately determined by fringes appearing on spectra: 4.3 µm ± 0.7 µm in 8 successive sample mountings. The system was placed on the motorized stage of the Nicolet IN10 IR microscope (Thermo Scientific, USA). A background spectrum was recorded in an air bubble and spectra were recorded from the diluent and bacterial locations at different positions (128 co-added scans, 8 cm^{-1} resolution). Apertures were set at 50 x 50 $µm^2$, making a sampled volume of approximately 10^4 $µm^3$. The approximate volume of *L. bulgaricus* cells being a few $µm^3$ (about 6 $µm^3$ for *L. bulgaricus* CFL1 and about 3 $µm^3$ for *L. bulgaricus* ATCC 11842), the estimated number of probed bacterial cells with this experimental setup could therefore be roughly estimated at a few thousands. Sample drying was never observed following chamber dismounting.

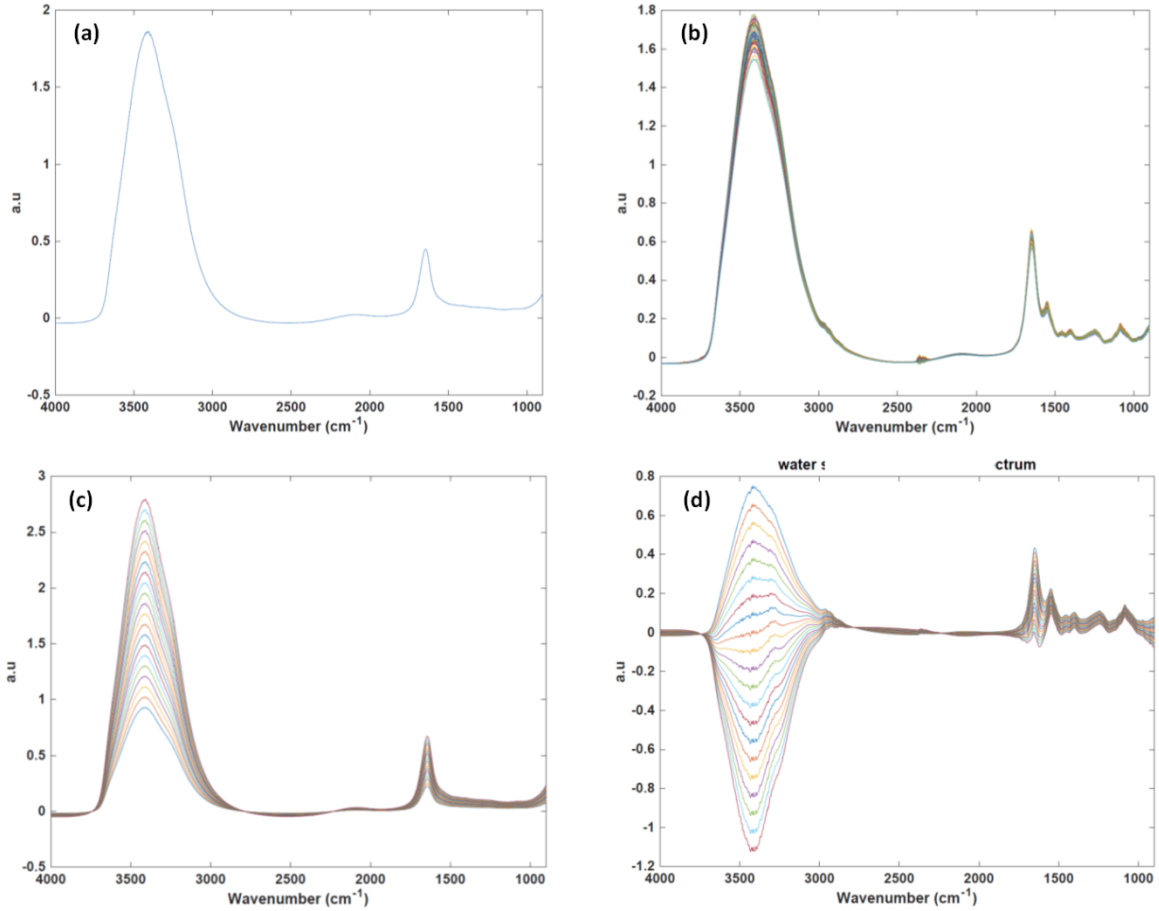

Figure IV.4-7: Illustration of the water subtraction procedure using Matlab R2014a (version: 8.3.0.532) on spectra recorded with the Nicolet IN10 IR microscope (Thermo Scientific, USA) **(a)** raw diluent spectrum, **(b)** raw sample spectra, **(c)** diluent spectrum multiplied by a range of coefficients, and **(d)** results of the subtractions between the first sample spectrum and the matrix of diluent spectra.

Spectral processing

Pre-processing

The Omnic software (Version 8.1, Thermo Scientific, USA) was used for spectral sorting and automatic atmospheric suppression. The advanced ATR correction provided by Omnic was additionally applied to ATR-FTIR spectra to correct for the wavelength dependent penetration depth of the IR radiation (parameters: RI_{Ge} = 4.01; sample RI = 1.5; angle of incidence = 30°; number of bounces = 1). In total, 282 and 267 spectra from individual *L. bulgaricus* CFL1 and ATCC 11842 cells (recorded with the inverted microscope) and 225 and 181 spectra from a few thousands of *L. bulgaricus* CFL1 and *L. bulgaricus* ATCC 11842 cells (recorded with the Nicolet IN10 IR microscope) were kept for analysis.

Water subtraction

The vibrational modes of water molecule are superimposed with some of the vibrational modes of biomolecules. In particular, the H-O-H bending mode of water which is centred around 1650 cm^{-1} interferes with the amide I of proteins. Removing spectral contributions of water has to be performed without affecting the shape and frequency position of the vibrational modes of interest in the IR spectra and avoiding over- or under-subtraction (Kong and Yu 2007). A program implemented in Matlab R2014a (version: 8.3.0.532) was specifically developed and used to perform a reproducible and accurate subtraction of water from all sample spectra recorded in this work. ATR FTIR spectra of dried cells of *L. bulgaricus* CFL1 and ATCC 11842 were recorded on Ge hemispheres from which the areas of the amide I and amide II bands were calculated. This calculation was performed on pre-processed spectra between 1727 cm^{-1} and 1584 cm^{-1}, and between 1584 cm^{-1} and 1481 cm^{-1}, respectively, with a baseline extending from 1727 cm^{-1} to 1481 cm^{-1}. The amide I/II area ratios for both strains in the dry state could thus be defined as 2.17 for *L. bulgaricus* CFL1 and 2.34 for *L. bulgaricus* ATCC 11842. The aim of the program was to optimize the subtraction coefficient that is applied to the diluent spectrum in order to approach the target amide I/II area ratios of dried samples and the procedure is illustrated in **Fig. IV.4-7**. A range of coefficients was applied to the diluent spectrum to get a spectral matrix of the diluent (number of columns = number of spectral points; number of lines = number of coefficients). Based on the work of Vaccari *et al*. (2012a), this range of coefficients was set at 0.8 to 1.0 with a step of 0.001 (**Fig. IV.4-7c**). Each line of the diluent matrix was subtracted from a sample spectrum, as shown in **Fig. IV.4-7d**. From each subtraction result, the amide I/II area ratio was calculated. The subtraction spectrum with the closest amide I/II area ratio from the target values (2.17 and 2.34) was kept.

Post-processing

Post processing of water subtracted spectra was performed with the Unscrambler® X software package (Version 10.2, CAMO Software AS, Oslo, Norway) on three spectral regions containing information about

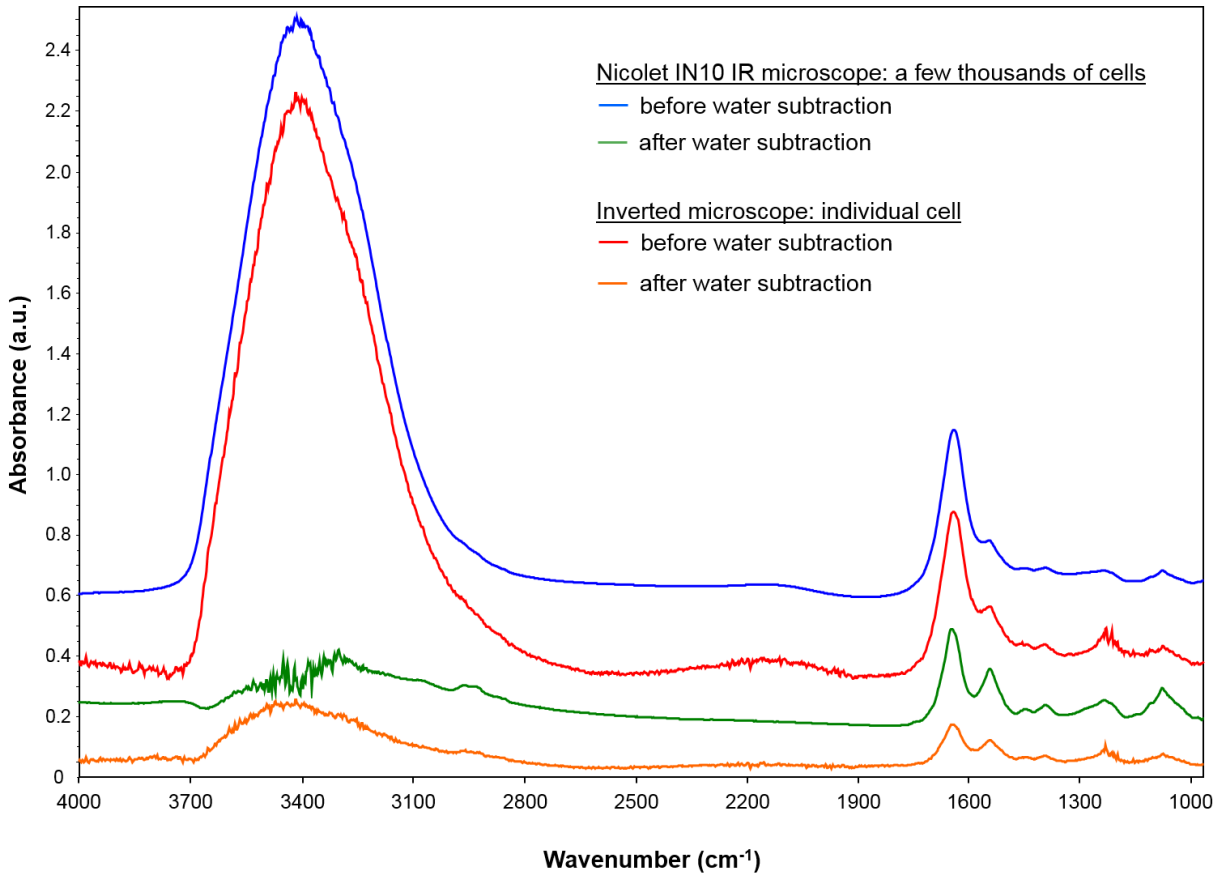

Figure IV.4-8: Example of a FTIR spectrum recorded with the commercial Nicolet IN10 IR microscope and with the new inverted ATR-FTIR micro-spectroscopy device (128 co-added scans; 4 cm^{-1} resolution) on a bacterial suspension of *Lactobacillus delbrueckii* subsp. *bulgaricus* ATCC 11842 in saline water after automatic atmospheric suppression and ATR correction. Blue and green: spectra recorded with the Nicolet IN10 IR microscope (thus probing a few thousands of cells) before and after water subtraction, respectively; red and orange: spectrum: spectra recorded with the inverted microscope (thus probing a single cell) before and after water subtraction, respectively.

lipids, proteins, and carbohydrates plus phosphorylated molecules. They spanned from 3016 to 2800 cm^{-1}, 1800 to 1300 cm^{-1} and 1363 to 975 cm^{-1}, respectively. The extended multiplicative scatter correction (EMSC) was used to normalize and correct the baseline of spectra in each of the spectral region of interest. The spectra were additionally smoothed with a 9-points smoothing factor when considering the 1800 to 1300 cm^{-1} region, and with a 5-points smoothing factor otherwise.

Spectra could then be statistically analysed by Principal Component Analysis (PCA) to visualize the variance of the data (loadings and score plots). To resolve protein secondary structures or identify precise peak locations, the second-order derivatives of FTIR spectra were calculated using a 7-points Savitzky-Golay algorithm (3^{rd} order). No relevant information could have been extracted from the analysis of the lipid spectral region, which is therefore not presented thereafter.

Results and discussion

ATR-FTIR inverted microscope reveals bacterial population protein heterogeneity

L. bulgaricus CFL1 and *L. bulgaricus* ATCC 11842 were analysed in an aqueous solution at two spatial resolutions using two FTIR spectroscopy approaches: (i) an association between demountable micro-chambers and a commercial Nicolet IN10 IR microscope in transmission mode targeting at a few thousands of cells and (ii) a custom-design inverted ATR configuration combined with microscopy and synchrotron radiation targeting at individual cells. In both cases, water subtraction procedure removed water spectral features and enhanced those arising from bacterial cells (**Fig. IV.4-8**), noticeable through the recovery of the particular shape of the amide I and II bands (1500 - 1700 cm^{-1}). The broad and intense band around 3400 cm^{-1} corresponding to O-H stretching vibration was indeed dramatically reduced and the removal of the H-O-H bending and libration combination band approximately spanning from 2500 to 1900 cm^{-1} could be evaluated through the flat baseline produced by the subtraction procedure in this region (Kong and Yu 2007). When probing a few thousands of bacterial cells, the spectral features were fairly well resolved in the region 3000 – 975 cm^{-1}, especially in the low wavenumbers (1800 – 975 cm^{-1}, blue and green spectra, **Fig. IV.4-8**). This region was limited to 1800 cm^{-1} – 1300 cm^{-1} when considering individual cells (red and orange spectra, **Fig. IV.4-8**), but constitutes an important spectral region containing information about proteins and their secondary structures. The noisy ("hairy") region between 1300 and 1150 cm^{-1} was due to high absorption of the synchrotron infrared beam when reflecting from some optical components of the beamline (aluminium-protected focusing mirrors) and could not be corrected. Regarding the higher wavenumbers (around 2800-3000 cm^{-1}), it was not possible to accurately resolve the CH stretching vibrations of lipids from the spectra recorded with the new device.

In ATR mode, the intensity of the evanescent wave decays exponentially with distance from the ATR hemisphere interface. The higher the refractive index (RI) of the ATR material is, the higher the decay is. Besides, the penetration depth (d_p) of the evanescent wave is dependent on wavelength, with shorter d_p in these high wavenumbers compared to other mid-IR spectral regions. Therefore, in the present configuration,

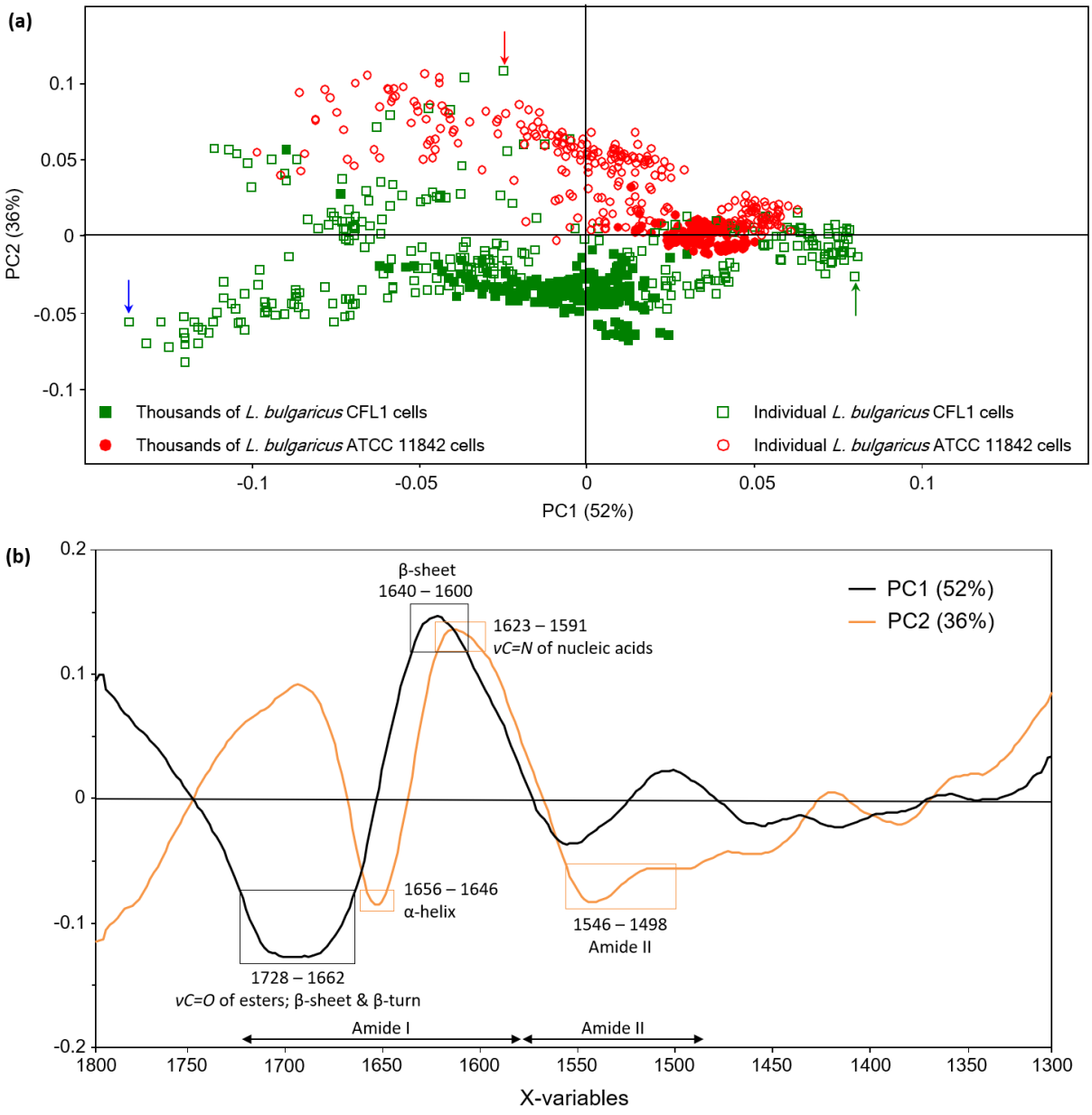

Figure IV.4-9: Principal Component Analysis (PCA) of FTIR spectra obtained on *Lactobacillus delbrueckii* subsp. *bulgaricus* samples in the 1800 – 1300 cm^{-1} region after smoothing (9-points smoothing factor). **(a)** Principal component 1 (PC1) vs. principal component 2 (PC2) score plot of *L. bulgaricus* CFL1 (green symbols) and *L. bulgaricus* ATCC 11842 (red symbols) arising from a few thousands of cells (filled symbols; spectra recorded with the Nicolet IN10 IR microscope) or individual cells (open symbols; spectra recorded with the new inverted microscope device) and **(b)** loading plots of PC1 (black) and PC2 (orange) in which the most significant variables (accounting for more than 70 % of the explained variance in correlation loadings) are highlighted by boxes.

the most external cellular components mainly contributed to the resulting ATR spectra, especially in the high wavenumbers. Extracellular cellular components of LAB are exopolysaccharides, as well as wall peptidoglycan, teichoic acids and proteins (Delcour *et al*. 1999; Kleerebezem *et al*. 2010; Chapot-Chartier and Kulakauskas 2014). In comparison, the ATR-FTIR micro-spectroscopy experiments on dried bacterial cells of Saulou *et al*. (2013) and Passot *et al*. (2015) made it possible to exploit the lipid spectral region and compare different experimental conditions. In their works, ATR hemispheres in ZnSe were used. The lower RI of ZnSe compared to Ge provided the authors with a deeper d_p of the evanescent wave. Moreover, drying cells over the surface of ATR hemispheres ensured an intimate contact allowing them to investigate deeper the biochemistry of cells compared to this liquid sampling approach, and contributes to explain the different spectral regions that could be finally exploited. A schematic drawing (**Fig. IV.4-10**) attempts to illustrate the different cellular depths probed by the different sampling modes used in this study, compared to the one used by Saulou *et al*. (2013) and Passot *et al*. (2015). Furthermore, scientific works performed on liquid ATR-FTIR spectroscopy, analysing biofilms (Comeau *et al*. 2009; Holman *et al*. 2009) or planktonic cells (Kazarian and Chan, 2013), mainly focused on the 1800 – 900 cm^{-1} region to analyse extracellular polymeric substances.

The comparison of *L. bulgaricus* strains with both approaches used in this work could thus be performed in the 1800 – 1300 cm^{-1} spectral region, containing important information especially about proteins and their secondary structure. A Principal Component Analysis (PCA) was thus performed on pre-processed and water-subtracted spectra after normalization and smoothing (**Fig. IV.4-9**). Equivalent processing – except for ATR correction – was indeed applied to all spectra to enable their comparison. The PCA score plot is presented in **Fig. IV.4-9a**, in which each data point represents a spectrum. The green ones represent *L. bulgaricus* CFL1, and the red ones *L. bulgaricus* ATCC 11842. The filled symbols correspond to spectra recorded with the Nicolet IN10 IR microscope and arise from a few thousands of bacteria, while the open symbols correspond to spectra recorded with the new inverted microscope device and represent individual cells. For each strain, the scatter plot arising from thousands of cells appeared included within the scatter plot arising from individual cells, indicating the consistency of both approaches and validating the proof of principle of the newly developed inverted microscope.

Besides, the higher dispersion characterising individual cells was mostly described by principal component 1 (PC1) which carried 52 % of the spectral variance. According to the loading plot of PC1 **Fig. IV.4-9b**, population heterogeneity was thus ascribed to various degrees of β-sheet structures (1640 – 1600 cm^{-1}) as well as C=O stretching vibrations of ester bonds, antiparallel β-sheet and β-turn structures (1728 – 1662 cm^{-1}) (Naumann 2000; Barth 2007). When considering only the spectra from thousands of cells (filled symbols, **Fig. IV.4-9a**), β-sheet structures (1640 – 1600 cm^{-1}) appeared strongly correlated to *L. bulgaricus* ATCC 11842. Furthermore, both strains were almost separated along principal component 2 (PC2), regardless of the sampling method and thus regardless of spatial resolution. Although both *L. bulgaricus* samples were genetically very close (two strains of the same subspecies) and cultivated and harvested according to the same conditions, FTIR micro-spectroscopy at single cell level could differentiate them based on their protein spectral features. This means that the IR spectra produced by individual *L. bulgaricus* CFL1 cells under

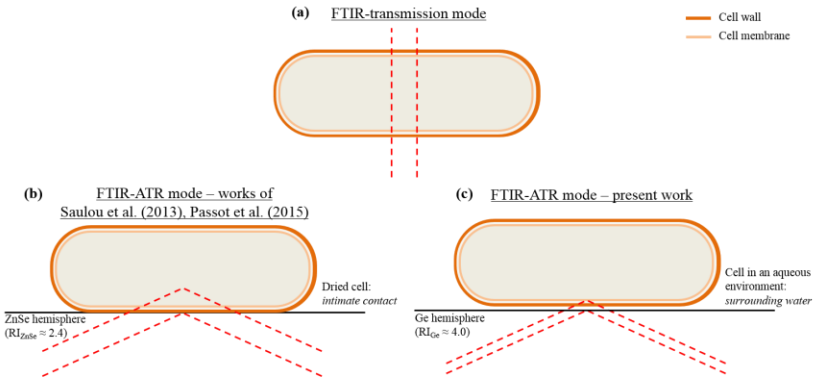

Figure IV.4-10: Schematic drawings illustrating the different cellular depths probed by **(a)** transmission-FTIR spectroscopy and ATR-FTIR spectroscopy associated with two sampling methods: **(b)** bacterial cells dried over ZnSe hemispheres ensuring an intimate contact between cells and the hemisphere surface such as in the work of Saulou *et al*. (2013) and Passot *et al*. (2015) and **(c)** cells in an aqueous environment dropping down on Ge hemisphere (present work). RI: refractive index.

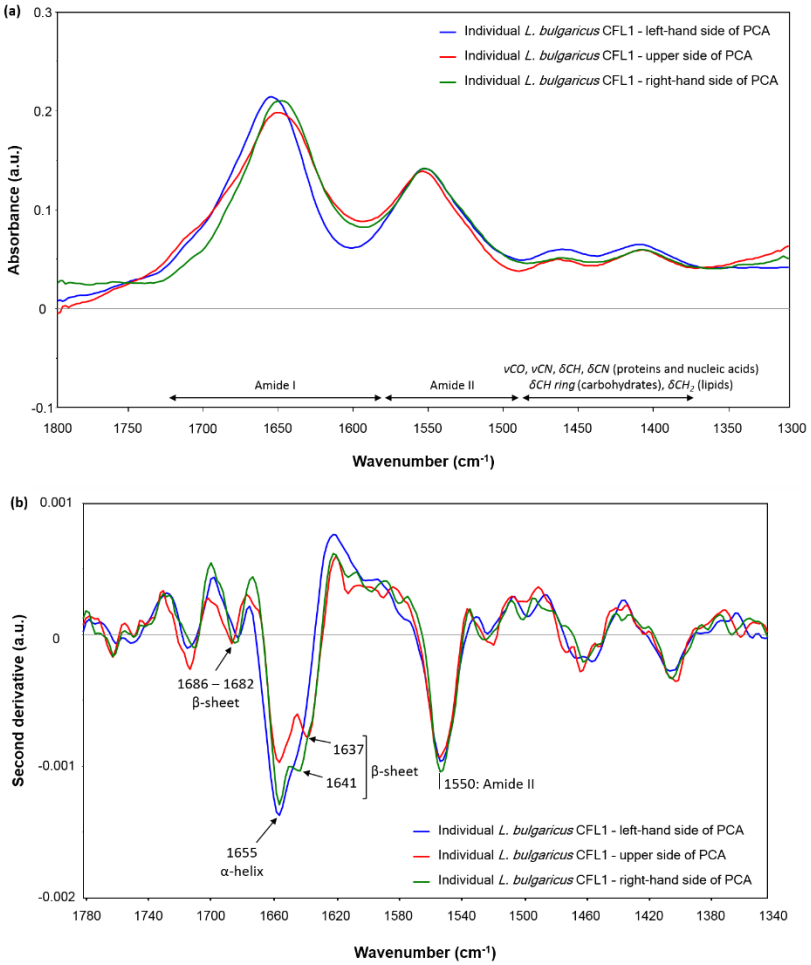

Figure IV.4-11: Selection of three of the most distant data points from the Principal Component Analysis (PCA) score plots of **Fig. III.4-9a**. **(a)** Spectra in the 1800–1300 cm^{-1} region and **(b)** their second derivatives (Savitsky-Golay algorithm; 9 points) corresponding to three different individual *Lactobacillus delbrueckii* subsp. *bulgaricus* CFL1 cells. The curve colour refers to the corresponding arrow in **Fig. IV.4-9**.

native conditions were different from the IR spectra produced by individual *L. bulgaricus* ATCC 11842 cells in the amide region, and that the signal-to-noise ratio was sufficiently good to reveal them, thanks to the use of synchrotron radiation. PC2 carried 36 % of the spectral variance and indicated a positive correlation between *L. bulgaricus* ATCC 11842 and stretching vibrations of nucleic acids (1623 – 1591 cm^{-1}) and a negative correlation with protein α-helix structures (1658 – 1646 cm^{-1}). On the contrary, most individual *L. bulgaricus* CFL1 cells were correlated to α-helix structures although a few of them spread along the upper axis of PC2.

In the literature, β-sheet structures have often been associated to lethality or stress-sensitivity. By cultivating *L. bulgaricus* CFL1 in two different media, Passot *et al*. (2015) generated a cryoresistant and a cryosensitive population of cells. The cryosensitive *L. bulgaricus* CFL1 cells were more associated with protein structures in β-sheets, and the cryoresistant cells with α-helices. In another work involving prokaryotes, Saulou *et al*. (2013) noticed a shift from α-helices towards β-sheets in *Escherichia coli* cells subjected to a lethal silver stress, suggesting a degradation of proteins secondary structures caused by silver stress. However, some elements must be kept in mind when interpreting PCA analyses and working in ATR configuration. Firstly, a PCA enables to perform a relative comparison between the input data from different experimental conditions, and prevents from directly comparing different works. Secondly and as mentioned previously, the sample preparation and material of the ATR hemispheres used in the works of Saulou *et al*. (2013) and Passot *et al*. (2015) differ from our approach. This leads to different cellular analysis depths, and thus to the assessment of proteins at different subcellular locations (**Fig. IV.4-10**). And thirdly, β-sheets may not necessarily be associated to bacterial sensitivity to cryopreservation as many cellular and membrane proteins harbour this type of conformation (Galdiero *et al*. 2007). It could be interesting to further compare the FTIR spectra of *L. bulgaricus* cells recorded in this work with the same samples in the dry state (dried over the Ge hemisphere), and evaluate whether accessing to cellular components at a deeper subcellular level leads to a different and complementary FTIR signal in the protein region.

To further analyse the spectral heterogeneity within *L. bulgaricus* in the protein region, the FTIR spectra of three of the most distant data points of the PCA arising from individual *L. bulgaricus* CFL1 cells (arrows in **Fig. IV.4-9a**) were plotted and their second derivatives were calculated. The results are presented in **Fig. IV.4-11**, in which the intensity variation of the peaks centred at 1641 – 1637 cm^{-1} and 1655 cm^{-1} (corresponding to β-sheet and α-helix structures, respectively) displays their different proportions in cells. In addition, both peaks assigned to β-sheet structures appeared to be centred at slightly different positions (between 1686 and 1682 cm^{-1} and between 1641 and 1637 cm^{-1}, **Fig. IV.4-11b**), indicating differences in terms of number of strands within the β-sheets (Barth, 2007).

The new inverted microscope device thus afforded additional information compared to lower-resolution FTIR spectroscopy: an inter-cellular level of population heterogeneity when analysing the protein spectral region. Besides, a higher population heterogeneity characterised the cryosensitive *L. bulgaricus* CFL1 compared to the cryoresistant *L. bulgaricus* ATCC 11842. In our previous work, the membrane fluidity of these *L. bulgaricus* strains cultivated under the same conditions has been analysed at subcellular resolution by UV fluorescence microscopy using synchrotron radiation (Meneghel *et al*. 2017). A higher heterogeneity

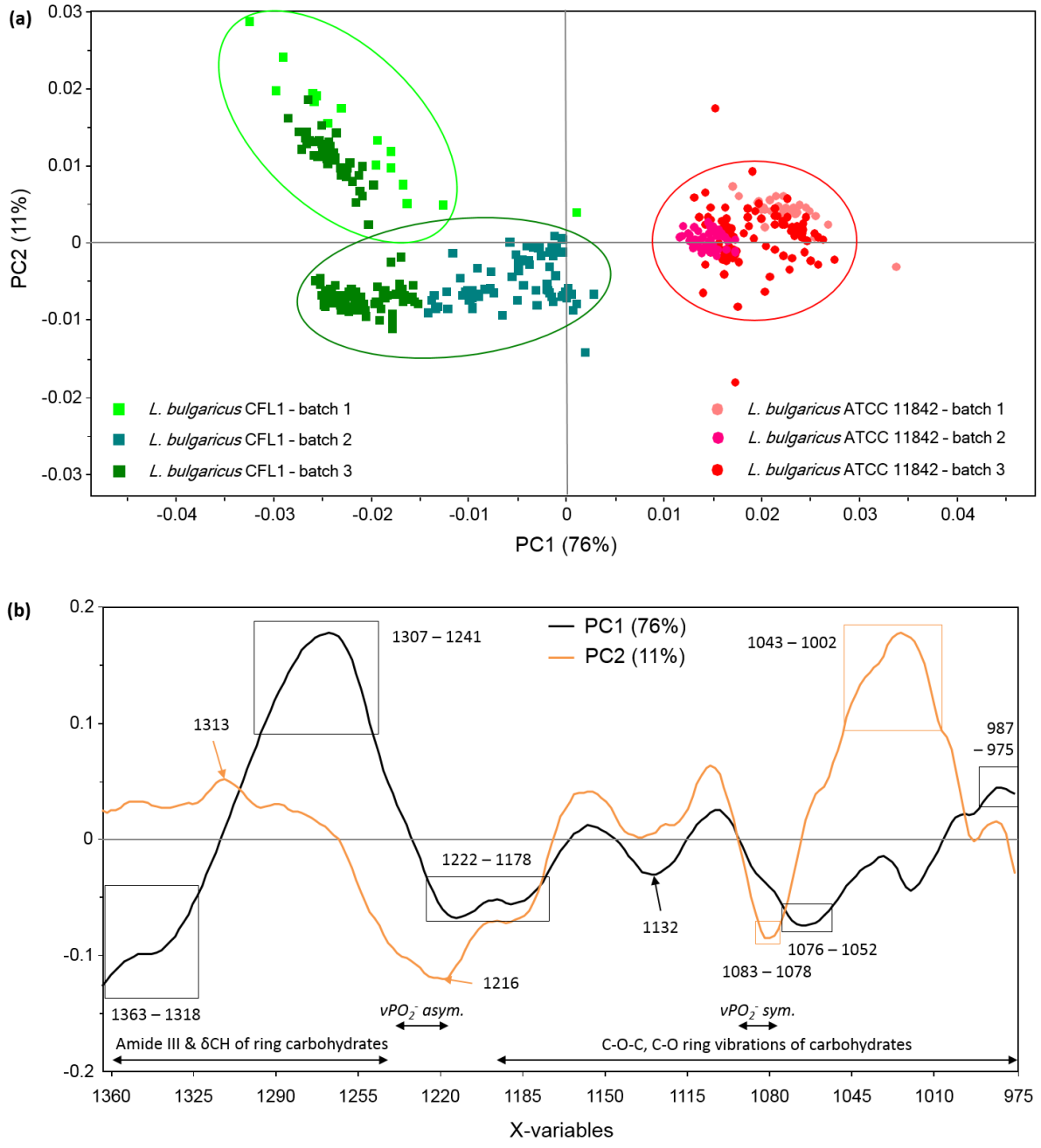

Figure IV.4-12: Principal Component Analysis (PCA) of FTIR spectra obtained from *Lactobacillus delbrueckii* subsp. *bulgaricus* samples with the Nicolet IN10 IR microscope on in the 1363 – 975 cm^{-1} region after smoothing (5-points smoothing factor). **(a)** Principal component 1 (PC1) vs. principal component 2 (PC2) score plot of *L. bulgaricus* CFL1 (green symbols) and *L. bulgaricus* ATCC 11842 (red symbols), **(b)** and corresponding loading plot of PC1 (black) and PC2 (orange) in which the most significant variables (accounting for more than 70 % of the explained variance in correlation loadings) are highlighted by boxes. Each data point represents a few thousands of cells. Shades of green and red represent different cell production batches.

in the distribution of membrane fluidity was identified between different *L. bulgaricus* CFL1 cryosensitive cells compared to *L. bulgaricus* ATCC 11842 cryoresistant cells. The present work therefore confirmed the existence of a relationship between population heterogeneity and cryosensitivity.
Characterising bacterial population heterogeneity presents several advantages. Having access to cell-to-cell variations enables to gain further knowledge on microbiological mechanisms and physiological processes that could be masked by bulk measurements (Schmid *et al*. 2010; Wang and Bodovitz 2010; Lencastre Fernandes *et al*. 2011). It could be used to control production processes and detect defects (such as batch issues), and serve as a reverse engineering tool to define the experimental conditions (strains, cultivation harvest and cryopreservation conditions) leading to the production of homogeneous cryoresistant populations of bacterial cells for industrial use, as suggested by Passot *et al*. (2015).

Transmission-FTIR IN10 microscope discriminates bacterial strains in terms of cell envelope

The lower-resolution transmission-FTIR spectroscopy approach developed in this work made it possible to analyse spectra from a few thousands of cells down to 975 cm^{-1}. The analysis of the 1363 – 975 cm^{-1} region thus provided biochemical information about carbohydrates and phosphorylated molecules, and the corresponding PCA is presented in **Fig. IV.4-12**. The PCA clustered both strains according to PC1 (76% of total variance) and revealed a higher heterogeneity within the population of *L. bulgaricus* CFL1 compared to *L. bulgaricus* ATCC 11842. Furthermore, PC2 (11% of total variance) separated the first as well as some data points of the third cell production batches of *L. bulgaricus* CFL1. Three clusters could thus be defined: a first one containing all batches of *L. bulgaricus* ATCC 11842 cells (red circle, **Fig. IV.4-12a**) and two others containing different batches of *L. bulgaricus* CFL1 cells (light and dark green circles, **Fig. IV.4-12a**). The discrimination of different cell production batches of *L. bulgaricus* CFL1, but not of *L. bulgaricus* ATCC 11842, can be related to the different growth kinetics of both strains. *L. bulgaricus* CFL1 presents a higher growth rate than *L. bulgaricus* ATCC 11842 (1.94 and 1.71 h^{-1}, respectively; **CHAPTER I** of this manuscript), and unintentional variations in the harvesting conditions between different cell production batches could thus result in more important differences in terms of protein and envelope composition of *L. bulgaricus* CFL1.

The spectral region here considered is complex and carries multiple and overlapping vibrational bands arising from carbohydrates, phosphorylated molecules and proteins. The attribution of specific bond vibration to these clusters with the loading plots of the PC1 and PC2 is thus not straightforward (**Fig. IV.4-12b**). The average spectra of each of the three clusters identified in **Fig. IV.4-12a**, as well as their inverted second-order derivatives were therefore calculated and are presented in **Fig. IV.4-13**. The second-order derivatives revealed peaks whose assignments are detailed in **Table IV.4-1**. Large spectral differences between both strains were clearly visible from the average spectra between 1363 and 1220 cm^{-1}, comprising the CH bending of polysaccharides, the amide III band and the PO_2^- asymmetric stretching of phosphorylated molecules (*νPO_2^- asym.*). The second-order derivatives confirmed these differences and revealed a higher intensity of the bands centred at 1243 and 1218 cm^{-1} in both *L. bulgaricus* CFL1 clusters

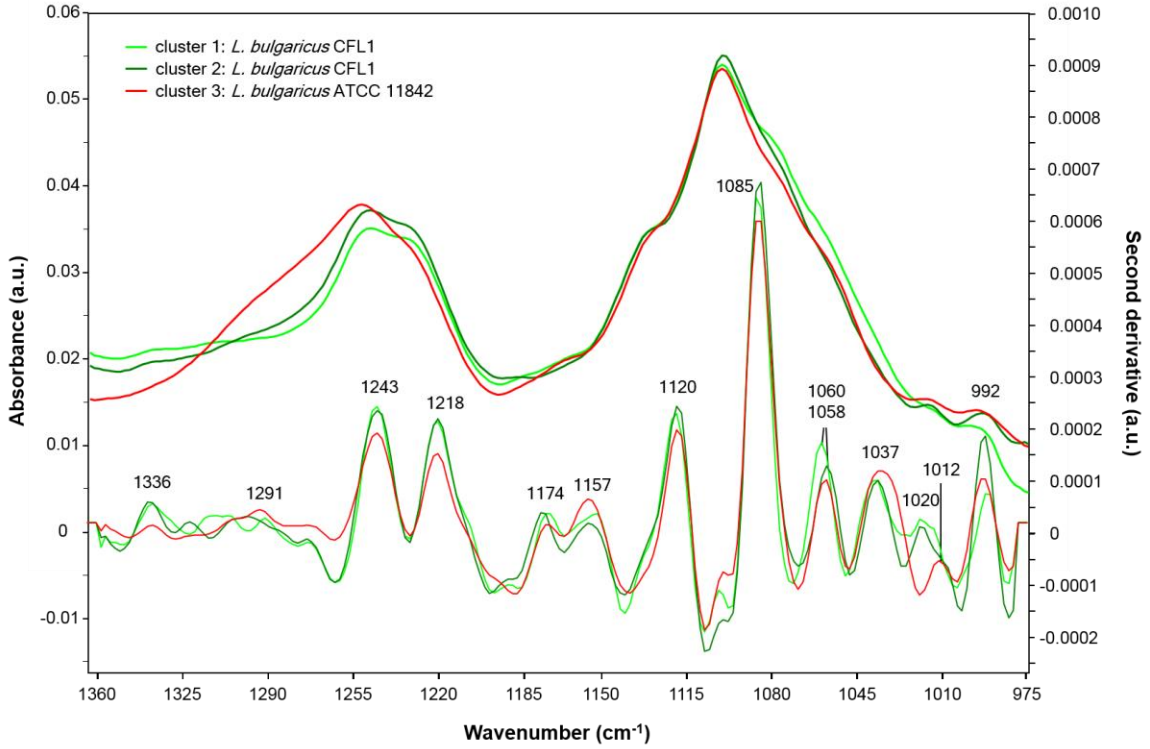

Figure IV.4-13: FTIR spectra of *Lactobacillus delbrueckii* subsp. *bulgaricus* recorded with the Nicolet IN10 IR microscope in the 1363 – 975 cm^{-1} region. Average spectra (thick lines, above) and inverted second-order derivatives following a 7-points Savitsky-Golay algorithm (thin lines, below) of two clusters of *L. bulgaricus* CFL1 cells (shades of green) and one cluster of ATCC 11842 cells (red) as revealed by the Principal Component Analysis of **Fig. IV.4-12**.

Table IV.4-1: Average position and assignments of infrared vibrational bands of the 1363 – 975 cm^{-1} region of the second derivative transmission FTIR spectra of fresh cell monolayers of *L. bulgaricus* in solution

Peak position (cm^{-1})	Assignment and main biomolecules associated	References
1336	*δCH* ring (polysaccharides)	Movasaghi *et al*. 2008
1291	-	-
1243 1218	vPO_2^- *asym.* (phospholipids, teichoic acids, nucleic acids)	Naumann, 2000; Movasaghi *et al*. 2008
1174	*vCO* (non hydrogen-bonded carbohydrates)	Movasaghi *et al*. 2008
1157	*vCO* (hydrogen-bonded carbohydrates) β 1 → 3 (glucans)	Movasaghi *et al*. 2008, Kuanyshev *et al*. 2016
1120	*vPOC sym.* (phosphorylated carbohydrates)	Movasaghi *et al*. 2008
1085	vPO_2^- *sym*. (phospholipids, teichoic acids, nucleic acids)	Naumann, 2000; Movasaghi *et al*. 2008
1060-1058	*vCOC sym.*, *vPOC sym.* (polysaccharides)	Quilès *et al*. 2010
1037	*vOH* coupled with *δCO* (polysaccharides)	Quilès *et al*. 2010
1020-1012	*vCO*, *vCC*, *δOCH* ring (polysaccharides)	Movasaghi *et al*. 2008
992	CC ribose skeleton β 1 → 6 (glucans)	Galichet *et al*. 2001; Quilès *et al*. 2010; Kuanyshev *et al*. 2016

(ν: stretching, δ: bending, sym.: symmetric, asym.: antisymmetric)

compared to the *L. bulgaricus* ATCC 11842 cluster. These vibrations arise from the vPO_2^- *asym.* and suggest differences within the phosphorylated molecules of both strains, such as phospholipids, nucleic acids, teichoic acids, cofactors (such as ATP, FAD, NAD^+…) and phosphorylated proteins. The second-order derivatives revealed additional differences between all three clusters in the lower wavenumbers of this spectral region, from 1040 to 975 cm^{-1}, which contains ring vibrations of polysaccharides (**Table IV.4-1**). In particular, the vibration centred at 1020 cm^{-1} in both *L. bulgaricus* CFL1 clusters shifted to 1012 cm^{-1} in the *L. bulgaricus* ATCC 11842 cluster. Also, the peak centred at 992 cm^{-1} was stronger for the cluster 2 of *L. bulgaricus* CFL1 compared to the other two clusters. The main sources of polysaccharides in Gram-positive bacteria are the cell wall peptidoglycan, teichoic acids, exopolysaccharides and glycogen (Jiang *et al*. 2004), but *L. bulgaricus* ATCC 11842 and CFL1 do not synthesize glycogen (van de Guchte *et al*. 2006; Meneghel *et al*. 2016). The results therefore suggest important differences in the composition and/or conformation of the cells envelope (cell wall, teichoic acids and exopolysaccharides). Since it is directly at the interface with the environment, extracellular components (*e.g.*, exopolysaccharides) are highly suspected to be implicated in the capacity of cells to survive freezing (Boetius *et al*. 2015). Strain as well as batch differences in the composition and/or conformation of cell surface could thus contribute to different levels of cryoresistance.

Conclusion

The new SR FTIR micro-spectroscopy device using an inverted ATR configuration developed in this work enabled to analyse the 1800 – 1300 cm^{-1} spectral region, and thus protein secondary structures arising from individual bacteria in solution (*i.e.*, under fully native conditions, without disturbing cellular processes). It provided access to cell-to-cell spectral differences and thus enabled to characterise population heterogeneity. The cryosensitive *L. bulgaricus* CFL1 population was identified as more heterogeneous than the cryoresistant *L. bulgaricus* ATCC 11842 population, associated with various proportions of α-helix and β-sheet structures, and β-sheets with various number of strands. This device could be used further to test cell productions conditions leading to homogeneous populations of resistant cells. Associating the Nicolet IN10 IR microscope with sampling micro-chambers also appeared as an interesting approach for the analysis of cells in aqueous environment. It provided an intermediate access to population heterogeneity between traditional bulk FTIR spectroscopy (which likely probes $10^{5\text{-}6}$ cells) and single-cell analysis with a satisfactory signal-to-noise ratio in the 1800 – 975 cm^{-1} region. It also revealed probable differences in the envelope between both strains and between different cell production batches of *L. bulgaricus* CFL1. It could be used for screening works before moving to higher spectral resolution and synchrotron radiation experiments with the new device. Finally, this proof of principle opens up the area for future development of the inverted microscope, whose sampling liquid chamber could be connected to microfluidics for long-term process monitoring.

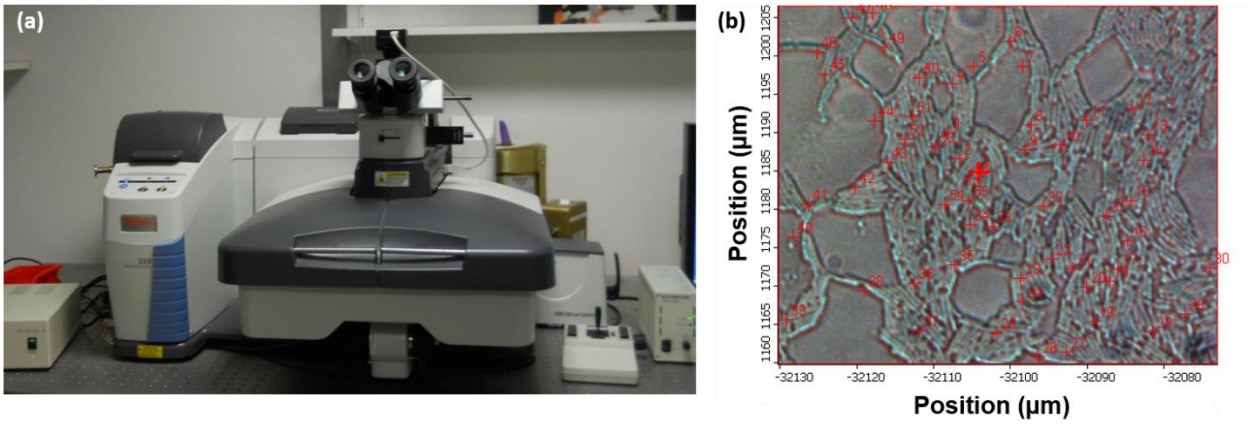

Figure IV.4-14: Pictures of **(a)** the DXR Raman confocal microscope (ThermoFisher Scientific; USA), and **(b)** a *Lactobacillus delbrueckii* subsp. *bulgaricus* ATCC 11842 sample dried over a CaF_2 Raman-grade window (Crystran; Poole, UK) using a MPLN100x microscope objective (Olympus; Tokyo, Japan); the red crosses indicate the different mapping points.

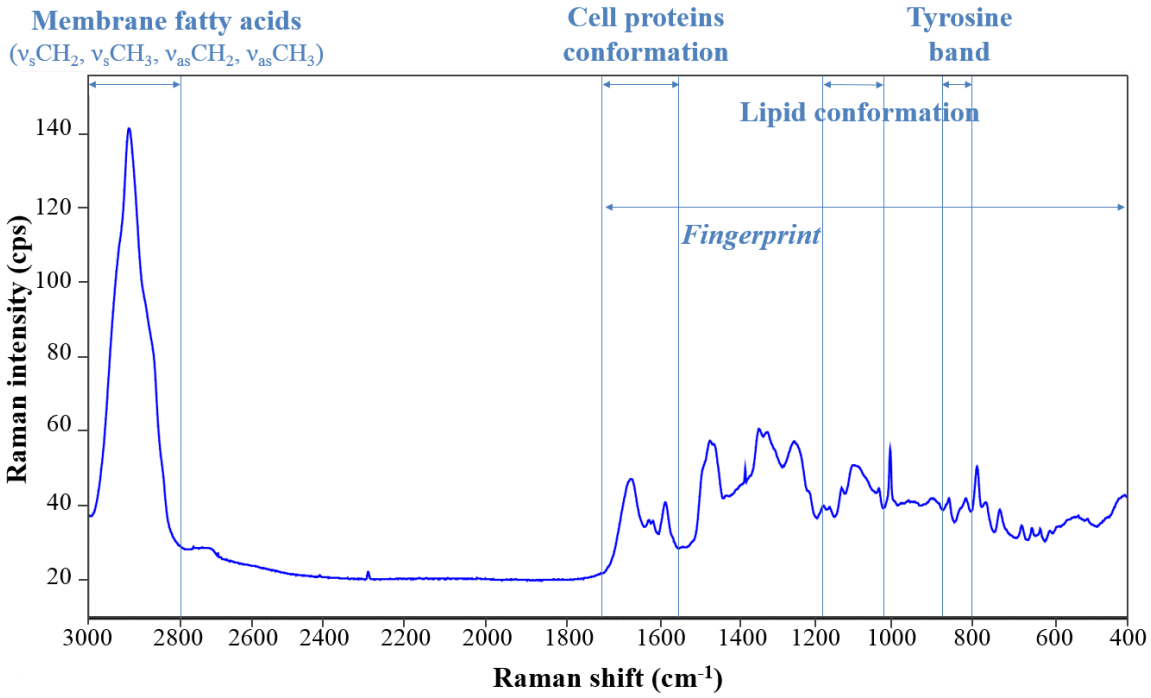

Figure IV.4-15: Averaged Raman spectrum from approximately 50 *Lactobacillus delbrueckii* subsp. *bulgaricus* CFL1 cells dried over Raman-grade CaF_2 windows in the 3000 – 400 cm^{-1} region.

Acknowledgements

This work was supported by the National Institute for Agricultural Research (INRA) and the French National Research Agency (ANR) under the Investing in the Future Program, Grant n°ANR-10-IDEX-0003-02. It was conducted on the SMIS beamline of the French national synchrotron facility SOLEIL (Gif-sur-Yvette, France) under the project 20150220 and we are grateful to the beamline staff for designing and implementing the new experimental device, and for providing assistance on the experimental work and data treatment.

4.3. Complementary information from dried bacteria by Raman micro-spectroscopy

Raman and FTIR spectroscopies are known to provide complementary vibrational information according to their respective selection rules (Naumann 2001; Maquelin *et al*. 2002). In addition, low wavenumbers regions are more easily accessible by Raman spectroscopy compared to FTIR spectroscopy. In order to complement the work done by infrared spectroscopy, we also initiated a Raman spectroscopy study of *L. bulgaricus* ATCC 11842 and *L. bulgaricus* CFL1.

Preliminary tests were kindly performed by Prof. Ganesh Sockalingum (URCA, Reims) on a high spectral resolution LabRAM ARAMIS (Horiba; Kyoto, Japan) in the 1750 – 600 cm^{-1} region. A satisfactory signal-to-noise ratio was obtained from spectra of dried *L. bulgaricus* CFL1 single cells. Further experiments were subsequently performed on the DXR Raman confocal microscope (ThermoFisher Scientific, USA) of the SMIS beamline (SOLEIL synchrotron, Gif-sur-Yvette).

A volume of 100 µL of washed bacterial sample was resuspended in saline water, spread over a Raman-grade CaF_2 window (Crystran, Poole, UK) and it was allowed to dry in air before analysis on the DXR Raman confocal microscope (ThermoFisher Scientific, USA) (**Fig. IV.4-14a**). The 512 nm laser and filter (grating: 900 lines mm^{-1}) were used since this wavelength produced minimum fluorescence while avoiding sample heat damage during 4 x 60 s exposures at 10 mW through a 50 µm pinhole. Samples were observed through an MPLN100x objective (Olympus, Tokyo, Japan). A background and approximately 50 locations corresponding to different cells were recorded for each strain (**Fig. IV.4-14b**) by co-adding 512 scans (Omnic software, Version 8.1; Thermo Scientific, USA). The spectra were normalized (EMSC algorithm) and averaged in different spectral regions. The Raman spectra of both strains did not reveal significant changes in the lipid (3000 – 2800 cm^{-1}; 1190 – 1010 cm^{-1}) and protein (1750 – 1590 cm^{-1}) regions (**Fig. IV.4-15**). However, the analysis of the low wavenumbers fingerprint region (910 – 550 cm^{-1}, **Fig. IV.4-16**) revealed interesting results that are presented thereafter.

The average spectra for both strains in the 910 – 550 cm^{-1} region are presented in **Fig. IV.4-16**. They appeared highly similar with extensive overlapping, except in the 875 – 830 cm^{-1} region (yellow dotted box, **Fig. IV.4-16**), where *L. bulgaricus* ATCC 11842 showed higher Raman intensity than *L. bulgaricus* CFL1 (red and green curves, respectively, **Fig. IV.4-16**). This region contains the band centred at 854 cm^{-1} attributed to the vibration of tyrosine residues of proteins. This band actually belongs to a doublet: the

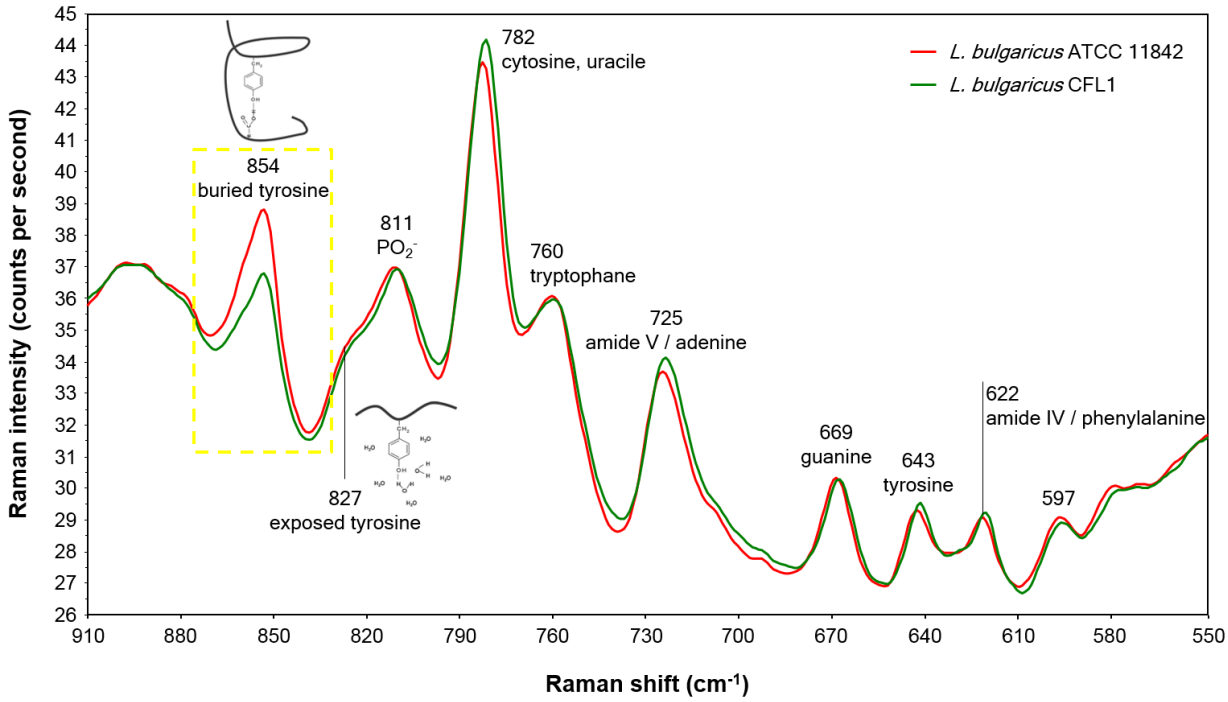

Figure IV.4-16: Averaged Raman spectra from approximately 50 *Lactobacillus delbrueckii* subsp. *bulgaricus* CFL1 (green) and approximately 50 *L. bulgaricus* ATCC 11842 (red) cells in the 910 – 550 cm^{-1} region. Band assignments are given, as well as illustrations of buried and exposed tyrosine residues within proteins (the inserted drawings were taken from Vyumvuhore *et al.* 2013). The spectral region of high variance between both strains is highlighted by a yellow dotted box.

854/827 cm^{-1} tyrosine doublet which carries information about the conformational state of this hydrophobic amino acyl residue. When tyrosine is buried inside proteins, the band centred at approximately 854 cm^{-1} dominates, whereas denaturation leads the band centred at approximately 827 cm^{-1} to dominate (inserted illustrations, **Fig. IV.4-16**) (Naumann 2001; Maquelin *et al*. 2002). Both bands are thus commonly attributed to "buried" and "exposed" tyrosyl residues, respectively. The average 854/827 cm^{-1} intensity ratios of *L. bulgaricus* ATCC 11842 and *L. bulgaricus* CFL1 were calculated as 1.12 and 1.07, respectively, indicating a slightly higher proportion of "buried" with respect to "exposed" tyrosine residues within the proteins of *L. bulgaricus* ATCC 11842 compared to *L. bulgaricus* CFL1. This result suggests the existence of a different degree of overall protein folding between both strains, which could explain, at least partly, their different cryosensitivities.

To go further in the investigation of bacterial cells by Raman spectroscopy and achieve measurements in solution, experimental trials were performed on liquid bacterial samples sandwiched between two substrate windows. However, the spectral signal-to-noise ratio decreased and cell immobilization was difficult to obtain due to Brownian motions of cells, especially during the long acquisition times that were required. In the literature, successful analyses of single bacterial cells in solution by Raman spectroscopy have been reported (Huang *et al*. 2009; Avetisyan *et al*. 2013). Such experiments required the use of a specific equipment though, called laser tweezers or optical tweezers, in which a laser is used to trap individual cells by thermal effect while the other one serves as probing light source. This interesting cutting-edge technology could constitute a possible perspective for future work.

4.4. Key points

- Possibility to analyse spectra recorded from individual bacteria in an aqueous environment with the newly developed inverted microscope in the 1800 – 1300 cm^{-1} spectral region; extension of the exploitable region to 975 cm^{-1} with the Nicolet IN10 IR microscope;
- Accurate and reproducible water subtraction procedure from sample spectra recorded with either approaches (using the inverted microscope or the Nicolet IN10 IR microscope) and the dedicated in-house program;
- Association of the cryoresistant *L. bulgaricus* ATCC 11842 population with dominant β-sheet protein secondary structures;
- Differences at the composition and/or conformation level in the cell envelope of both strains in terms of carbohydrates and phosphorylated molecules;
- Access to different and complementary levels of population heterogeneity with both approaches: a single-cell level with the inverted microscope and an intermediate level between bulk and single-cell with the Nicolet IN10 IR microscope;
- Confirmation of a relationship between heterogeneity and cryosensitivity.

CONCLUSIONS & FUTURE PERSPECTIVES

CONCLUSIONS & FUTURE PERSPECTIVES

Conclusions

Cryopreservation, the most widely used cell preservation technique (De Paoli 2005), was at the heart of this thesis work. The lactic acid bacterium (LAB) *Lactobacillus delbrueckii* subsp. *bulgaricus*, exhibiting variable cryosensitivity according to strains and environmental conditions, was here examined. This work aimed at studying the response of *L. bulgaricus* to cryopreservation-related stresses by complementary approaches, including physiological, genomic and biophysical characterisations. Moreover, it intended to investigate the relative importance of cell responses to the main freeze-thaw stresses at different scales: from the population to the single cell responses. The principal working hypotheses relate to consider the cryopreservation as a combination of cold and osmotic stresses and the membrane as the primary target of freeze-injury but without neglecting the potential impact of other components, in particular the cell wall and proteins. Furthermore, the development of non invasive and multiscale methodologies down to the single cell is considered as essential for better understanding the mechanisms of cryoinjury and for delivering in the future homogeneous LAB populations with desired characteristics (functions, storage stability, …).
The most relevant results obtained from this work are grouped thereafter in four items, and are schematically presented in **Fig. V.1-1**:

Selection of strains and cultivation conditions (**Fig. V.1-1a**)

To reduce the factors of experimental variability, the cryoresistance of three *L. bulgaricus* strains cultivated according to various growth conditions (two growth media and two growth phases upon harvest) was screened under standardized conditions of cryopreservation (addition of a cryoprotective agent and controlled cooling rate) (**CHAPTER I**). Bacterial cryoresistance was evaluated through the losses of culturability and functionality (acidifying activity) following freeze-thawing. *L. bulgaricus* ATCC BAA-365 and ATCC 11842 appeared cryoresistant regardless of the conditions tested. When grown in whey-based medium, *L. bulgaricus* CFL1 appeared sensitive to freeze-thawing, with significant culturability and acidification activity losses. Difference in freeze-thaw sensitivity was particularly pronounced between *L. bulgaricus* CFL1 and *L. bulgaricus* ATCC 11842 when cells were harvested at the end of exponential growth phase. These growth conditions were thus selected for the rest of this work.

(a) Selection of strains and cultivation conditions

> *L. bulgaricus* CFL1: **cryosensitive**; *L. bulgaricus* ATCC 11842: **cryoresistant**
> Whey-based medium & late exponential growth phase → most different strain cryoresistances

(b) Determination of the relative impact of the main cryopreservation-related stresses

> Freezing = mainly cold + hyperosmotic stresses
> Osmotic stress: most important biological activity losses when cryopreserving the **cryosensitive cells**
> Neither osmotic stress nor cold stress affected the biological activity of the **cryoresistant cells**

(c) Identification of cellular markers related to cryoinjury/cryoresistance

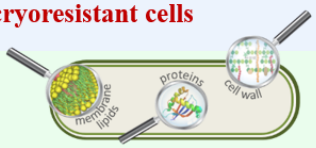

Genetic markers

> 3 genes including a *csp* in the cryoresistant strains, with orthology to a psychrophilic LAB
> Differences in the *epsI* loci and transporters → differences in the membrane composition/properties?

Membrane markers

> **Cryosensitive cells**: + SFA & short-chain FA; higher $T_{s\ lip}$ (less flexible membrane at low T °C); preferential interaction of sucrose with phospholipid headgroups?
> **Cryoresistant cells**: + UFA & long-chain FA; lower $T_{s\ lip}$ (more flexible membrane at low T °C); preferential exclusion of sucrose with phospholipid headgroups?

Cell wall and protein markers

> Strain-dependent cell wall composition/conformation with differences related to carbohydrates and phosphorylated molecules
> Strain-dependent protein conformation with β-sheets preferentially associated to **cryoresistant cells**
> Buried tyrosine residues preferentially associated to **cryoresistant cells**
→ more native protein structure?

(d) Assessment of population heterogeneity

Proteins conformation

> **Cryosensitive cells**: Higher inter-cellular heterogeneity
> **Cryoresistant cells**: Higher inter-cellular homogeneity

Membrane fluidity

> **Cryosensitive cells**: Higher intra and inter-cellular heterogeneities with high rigidity domains, especially under stressful conditions;
> **Cryoresistant cells**: Higher intra and inter-cellular homogeneities with fewer rigidity domains

Observation scale

Figure V.1-1: Schematic overview of the main results obtained from the present work. It is divided into four main topics (*csp*: gene encoding a cold-shock protein; *epsI* loci: group of genes encoding the proteins for the biosynthesis of exopolysaccharides; FA: fatty acid; SFA: saturated fatty acid; UFA: unsaturated fatty acid; $T_{s\ lip}$: membrane lipid solidification (phase transition) temperature).

Determination of the relative impact of the main cryopreservation-related stresses (Fig. V.1-1b)

For better understanding the mechanisms leading to such different behaviours, the cryopreservation process was associated to two main unitary stresses: cold and osmotic.
The relative impact of cold and osmotic stresses on culturability and acidifying activity losses of *L. bulgaricus* CFL1 and *L. bulgaricus* ATCC 11842 was investigated and compared to freeze-thawing sensitivity (**CHAPTER II**). The osmotic stress due to cryoconcentration of extracellular solutes induced by ice formation was identified as the primary cause of lethality and functionality loss in the cryosensitive strain. In contrast, it did not cause any damage to the cryoresistant strain.

Identification of cellular markers related to cryoinjury/cryoresistance (Fig. V.1-1c)

Different approaches were applied with the aim of identifying markers of cellular cryoinjury or cryoresistance: the genomic comparison, the assessment of cell membrane biophysical properties and their modification when applying stress-treatments, and the evaluation of biochemical information arising from other cell components such as proteins and cell wall constituents.

Genetic markers

Sequencing the genome of *L. bulgaricus* CFL1, that had not been done so far, interestingly revealed the presence of two different CRISPR-Cas system types whereas *L. bulgaricus* ATCC BAA-365 and ATCC 11842 possessed a unique CRISPR-Cas system of another type (**CHAPTER I**). To determine the potential existence of other genomic differences between the cryosensitive *L. bulgaricus* CFL1 and the cryoresistant *L. bulgaricus* ATCC BAA-365 and ATCC 11842 that could provide some clues for the elucidation of cryoresistance, a deeper genomic comparison was performed (**CHAPTER I**). Few relevant genes were identified, especially the presence in the cryoresistant strains of genes encoding a cold shock protein and two ribosomal subunits with orthology to that of a psychrophilic LAB. Also, some strain-specific genes for the biosynthesis of exopolysaccharides (*epsI* loci) and transporters (PTS^{Cel}; spermidine/putrescine ABC transporters) could account, at least partly, for the strain-dependant cryoresistances observed and suggested different composition and organization of the cell envelope between strains.

Membrane markers

The characterisation of bacterial membranes included the assessment of their fatty acid composition, the conformational order existing at the level of the fatty acyl chains (enabling the evaluation of membrane lipid phase transition temperature) and phospholipid headgroups; and the membrane fluidity (**CHAPTER II**).
Both strains were characterised by various degrees of unsaturated and long chain membrane fatty acyl residues, with higher proportions in the membrane of the resistant strain compared to the sensitive one. Unsaturated fatty acids induce a lower phase transition than saturated counterparts, whereas long chain fatty

acids melt at higher temperature. A lower membrane lipid phase transition temperature characterised the cryoresistant *L. bulgaricus* ATCC 11842 compared to *L. bulgaricus* CFL1, indicating a probable higher influence of unsaturations compared to chain length on lipid phase transition temperature. This could, in turn, provide cells with a more flexible membrane upon cooling and ice formation, and facilitate water efflux from cells following extracellular cryoconcentration, confirming previous work (Gautier *et al*. 2013). Cooling thus induced an important modification of the conformational order of neighbouring fatty acyl residues, contrary to hyperosmotic stress.

When considering the conformational order existing among neighbouring phospholipid headgroups under cold and osmotic stress, this membrane biophysical property was evaluated by monitoring the position of the vPO_2^- *asym.* FTIR vibrational band. Such investigation, usually performed on model membranes (Arrondo and Goñi 1998; Díaz *et al*. 2003; Wolkers *et al*. 2010), was originally applied to intact cell in this work. Cooling had no particular influence on the vPO_2^- *asym.* position, but the osmotic stress extensively downshifted this peak position in the FTIR spectra of sensitive cells. This result suggests the existence of different types of interactions between the concentrated sucrose matrix and the membrane phospholipid headgroups of both strains. Preferential interaction was thus proposed to be occurring between sucrose and the membrane phospholipid headgroups of *L. bulgaricus* CFL1, leading to membrane disruption, possible leakages and eventually, lethality. In contrast, preferential exclusion of sucrose considering the cryoresistant *L. bulgaricus* ATCC 11842 was proposed to explain the preservation of its membrane.

In addition, the assessment of membrane fluidity by fluorescence anisotropy at a population scale of both strains did not reveal any significant difference, but the elevated standard deviations may have masked subtle variations.

Cell wall and proteins markers

Vibrational spectroscopies carry information about the other cell biomolecules, and enabled the characterisation of cell proteins and wall (**CHAPTER IV**).

Different infrared signatures in the carbohydrates and phosphorylated molecules region between both strains indicated possible differences in the composition of their envelope (in terms of peptidoglycan, teichoic acids and/or exopolysaccharides).

Regarding proteins, a higher proportion of β-sheet secondary structures could be associated to bacterial cryoresistance. A complimentary investigation using Raman micro-spectroscopy was performed. It revealed that the amino acyl residues tyrosyl had a more buried position relatively to the ones exposed to the environment within the proteins of *L. bulgaricus* ATCC 11842 compared to proteins of *L. bulgaricus* CFL1, suggesting protein structures more prone to denaturation for the latter cryosensitive strain.

Assessment of population heterogeneity (Fig. V.1-1d)

In order to investigate bacteria down to the single-cell level and in aqueous environment and to quantify population heterogeneity, different approaches exploiting the high brilliance of SOLEIL synchrotron

radiation were developed. They involved deep UV-fluorescence microscopy (DISCO beamline) and FTIR micro-spectroscopy (SMIS beamline).

By deep UV-fluorescence microscopy it was possible to investigate subcellular membrane fluidity under conditions of cold and osmotic stresses, in relation to cryoresistance (**CHAPTER III**), and therefore to go further compared to the previous population-scale analysis. This work confirmed that a cold stress to 0 °C (without ice formation) induced a membrane rigidification in both strains that was not correlated to cell lethality. A membrane rigidification under osmotic stress was also evidenced in the case of the resistant *L. bulgaricus* ATCC 11842. Instead, the membrane of the sensitive strain did not significantly rigidify under a lethal osmotic stress. More interestingly, inter- and intra-cellular heterogeneities were quantified for the first time in this work. The sensitive strain thus revealed higher inter- and intra-cellular heterogeneities compared to the resistant one, with the presence of more domains of high rigidity. The application of a hyperosmotic treatment further increased this heterogeneity in the sensitive strain with more numerous and larger rigid domains along the membrane of individual cells, further supporting the existence of disruptive interactions between sucrose and the membrane of this strain.

The analysis of bacterial cells at high resolution was also achieved by FTIR micro-spectroscopy, and in an aqueous environment for an examination of cells under native conditions (**CHAPTER IV**). Two levels of resolution were accessed: either groups of approximately $10^{3\text{-}4}$ cells (intermediate level between bulk and single-cell measurements), or individual cells with a 1 x 1 µm² spatial resolution. In both cases water features, that submerge bacterial vibration bands to a large extent, were removed in an optimized way thanks to an in-house program. The first approach combined the use of micro-chambers and dedicated sample holders to hold them tightly close, minimize and control the optical path (mandatory for allowing water subtraction). It provided access to a large spectral region for sample analysis (proteins, carbohydrates and phosphorylated molecules) and to quantify population heterogeneity, making possible to differentiate cell production batches of *L. bulgaricus* CFL1.
The second "single-bacterial cells" approach resulted from a technical development undertaken by the SMIS beamline staff, since high spatial resolution analysis by FTIR spectroscopy was limited to large eukaryotic cells in solution or dried bacterial cells up to now. An inverted ATR configuration was thus custom-designed and connected to synchrotron radiation and microscopy. Using high refractive index ATR hemispheres and a liquid chamber, it was possible to record IR spectra from individual *L. bulgaricus* cells in solution, by minimizing the quantity of water that was probed. With this approach, the examination of individual *L. bulgaricus* CFL1 and *L. bulgaricus* ATCC 11842 cells in an aqueous environment focused on their cellular envelope. The protein spectral region could be analysed and revealed more heterogeneous protein secondary structures in the cryosensitive cells compared to the cryoresistant cells.

In summary, this work confirmed that the resistance to cryopreservation of the LAB *L. bulgaricus* is highly strain- and culture conditions-dependant. It highlighted that culturability and acidification activity losses following freeze-thawing can be mainly attributed to the deleterious effects of osmotic stress resulting from

solutes cryoconcentration. Moreover, it confirmed the decisive implication of the envelope in the resistance of *L. bulgaricus* to such environmental stresses, including the membrane and the cell wall composition and organisation. The multi-scale analysis performed in this work, especially through synchrotron-radiation high-resolution experiments, was novel and indicated a link between intercellular heterogeneity (of both the membrane fluidity and protein conformation) and cryosensitivity. Heterogeneity of membrane fluidity was also more pronounced at an intracellular level in cryosensitive cells. Consequently, identifying the strains, cultivation, harvest and cryopreservation conditions leading to homogeneous populations of resistant cells constitutes a challenge for the dairy industry to produce and cryopreserve highly viable and functional starters upon thawing.

Characterising cryoresistant and cryosensitive bacterial populations with complementary analytical techniques has provided an overview of the biomolecules that are implicated in bacterial cryoresistance, thus increasing the understanding of the mechanisms involved. It was possible to identify molecules (membrane fatty acid composition) or fractions of macromolecules (genes), to characterise cellular entities (membrane fluidity; protein secondary structure; cell envelope) and to associate their analysis to the final functionality of bacterial populations (culturability and acidifying activity).

This study has been performed applying more or less invasive techniques. Biological activity (to report culturability and acidifying activity) data were thus obtained under fully native conditions and FTIR spectroscopy data in an aqueous environment. In contrast, cell fixation by air-drying (Raman micro-spectroscopy), the use of membrane fluorophores and ionising UV radiations (fluorescence anisotropy), or extraction procedures (accelerated solvent extraction of lipids) could have introduced some chemical modifications to the samples. This assumption should be kept in mind for careful interpretations.

FTIR spectroscopy in the mid-IR region allowed a wide choice of experimental spatial resolutions. By combining different analysis modes to a thermal or a synchrotron source, and to sampling techniques and water subtraction procedures for analysing aqueous samples, it is possible to reach a custom use of FTIR spectroscopy for the full exploitation of its analytical potential. However, the non-specificity of FTIR spectroscopy may be a drawback that needs the utilisation of complementary, and often more invasive techniques. Combining different analytical techniques presenting diverse advantages and drawbacks is thus today the required approach to provide a comprehensive characterisation of biological samples.

Perspectives

The future perspectives to this work are numerous and are presented according to short-, medium- and long-term views.

Short-term perspectives

The comparative cryoresistance analysis revealed a significant growth medium dependent cryoresistance of *L. bulgaricus* CFL1 (confirming the work of (Gautier *et al*. 2013)) and a tendency for the implication of the growth phase upon harvest (**CHAPTER I**). The genomic comparison did not provide relevant information to explain these observations, but great expectations are placed in a quantitative proteomic study. By sequencing the proteomes of this strain when cultivated in MRS broth or whey-based medium until late exponential or early stationary phases, both in the fresh state and following freeze-thawing, this ongoing work aims at completing the information obtained from the genomic comparison. The pool of proteins of cells in a specific experimental condition indeed results from the expression of the genome and the translation of messenger RNAs in response to environmental conditions (parameter that the genomic comparison was blind to). For instance, proteins that are only or over-produced by *L. bulgaricus* CFL1 grown in MRS medium compared to whey-based medium could be implicated in its cryoresistance mechanism, especially if these proteins are localized in the envelope, *i.e.*, at the interface with the changing environment. The samples have been generated, the cytoplasmic and envelope proteomes have been separated and sequenced (PAPPSO platform, INRA Jouy-en-Josas), and data exploitation remains to be performed (Séverine Layec, GMPA laboratory, INRA Grignon).

The assessment of membrane fatty acid composition (**CHAPTER II**) has raised the interest for assessing the membrane phospholipid composition as well, to have a complete description of membrane lipids from *L. bulgaricus* CFL1 and ATCC 11842. This work has been initiated by Michele Da Silva Pinto as part of her post-doctoral project in the GMPA laboratory (INRA Grignon), in collaboration with Yann Gohon (IJPB[7], INRA Versailles) and Marie-Hélène Ropers (BIA[8], INRA Nantes). This project also aims at understanding the role of specific fatty acids and phospholipids on the membrane properties of *L. bulgaricus*, in relation to cryoresistance.

[7] IJPB, acronym for Institute Jean-Pierre Bourgin, is a plant sciences joint research unit (INRA, AgroParisTech, CNRS) with various research topics, including the dynamics and structure of lipid bodies (http://www-ijpb.versailles.inra.fr/en/index.htm).

[8] BIA, acronym for Biopolymers, Interactions, Assemblies, in an INRA research unit focusing on the **sustainable transformation of agricultural resources and plant biomass** with various research topics, **including the** construction and stabilization of complex matrices of assemblies of proteins, polysaccharides and/or lipids (https://www6.angers-nantes.inra.fr/bia_eng/).

Besides, the present work focused on studying the response of *L. bulgaricus* to cryopreservation. The decomposition of this process into major underlying stresses has enabled to investigate the relative contribution of cold and osmotic stresses on some biophysical properties, but also to circumvent some technical limitations. For instance, the assessment of subcellular membrane fluidity under cold stress was limited to 0 °C. A possible upgrade of the experimental setup could allow to cool samples down to lower temperatures, and monitor subcellular membrane fluidity in real-time down to negative temperatures, and possibly during a freezing process.

Moreover, some experimental conditions have been set: growth medium and cryopreservation conditions. Nevertheless, the identification of cryoresistance markers of *L. bulgaricus* could be performed by considering other cultivation and protection conditions. Likewise, stresses associated to other LAB production processes could be studied, such as the oxidative or the acidic stress. The effect of these additional experimental conditions on the biophysical properties of cells could be investigated by FTIR spectroscopy using the approach developed to analyse groups of $10^{3\text{-}4}$ cells in an aqueous environment. It could serve to screen experimental conditions in a rapid and easy way before using synchrotron radiation at high spatial resolution with the new device developed on the SMIS beamline of SOLEIL synchrotron (**CHAPTER IV**).

Medium and long-term perspectives

A perspective that would require some methodological development may be suggested, further to the identification of rigid domains within bacterial membranes (**CHAPTER III**), is the assessment of their lipid composition. The visualisation of the subcellular localisation of cardiolipin and phosphatidylglycerol within bacterial membranes is possible by combing confocal fluorescence microscopy with the use of specific dyes (Barák *et al*. 2008). After applying this methodology to *L. bulgaricus*, analysing simultaneously the subcellular localisation of anionic lipids and distribution of membrane fluidity could indicate whether or not the rigid domains are mainly composed of these anionic lipids.

Then, the effective expression of the few candidate genes identified as possibly involved in the cryoresistance mechanisms of *L. bulgaricus* (**CHAPTER I**) should be confirmed. Their implication in bacterial cryoresistance could be further examined by mutagenesis (by introducing the candidate genes in the cryosensitive *L. bulgaricus* CFL1 strain, or by inactivating them from the genomes of the cryoresistant strains), *e.g.*, by eletrotransformation (Serror *et al*. 2002), and measuring the biological activity loss of mutants following freeze-thawing.

The proof of principle of the new device developed on the SMIS beamline of SOLEIL synchrotron for the analysis of single bacteria in an aqueous environment by FTIR spectroscopy has been given (**CHAPTER IV**). This device offers a great analytical potential for future studies, especially for monitoring a variety of stressful treatments and cellular processes under native conditions and in real-time. This would require

significant research and development (including the adaptation of microfluidics channels), but opens the way towards the possibility to monitor one cell in its native environment during the application of any desired process. Such real-time single-cell spectroscopy experiment under native conditions could be completed by Raman micro-spectroscopy using optical tweezers. Otherwise, labelling and sorting cells according to defined physiological parameters (*e.g.*, esterase activity and membrane permeabilization) before spectral analysis could enable to split populations into live, damaged, and dead cells for instance, thus allowing further analyses to be performed on several thousands of cells instead of single cell level approaches. Hopefully, continuous progress in cell sorting would soon allow the delivery of sorting technologies that do not introduce additional damage to cells.

The progress of such challenging research should hopefully make it possible at some point to deeply understand cryopreservation mechanisms and identify the cultivation conditions generating homogeneous populations of microorganisms with desired and stable functionalities.

REFERENCES

REFERENCES

Abe F, Hiraki T (2009) Mechanistic role of ergosterol in membrane rigidity and cycloheximide resistance in *Saccharomyces cerevisiae*. Biochim Biophys Acta BBA - Biomembr 1788:743–752. doi: 10.1016/j.bbamem.2008.12.002

Alberts B, Johnson A, Lewis J, Raff M, Roberts K, Walter P (2002) The lipid bilayer. In: Molecular biology of the cell. 4th edition, Garland Science. New York, USA

Álvarez-Ordóñez A, Fernández A, López M, Arenas R, Bernardo A (2008) Modifications in membrane fatty acid composition of *Salmonella typhimurium* in response to growth conditions and their effect on heat resistance. Int J Food Microbiol 123:212–219. doi: 10.1016/j.ijfoodmicro.2008.01.015

Alvarez-Ordóñez A, Mouwen DJM, López M, Prieto M (2011) Fourier transform infrared spectroscopy as a tool to characterize molecular composition and stress response in foodborne pathogenic bacteria. J Microbiol Methods 84:369–378. doi: 10.1016/j.mimet.2011.01.009

Ami D, Posteri R, Mereghetti P, Porro D, Doglia SM, Branduardi P (2014) Fourier transform infrared spectroscopy as a method to study lipid accumulation in oleaginous yeasts. Biotechnol Biofuels 7:12. doi: 10.1186/1754-6834-7-12

Amiel C, Mariey L, Curk-Daubié M-C, Pichon P, Travert J (2000) Potentiality of Fourier Transform Infrared Spectroscopy (FTIR) for discrimination and identification of dairy lactic acid bacteria. Le Lait 80:445–459. doi: 10.1051/lait:2000137

Amor KB, Breeuwer P, Verbaarschot P, Rombouts FM, Akkermans ADL, Vos WMD, Abee T (2002) Multiparametric flow cytometry and cell sorting for the assessment of viable, injured, and dead *Bifidobacterium* cells during bile salt stress. Appl Environ Microbiol 68:5209–5216. doi: 10.1128/AEM.68.11.5209-5216.2002

Anchordoguy TJ, Rudolph AS, Carpenter JF, Crowe JH (1987) Modes of interaction of cryoprotectants with membrane phospholipids during freezing. Cryobiology 24:324–331

Andersen HD, Wang C, Arleth L, Peters GH, Westh P (2011) Reconciliation of opposing views on membrane–sugar interactions. Proc Natl Acad Sci 108:1874–1878. doi: 10.1073/pnas.1012516108

Arias JM, Tuttolomondo ME, Díaz SB, Altabef AB (2015) FTIR and Raman analysis of L-cysteine ethyl ester HCl interaction with dipalmitoylphosphatidylcholine in anhydrous and hydrated states. J Raman Spectrosc 46:369–376. doi: 10.1002/jrs.4659

Arndt D, Grant JR, Marcu A, Sajed T, Pon A, Liang Y, Wishart DS (2016) PHASTER: a better, faster version of the PHAST phage search tool. Nucleic Acids Res 44:W16–W21. doi: 10.1093/nar/gkw387

Arrondo JL, Goñi FM (1998) Infrared studies of protein-induced perturbation of lipids in lipoproteins and membranes. Chem Phys Lipids 96:53–68

Avetisyan A, Jensen JB, Huser T (2013) Monitoring trehalose uptake and conversion by single bacteria using laser tweezers Raman spectroscopy. Anal Chem 85:7264–7270. doi: 10.1021/ac4011638

Bâati L, Fabre-Gea C, Auriol D, Blanc PJ (2000) Study of the cryotolerance of *Lactobacillus acidophilus*: effect of culture and freezing conditions on the viability and cellular protein levels. Int J Food Microbiol 59:241–247. doi: 10.1016/S0168-1605(00)00361-5

Bajaj R, Bruce KE, Davidson AL, Rued BE, Stauffacher CV, Winkler ME (2016) Biochemical characterization of essential cell division proteins FtsX and FtsE that mediate peptidoglycan hydrolysis by PcsB in *Streptococcus pneumoniae*. MicrobiologyOpen 5:738–752. doi: 10.1002/mbo3.366

Baker MJ, Trevisan J, Bassan P, Bhargava R, Butler HJ, Dorling KM, Fielden PR, Fogarty SW, Fullwood NJ, Heys KA, Hughes C, Lasch P, Martin-Hirsch PL, Obinaju B, Sockalingum GD, Sulé-Suso J, Strong RJ, Walsh MJ, Wood BR, Gardner P, Martin FL (2014) Using Fourier transform IR spectroscopy to analyze biological materials. 9:1771–1791. doi: 10.1038/nprot.2014.110

Bandekar J (1992) Amide modes and protein conformation. Biochim Biophys Acta 1120:123–143

Bank H, Mazur P (1973) Visualization of freezing damage. J Cell Biol 57:729–742

Bar Dolev M, Braslavsky I, Davies PL (2016) Ice-binding proteins and their function. Annu Rev Biochem 85:515–542. doi: 10.1146/annurev-biochem-060815-014546

Barák I, Muchová K (2013) The role of lipid domains in bacterial cell processes. Int J Mol Sci 14:4050–4065. doi: 10.3390/ijms14024050

Barák I, Muchová K, Wilkinson AJ, O'Toole PJ, Pavlendová N (2008) Lipid spirals in *Bacillus subtilis* and their role in cell division. Mol Microbiol 68:1315–1327. doi: 10.1111/j.1365-2958.2008.06236.x

Barinov A, Loux V, Hammani A, Nicolas P, Langella P, Ehrlich D, Maguin E, van de Guchte M (2009) Prediction of surface exposed proteins in *Streptococcus pyogenes*, with a potential application to other Gram-positive bacteria. Proteomics 9:61–73. doi: 10.1002/pmic.200800195

Barrangou R, Azcarate-Peril MA, Duong T, Conners SB, Kelly RM, Klaenhammer TR (2006) Global analysis of carbohydrate utilization by *Lactobacillus acidophilus* using cDNA microarrays. Proc Natl Acad Sci U S A 103:3816–3821. doi: 10.1073/pnas.0511287103

Barth A (2007) Infrared spectroscopy of proteins. Biochim Biophys Acta 1767:1073–1101. doi: 10.1016/j.bbabio.2007.06.004

Barth A, Zscherp C (2002) What vibrations tell us about proteins. Q Rev Biophys 35:369–430

Baumann DP, Reinbold GW (1966) Freezing of lactic cultures. J Dairy Sci 49:259–264. doi: 10.3168/jds.S0022-0302(66)87846-3

Beal C, Fonseca F, Corrieu G (2001) Resistance to freezing and frozen storage of *Streptococcus thermophilus* is related to membrane fatty acid composition. J Dairy Sci 84:2347–2356. doi: 10.3168/jds.S0022-0302(01)74683-8

Beal C, Marin M, Fontaine E, Fonseca F, Obert J (2008) Production et conservation des ferments lactiques et probiotiques. In: Corrieu G, Luquet F (eds) Bactéries lactiques : de la génétique aux ferments., Lavoisier. pp 511–611

Behare PV, Singh R, Kumar M, Prajapati JB, Singh RP (2009) Exopolysaccharides of lactic acid bacteria: a review. J Food Sci Technol Mysore 46:1–11

Beney L, Gervais P (2001) Influence of the fluidity of the membrane on the response of microorganisms to environmental stresses. Appl Microbiol Biotechnol 57:34–42. doi: 10.1007/s002530100754

Beney L, Mille Y, Gervais P (2004) Death of *Escherichia coli* during rapid and severe dehydration is related to lipid phase transition. Appl Microbiol Biotechnol 65:457–464. doi: 10.1007/s00253-004-1574-x

Beney L, Simonin H, Mille Y, Gervais P (2007) Membrane physical state as key parameter for the resistance of the gram-negative *Bradyrhizobium japonicum* to hyperosmotic treatments. 187:387–396. doi: 10.1007/s00203-006-0203-8

Ben-Yashar V, Barenholz Y (1991) Characterization of the core and surface of human plasma lipoproteins. A study based on the use of five fluorophores. Chem Phys Lipids 60:1–14. doi: 10.1016/0009-3084(91)90009-Z

Berg DE, Weiss A, Crossland L (1980) Polarity of Tn5 insertion mutations in *Escherichia coli*. J Bacteriol 142:439–446

Berg JM, Tymoczko JL, Stryer L (2002) Lipids and many membrane proteins diffuse rapidly in the plane of the membrane. In: Freeman W (ed) Biochemistry. 5th edition. New York, USA

Bernal P, Muñoz-Rojas J, Hurtado A, Ramos JL, Segura A (2007) A *Pseudomonas putida* cardiolipin synthesis mutant exhibits increased sensitivity to drugs related to transport functionality. Environ Microbiol 9:1135–1145. doi: 10.1111/j.1462-2920.2006.01236.x

Bertelli C, Laird MR, Williams KP, Lau BY, Hoad G, Winsor GL, Brinkman FS (2017) IslandViewer 4: expanded prediction of genomic islands for larger-scale datasets. Nucleic Acids Res. doi: 10.1093/nar/gkx343

Beshkova D, Simova E, Frengova G, Simov Z (1998) Production of flavour compounds by yogurt starter cultures. J Ind Microbiol Biotechnol 20:180–186. doi: 10.1038/sj.jim.2900504

Bhaya D, Davison M, Barrangou R (2011) CRISPR-Cas systems in bacteria and archaea: versatile small RNAs for adaptive defense and regulation. Annu Rev Genet 45:273–297. doi: 10.1146/annurev-genet-110410-132430

Birarda G, Grenci G, Businaro L, Marmiroli B, Pacor S, Vaccari L (2010b) Fabrication of a microfluidic platform for investigating dynamic biochemical processes in living samples by FTIR microspectroscopy. Microelectron Eng 87:806–809. doi: 10.1016/j.mee.2009.11.081

Bischof JC, Wolkers WF, Tsvetkova NM, Oliver AE, Crowe JH (2002) Lipid and protein changes due to freezing in dunning AT-1 cells. 45:22–32. doi: 10.1016/S0011-2240(02)00103-7

Blond G, Simatos D, Catté M, Dussap CG, Gros JB (1997) Modeling of the water-sucrose state diagram below 0 °C. Carbohydr Res 298:139–145. doi: 10.1016/S0008-6215(96)00313-8

Boetius A, Anesio AM, Deming JW, Mikucki JA, Rapp JZ (2015) Microbial ecology of the cryosphere: sea ice and glacial habitats. Nat Rev Microbiol 13:677–690. doi: 10.1038/nrmicro3522

Borchman D, Yappert MC, Herrell P (1991) Structural characterization of human lens membrane lipid by infrared spectroscopy. Invest Ophthalmol Vis Sci 32:2404–2416

Bravo-Ferrada BM, Brizuela N, Gerbino E, Gómez-Zavaglia A, Semorile L, Tymczyszyn EE (2015) Effect of protective agents and previous acclimation on ethanol resistance of frozen and freeze-dried *Lactobacillus plantarum* strains. Cryobiology 71:522–528. doi: 10.1016/j.cryobiol.2015.10.154

Broadbent JR, Lin C (1999) Effect of heat shock or cold shock treatment on the resistance of *Lactococcus lactis* to freezing and lyophilization. Cryobiology 39:88–102. doi: 10.1006/cryo.1999.2190

Burgess CM, Slotboom DJ, Geertsma ER, Duurkens RH, Poolman B, van Sinderen D (2006) The riboflavin transporter RibU in *Lactococcus lactis*: molecular characterization of gene expression and the transport mechanism. J Bacteriol 188:2752–2760. doi: 10.1128/JB.188.8.2752-2760.2006

Cárcoba R, Rodríguez A (2000) Influence of cryoprotectants on the viability and acidifying activity of frozen and freeze-dried cells of the novel starter strain *Lactococcus lactis* ssp. *lactis* CECT 5180. Eur Food Res Technol 211:433–437. doi: 10.1007/s002170000194

Carr GL (2001) Resolution limits for infrared microspectroscopy explored with synchrotron radiation. Rev Sci Instrum 72:1613–1619. doi: 10.1063/1.1347965

Carvalho AL, Turner DL, Fonseca LL, Solopova A, Catarino T, Kuipers OP, Voit EO, Neves AR, Santos H (2013) Metabolic and transcriptional analysis of acid stress in *Lactococcus lactis*, with a focus on the kinetics of lactic acid pools. PLOS ONE 8:e68470. doi: 10.1371/journal.pone.0068470

Castro R, Neves AR, Fonseca LL, Pool WA, Kok J, Kuipers OP, Santos H (2009) Characterization of the individual glucose uptake systems of *Lactococcus lactis*: mannose-PTS, cellobiose-PTS and the novel GlcU permease. Mol Microbiol 71:795–806. doi: 10.1111/j.1365-2958.2008.06564.x

Chadeau E, Dumas E, Adt I, Degraeve P, Noël C, Girodet C, Oulahal N (2012) Assessment of the mode of action of polyhexamethylene biguanide against *Listeria innocua* by Fourier transformed infrared spectroscopy and fluorescence anisotropy analysis. Can J Microbiol 58:1353–1361. doi: 10.1139/w2012-113

Champagne CP, Gélinas P (1998) Ferments commerciaux. In: Champagne CP (ed) Production de ferments lactiques dans l'industrie laitière. Edisem, Incorporated, Canada, pp 65–87

Chan JW, Esposito AP, Talley CE, Hollars CW, Lane SM, Huser T (2004) Reagentless identification of single bacterial spores in aqueous solution by confocal laser tweezers Raman spectroscopy. Anal Chem 76:599–603. doi: 10.1021/ac0350155

Chapot-Chartier M-P, Kulakauskas S (2014) Cell wall structure and function in lactic acid bacteria. Microb Cell Factories 13 Suppl 1:S9. doi: 10.1186/1475-2859-13-S1-S9

Chattopadhyay MK (2006) Mechanism of bacterial adaptation to low temperature. J Biosci 31:157–165. doi: 10.1007/BF02705244

Chavarri FJ, Paz MD, Nuñez M (1988) Cryoprotective agents for frozen concentrated starters from non-bitter *Streptococcus lactis* strains. Biotechnol Lett 10:11–16. doi: 10.1007/BF01030016

Chervaux C, Ehrlich SD, Maguin E (2000) Physiological study of *Lactobacillus delbrueckii* subsp. *bulgaricus* strains in a novel chemically defined medium. 66:5306–5311. doi: 10.1128/AEM.66.12.5306-5311.2000

Chu-Ky S, Tourdot-Marechal R, Marechal P-A, Guzzo J (2005) Combined cold, acid, ethanol shocks in *Oenococcus oeni*: Effects on membrane fluidity and cell viability. Biochim Biophys Acta BBA - Biomembr 1717:118–124. doi: 10.1016/j.bbamem.2005.09.015

Clarke A, Morris GJ, Fonseca F, Murray BJ, Acton E, Price HC (2013) A low temperature limit for life on Earth. PLoS ONE 8:e66207. doi: 10.1371/journal.pone.0066207

Cohen DPA, Renes J, Bouwman FG, Zoetendal EG, Mariman E, de Vos WM, Vaughan EE (2006) Proteomic analysis of log to stationary growth phase *Lactobacillus plantarum* cells and a 2-DE database. Proteomics 6:6485–6493. doi: 10.1002/pmic.200600361

Comeau JWD, Pink J, Bezanson E, Douglas CD, Pink D, Smith-Palmer T (2009) A comparison of *Pseudomonas aeruginosa* biofilm development on ZnSe and TiO2 using attenuated total reflection Fourier transform infrared spectroscopy. Appl Spectrosc 63:1000–1007. doi: 10.1366/000370209789379259

Crowe JH (2015) Anhydrobiosis: an unsolved problem with applications in human welfare. Subcell Biochem 71:263–280. doi: 10.1007/978-3-319-19060-0_11

Crowe JH, Carpenter JF, Crowe LM, Anchordoguy TJ (1990) Are freezing and dehydration similar stress vectors? A comparison of modes of interaction of stabilizing solutes with biomolecules. Cryobiology 27:219–231. doi: 10.1016/0011-2240(90)90023-W

Crowe JH, Crowe LM, Carpenter JF, Rudolph AS, Wistrom CA, Spargo BJ, Anchordoguy TJ (1988) Interactions of sugars with membranes. Biochim Biophys Acta BBA - Rev Biomembr 947:367–384. doi: 10.1016/0304-4157(88)90015-9

Crowe JH, Hoekstra FA, Crowe LM, Anchordoguy TJ, Drobnis E (1989) Lipid phase transitions measured in intact cells with Fourier transform infrared spectroscopy. Cryobiology 26:76–84. doi: 10.1016/0011-2240(89)90035-7

Cuevas JC, López-Cobollo R, Alcázar R, Zarza X, Koncz C, Altabella T, Salinas J, Tiburcio AF, Ferrando A (2008) Putrescine is involved in Arabidopsis freezing tolerance and cold acclimation by regulating abscisic acid levels in response to low temperature. Plant Physiol 148:1094–1105. doi: 10.1104/pp.108.122945

Davidson AL, Maloney PC (2007) ABC transporters: how small machines do a big job. Trends Microbiol 15:448–455. doi: 10.1016/j.tim.2007.09.005

De Man JC, Rogosa M, Sharpe ME (1960) A medium for the cultivation of lactobacilli. 23:130–135. doi: 10.1111/j.1365-2672.1960.tb00188.x

De Paoli P (2005) Bio-banking in microbiology: from sample collection to epidemiology, diagnosis and research. FEMS Microbiol Rev 29:897–910. doi: 10.1016/j.femsre.2005.01.005

de Sarrau B, Clavel T, Zwickel N, Despres J, Dupont S, Beney L, Tourdot-Maréchal R, Nguyen-the C (2013) Unsaturated fatty acids from food and in the growth medium improve growth of *Bacillus cereus* under cold and anaerobic conditions. Food Microbiol 36:113–122. doi: 10.1016/j.fm.2013.04.008

de Urraza P, De Antoni G (1997) Induced cryotolerance of *Lactobacillus delbrueckii* subsp. *bulgaricus* LBB by preincubation at suboptimal temperatures with a fermentable sugar. Cryobiology 35:159–164. doi: 10.1006/cryo.1997.2036

De Valdéz GF, De Giori GS (1993) Effect of freezing and thawing on the viability and uptake of amino acids by *L. delbrueckii* ssp. *bulgaricus*. Cryobiology 30:329–334. doi: 10.1006/cryo.1993.1032

Delcour J, Ferain T, Deghorain M, Palumbo E, Hols P (1999) The biosynthesis and functionality of the cell-wall of lactic acid bacteria. Antonie Van Leeuwenhoek 76:159–184

Delille A, Quilès F, Humbert F (2007) In situ monitoring of the nascent *Pseudomonas fluorescens* biofilm response to variations in the dissolved organic carbon level in low-nutrient water by attenuated total reflectance-Fourier transform infrared spectroscopy. Appl Environ Microbiol 73:5782–5788. doi: 10.1128/AEM.00838-07

Denich TJ, Beaudette LA, Lee H, Trevors JT (2003) Effect of selected environmental and physico-chemical factors on bacterial cytoplasmic membranes. J Microbiol Methods 52:149–182. doi: 10.1016/S0167-7012(02)00155-0

Derzelle S, Hallet B, Ferain T, Delcour J, Hols P (2003) Improved adaptation to cold-shock, stationary-phase, and freezing stresses in *Lactobacillus plantarum* overproducing cold-shock proteins. Appl Environ Microbiol 69:4285–4290. doi: 10.1128/AEM.69.7.4285-4290.2003

Deutscher MP (2003) Degradation of stable RNA in bacteria. J Biol Chem. doi: 10.1074/jbc.R300031200

Dianawati D, Mishra V, Shah NP (2012) Role of calcium alginate and mannitol in protecting *Bifidobacterium*. Appl Environ Microbiol 78:6914–6921. doi: 10.1128/AEM.01724-12

Díaz SB, Biondi de Lopez AC, Disalvo EA (2003) Dehydration of carbonyls and phosphates of phosphatidylcholines determines the lytic action of lysoderivatives. Chem Phys Lipids 122:153–157. doi: 10.1016/S0009-3084(02)00186-X

Disalvo EA, Bouchet AM, Frias MA (2013) Connected and isolated CH_2 populations in acyl chains and its relation to pockets of confined water in lipid membranes as observed by FTIR spectrometry. Biochim Biophys Acta BBA - Biomembr 1828:1683–1689. doi: 10.1016/j.bbamem.2013.02.007

Dmitriev B, Toukach F, Ehlers S (2005) Towards a comprehensive view of the bacterial cell wall. Trends Microbiol 13:569–574. doi: 10.1016/j.tim.2005.10.001

Donovan C, Bramkamp M (2009) Characterization and subcellular localization of a bacterial flotillin homologue. Microbiology 155:1786–1799. doi: 10.1099/mic.0.025312-0

Dubas E, Janowiak F, Krzewska M, Hura T, Żur I (2013) Endogenous ABA concentration and cytoplasmic membrane fluidity in microspores of oilseed rape (*Brassica napus* L.) genotypes differing in responsiveness to androgenesis induction. Plant Cell Rep 32:1465–1475. doi: 10.1007/s00299-013-1458-6

Dumas P, Miller L (2003) Biological and biomedical applications of synchrotron infrared microspectroscopy. J Biol Phys 29:201–218. doi: 10.1023/A:1024448910761

Dumont F, Marechal PA, Gervais P (2003) Influence of cooling rate on *Saccharomyces cerevisiae* destruction during freezing: unexpected viability at ultra-rapid cooling rates. Cryobiology 46:33–42

Dumont F, Marechal P-A, Gervais P (2004) Cell size and water permeability as determining factors for cell viability after freezing at different cooling rates. Appl Environ Microbiol 70:268–272. doi: 10.1128/AEM.70.1.268-272.2004

Dumont F, Marechal P-A, Gervais P (2006) Involvement of two specific causes of cell mortality in freeze-thaw cycles with freezing to -196 degrees C. Appl Environ Microbiol 72:1330–1335. doi: 10.1128/AEM.72.2.1330-1335.2006

Egelie KJ, Graff GD, Strand SP, Johansen B (2016) The emerging patent landscape of CRISPR-Cas gene editing technology. Nat Biotechnol 34:1025–1031. doi: 10.1038/nbt.3692

Eiteman MA, Ramalingam S (2015) Microbial production of lactic acid. Biotechnol Lett 37:955–972. doi: 10.1007/s10529-015-1769-5

El Kafsi H, Binesse J, Loux V, Buratti J, Boudebbouze S, Dervyn R, Kennedy S, Galleron N, Quinquis B, Batto J-M, Moumen B, Maguin E, van de Guchte M (2014) *Lactobacillus delbrueckii* ssp. *lactis* and ssp. bulgaricus: a chronicle of evolution in action. BMC Genomics 15:407. doi: 10.1186/1471-2164-15-407

Endo A, Dicks LMT (2014) Physiology of the LAB. In: Holzapfel WH, Wood BJB (eds) Lactic acid bacteria. John Wiley & Sons, Ltd, pp 13–30

Exterkate FA, Otten BJ, Wassenberg HW, Veerkamp JH (1971) Comparison of the phospholipid composition of *Bifidobacterium* and *Lactobacillus* strains. 106:824–829

Fakruddin M, Mannan KSB, Andrews S (2013) Viable but nonculturable bacteria: food safety and public health perspective. Int Sch Res Not Microbiol. doi: 10.1155/2013/703813

Felis GE, Pot B (2014) The family Lactobacillaceae. In: Holzapfel WH, Wood BJB (eds) Lactic acid bacteria. John Wiley & Sons, Ltd, pp 245–247

Fencl Z, Málek I, Fencl Z (1966) Theoretical analysis of continuous culture systems. In: Theoretical and methodological basis of continuous culture of microorganisms. Academic Press, pp 67–153

Fernández Murga ML, Cabrera GM, Font De Valdez G, Disalvo A, Seldes AM (2000) Influence of growth temperature on cryotolerance and lipid composition of *Lactobacillus acidophilus*. J Appl Microbiol 88:342–348. doi: 10.1046/j.1365-2672.2000.00967.x

Fernández Murga ML, de Valdez GF, Disalvo EA (2001) Effect of lipid composition on the stability of cellular membranes during freeze–thawing of *Lactobacillus acidophilus* grown at different temperatures. Arch Biochem Biophys 388:179–184. doi: 10.1006/abbi.2001.2274

Fisberg M, Machado R (2015) History of yogurt and current patterns of consumption. Nutr Rev 73:4–7. doi: 10.1093/nutrit/nuv020

Fonseca F, Béal C, Corrieu G (2000) Method of quantifying the loss of acidification activity of lactic acid starters during freezing and frozen storage. J Dairy Res 67:83–90

Fonseca F, Béal C, Corrieu G (2001) Operating conditions that affect the resistance of lactic acid bacteria to freezing and frozen storage. Cryobiology 43:189–198. doi: 10.1006/cryo.2001.2343

Fonseca F, Béal C, Mihoub F, Marin M, Corrieu G (2003) Improvement of cryopreservation of *Lactobacillus delbrueckii* subsp. *bulgaricus* CFL1 with additives displaying different protective effects. 13:917–926. doi: 10.1016/S0958-6946(03)00119-5

Fonseca F, Marin M, Morris GJ (2006) Stabilization of frozen *Lactobacillus delbrueckii* subsp. *bulgaricus* in glycerol suspensions: Freezing kinetics and storage temperature effects. Appl Environ Microbiol 72:6474–6482. doi: 10.1128/AEM.00998-06

Fonseca F, Meneghel J, Cenard S, Passot S, Morris GJ (2016) Determination of intracellular vitrification temperatures for unicellular micro organisms under conditions relevant for cryopreservation. PloS One 11:e0152939. doi: 10.1371/journal.pone.0152939

Foschino R, Fiori E, Galli A (1996) Survival and residual activity of *Lactobacillus acidophilus* frozen cultures under different conditions. J Dairy Res 63:295–303. doi: 10.1017/S0022029900031782

Fox J (2005) The R Commander: a basic-statistics graphical user interface to R. J Stat Softw 14:1–42. doi: 10.18637/jss.v014.i09

Franks F (1998) Freeze-drying of bioproducts: putting principles into practice. Eur J Pharm Biopharm 45:221–229. doi: 10.1016/S0939-6411(98)00004-6

Frías MA, Díaz SB, Ale NM, Ben Altabef A, Disalvo EA (2006) FTIR analysis of the interaction of arbutin with dimyristoyl phosphatidylcholine in anhydrous and hydrated states. Biochim Biophys Acta BBA - Biomembr 1758:1823–1829. doi: 10.1016/j.bbamem.2006.06.024

Galdiero S, Galdiero M, Pedone C (2007) beta-barrel membrane bacterial proteins: structure, function, assembly and interaction with lipids. Curr Protein Pept Sci 8:63–82

Galichet A, Sockalingum GD, Belarbi A, Manfait M (2001) FTIR spectroscopic analysis of *Saccharomyces cerevisiae* cell walls: study of an anomalous strain exhibiting a pink-colored cell phenotype. FEMS Microbiol Lett 197:179–186

Gautier J, Passot S, Pénicaud C, Guillemin H, Cenard S, Lieben P, Fonseca F (2013) A low membrane lipid phase transition temperature is associated with a high cryotolerance of *Lactobacillus delbrueckii* subspecies *bulgaricus* CFL1. J Dairy Sci 96:5591–5602. doi: 10.3168/jds.2013-6802

Gill SS, Tuteja N (2010) Polyamines and abiotic stress tolerance in plants. Plant Signal Behav 5:26–33

Gilliland SE, Kim HS (1984) Effect of viable starter culture bacteria in yogurt on lactose utilization in humans. J Dairy Sci 67:1–6. doi: 10.3168/jds.S0022-0302(84)81260-6

Giuliani A, Jamme F, Rouam V, Wien F, Giorgetta J-L, Lagarde B, Chubar O, Bac S, Yao I, Rey S, Herbeaux C, Marlats J-L, Zerbib D, Polack F, Réfrégiers M (2009) DISCO: a low-energy multipurpose beamline at synchrotron SOLEIL. J Synchrotron Radiat 16:835–841. doi: 10.1107/S0909049509034049

Glaasker E, Heuberger EH, Konings WN, Poolman B (1998) Mechanism of osmotic activation of the quaternary ammonium compound transporter (QacT) of *Lactobacillus plantarum*. J Bacteriol 180:5540–5546

Goldberg I, Eschar L (1977) Stability of lactic acid bacteria to freezing as related to their fatty acid composition. Appl Environ Microbiol 33:489–496

Gomez Zavaglia A, Disalvo EA, De Antoni GL (2000) Fatty acid composition and freeze-thaw resistance in lactobacilli. J Dairy Res 67:241–247

Goñi FM, Arrondo JLR (1986) A study of phospholipid phosphate groups in model membranes by Fourier transform infrared spectroscopy. Faraday Discuss Chem Soc 81:117–126. doi: 10.1039/DC9868100117

Grangeteau C, Gerhards D, Terrat S, Dequiedt S, Alexandre H, Guilloux-Benatier M, von Wallbrunn C, Rousseaux S (2016) FT-IR spectroscopy: a powerful tool for studying the inter- and intraspecific biodiversity of cultivable non-*Saccharomyces* yeasts isolated from grape must. J Microbiol Methods 121:50–58. doi: 10.1016/j.mimet.2015.12.009

Graumann P, Schröder K, Schmid R, Marahiel MA (1996) Cold shock stress-induced proteins in *Bacillus subtilis*. J Bacteriol 178:4611–4619

Grenci G, Birarda G, Mitri E, Businaro L, Pacor S, Vaccari L, Tormen M (2012) Optimization of microfluidic systems for IRMS long term measurement of living cells. Microelectron Eng 98:698–702. doi: 10.1016/j.mee.2012.05.049

Hachmann A-B, Angert ER, Helmann JD (2009) Genetic analysis of factors affecting susceptibility of *Bacillus subtilis* to daptomycin. Antimicrob Agents Chemother 53:1598–1609. doi: 10.1128/AAC.01329-08

Haris PI, Coke M, Chapman D (1989) Fourier transform infrared spectroscopic investigation of rhodopsin structure and its comparison with bacteriorhodopsin. Biochim Biophys Acta 995:160–167

Harz M, Rösch P, Popp J (2009) Vibrational spectroscopy--a powerful tool for the rapid identification of microbial cells at the single-cell level. Cytom Part J Int Soc Anal Cytol 75:104–113. doi: 10.1002/cyto.a.20682

Hati S, Mandal S, Prajapati JB (2013) Novel starters for value added fermented dairy products. Curr Res Nutr Food Sci J 1:83–91

Helm D, Labischinski H, Schallehn G, Naumann D (1991) Classification and identification of bacteria by Fourier-transform infrared spectroscopy. J Gen Microbiol 137:69–79. doi: 10.1099/00221287-137-1-69

Heylen K, Hoefman S, Vekeman B, Peiren J, De Vos P (2012) Safeguarding bacterial resources promotes biotechnological innovation. Appl Microbiol Biotechnol 94:565–574. doi: 10.1007/s00253-011-3797-y

Hickey MW, Hillier AJ, Jago GR (1986) Transport and metabolism of lactose, glucose, and galactose in homofermentative lactobacilli. Appl Environ Microbiol 51:825–831

Hincha DK, Crowe JH (1998) Trehalose increases freeze–thaw damage in liposomes containing chloroplast glycolipids. Cryobiology 36:245–249. doi: 10.1006/cryo.1998.2074

Holman HY, Martin MC, Blakely EA, Bjornstad K, McKinney WR (2000) IR spectroscopic characteristics of cell cycle and cell death probed by synchrotron radiation based Fourier transform IR spectromicroscopy. Biopolymers 57:329–335. doi: 10.1002/1097-0282(2000)57:6<329::AID-BIP20>3.0.CO;2-2

Holman H-YN, Martin MC, McKinney WR (2003) Synchrotron-based FTIR spectromicroscopy: cytotoxicity and heating considerations. J Biol Phys 29:275–286. doi: 10.1023/A:1024465414395

Holman H-YN, Miles R, Hao Z, Wozei E, Anderson LM, Yang H (2009) Real-time chemical imaging of bacterial activity in biofilms using open-channel microfluidics and synchrotron FTIR spectromicroscopy. Anal Chem 81:8564–8570. doi: 10.1021/ac9015424

Holzapfel WH, Wood BJB (2014) Introduction to the LAB. In: Holzapfel WH, Wood BJB (eds) Lactic Acid Bacteria. John Wiley & Sons, Ltd, pp 1–12

Hoopes L (2008) Introduction to the gene expression and regulation topic room. Nat Educ 1:160

Huang WE, Ward AD, Whiteley AS (2009) Raman tweezers sorting of single microbial cells. Environ Microbiol Rep 1:44–49. doi: 10.1111/j.1758-2229.2008.00002.x

Hubálek Z (1996) Cryopreservation of microorganisms at ultra-low temperatures. Academia Praha

Hubálek Z (2003) Protectants used in the cryopreservation of microorganisms. Cryobiology 46:205–229. doi: 10.1016/S0011-2240(03)00046-4

Humbert F, Quilès F (2011) *In situ* study of early stages of biofilm formation under different environmental stresses by ATR-FTIR spectroscopy. In: Mendez-Villas A (ed) Science against microbial pathogens: communicating current research and technological advances, Formatex Research Center, Badajoz, Spain

Hynönen U, Palva A (2013) *Lactobacillus* surface layer proteins: structure, function and applications. Appl Microbiol Biotechnol 97:5225–5243. doi: 10.1007/s00253-013-4962-2

Iwamori M, Sakai A, Minamimoto N, Iwamori Y, Tanaka K, Aoki D, Adachi S, Nomura T (2011) Characterization of novel glycolipid antigens with an α-galactose epitope in lactobacilli detected with rabbit anti-*Lactobacillus* antisera and occurrence of antibodies against them in human sera. J Biochem (Tokyo) 150:515–523. doi: 10.1093/jb/mvr091

Jamin N, Dumas P, Moncuit J, Fridman WH, Teillaud JL, Carr GL, Williams GP (1998) Highly resolved chemical imaging of living cells by using synchrotron infrared microspectrometry. Proc Natl Acad Sci U S A 95:4837–4840

Jamme F, Villette S, Giuliani A, Rouam V, Wien F, Lagarde B, Réfrégiers M (2010) Synchrotron UV fluorescence microscopy uncovers new probes in cells and tissues. Microsc Microanal 16:507–514. doi: 10.1017/S1431927610093852

Janer C, Arigoni F, Lee BH, Peláez C, Requena T (2005) Enzymatic ability of *Bifidobacterium animalis* subsp. *lactis* to hydrolyze milk proteins: identification and characterization of endopeptidase O. Appl Environ Microbiol 71:8460–8465. doi: 10.1128/AEM.71.12.8460-8465.2005

Jansson JK, Taş N (2014) The microbial ecology of permafrost. Nat Rev Microbiol 12:414–425. doi: 10.1038/nrmicro3262

Jantaro S, Mäenpää P, Mulo P, Incharoensakdi A (2003) Content and biosynthesis of polyamines in salt and osmotically stressed cells of *Synechocystis* sp. PCC 6803. FEMS Microbiol Lett 228:129–135. doi: 10.1016/S0378-1097(03)00747-X

Jiang W, Saxena A, Song B, Ward BB, Beveridge TJ, Myneni SCB (2004) Elucidation of functional groups on Gram-positive and Gram-negative bacterial surfaces using infrared spectroscopy. Langmuir ACS J Surf Colloids 20:11433–11442. doi: 10.1021/la049043+

Johler S, Stephan R, Althaus D, Ehling-Schulz M, Grunert T (2016) High-resolution subtyping of *Staphylococcus aureus* strains by means of Fourier-transform infrared spectroscopy. Syst Appl Microbiol 39:189–194. doi: 10.1016/j.syapm.2016.03.003

Johnson BR, Hymes J, Sanozky-Dawes R, Henriksen ED, Barrangou R, Klaenhammer TR (2015) Conserved S-layer-associated proteins revealed by exoproteomic survey of S-layer-forming Lactobacilli. Appl Environ Microbiol 82:134–145. doi: 10.1128/AEM.01968-15

Jones PG, Cashel M, Glaser G, Neidhardt FC (1992) Function of a relaxed-like state following temperature downshifts in *Escherichia coli*. J Bacteriol 174:3903–3914

Kaiser RD, London E (1998) Location of diphenylhexatriene (DPH) and its derivatives within membranes: comparison of different fluorescence quenching analyses of membrane depth. Biochemistry (Mosc) 37:8180–8190. doi: 10.1021/bi980064a

Kapla J (2016) Computer simulations of membrane-sugar interactions. Stockholm University

Kawai F, Shoda M, Harashima R, Sadaie Y, Hara H, Matsumoto K (2004) Cardiolipin domains in *Bacillus subtilis* Marburg membranes. J Bacteriol 186:1475–1483. doi: 10.1128/JB.186.5.1475-1483.2004

Kazarian SG, Chan KLA (2013) ATR-FTIR spectroscopic imaging: recent advances and applications to biological systems. Analyst 138:1940–1951. doi: 10.1039/c3an36865c

Keto-Timonen R, Hietala N, Palonen E, Hakakorpi A, Lindström M, Korkeala H (2016) Cold shock proteins: A minireview with special emphasis on Csp-family of enteropathogenic *Yersinia*. Front Microbiol. doi: 10.3389/fmicb.2016.01151

Kets E, Teunissen P, de Bont J (1996) Effect of compatible solutes on survival of lactic acid bacteria subjected to drying. Appl Environ Microbiol 62:259–261

Kets EPW, Galinski EA, Bont JAM de (1994) Carnitine: a novel compatible solute in *Lactobacillus plantarum*. Arch Microbiol 162:243–248. doi: 10.1007/BF00301845

Kim WS, Khunajakr N, Ren J, Dunn NW (1998) Conservation of the major cold shock protein in lactic acid bacteria. Curr Microbiol 37:333–336. doi: 10.1007/s002849900387

Kim WS, Ren J, Dunn NW (1999) Differentiation of *Lactococcus lactis* subspecies *lactis* and subspecies *cremoris* strains by their adaptive response to stresses. FEMS Microbiol Lett 171:57–65

Kleerebezem M, Hols P, Bernard E, Rolain T, Zhou M, Siezen RJ, Bron PA (2010) The extracellular biology of the lactobacilli. FEMS Microbiol Rev 34:199–230. doi: 10.1111/j.1574-6976.2010.00208.x

Koch AL (1995) The geometry and osmotic relations of plasmolysis spaces in bacteria and the role of endocytosis, tubular structures and Scheie structures in their formation. J Theor Biol 176:471–492. doi: 10.1006/S0022-5193(85)90300-5

Koch AL (1998) How did bacteria come to be? Adv Microb Physiol 40:353–399

Kong J, Yu S (2007) Fourier transform infrared spectroscopic analysis of protein secondary structures. Acta Biochim Biophys Sin Shanghai 39:549–559. doi: 10.1111/j.1745-7270.2007.00320.x

Koppelman C-M, Blaauwen TD, Duursma MC, Heeren RMA, Nanninga N (2001) *Escherichia coli* minicell membranes are enriched in cardiolipin. J Bacteriol 183:6144–6147. doi: 10.1128/JB.183.20.6144-6147.2001

Kuanyshev N, Ami D, Signori L, Porro D, Morrissey JP, Branduardi P (2016) Assessing physio-macromolecular effects of lactic acid on *Zygosaccharomyces bailii* cells during microaerobic fermentation. FEMS Yeast Res. doi: 10.1093/femsyr/fow058

Laczkó-Dobos H, Szalontai B (2009) Lipids, proteins, and their interplay in the dynamics of temperature-stressed membranes of a cyanobacterium, *Synechocystis* PCC 6803. Biochemistry (Mosc) 48:10120–10128. doi: 10.1021/bi9011034

Lahtinen SJ, Ouwehand AC, Reinikainen JP, Korpela JM, Sandholm J, Salminen SJ (2006) Intrinsic properties of so-called dormant probiotic bacteria, determined by flow cytometric viability assays. Appl Environ Microbiol 72:5132–5134. doi: 10.1128/AEM.02897-05

Laiño JE, Hebert EM, Savoy de Giori G, LeBlanc JG (2015) Draft genome sequence of *Lactobacillus delbrueckii* subsp. *bulgaricus* CRL871, a folate-producing strain isolated from a northwestern Argentinian yogurt. Genome Announc. doi: 10.1128/genomeA.00693-15

Lakowicz JR (ed) (2006) Instrumentation for fluorescence spectroscopy. In: Principles of fluorescence spectroscopy. Springer US, pp 27–61

Lamothe GT, Jolly L, Mollet B, Stingele F (2002) Genetic and biochemical characterization of exopolysaccharide biosynthesis by *Lactobacillus delbrueckii* subsp. *bulgaricus*. Arch Microbiol 178:218–228. doi: 10.1007/s00203-002-0447-x

Le Marrec C (2011) Responses of lactic acid bacteria to osmotic stress. In: Tsakalidou E, Papadimitriou K (eds) Stress responses of lactic acid bacteria. Springer, Boston, MA, pp 67–90

Leibo S, Farrant J, Mazur P, Hanna MJ, Smith L (1970) Effects of freezing on marrow stem cell suspensions: interactions of cooling and warming rates in the presence of PVP, sucrose, or glycerol. Cryobiology 6:315–332

Lencastre Fernandes R, Nierychlo M, Lundin L, Pedersen AE, Puentes Tellez PE, Dutta A, Carlquist M, Bolic A, Schäpper D, Brunetti AC, Helmark S, Heins A-L, Jensen AD, Nopens I, Rottwitt K, Szita N, van Elsas JD, Nielsen PH, Martinussen J, Sørensen SJ, Lantz AE, Gernaey KV (2011)

Experimental methods and modeling techniques for description of cell population heterogeneity. Biotechnol Adv 29:575–599. doi: 10.1016/j.biotechadv.2011.03.007

Lentz BR (1989) Membrane "fluidity" as detected by diphenylhexatriene probes. Chem Phys Lipids 50:171–190. doi: 10.1016/0009-3084(89)90049-2

Lentz BR (1993) Use of fluorescent probes to monitor molecular order and motions within liposome bilayers. Chem Phys Lipids 64:99–116. doi: 10.1016/0009-3084(93)90060-G

Leslie SB, Israeli E, Lighthart B, Crowe JH, Crowe LM (1995) Trehalose and sucrose protect both membranes and proteins in intact bacteria during drying. Appl Environ Microbiol 61:3592–3597

Letellier L, Moudden H, Shechter E (1977) Lipid and protein segregation in *Escherichia coli* membrane: morphological and structural study of different cytoplasmic membrane fractions. Proc Natl Acad Sci U S A 74:452–456

Levin IW, Bhargava R (2005) Fourier transform infrared vibrational spectroscopic imaging: integrating microscopy and molecular recognition. Annu Rev Phys Chem 56:429–474. doi: 10.1146/annurev.physchem.56.092503.141205

Lewis RNAH, McElhaney RN (1998) The structure and organization of phospholipid bilayers as revealed by infrared spectroscopy. Chem Phys Lipids 96:9–21. doi: 10.1016/S0009-3084(98)00077-2

Lewis RNAH, McElhaney RN (2013) Membrane lipid phase transitions and phase organization studied by Fourier transform infrared spectroscopy. Biochim Biophys Acta 1828:2347–2358. doi: 10.1016/j.bbamem.2012.10.018

Lewis RNAH, Sykes BD, McElhaney RN (1987) Thermotropic phase behavior of model membranes composed of phosphatidylcholines containing *dl*-methyl anteisobranched fatty acids. Differential scanning calorimetric and phosphorus-31P NMR spectroscopic studies. Biochemistry (Mosc) 26:4036–4044. doi: 10.1021/bi00387a044

Lin T-Y, Weibel DB (2016) Organization and function of anionic phospholipids in bacteria. Appl Microbiol Biotechnol 100:4255–4267. doi: 10.1007/s00253-016-7468-x

Linders LJM, Wolkers WF, Hoekstra FA, van 't Riet K (1997) Effect of added carbohydrates on membrane phase behavior and survival of dried *Lactobacillus plantarum*. Cryobiology 35:31–40. doi: 10.1006/cryo.1997.2021

Lippert K, Galinski EA (1992) Enzyme stabilization be ectoine-type compatible solutes: protection against heating, freezing and drying. Appl Microbiol Biotechnol 37:61–65. doi: 10.1007/BF00174204

López CS, Alice AF, Heras H, Rivas EA, Sánchez-Rivas C (2006) Role of anionic phospholipids in the adaptation of *Bacillus subtilis* to high salinity. Microbiology 152:605–616. doi: 10.1099/mic.0.28345-0

López D, Kolter R (2010) Functional microdomains in bacterial membranes. Genes Dev 24:1893–1902. doi: 10.1101/gad.1945010

Lorca G, Font de Valdez G (1999) The effect of suboptimal growth temperature and growth phase on resistance of *Lactobacillus acidophilus* to environmental stress. Cryobiology 39:144–149. doi: 10.1006/cryo.1999.2193

Lorca GL, de Valdez GF (1998) Temperature adaptation and cryotolerance in *Lactobacillus acidophilus*. Biotechnol Lett 20:847–849. doi: 10.1023/A:1005359424973

Louesdon S, Charlot-Rougé S, Tourdot-Maréchal R, Bouix M, Béal C (2015) Membrane fatty acid composition and fluidity are involved in the resistance to freezing of *Lactobacillus buchneri* R1102 and *Bifidobacterium longum* R0175. Microb Biotechnol 8:311–318. doi: 10.1111/1751-7915.12132

Luzardo MC, Amalfa F, Nuñez AM, Díaz S, Biondi De Lopez AC, Disalvo EA (2000) Effect of trehalose and sucrose on the hydration and dipole potential of lipid bilayers. Biophys J 78:2452–2458

Makarova K, Slesarev A, Wolf Y, Sorokin A, Mirkin B, Koonin E, Pavlov A, Pavlova N, Karamychev V, Polouchine N, Shakhova V, Grigoriev I, Lou Y, Rohksar D, Lucas S, Huang K, Goodstein DM, Hawkins T, Plengvidhya V, Welker D, Hughes J, Goh Y, Benson A, Baldwin K, Lee J-H, Díaz-Muñiz I, Dosti B, Smeianov V, Wechter W, Barabote R, Lorca G, Altermann E, Barrangou R, Ganesan B, Xie Y, Rawsthorne H, Tamir D, Parker C, Breidt F, Broadbent J, Hutkins R, O'Sullivan D, Steele J, Unlu G, Saier M, Klaenhammer T, Richardson P, Kozyavkin S, Weimer B, Mills D (2006a) Comparative genomics of the lactic acid bacteria. Proc Natl Acad Sci U S A 103:15611–15616. doi: 10.1073/pnas.0607117103

Makarova KS, Grishin NV, Shabalina SA, Wolf YI, Koonin EV (2006b) A putative RNA-interference-based immune system in prokaryotes: computational analysis of the predicted enzymatic machinery, functional analogies with eukaryotic RNAi, and hypothetical mechanisms of action. Biol Direct 1:7. doi: 10.1186/1745-6150-1-7

Maquelin K, Kirschner C, Choo-Smith L-P, van den Braak N, Endtz HP, Naumann D, Puppels GJ (2002) Identification of medically relevant microorganisms by vibrational spectroscopy. J Microbiol Methods 51:255–271

Marcotte L, Therien-Aubin H, Sandt C, Barbeau J, Lafleur M (2004) Solute size effects on the diffusion in biofilms of *Streptococcus mutans*. Biofouling 20:189–201. doi: 10.1080/08927010400010494

Markowitz VM, Chen I-MA, Palaniappan K, Chu K, Szeto E, Grechkin Y, Ratner A, Jacob B, Huang J, Williams P, Huntemann M, Anderson I, Mavromatis K, Ivanova NN, Kyrpides NC (2012) IMG: the Integrated Microbial Genomes database and comparative analysis system. Nucleic Acids Res 40:D115-122. doi: 10.1093/nar/gkr1044

Martos G i., Minahk C j., Font de Valdez G, Morero R (2007) Effects of protective agents on membrane fluidity of freeze-dried *Lactobacillus delbrueckii* ssp. *bulgaricus*. Lett Appl Microbiol 45:282–288. doi: 10.1111/j.1472-765X.2007.02188.x

Mazur P (1970) Cryobiology: the freezing of biological systems. Science 168:939–949

Mazur P (1977) The role of intracellular freezing in the death of cells cooled at supraoptimal rates. Cryobiology 14:251–272

Mazur P (1984) Freezing of living cells: mechanisms and implications. Am J Physiol 247:C125-142

Mazur P, Leibo SP, Chu EH (1972) A two-factor hypothesis of freezing injury. Evidence from Chinese hamster tissue-culture cells. Exp Cell Res 71:345–355

Mazur P, Rigopoulos N (1983) Contributions of unfrozen fraction and of salt concentration to the survival of slowly frozen human erythrocytes: influence of warming rate. Cryobiology 20:274–289

McElhaney RN (1982) The use of differential scanning calorimetry and differential thermal analysis in studies of model and biological membranes. Chem Phys Lipids 30:229–259

McGibbon L, Cossins AR, Quinn PJ, Russell NJ (1985) A differential scanning calorimetry and fluorescence polarisation study of membrane lipid fluidity in a psychrophilic bacterium. Biochim Biophys Acta BBA - Biomembr 820:115–121. doi: 10.1016/0005-2736(85)90222-6

McGuffee SR, Elcock AH (2010) Diffusion, crowding & protein stability in a dynamic molecular model of the bacterial cytoplasm. PLoS Comput Biol 6:e1000694. doi: 10.1371/journal.pcbi.1000694

Meadows JA, Wargo MJ (2015) Carnitine in bacterial physiology and metabolism. Microbiol Read Engl 161:1161–1174. doi: 10.1099/mic.0.000080

Meneghel J, Dugat-Bony E, Irlinger F, Loux V, Vidal M, Passot S, Béal C, Layec S, Fonseca F (2016) Draft genome sequence of *Lactobacillus delbrueckii* subsp. *bulgaricus* CFL1, a lactic acid bacterium isolated from French handcrafted fermented milk. Genome Announc 4:e00052-16. doi: 10.1128/genomeA.00052-16

Meneghel J, Passot S, Dupont S, Fonseca F (2017) Biophysical characterization of the *Lactobacillus delbrueckii* subsp. *bulgaricus* membrane during cold and osmotic stress and its relevance for cryopreservation. Appl Microbiol Biotechnol 101:1427–1441. doi: 10.1007/s00253-016-7935-4

Mercenier A, Pavan S, Pot B (2003) Probiotics as biotherapeutic agents: Present knowledge and future prospects. 9:175–191. doi: 10.2174/1381612033392224

Meryman HT (1968) Modified model for the mechanism of freezing injury in erythrocytes. Nature 218:333–336

Mika JT, Schavemaker PE, Krasnikov V, Poolman B (2014) Impact of osmotic stress on protein diffusion in *Lactococcus lactis*. Mol Microbiol 94:857–870. doi: 10.1111/mmi.12800

Mileykovskaya E, Dowhan W (2000) Visualization of phospholipid domains in *Escherichia coli* by using the cardiolipin-specific fluorescent dye 10-N-nonyl acridine orange. J Bacteriol 182:1172–1175. doi: 10.1128/JB.182.4.1172-1175.2000

Mille Y, Beney L, Gervais P (2003) Magnitude and kinetics of rehydration influence the viability of dehydrated *E. coli* K-12. Biotechnol Bioeng 83:578–582. doi: 10.1002/bit.10706

Mille Y, Beney L, Gervais P (2005) Compared tolerance to osmotic stress in various microorganisms: towards a survival prediction test. Biotechnol Bioeng 92:479–484. doi: 10.1002/bit.20631

Miller LM, Dumas P (2006) Chemical imaging of biological tissue with synchrotron infrared light. Biochim Biophys Acta BBA - Biomembr 1758:846–857. doi: 10.1016/j.bbamem.2006.04.010

Miller LM, Smith GD, Carr GL (2003) Synchrotron-based biological microspectroscopy: from the mid-infrared through the far-infrared regimes. J Biol Phys 29:219–230. doi: 10.1023/A:1024401027599

Molina-Höppner A, Doster W, Vogel RF, Gänzle MG (2004) Protective effect of sucrose and sodium chloride for *Lactococcus lactis* during sublethal and lethal high-pressure treatments. Appl Environ Microbiol 70:2013–2020. doi: 10.1128/AEM.70.4.2013-2020.2004

Monnet C, Béal C, Corrieu G (2003) Improvement of the resistance of *Lactobacillus delbrueckii* ssp. *bulgaricus* to freezing by natural selection. 86:3048–3053. doi: 10.3168/jds.S0022-0302(03)73904-6

Monnet C, Latrille E, Béal C, Corrieu G (2008) Croissance et propriétés fonctionnelles des bactéries lactiques. In: Corrieu G, Luquet F-M (eds) Bactéries lactiques. De la génétique aux ferments. Lavoisier, pp 511–611

Morice M, Bracquart P, Linden G (1992) Colonial variation and freeze-thaw resistance of *Streptococcus thermophilus*. J Dairy Sci 75:1197–1203. doi: 10.3168/jds.S0022-0302(92)77867-9

Morris GJ (2007) Asymptote guide to cryopreservation

Morris GJ, Acton E (2013) Controlled ice nucleation in cryopreservation--a review. Cryobiology 66:85–92. doi: 10.1016/j.cryobiol.2012.11.007

Morris GJ, Acton E, Murray BJ, Fonseca F (2012) Freezing injury: the special case of the sperm cell. Cryobiology 64:71–80. doi: 10.1016/j.cryobiol.2011.12.002

Morris GJ, Goodrich M, Acton E, Fonseca F (2006) The high viscosity encountered during freezing in glycerol solutions: effects on cryopreservation. Cryobiology 52:323–334. doi: 10.1016/j.cryobiol.2006.01.003

Moss DA, Keese M, Pepperkok R (2005) IR microspectroscopy of live cells. Vib Spectrosc 38:185–191. doi: 10.1016/j.vibspec.2005.04.004

Moussa M, Dumont F, Perrier-Cornet J-M, Gervais P (2008) Cell inactivation and membrane damage after long-term treatments at sub-zero temperature in the supercooled and frozen states. Biotechnol Bioeng 101:1245–1255. doi: 10.1002/bit.21981

Movasaghi Z, Rehman S, Rehman DI ur (2008) Fourier transform infrared (FTIR) spectroscopy of biological tissues. Appl Spectrosc Rev 43:134–179. doi: 10.1080/05704920701829043

Muchová K, Jamroškovič J, Barák I (2010) Lipid domains in *Bacillus subtilis* anucleate cells. Res Microbiol 161:783–790. doi: 10.1016/j.resmic.2010.07.006

Muchová K, Wilkinson AJ, Barák I (2011) Changes of lipid domains in *Bacillus subtilis* cells with disrupted cell wall peptidoglycan. FEMS Microbiol Lett 325:92–98. doi: 10.1111/j.1574-6968.2011.02417.x

Munro KL, Bambery KR, Carter EA, Puskar L, Tobin MJ, Wood BR, Dillon CT (2010) Synchrotron radiation infrared microspectroscopy of arsenic-induced changes to intracellular biomolecules in live leukemia cells. Vib Spectrosc 53:39–44. doi: 10.1016/j.vibspec.2010.02.004

Mykytczuk NCS, Trevors JT, Leduc LG, Ferroni GD (2007) Fluorescence polarization in studies of bacterial cytoplasmic membrane fluidity under environmental stress. Prog Biophys Mol Biol 95:60–82. doi: 10.1016/j.pbiomolbio.2007.05.001

Naumann D (2000) Infrared spectroscopy in microbiology. In: Meyer RA (ed) Encyclopedia of Analytical Chemistry. John Wiley & Sons, Ltd, Chichester, UK, pp 102–131

Naumann D (2001) FT-infrared and FT-Raman spectroscopy in biomedical research. Appl Spectrosc Rev 36:239–298. doi: 10.1081/ASR-100106157

Naumann D, Fijala V, Labischinski H, Giesbrecht P (1988) The rapid differentiation and identification of pathogenic bacteria using Fourier transform infrared spectroscopic and multivariate statistical analysis. J Mol Struct 174:165–170. doi: 10.1016/0022-2860(88)80152-2

Naumann D, Helm D, Labischinski H (1991) Microbiological characterizations by FT-IR spectroscopy. Nature 351:81–82. doi: 10.1038/351081a0

Nei T (1973) Proceedings: some aspects of freezing and drying of microorganisms on the basis of cellular water. Cryobiology 10:403–408

Norris KP (1959) Infra-red spectroscopy and its application to microbiology. J Hyg (Lond) 57:326–345

Obis D, Guillot A, Gripon J-C, Renault P, Bolotin A, Mistou M-Y (1999) Genetic and biochemical characterization of a high-affinity betaine uptake system (BusA) in *Lactococcus lactis* reveals a new functional organization within bacterial ABC transporters. J Bacteriol 181:6238–6246

Oldenhof H, Wolkers WF, Fonseca F, Passot S, Marin M (2005) Effect of sucrose and maltodextrin on the physical properties and survival of air-dried *Lactobacillus bulgaricus*: an in situ Fourier transform infrared spectroscopy study. Biotechnol Prog 21:885–892. doi: 10.1021/bp049559j

Olsen I, Jantzen E (2001) Sphingolipids in bacteria and fungi. Anaerobe 7:103–112. doi: 10.1006/anae.2001.0376

Panoff JM (Universite de C, Thammavongs B, Laplace JM, Hartke A, Boutibonnes P, Auffray Y (1995) Cryotolerance and cold adaptation in *Lactococcus lactis* subsp. *lactis* IL1403.

Panoff J-M, Thammavongs B, Guéguen M (2000) Cryoprotectants Lead to Phenotypic Adaptation to Freeze–Thaw Stress in Lactobacillus delbrueckii ssp. bulgaricus CIP 101027T. 40:264–269. doi: 10.1006/cryo.2000.2240

Passot S, Gautier J, Jamme F, Cenard S, Dumas P, Fonseca F (2015) Understanding the cryotolerance of lactic acid bacteria using combined synchrotron infrared and fluorescence microscopies. Analyst 140:5920–5928. doi: 10.1039/C5AN00654F

Passot S, Jamme F, Réfrégiers M, Gautier J, Cenard S, Fonseca F (2014) Synchrotron UV fluorescence microscopy for determining membrane fluidity modification of single bacteria with temperatures. Biomed Spectrosc Imaging 3:203–210. doi: 10.3233/BSI-140062

Pegg DE (2002) The history and principles of cryopreservation. Semin Reprod Med 20:5–13. doi: 10.1055/s-2002-23515

Pénicaud C, Landaud S, Jamme F, Talbot P, Bouix M, Ghorbal S, Fonseca F (2014) Physiological and biochemical responses of *Yarrowia lipolytica* to dehydration induced by air-drying and freezing. PloS One 9:e111138. doi: 10.1371/journal.pone.0111138

Péter G, Reichart O (2001) The effect of growth phase, cryoprotectants and freezing rates on the survival of selected micro-organisms during freezing and thawing. Acta Aliment 30:89–97. doi: 10.1556/AAlim.30.2001.1.10

Picque D, Perret B, Latrille E, Corrieu G (1992) Caractérisation et classification de bactéries lactiques à partir de la mesure de leur cinetique d'acidification. Lebensm - Wiss Technol 24:2–6

Pikuta EV, Marsic D, Bej A, Tang J, Krader P, Hoover RB (2005) *Carnobacterium pleistocenium* sp. nov., a novel psychrotolerant, facultative anaerobe isolated from permafrost of the Fox Tunnel in Alaska. Int J Syst Evol Microbiol 55:473–478. doi: 10.1099/ijs.0.63384-0

Polge C, Smith AU, Parkes AS (1949) Revival of spermatozoa after vitrification and dehydration at low temperatures. Nature 164:666

Poolman B, Glaasker E (1998) Regulation of compatible solute accumulation in bacteria. Mol Microbiol 29:397–407

Pothipongsa A, Jantaro S, Incharoensakdi A (2016) Spermidine synthase is required for growth of *Synechococcus* sp. PCC 7942 under osmotic stress. Curr Microbiol 73:639–645. doi: 10.1007/s00284-016-1107-8

Prakash O, Nimonkar Y, Shouche YS (2013) Practice and prospects of microbial preservation. FEMS Microbiol Lett 339:1–9. doi: 10.1111/1574-6968.12034

Prasad J, McJarrow P, Gopal P (2003) Heat and osmotic stress responses of probiotic *Lactobacillus rhamnosus* HN001 (DR20) in relation to viability after drying. Appl Environ Microbiol 69:917–925. doi: 10.1128/AEM.69.2.917-925.2003

Puzey KA, Gardner PJ, Petrova VK, Donnelly CW, Petrucci GA (2008) Automated species and strain identification of bacteria in complex matrices using FTIR spectroscopy. Proc. SPIE 6954, Chemical, Biological, Radiological, Nuclear, and Explosives (CBRNE) Sensing IX, 695412

Quilès F, Humbert F, Delille A (2010) Analysis of changes in attenuated total reflection FTIR fingerprints of *Pseudomonas fluorescens* from planktonic state to nascent biofilm state. Spectrochim Acta A Mol Biomol Spectrosc 75:610–616. doi: 10.1016/j.saa.2009.11.026

Quinn PJ (1985) A lipid-phase separation model of low-temperature damage to biological membranes. Cryobiology 22:128–146. doi: 10.1016/0011-2240(85)90167-1

Ragoonanan V, Malsam J, Bond DR, Aksan A (2008) Roles of membrane structure and phase transition on the hyperosmotic stress survival of *Geobacter sulfurreducens*. Biochim Biophys Acta BBA - Biomembr 1778:2283–2290. doi: 10.1016/j.bbamem.2008.06.006

Ragoonanan V, Wiedmann T, Aksan A (2010) Characterization of the effect of NaCl and trehalose on the thermotropic hysteresis of DOPC lipids during freeze/thaw. J Phys Chem B 114:16752–16758. doi: 10.1021/jp103960r

Räisänen L, Draing C, Pfitzenmaier M, Schubert K, Jaakonsaari T, von Aulock S, Hartung T, Alatossava T (2007) Molecular interaction between lipoteichoic acids and *Lactobacillus delbrueckii* phages depends on D-alanyl and alpha-glucose substitution of poly(glycerophosphate) backbones. J Bacteriol 189:4135–4140. doi: 10.1128/JB.00078-07

Raksajit W, Yodsang P, Mäenpää P, Incharoensakdi A (2009) Characterization of spermidine transport system in a cyanobacterium, *Synechocystis* sp. PCC 6803. J Microbiol Biotechnol 19:447–454

Rault A, Béal C, Ghorbal S, Ogier J-C, Bouix M (2007) Multiparametric flow cytometry allows rapid assessment and comparison of lactic acid bacteria viability after freezing and during frozen storage. Cryobiology 55:35–43. doi: 10.1016/j.cryobiol.2007.04.005

Rault A, Bouix M, Béal C (2010) Cryotolerance of *Lactobacillus delbrueckii* subsp. *bulgaricus* CFL1 is influenced by the physiological state during fermentation. Int Dairy J 20:792–799. doi: 10.1016/j.idairyj.2010.05.002

Rawlings ND, Barrett AJ (1995) Evolutionary families of metallopeptidases. Methods Enzymol 248:183–228

Rhee HJ, Kim E-J, Lee JK (2007) Physiological polyamines: simple primordial stress molecules. J Cell Mol Med 11:685–703. doi: 10.1111/j.1582-4934.2007.00077.x

Rivals J-P, Béal C, Thammavongs B, Guéguen M, Panoff J-M (2007) Cryotolerance of *Lactobacillus delbrueckii* subsp. *bulgaricus* CFL1 is modified by acquisition of antibiotic resistance. Cryobiology 55:19–26. doi: 10.1016/j.cryobiol.2007.04.003

Roberts IS (1996) The biochemistry and genetics of capsular polysaccharide production in bacteria. Annu Rev Microbiol 50:285–315. doi: 10.1146/annurev.micro.50.1.285

Robinson JW, Skelly Frame EM, Frame GMI (2005) Infrared, near-infrared, and Raman spectroscopy. In: Undergraduate instrumental analysis. Sixth edition, Marcel Dekker. CRC Press, New York, USA, pp 213–316

Romanazzi V, Traversi D, Lorenzi E, Gilli G (2015) Effects of freezing storage on the DNA extraction and microbial evaluation from anaerobic digested sludges. BMC Res Notes. doi: 10.1186/s13104-015-1407-2

Romantsov T, Stalker L, Culham DE, Wood JM (2008) Cardiolipin controls the osmotic stress response and the subcellular location of transporter ProP in *Escherichia coli*. J Biol Chem 283:12314–12323. doi: 10.1074/jbc.M709871200

Romeo Y, Bouvier J, Gutierrez C (2001) La réponse au stress osmotique des bactéries lactiques *Lactococcus lactis* et *Lactobacillus plantarum* (mini-revue). Le Lait 81:49–55. doi: 10.1051/lait:2001100

Ronholm J, Raymond-Bouchard I, Creskey M, Cyr T, Cloutis EA, Whyte LG (2015) Characterizing the surface-exposed proteome of *Planococcus halocryophilus* during cryophilic growth. Extrem Life Extreme Cond 19:619–629. doi: 10.1007/s00792-015-0743-4

Sandt C, Madoulet C, Kohler A, Allouch P, De Champs C, Manfait M, Sockalingum GD (2006) FT-IR microspectroscopy for early identification of some clinically relevant pathogens. J Appl Microbiol 101:785–797. doi: 10.1111/j.1365-2672.2006.02969.x

Sanguansermsri J, György P, Zilliken F (1974) Polyamines in human and cow's milk. Am J Clin Nutr 27:859–865

Santivarangkna C, Higl B, Foerst P (2008a) Protection mechanisms of sugars during different stages of preparation process of dried lactic acid starter cultures. Food Microbiol 25:429–441. doi: 10.1016/j.fm.2007.12.004

Santivarangkna C, Kulozik U, Foerst P (2008b) Inactivation mechanisms of lactic acid starter cultures preserved by drying processes. J Appl Microbiol 105:1–13. doi: 10.1111/j.1365-2672.2008.03744.x

Santivarangkna C, Wenning M, Foerst P, Kulozik U (2007) Damage of cell envelope of *Lactobacillus helveticus* during vacuum drying. J Appl Microbiol 102:748–756. doi: 10.1111/j.1365-2672.2006.03123.x

Saulou C, Jamme F, Girbal L, Maranges C, Fourquaux I, Cocaign-Bousquet M, Dumas P, Mercier-Bonin M (2013) Synchrotron FTIR microspectroscopy of *Escherichia coli* at single-cell scale under silver-induced stress conditions. Anal Bioanal Chem 405:2685–2697. doi: 10.1007/s00216-013-6725-4

Saulou C, Jamme F, Maranges C, Fourquaux I, Despax B, Raynaud P, Dumas P, Mercier-Bonin M (2010) Synchrotron FTIR microspectroscopy of the yeast *Saccharomyces cerevisiae* after exposure to plasma-deposited nanosilver-containing coating. Anal Bioanal Chem 396:1441–1450. doi: 10.1007/s00216-009-3316-5

Savaiano DA (2014) Lactose digestion from yogurt: mechanism and relevance. Am J Clin Nutr 99:1251S–5S. doi: 10.3945/ajcn.113.073023

Savić D, Joković N, Topisirović L (2008) Multivariate statistical methods for discrimination of lactobacilli based on their FTIR spectra. Dairy Sci Technol 88:273–290. doi: 10.1051/dst:2008003

Schiller D, Kruse D, Kneifel H, Krämer R, Burkovski A (2000) Polyamine transport and role of potE in response to osmotic stress in *Escherichia coli*. J Bacteriol 182:6247–6249. doi: 10.1128/JB.182.21.6247-6249.2000

Schlame M (2008) Cardiolipin synthesis for the assembly of bacterial and mitochondrial membranes. J Lipid Res 49:1607–1620. doi: 10.1194/jlr.R700018-JLR200

Schmid A, Kortmann H, Dittrich PS, Blank LM (2010) Chemical and biological single cell analysis. Curr Opin Biotechnol 21:12–20. doi: 10.1016/j.copbio.2010.01.007

Schuster KC, Reese I, Urlaub E, Gapes JR, Lendl B (2000) Multidimensional information on the chemical composition of single bacterial cells by confocal Raman microspectroscopy. Anal Chem 72:5529–5534. doi: 10.1021/ac000718x

Schwarz H, Koch AL (1995) Phase and electron microscopic observations of osmotically induced wrinkling and the role of endocytotic vesicles in the plasmolysis of the Gram-negative cell wall. Microbiol Read Engl 141 (Pt 12):3161–3170. doi: 10.1099/13500872-141-12-3161

Serror P, Sasaki T, Ehrlich SD, Maguin E (2002) Electrotransformation of *Lactobacillus delbrueckii* subsp. *bulgaricus* and *L. delbrueckii* subsp. *lactis* with various plasmids. Appl Environ Microbiol 68:46–52. doi: 10.1128/AEM.68.1.46-52.2002

Seydlová G, Fišer R, Čabala R, Kozlík P, Svobodová J, Pátek M (2013) Surfactin production enhances the level of cardiolipin in the cytoplasmic membrane of *Bacillus subtilis*. Biochim Biophys Acta BBA - Biomembr 1828:2370–2378. doi: 10.1016/j.bbamem.2013.06.032

Shao Y, Gao S, Guo H, Zhang H (2014) Influence of culture conditions and preconditioning on survival of *Lactobacillus delbrueckii* subspecies *bulgaricus* ND02 during lyophilization. 97:1270–1280. doi: 10.3168/jds.2013-7536

She RC, Petti CA (2015) Procedures for the storage of microorganisms. In: Jorgensen J, Pfaller M, Carroll K, Funke G, Landry M, Richter S, Warnock D (eds) Manual of clinical microbiology, 11th edition, ASM press. Washington, DC, pp 161–168

She RC, Petti CA (2015) Procedures for the storage of microorganisms. In: Jorgensen J, Pfaller M, Carroll K, Funke G, Landry M, Richter S, Warnock D (eds) Manual of clinical microbiology, 11th edition, ASM press. Washington, DC, pp 161–168

Shivaji S, Prakash JSS (2010) How do bacteria sense and respond to low temperature? Arch Microbiol 192:85–95. doi: 10.1007/s00203-009-0539-y

Simonin H, Beney L, Gervais P (2008) Controlling the membrane fluidity of yeasts during coupled thermal and osmotic treatments. Biotechnol Bioeng 100:325–333. doi: 10.1002/bit.21749

Simonin H, Bergaoui IM, Perrier-Cornet JM, Gervais P (2015) Cryopreservation of *Escherichia coli* K12TG1: Protection from the damaging effects of supercooling by freezing. Cryobiology 70:115–121. doi: 10.1016/j.cryobiol.2014.12.006

Singer SJ, Nicolson GL (1972) The fluid mosaic model of the structure of cell membranes. Science 175:720–731

Smeianov VV, Wechter P, Broadbent JR, Hughes JE, Rodríguez BT, Christensen TK, Ardö Y, Steele JL (2007) Comparative high-density microarray analysis of gene expression during growth of *Lactobacillus helveticus* in milk versus rich culture medium. Appl Environ Microbiol 73:2661–2672. doi: 10.1128/AEM.00005-07

Smith D, Ryan M, Stackebrandt E (2008) The ex situ conservation of microorganisms: aiming at a certified quality management. In: Doelle H, Rokem S, Berovic M (eds) Biotechnology - fundamentals in biotechnology, Eolss Publishers Co. Ltd. Oxford, UK

Smittle RB, Gilliland SE, Speck ML (1972) Death of *Lactobacillus bulgaricus* resulting from liquid nitrogen freezing. Appl Microbiol 24:551–554

Smittle RB, Gilliland SE, Speck ML, Walter WM (1974) Relationship of cellular fatty acid composition to survival of *Lactobacillus bulgaricus* in liquid nitrogen. Appl Microbiol 27:738–743

Sohlenkamp C, Geiger O (2016) Bacterial membrane lipids: diversity in structures and pathways. FEMS Microbiol Rev 40:133–159. doi: 10.1093/femsre/fuv008

Sommer A, Tisinger L, Marcott C, Story G (2001) Attenuated total internal reflection infrared mapping microspectroscopy using an imaging microscope. Appl Spectrosc 55:252–256

Song S, Bae D-W, Lim K, Griffiths MW, Oh S (2014) Cold stress improves the ability of *Lactobacillus plantarum* L67 to survive freezing. Int J Food Microbiol 191:135–143. doi: 10.1016/j.ijfoodmicro.2014.09.017

Sorek R, Kunin V, Hugenholtz P (2008) CRISPR--a widespread system that provides acquired resistance against phages in bacteria and archaea. Nat Rev Microbiol 6:181–186. doi: 10.1038/nrmicro1793

Sørensen KI, Curic-Bawden M, Junge MP, Janzen T, Johansen E (2016) Enhancing the sweetness of yoghurt through metabolic remodeling of carbohydrate metabolism in *Streptococcus thermophilus* and *Lactobacillus delbrueckii* subsp. *bulgaricus*. Appl Environ Microbiol AEM.00462-16. doi: 10.1128/AEM.00462-16

Spinnler HE, Corrieu G (1989) Automatic method to quantify starter activity based on pH measurement. J Dairy Res 56:755–764. doi: 10.1017/S0022029900029332

Stöckel S, Kirchhoff J, Neugebauer U, Rösch P, Popp J (2016) The application of Raman spectroscopy for the detection and identification of microorganisms. J Raman Spectrosc 47:89–109. doi: 10.1002/jrs.4844

Strasser S, Neureiter M, Geppl M, Braun R, Danner H (2009) Influence of lyophilization, fluidized bed drying, addition of protectants, and storage on the viability of lactic acid bacteria. J Appl Microbiol 107:167–177. doi: 10.1111/j.1365-2672.2009.04192.x

Strauss G, Hauser H (1986) Stabilization of lipid bilayer vesicles by sucrose during freezing. Proc Natl Acad Sci U S A 83:2422–2426

Streit F, Athès V, Bchir A, Corrieu G, Béal C (2011) Microfiltration conditions modify *Lactobacillus bulgaricus* cryotolerance in response to physiological changes. Bioprocess Biosyst Eng 34:197–204. doi: 10.1007/s00449-010-0461-3

Streit F, Delettre J, Corrieu G, Béal C (2008) Acid adaptation of *Lactobacillus delbrueckii* subsp. *bulgaricus* induces physiological responses at membrane and cytosolic levels that improves cryotolerance. J Appl Microbiol 105:1071–1080. doi: 10.1111/j.1365-2672.2008.03848.x

Stuurman N, Edelstein AD, Amodaj N, Hoover KH, Vale RD (2010) Computer control of microscopes using μManager. Curr Protoc Mol Biol Chapter 14:Unit14.20. doi: 10.1002/0471142727.mb1420s92

Sun Z, Chen X, Wang J, Zhao W, Shao Y, Guo Z, Zhang X, Zhou Z, Sun T, Wang L, Meng H, Zhang H, Chen W (2011) Complete genome sequence of *Lactobacillus delbrueckii* subsp. *bulgaricus* strain ND02. J Bacteriol 193:3426–3427. doi: 10.1128/JB.05004-11

Sutton S (2010) The most probable number method and its uses in enumeration, qualification and validation. J Valid Technol 35–38

Tablin F, Wolkers WF, Walker NJ, Oliver AE, Tsvetkova NM, Gousset K, Crowe LM, Crowe JH (2001) Membrane reorganization during chilling: implications for long-term stabilization of platelets. Cryobiology 43:114–123. doi: 10.1006/cryo.2001.2355

Taniguchi Y, Choi PJ, Li G-W, Chen H, Babu M, Hearn J, Emili A, Xie XS (2010) Quantifying *E. coli* proteome and transcriptome with single-molecule sensitivity in single cells. Science 329:533–538. doi: 10.1126/science.1188308

Teixeira P, Castro H, Kirby R (1996) Evidence of membrane lipid oxidation of spray-dried *Lactobacillus bulgaricus* during storage. Lett Appl Microbiol 22:34–38. doi: 10.1111/j.1472-765X.1996.tb01103.x

Thoury M, Echard J-P, Réfrégiers M, Berrie B, Nevin A, Jamme F, Bertrand L (2011) Synchrotron UV−visible multispectral luminescence microimaging of historical samples. Anal Chem 83:1737–1745. doi: 10.1021/ac102986h

To BCS, Etzel MR (1997) Spray drying, freeze drying, or freezing of three different lactic acid bacteria species. J Food Sci 62:576–578. doi: 10.1111/j.1365-2621.1997.tb04434.x

Tobin MJ, Chesters MA, Chalmers JM, Rutten FJM, Fisher SE, Symonds IM, Hitchcock A, Allibone R, Dias-Gunasekara S (2004) Infrared microscopy of epithelial cancer cells in whole tissues and in tissue culture, using synchrotron radiation. Faraday Discuss 126:27-39; discussion 77-92

Tobin MJ, Puskar L, Barber RL, Harvey EC, Heraud P, Wood BR, Bambery KR, Dillon CT, Munro KL (2010) FTIR spectroscopy of single live cells in aqueous media by synchrotron IR microscopy using microfabricated sample holders. Vib Spectrosc 53:34–38. doi: 10.1016/j.vibspec.2010.02.005

Tourdot-Maréchal R, Gaboriau D, Beney L, Diviès C (2000) Membrane fluidity of stressed cells of *Oenococcus oeni*. Int J Food Microbiol 55:269–273. doi: 10.1016/S0168-1605(00)00202-6

Trevors JT (2003) Fluorescent probes for bacterial cytoplasmic membrane research. J Biochem Biophys Methods 57:87–103

Tsvetkov T, Brankova R (1983) Viability of micrococci and lactobacilli upon freezing and freeze-drying in the presence of different cryoprotectants. Cryobiology 20:318–323

Tsvetkov T, Shishkova I (1982) Studies on the effects of low temperatures on lactic acid bacteria. Cryobiology 19:211–214. doi: 10.1016/0011-2240(82)90143-2

Tymczyszyn EE, Gómez-Zavaglia A, Disalvo EA (2005) Influence of the growth at high osmolality on the lipid composition, water permeability and osmotic response of *Lactobacillus bulgaricus*. Arch Biochem Biophys 443:66–73. doi: 10.1016/j.abb.2005.09.004

Ulmer HM, Herberhold H, Fahsel S, Gänzle MG, Winter R, Vogel RF (2002) Effects of pressure-induced membrane phase transitions on inactivation of HorA, an ATP-dependent multidrug resistance transporter, in *Lactobacillus plantarum*. Appl Environ Microbiol 68:1088–1095

Uribe S, Sampedro JG (2003) Measuring solution viscosity and its effect on enzyme activity. Biol Proced Online 5:108–115. doi: 10.1251/bpo52

Urshev Z, Ishlimova D (2015) Distribution of clustered regularly interspaced palindrome repeats CRISPR2 and CRISPR3 in *Lactobacillus delbrueckii* ssp. *bulgaricus* strains. Biotechnol Biotechnol Equip 29:541–546. doi: 10.1080/13102818.2015.1013351

Vaccari L, Birarda G, Businaro L, Pacor S, Grenci G (2012a) Infrared microspectroscopy of live cells in microfluidic devices (MD-IRMS): toward a powerful label-free cell-based assay. Anal Chem 84:4768–4775. doi: 10.1021/ac300313x

Vaccari L, Birarda G, Grenci G, Pacor S, Businaro L (2012b) Synchrotron radiation infrared microspectroscopy of single living cells in microfluidic devices: advantages, disadvantages and future perspectives. J Phys Conf Ser 359:012007. doi: 10.1088/1742-6596/359/1/012007

van de Guchte M, Chaze T, Jan G, Mistou M-Y (2012) Properties of probiotic bacteria explored by proteomic approaches. Curr Opin Microbiol 15:381–389. doi: 10.1016/j.mib.2012.04.003

van de Guchte M, Penaud S, Grimaldi C, Barbe V, Bryson K, Nicolas P, Robert C, Oztas S, Mangenot S, Couloux A, Loux V, Dervyn R, Bossy R, Bolotin A, Batto J-M, Walunas T, Gibrat J-F, Bessières P, Weissenbach J, Ehrlich SD, Maguin E (2006) The complete genome sequence of *Lactobacillus bulgaricus* reveals extensive and ongoing reductive evolution. Proc Natl Acad Sci U S A 103:9274–9279. doi: 10.1073/pnas.0603024103

van de Guchte M, Serror P, Chervaux C, Smokvina T, Ehrlich SD, Maguin E (2002) Stress responses in lactic acid bacteria. Antonie Van Leeuwenhoek 82:187–216

VanBogelen RA, Neidhardt FC (1990) Ribosomes as sensors of heat and cold shock in *Escherichia coli*. Proc Natl Acad Sci U S A 87:5589–5593

Veerkamp JH (1971) Fatty acid composition of *Bifidobacterium* and *Lactobacillus* strains. J Bacteriol 108:861–867

Velly H, Bouix M, Passot S, Penicaud C, Beinsteiner H, Ghorbal S, Lieben P, Fonseca F (2015) Cyclopropanation of unsaturated fatty acids and membrane rigidification improve the freeze-drying resistance of *Lactococcus lactis* subsp. *lactis* TOMSC161. Appl Microbiol Biotechnol 99:907–918. doi: 10.1007/s00253-014-6152-2

Velly H, Fonseca F, Passot S, Delacroix-Buchet A, Bouix M (2014) Cell growth and resistance of *Lactococcus lactis* subsp. *lactis* TOMSC161 following freezing, drying and freeze-dried storage are differentially affected by fermentation conditions. 117:729–740. doi: 10.1111/jam.12577

Vinogradov E, Sadovskaya I, Cornelissen A, van Sinderen D (2015) Structural investigation of cell wall polysaccharides of *Lactobacillus delbrueckii* subsp. *bulgaricus* 17. Carbohydr Res 413:93–99. doi: 10.1016/j.carres.2015.06.001

Vollmer W, Blanot D, de Pedro MA (2008) Peptidoglycan structure and architecture. FEMS Microbiol Rev 32:149–167. doi: 10.1111/j.1574-6976.2007.00094.x

Vyumvuhore R, Tfayli A, Duplan H, Delalleau A, Manfait M, Baillet-Guffroy A (2013) Effects of atmospheric relative humidity on Stratum Corneum structure at the molecular level: ex vivo Raman spectroscopy analysis. Analyst 138:4103–4111. doi: 10.1039/c3an00716b

Wang D, Bodovitz S (2010) Single cell analysis: the new frontier in 'Omics.' Trends Biotechnol 28:281–290. doi: 10.1016/j.tibtech.2010.03.002

Wang Y, Corrieu G, Béal C (2005a) Fermentation pH and temperature influence the cryotolerance of *Lactobacillus acidophilus* RD758. J Dairy Sci 88:21–29. doi: 10.3168/jds.S0022-0302(05)72658-8

Wang Y, Delettre J, Guillot A, Corrieu G, Béal C (2005b) Influence of cooling temperature and duration on cold adaptation of *Lactobacillus acidophilus* RD758. Cryobiology 50:294–307. doi: 10.1016/j.cryobiol.2005.03.001

Wassenaar TM, Lukjancenko O (2014) Comparative genomics of Lactobacillus and other LAB. In: Holzapfel WH, Wood BJB (eds) Lactic Acid Bacteria. John Wiley & Sons, Ltd, pp 55–69

Weiss N, Schillinger U, Kandler O (1983) *Lactobacillus lactis*, *Lactobacillus leichmannii* and *Lactobacillus bulgaricus*, subjective synonyms of *Lactobacillus delbrueckii*, and description of *Lactobacillus delbrueckii* subsp. *lactis* comb. nov. and *Lactobacillus delbrueckii* subsp. *bulgaricus* comb. nov. Syst Appl Microbiol 4:552–557. doi: 10.1016/S0723-2020(83)80012-5

Wenning M, Breitenwieser F, Konrad R, Huber I, Busch U, Scherer S (2014) Identification and differentiation of food-related bacteria: a comparison of FTIR spectroscopy and MALDI-TOF mass spectrometry. J Microbiol Methods 103:44–52. doi: 10.1016/j.mimet.2014.05.011

Wenning M, Büchl NR, Scherer S (2010) Species and strain identification of lactic acid bacteria using FTIR spectroscopy and artificial neural networks. J Biophotonics 3:493–505. doi: 10.1002/jbio.201000015

Wolkers W, Oldenhof H (2015) Use of in situ Fourier transform infrared spectroscopy to study freezing and drying of cells. In: Wolkers WF, Oldenhof H (eds) Cryopreservation and freeze-drying protocols. Springer New York, pp 147–161

Wolkers WF, Balasubramanian SK, Ongstad EL, Zec HC, Bischof JC (2007) Effects of freezing on membranes and proteins in LNCaP prostate tumor cells. 1768:728–736. doi: 10.1016/j.bbamem.2006.12.007

Wolkers WF, Oldenhof H, Glasmacher B (2010) Dehydrating phospholipid vesicles measured in real-time using ATR Fourier transform infrared spectroscopy. Cryobiology 61:108–114. doi: 10.1016/j.cryobiol.2010.06.001

Wood JM, Bremer E, Csonka LN, Kraemer R, Poolman B, van der Heide T, Smith LT (2001) Osmosensing and osmoregulatory compatible solute accumulation by bacteria. Comp Biochem Physiol A Mol Integr Physiol 130:437–460

Wouters JA, Frenkiel H, Vos WM de, Kuipers OP, Abee T (2001) Cold shock proteins of *Lactococcus lactis* MG1363 are involved in cryoprotection and in the production of cold-induced proteins. Appl Environ Microbiol 67:5171–5178. doi: 10.1128/AEM.67.11.5171-5178.2001

Wouters JA, Mailhes M, Rombouts FM, Vos WM de, Kuipers OP, Abee T (2000) Physiological and regulatory effects of controlled overproduction of five cold shock proteins of *Lactococcus lactis* MG1363. Appl Environ Microbiol 66:3756–3763. doi: 10.1128/AEM.66.9.3756-3763.2000

Wouters JA, Rombouts FM, de Vos WM, Kuipers OP, Abee T (1999) Cold shock proteins and low-temperature response of *Streptococcus thermophilus* CNRZ302. Appl Environ Microbiol 65:4436–4442

Wright CT, Klaenhammer TR (1983) Survival of *Lactobacillus bulgaricus* during freezing and freeze-drying after growth in the presence of calcium. J Food Sci 48:773–777. doi: 10.1111/j.1365-2621.1983.tb14896.x

Wu R, Wang W, Yu D, Zhang W, Li Y, Sun Z, Wu J, Meng H, Zhang H (2009) Proteomics analysis of *Lactobacillus casei* Zhang, a new probiotic bacterium isolated from traditional home-made koumiss in inner Mongolia of China. Mol Cell Proteomics 8:2321–2338. doi: 10.1074/mcp.M800483-MCP200

Wurtmann EJ, Wolin SL (2009) RNA under attack: cellular handling of RNA damage. Crit Rev Biochem Mol Biol 44:34–49. doi: 10.1080/10409230802594043

Xie C, Mace J, Dinno MA, Li YQ, Tang W, Newton RJ, Gemperline PJ (2005) Identification of single bacterial cells in aqueous solution using confocal laser tweezers Raman spectroscopy. Anal Chem 77:4390–4397. doi: 10.1021/ac0504971

Xie X, Zubarev RA (2014) Effects of low-level deuterium enrichment on bacterial growth. PLoS ONE 9:e102071. doi: 10.1371/journal.pone.0102071

Yang L, Chen Y, Li Z, Shi Y, Li Z, Zhao X (2016) Correction for Yang *et al*., complete genome sequence of *Lactobacillus delbrueckii* subsp. *bulgaricus* MN-BM-F01. Genome Announc. doi: 10.1128/genomeA.00420-16

Yap TWC, Rabu A, Abu Bakar FD, Rahim RA, Mahadi NM, Illias RM, Murad AMA (2014) Growth phase-dependent proteomes of the Malaysian isolated *Lactococcus lactis* dairy strain M4 using label-free qualitative shotgun proteomics analysis. Sci World J 2014:642891. doi: 10.1155/2014/642891

Zanni E, Schifano E, Motta S, Sciubba F, Palleschi C, Mauri P, Perozzi G, Uccelletti D, Devirgiliis C, Miccheli A (2017) Combination of metabolomic and proteomic analysis revealed different features among *Lactobacillus delbrueckii* subspecies *bulgaricus* and *lactis* strains while in vivo testing in the model organism *Caenorhabditis elegans* highlighted probiotic properties. Front Microbiol. doi: 10.3389/fmicb.2017.01206

Zhang H-M, Li Z, Tsudome M, Ito S, Takami H, Horikoshi K (2005) An alkali-inducible flotillin-like protein from *Bacillus halodurans* C-125. Protein J 24:125–131

Zhong Z, Sun Z, Xu H, Zhang H (2016) Complete genome sequence of *Lactobacillus delbrueckii* subsp. *bulgaricus* strain ND04

Zhu D, Sun Y, Liu F, Li A, Yang L, Meng X-C (2016) Identification of surface-associated proteins of *Bifidobacterium animalis* ssp. *lactis* KLDS 2.0603 by enzymatic shaving. J Dairy Sci 99:5155–5172. doi: 10.3168/jds.2015-10581

APPENDICES

APPENDICES

I. Preparation of bacterial inocula

Colonies of *Lactobacillus delbrueckii* subsp. *bulgaricus* strains CFL1, ATCC 11842 or ATCC BA-365 were isolated on MRS agar plates (Biokar Diagnostics; Beauvais; France) after incubation for 72 h at 42 °C in anaerobic conditions (GENbox anaer, bioMerieux; Marcy l'Etoile, France). One colony was aseptically transferred into 30 mL of sterile MRS broth (Biokar Diagnostics; Beauvais, France) placed at 42 °C for 24 h. A volume of this preculture was transferred to 300 mL of sterile MRS broth, so that a dilution factor of 50 was applied, based on the measured optical density at 600 nm of the preculture (typically 1.5 mL). This culture was placed at 42 °C for 24 h of incubation without shaking. It was subsequently placed on ice to stop bacterial growth, and 10 % (wt/wt) of sterile glycerol of high purity (≥ 99 %, Sigma Aldrich; Saint-Louis, MO, USA) was added to the culture. After a thorough homogenization, aliquots of 1.2 mL into 2-mL sterile cryotubes (Sarstedt; Nümbrecht, Germany) were prepared, and kept on ice until storage in a mechanical freezer at -80 °C.

The absence of contamination of the bacterial preparation was verified at each step of the process (colony from the agar plate, end of preculture, end of culture) through Gram staining and observation of purple-stained straight rods under an optical microscope (Olympus Scop-Pro; Japan) with a 100x objective (A100, 1.30 oil immersion; Olympus; ville, Japan), resulting in a 1000x total magnification (eyepiece: 10x magnification).

II. SUPPLEMENTARY DATA TO CHAPTER I OF RESULTS & DISCUSSION

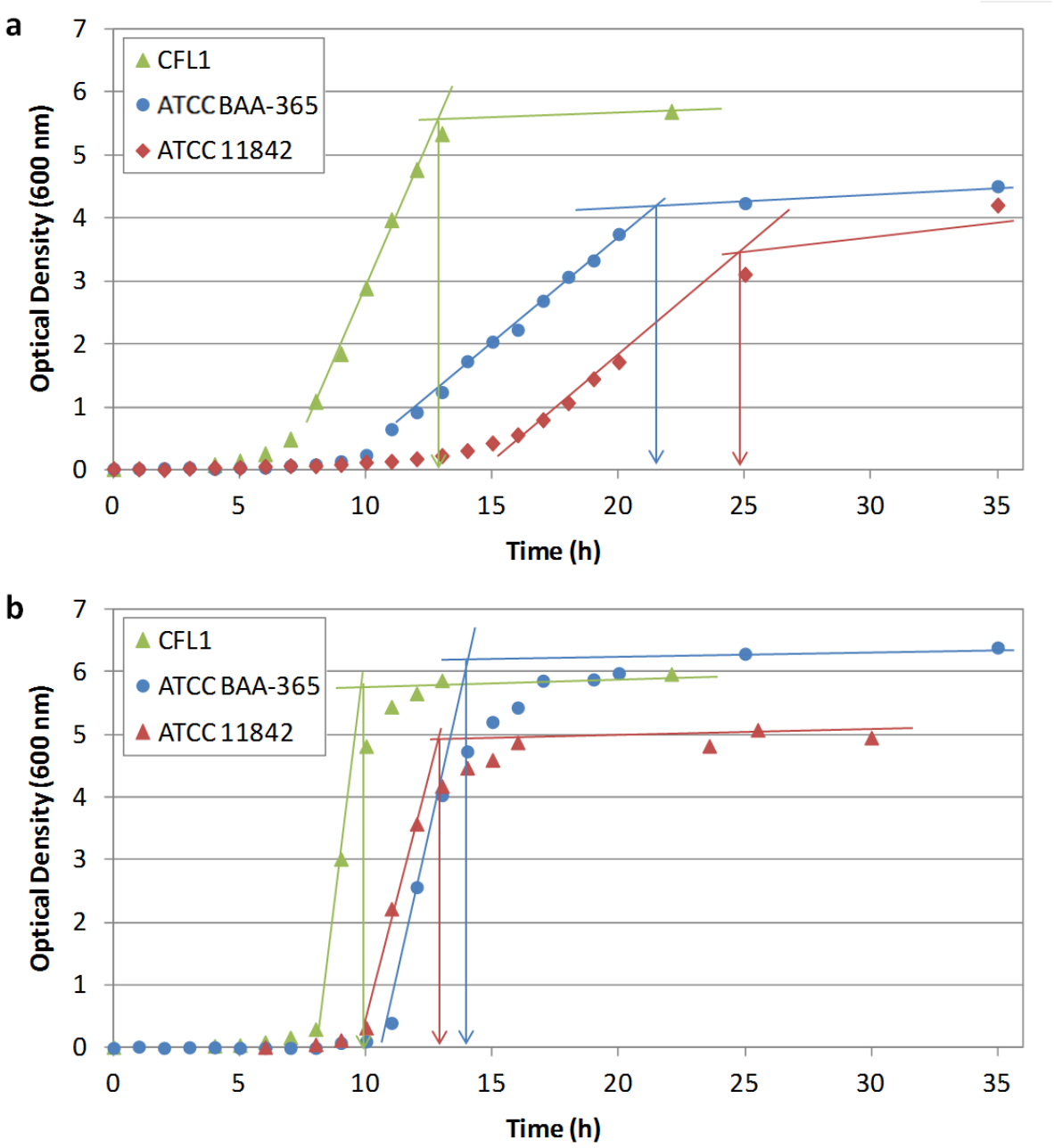

Figure S1: Growth kinetics of *Lactobacillus delbrueckii* subsp. *bulgaricus* CFL1 (green triangles), *L. bulgaricus* ATCC BAA-365 (blue dots) and *L. bulgaricus* ATCC 11842 (red diamonds) during culture in MRS broth (**a**) and whey-based medium (**b**) at 42 °C by optical density measurements at 600 nm. The arrows indicate the end of exponential growth phase and beginning of stationary phase used as references for cell harvest (see **Table IV.1-3** for harvest time details).

Table S1: Prophages identified in *Lactobacillus delbrueckii* subsp. *bulgaricus* CFL1, ATCC BAA-365 and ATCC 11842 and their main characteristics.

		Prophage characteristics: size (Kbp) - G+C content (%) – number of CDS - completeness		
# prophage	**Prophage BLAST hit**	**CFL1**	**ATCC BAA-365**	**ATCC 11842**
1	PHAGE_Clostr_c_st_NC_007581	8.5 - 46.49 - 15 - incomplete	23.0 - 45.68 - 9 - incomplete	21.6 - 46.72 - 8 - incomplete
2	PHAGE_Bacill_vB_BanS_Tsamsa_NC_023007	6.8 - 50.00 - 9 - incomplete	6.8 - 49.87 - 9 - incomplete	-
3	PHAGE_Plankt_PaV_LD_NC_016564	7.0 - 48.20 - 10 - incomplete	8.0 - 50.48 - 8 - incomplete	-
4	PHAGE_Arthro_KellEzio_NC_031231	8.5 - 46.49 - 15 - incomplete	-	-
5	PHAGE_Bacill_G_NC_023719	-	-	7.0 - 49.24 - 8 - incomplete
6	PHAGE_Strept_phiARI0460_1_NC_031913	-	-	34.3 - 47.94 - 7 - incomplete

CDS: coding DNA sequences; "–" phage absence.

Table S2: Other genes of interest present or not in the genomes of *Lactobacillus delbrueckii* subsp. *bulgaricus* CFL1, ATCC BAA-365 and ATCC 11842.

Locus tag: CFL1 (IMG / NCBI)	Locus tag: ATCC BAA-365	Locus tag: ATCC 11842	Protein name	Metabolic pathway	Protein size	Protein accession number: CFL1	Protein accession number: ATCC BAA-365	Protein accession number: ATCC 11842
Ga0063702_01030 / CFL1_RS04890	LBUL_1496	Ldb1617	molecular chaperone GroEL		537	WP_003619546	WP_003619546	WP_003619546
Ga0063702_01031 / CFL1_RS04895	LBUL_1497	Ldb1618	co-chaperone GroES		94	WP_011544118	WP_011544118	WP_011544118
Ga0063702_00019 / CFL1_RS00080	LBUL_0711	Ldb0778	ATP-dependent Clp protease ATP-binding subunit ClpX		417	WP_003619235	WP_011678151	WP_003623562
Ga0063702_00175 / CFL1_RS00805	LBUL_0559	Ldb0624	ATP-dependent Clp protease proteolytic subunit ClpP	Stress response	194	WP_003618944	WP_003618944	WP_011543732
Ga0063702_00222 / CFL1_RS01040	LBUL_0510	Ldb0574	ATP-dependent Clp protease ClpE		731	WP_014564694	WP_014564694	WP_011543713
Ga0063702_00810 / CFL1_RS03820	LBUL_0339	Ldb0383	ATP-dependent Clp protease ATP-binding subunit ClpC		819	WP_003620811	WP_003620811	WP_003622459
Ga0063702_00876 / CFL1_RS04140	LBUL_1944	Ldb2102	ATP-dependent Clp protease ATP-binding subunit ClpL		696	WP_003620469	WP_003620469	WP_011544327
Ga0063702_00151 / CFL1_RS00710	LBUL_0578	Ldb0647	Spermidine/putrescine ABC transporter, permease protein		362	WP_003622729	WP_011678091	WP_003622729
Ga0063702_00152 / CFL1_RS00705	LBUL_0579	Ldb0648	Spermidine/putrescine ABC transporter, permease protein		270	WP_003618983	WP_003618983	WP_003618983
Ga0063702_00153 / CFL1_RS00700	LBUL_0580	Ldb0649	Spermidine/putrescine ABC transporter, ATP-binding protein		267	WP_003618984	WP_003618984	WP_003618984
Ga0063702_00154 / CFL1_RS00695	LBUL_0581	Ldb0650	Spermidine/putrescine ABC transporter, substrate binding protein	Polyamine uptake	360	WP_003618985	WP_003622733	WP_011543738
-	-	Ldb2178	Spermidine/putrescine ABC transporter, permease protein		276	-	-	WP_011544348
-	-	Ldb2179	Spermidine/putrescine ABC transporter, permease protein		262	-	-	WP_011544349
-	-	Ldb2180	Spermidine/putrescine ABC transporter, ATP-binding protein		344	-	-	WP_011544350
-	-	Ldb2181	Spermidine/putrescine ABC transporter, substrate binding protein		353	-	-	WP_011544351

The proteins may be searched for *via* their protein accession numbers on: https://www.ncbi.nlm.nih.gov/protein; "–" gene absence.

III. Supplementary data to Chapter II of Results & Discussion

Table S3: Raw data for biological activity losses (culturability loss and acidification activity loss) following freeze-thawing and osmotic and cold stress treatments. Mean values ± standard deviations are indicated. Please refer to the material and methods section for experimental details.

	Strain	ATCC 11842			CFL1		
	Osmolarity	300 mOsm	600 mOsm	1800 mOsm	300 mOsm	600 mOsm	1800 mOsm
Culturability loss (log (CFU.mL^{-1})$^{-1}$)	Treatment						
	25 °C, 15 min	0.00 ± 0.00	0.05 ± 0.09	0.06 ± 0.07	0.00 ± 0.00	-0.28 ± 0.14	-1.69 ± 0.11
	25 °C, 3 hours	0.00 ± 0.00	0.05 ± 0.09	0.06 ± 0.07	0.05 ± 0.14	-0.36 ± 0.15	-1.80 ± 0.36
	-3 °C, 15 min	0.15 ± 0.10	-0.10 ± 0.07	-0.21 ± 0.08	0.00 ± 0.00	-0.38 ± 0.17	-1.88 ± 0.30
	-3 °C, 3 hours	0.15 ± 0.10	-0.10 ± 0.07	-0.21 ± 0.08	-0.07 ± 0.22	-0.76 ± 0.20	-2.01 ± 0.36
	Freezing (2°C.min^{-1})		-0.07 ± 0.16			-1.44 ± 0.12	
Acidification activity loss (min)	Treatment						
	25 °C, 15 min	0 ± 0	6 ± 12	11 ± 21	0 ± 0	58 ± 9	209 ± 68
	25 °C, 3 hours	16 ± 5	15 ± 11	29 ± 11	15 ± 10	77 ± 11	304 ± 74
	-3 °C, 15 min	0 ± 0	7 ± 3	8 ± 10	0 ± 0	65 ± 20	198 ± 39
	-3 °C, 3 hours	3 ± 3	16 ± 12	23 ± 15	49 ± 30	144 ± 19	301 ± 18
	Freezing (2°C.min^{-1})		9 ± 11			250 ± 10	

Table S4: Raw data for membrane properties assessments after an osmotic stress under selected temperatures. Membrane fluidity was measured by fluorescence anisotropy (*r*) using the probes DPH and TMA-DPH. Acyl chain order and phospholipid headgroup conformation were measured by FTIR spectroscopy by tracking the position of the symmetric CH_2 stretching vibration band (*sym.* vCH_2) and the asymmetric PO_2^- stretching vibration band (*asym.* vPO_2^-), respectively. Mean values ± standard deviations are indicated.

	Strain	ATCC 11842			CFL1		
	Osmolarity	300 mOsm	600 mOsm	1800 mOsm	300 mOsm	600 mOsm	1800 mOsm
Fluorescence anisotropy (*r*)	Temperature (°C)						
	DPH						
	42	0.123 ± 0.011	0.127 ± 0.005	0.128 ± 0.002	0.132 ± 0.004	0.135 ± 0.001	0.140 ± 0.015
	25	0.165 ± 0.016	0.160 ± 0.009	0.164 ± 0.007	0.188 ± 0.004	0.190 ± 0.008	0.183 ± 0.006
	5	0.235 ± 0.029	0.226 ± 0.010	0.227 ± 0.005	0.266 ± 0.022	0.263 ± 0.003	0.254 ± 0.001
	0	0.253 ± 0.025	0.192 ± 0.005	0.202 ± 0.003	0.282 ± 0.012	0.273 ± 0.009	0.260 ± 0.013
	TMA-DPH						
	42	0.228 ± 0.016	0.218 ± 0.004	0.220 ± 0.003	0.205 ± 0.010	0.212 ± 0.010	0.221 ± 0.015
	25	0.246 ± 0.017	0.239 ± 0.005	0.233 ± 0.007	0.233 ± 0.016	0.231 ± 0.008	0.236 ± 0.009
	5	0.283 ± 0.010	0.282 ± 0.007	0.265 ± 0.010	0.279 ± 0.027	0.300 ± 0.018	0.304 ± 0.011
	0	0.294 ± 0.022	0.262 ± 0.008	0.244 ± 0.001	0.289 ± 0.012	0.308 ± 0.008	0.314 ± 0.009
FTIR band position (cm^{-1})	Temperature (°C)						
	sym. vCH_2						
	42	2,853.34 ± 0.08	2,853.35 ± 0.09	2,853.39 ± 0.09	2,852.91 ± 0.63	2,852.89 ± 0.18	2,853.18 ± 0.30
	25	2,852.96 ± 0.09	2,852.97 ± 0.10	2,852.99 ± 0.09	2,852.06 ± 0.39	2,852.31 ± 0.18	2,852.56 ± 0.34
	5	2,851.62 ± 0.18	2,851.63 ± 0.15	2,851.64 ± 0.15	2,850.43 ± 0.08	2,850.72 ± 0.06	2,850.71 ± 0.04
	-50	2,850.18 ± 0.11	2,850.05 ± 0.14	2,849.97 ± 0.24	2,849.51 ± 0.25	2,849.44 ± 0.14	2,849.12 ± 0.20
	Ts	6.9 ± 1.3	6.1 ± 0.5	8.0 ± 1.5	17.5 ± 1.8	13.8 ± 1.4	13.6 ± 2.2
	asym. vPO_2^-						
	42	1,219.06 ± 0.05	1,218.62 ± 0.04	1,217.67 ± 0.17	1,218.20 ± 0.43	1,217.03 ± 0.47	1,210.24 ± 0.28
	25	1,219.26 ± 0.07	1,218.80 ± 0.03	1,217.76 ± 0.34	1,218.40 ± 0.72	1,217.02 ± 0.55	1,211.42 ± 0.06
	5	1,219.62 ± 0.03	1,219.07 ± 0.07	1,218.16 ± 0.15	1,218.83 ± 0.61	1,217.43 ± 0.60	1,213.67 ± 1.01
	-50	1,219.60 ± 0.06	1,218.94 ± 0.09	1,217.94 ± 0.16	1,218.55 ± 0.29	1,216.95 ± 0.63	1,214.22 ± 0.41

IV. Résumé substantiel de la thèse en français

Les bactéries lactiques sont d'une importance majeure pour l'industrie agro-alimentaire de par leur capacité à transformer des matières premières végétales en aliments fermentés. Le processus de fermentation est intéressant à plusieurs points de vue puisqu'il permet de modifier les caractéristiques organoleptiques de l'aliment ainsi transformé (arômes, goût, texture), d'en étendre la durée de conservation et de réduire la probabilité de contamination par des germes pathogènes. En particulier, *Lactobacillus delbrueckii* subsp. *bulgaricus* (*L. bulgaricus*) est utilisée depuis des millénaires pour la fermentation de produits laitiers, notamment pour la production de yaourts en protocooperation avec *Steptococcus thermophilus*. Pour illustrer l'importance considérable que représente la production industrielle de yaourts en France, d'après Syndifrais, en 2016, près d'1 million de yaourts ont été vendus en France, générant un chiffre d'affaires de près de 2 milliards d'euros. Or, l'industriel laitier qui conduit ce type de procédé de fermentation doit pouvoir disposer à tout instant de ferments actifs. Pour cela, il est donc nécessaire de procéder à une étape de stabilisation des ferments fraîchement produits avant leur utilisation finale. Celle-ci consiste à suspendre le métabolisme des bactéries pour le réactiver le moment voulu, tout en conservant la viabilité et les propriétés technologiques des bactéries avant et après cette étape de stabilisation. Les méthodes couramment employées pour stabiliser les ferments sont la congélation et la lyophilisation. La lyophilisation conduit à une déshydratation sévère des cellules, à laquelle *L. bulgaricus* ne survit pas, et faisant donc de la congélation – ou cryopréservation – la seule option industriellement viable.

La cryopréservation était donc au cœur de cette thèse, avec comme modèle d'application la bactérie lactique *L. bulgaricus*, car présentant une cryosensibilité variable selon les souches et les conditions de croissance appliquées en amont. Ces travaux visaient à étudier au sens large la réponse de *L. bulgaricus* aux principaux stress liés à la cryopréservation. Pour cela, des approches complémentaires de caractérisation de l'échantillon ont été mis en œuvre, incluant des analyses physiologiques, génomiques et biophysiques. L'intention était également d'étudier l'importance relative des réponses cellulaires à ces stress à différentes échelles : de la population à la cellule unique. Les principales hypothèses de travail ont été de considérer la cryopréservation comme une combinaison de stress froid et osmotique et la membrane comme la cible principale de dégradation, sans toutefois négliger l'impact potentiel d'autres constituants cellulaires, en particulier la paroi cellulaire et l'ensemble des protéines de la cellule. De plus, le recours à des techniques d'analyse non invasives et multi-échelles a été privilégié, permettant ainsi de sonder ces réponses cellulaires au niveau des populations et jusqu'à aux cellules individuelles en causant un minimum de perturbations, essentiel pour mieux comprendre les mécanismes de dégradation cellulaires liés à la congélation. Certaines de ces techniques d'analyse ont même été spécifiquement développées dans le cadre de ces travaux de thèse. L'objectif étant, *in fine*, de fournir des outils permettant de tendre vers la production de populations homogènes de ferments lactiques présentant des caractéristiques et performances désirées (fonctions, stabilité au stockage, etc.).

(a) Selection des souches et des conditions de croissance

> *L. bulgaricus* CFL1: **souche cryosensible**; *L. bulgaricus* ATCC 11842: **souche cryorésistante**
> Milieu à base de lactosérum & phase de croissance exponentielle tardive → cryorésistances les plus contrastées entre ces souches

(b) Détermination de l'impact relatif des principales contraintes liées à la cryopréservation

> Stress principaux lies à la congélation = froid + hyperosmotique
> Stress osmotique: perte d'activité biologique la plus importante pour **les cellules cryosensibles**
> Ni le stress osmotique ni le stress froid n'ont affecté l'activité biologique **des cellules cryorésistantes**

(c) Identification des marqueurs cellulaires de cryosensibilité/cryorésistance

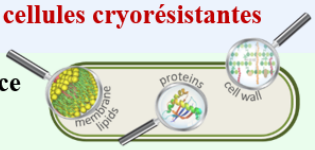

Marqueurs génétiques

> 3 gènes des souches cryorésistantes orthologues à une BL psychrophile, dont 1 codant pour une *csp*.
> Locus *epsI* + gènes codant pour certains transporteurs = souche-dépendants → différences de composition et/ou propriétés de leur membrane ?

Marqueurs membranaires

> **Cellules cryosensibles :** + SFA & CC-FA; $T_{s\ lip}$ plus élevé (membrane moins flexible aux faibles T°C) interaction préférentielle entre le saccharose et les têtes phospholipidiques ?
> **Cellules cryorésistantes :** + UFA & LC-FA; $T_{s\ lip}$ plus faible (membrane plus flexible aux faibles T°C) exclusion préférentielle entre le saccharose et les têtes phospholipidiques ?

Marqueurs au niveau de la paroi cellulaire et des protéines

> Composition/conformation de la paroi cellulaire = souche-dépendante avec des différences liées aux sucres et aux molécules phosphorylées
> Conformation des protéines = souche-dépendante avec des feuillets β préférentiellement associés aux **cellules cryorésistantes**
> Résidus d'acides amines tyrosine enfouis préférentiellement associés aux **cellules cryorésistantes** → structure protéiques plus natives ?

(d) Évaluation de l'hétérogénéité au sein des populations

Conformation des protéines

> **Cellules cryosensibles :** Hétérogénéité inter-cellulaire plus importante
> **Cellules cryorésistantes :** Homogénéité inter-cellulaire plus importante

Fluidité membranaire

> **Cellules cryosensibles :** Hétérogénéités intra- et inter-cellulaires plus importantes avec davantage de domaines rigides, en particulier en conditions de stress ;
> **Cellules cryorésistantes :** Homogénéités intra and inter-cellulaires plus importantes avec moins de domaines rigides

Echelle d'observation

Figure S2 : Aperçu schématique des principaux résultats obtenus de l'ensemble de ces travaux de thèse, divisé en quatre parties détaillées dans le texte (BL : bactérie lactique ; *csp* : gène codant pour une protéine cold-shock ; locus *epsI* : groupe de gènes codant pour des protéines de biosynthèse d'exopolysaccharides ; SFA : acide gras sature ; UFA : acide gras insaturé ; CC-FA : acide gras à courte chaine ; LC-FA : acide gras à longue chaine ; $T_{s\ lip}$: température de solidification de la membrane)

Les résultats les plus pertinents obtenus à la suite de ces travaux sont présentés ci-après en quatre points, et sont également regroupés schématiquement dans la **Fig. S2** :

Sélection des souches et des conditions de croissance (Fig. S2a)

Pour réduire les facteurs de variabilité expérimentale, la cryorésistance de trois souches de *L. bulgaricus* a été criblée selon plusieurs conditions de croissance (deux milieux de culture et deux phases de croissance au moment de la récolte) dans des conditions normalisées de cryopréservation (ajout d'un agent cryoprotecteur et vitesse de refroidissement contrôlée) (**CHAPITRE I**). La cryorésistance bactérienne a été évaluée par la perte de cultivabilité et de fonctionnalité (activité acidifiante) après congélation-décongélation. Les souches *L. bulgaricus* ATCC BAA-365 et ATCC 11842 se sont révélées être cryorésistantes, et ce quelles que soient les conditions de croissance testées. La souche *L. bulgaricus* CFL1 s'est révélée sensible à la congélation-décongélation lorsque cultivée dans un milieu à base de lactosérum, avec des pertes significatives de cultivabilité et d'activité d'acidifiante. La différence de sensibilité à la congélation-décongélation était particulièrement prononcée entre *L. bulgaricus* CFL1 et *L. bulgaricus* ATCC 11842 pour des cellules cultivées dans un milieu à base de lactosérum puis récoltées en fin de la phase exponentielle de croissance. Ce sont donc ces conditions de croissance qui ont été sélectionnées pour la suite de ce travail.

Détermination de l'impact relatif des principales contraintes liées à la cryopréservation (Fig. S2b)

Pour mieux comprendre les mécanismes conduisant à des comportements aussi différents, le processus de cryopréservation a été dissocié en deux stress unitaires principaux : le stress froid et le stress osmotique.
L'impact relatif des stress froid et osmotique sur la cultivabilité et les pertes d'activité acidifiante de *L. bulgaricus* CFL1 et *L. bulgaricus* ATCC 11842 a été étudié et comparé à la sensibilité à la congélation-décongélation (**CHAPITRE II)**. Le stress osmotique, dû à la cryoconcentration en solutés extracellulaires induite par la formation de glace au cours du refroidissement, a été identifié comme la cause principale de mort cellulaire et de perte de fonctionnalité de la souche cryosensible. En revanche, il n'a causé aucun dommage à la souche cryorésistante.

Identification des marqueurs cellulaires de cryosensibilité/cryorésistance (Fig. S2c)

Différentes approches ont été appliquées dans le but d'identifier les marqueurs de cryosensibilité cellulaire ou de cryorésistance chez plusieurs souches de *L. bulgaricus* : la comparaison génomique ; l'évaluation des propriétés biophysiques des membranes cellulaires et leur modification lors de l'application de traitements de stress ; et l'évaluation des informations biochimiques provenant d'autres composants cellulaires tels que les protéines et les constituants de la paroi cellulaire.

Marqueurs génétiques

Le séquençage du génome de *L. bulgaricus* CFL1, réalisé dans le cadre de ce travail de thèse, a révélé la présence de deux systèmes CRISPR-Cas distincts alors que *L. bulgaricus* ATCC BAA-365 et ATCC 11842 possèdent un unique système CRISPR-Cas d'un autre type (**CHAPITRE I**). Pour déterminer l'existence potentielle d'autres gènes différents entre la souche cryosensible (*L. bulgaricus* CFL1) et les souches cryorésistantes (*L. bulgaricus* ATCC BAA-365 et ATCC 11842), une comparaison génomique plus approfondie a été effectuée (**CHAPITRE I**). Un nombre restreint de gènes pertinents a ainsi été identifié chez les souches cryorésistantes, parmi lesquels un codant pour une protéine de choc froid et deux pour des sous-unités ribosomiques ayant la particularité d'être orthologues avec les gènes correspondants d'une bactérie lactique psychrophile. En outre, l'identification de certains gènes spécifiques à l'une ou l'autre des trois souches étudiées pourrait expliquer, au moins en partie, les cryorésistances souche-dépendantes qui ont pu être observées. Ces gènes codent pour la biosynthèse d'exopolysaccharides (loci *epsI*) et de transporteurs (PTS^{Cel} et transporteurs ABC à spermidine/putrescine), suggérant des différences en termes de composition et d'organisation de l'enveloppe cellulaire entre les trois souches.

Marqueurs membranaires

La caractérisation des membranes bactériennes de *L. bulgaricus* CFL1 et ATCC 11842 a englobé l'évaluation (**CHAPITRE II**) :

- de leur composition en acides gras,
- de l'ordre conformationnel existant au niveau de leurs chaînes acyl des acides gras (permettant l'évaluation de la température de transition de phase lipidique membranaire) ainsi qu'au niveau de leurs têtes phospholipidiques,
- et de leur fluidité membranaire.

Ces travaux ont révélé que les deux souches possèdent plus ou moins de résidus d'acides gras insaturés et à longue chaîne, avec des proportions plus élevées de ces acides gras dans la membrane de la souche résistante par rapport à la souche sensible. Les acides gras insaturés tendent à décaler la transition de phase lipidique membranaire vers les plus faibles températures (et vice versa pour les acides gras saturés), tandis que les acides gras à longue chaîne fondent à une température plus élevée. La température de transition de phase lipidique membranaire de la souche *L. bulgaricus* ATCC 11842, inférieure à celle de la souche *L. bulgaricus* CFL1, indique une influence probablement plus élevée des insaturations par rapport à la longueur de chaîne sur la température de transition de phase lipidique membranaire. Une faible température de transition de phase lipidique pourrait, également, être à l'origine d'une plus grande souplesse membranaire chez les cellules résistantes lors du refroidissement et de la formation de la glace, et ainsi faciliter l'écoulement de l'eau hors des cellules lors de la cryoconcentration extracellulaire. Ces résultats confirment des travaux antérieurs (Gautier *et al*. 2013). Le stress froid apparaît finalement comme induisant une modification importante de l'ordre conformationnel des résidus acyl des acides gras membranaires, contrairement au stress osmotique.

L'ordre conformationnel au niveau des têtes polaires phospholipidiques et sa modulation sous l'effet d'un stress froid et d'un stress osmotique ont ensuite été considérés. Cette propriété biophysique de la membrane a été évaluée en suivant, par spectroscopie infrarouge à transformée de Fourier (FTIR), la position de la bande de vibration issue de l'élongation asymétrique de la liaison PO^- (νPO^-_{asym}). Une telle étude, généralement réalisée sur des membranes modèles (Arrondo et Goñi 1998 ; Díaz *et al*. 2003 ; Wolkers *et al*. 2010), a ici été appliquée de façon originale à des cellules intactes. Le refroidissement n'a pas eu d'influence particulière sur le νPO^-_{asym}, mais le stress osmotique a décalé la position de cette bande de vibration dans les spectres FTIR des cellules sensibles vers des valeurs considérablement inférieures. Ce résultat suggère l'existence de différents types d'interactions entre la matrice concentrée en saccharose et les groupes PO^- des têtes phospholipidiques de la membrane des deux souches. L'existence d'une interaction préférentielle dans le cas de *L. bulgaricus* CFL1 a donc été proposée ; interaction pouvant conduire à des phénomènes de fuite au niveau de la membrane de composants cellulaires, pouvant finalement engendrer la rupture membranaire et la mort des cellules. En revanche, une exclusion préférentielle du saccharose de la membrane *L. bulgaricus* ATCC 11842 a été proposée pour expliquer la préservation de cette dernière en condition de stress hyperosmotique.
En parallèle, l'évaluation de la fluidité membranaire par anisotropie de fluorescence à l'échelle des populations des deux souches n'a pas révélé de différences significatives. Toutefois, la variabilité de ces résultats (écarts-types élevés) pourrait avoir masqué des variations subtiles.

Marqueurs au niveau de la paroi cellulaire et des protéines

Les spectroscopies vibrationnelles donnent des informations au niveau de la membrane, mais également sur d'autres biomolécules constitutrices des cellules et ont ainsi permis une caractérisation de la paroi cellulaire et des protéines de *L. bulgaricus* CFL1 et de *L. bulgaricus* ATCC 11842 (**CHAPITRE IV**).
L'observation de différences dans les empreintes infrarouges des deux souches au niveau de la région des glucides et des molécules phosphorylées a révélé des différences possibles dans la composition de leur enveloppe (en termes de peptidoglycane, d'acides téichoïques et/ou d'exopolysaccharides). En ce qui concerne les protéines, une proportion plus élevée de structures secondaires en feuillets β pourrait notamment être associée à la cryorésistance bactérienne. Une investigation complémentaire utilisant la microspectroscopie Raman a été réalisée. Elle a révélé que le ratio entre les localisations enfouie et exposée des résidus d'acides aminé tyrosyl au sein des protéines de *L. bulgaricus* était plus élevé dans le cas de la souche ATCC 11842 que dans le cas de la souche CFL1. Ces résultats suggèrent des structures protéiques plus sujettes à la dénaturation (plus exposées) pour cette dernière souche cryosensible.

Évaluation de l'hétérogénéité au sein des populations (Fig. S2d)

Afin de tendre vers l'étude de bactéries individuelles et dans un environnement aqueux et d'explorer ainsi l'hétérogénéité régnant au sein des populations de manière non invasive, différentes approches exploitant la brillance élevée du rayonnement synchrotron de SOLEIL ont été développées. Il s'agit de la microscopie à

fluorescence dans l'UV lointain (sur la ligne de lumière DISCO) et de la microspectroscopie FTIR (sur la ligne de lumière SMIS).

La microscopie de fluorescence dans l'UV profond a permis d'étudier la fluidité membranaire à un niveau sub-cellulaire en conditions de stress froid et osmotique, et de faire le lien avec la cryorésistance (**CHAPITRE III**). Elle a donc permis d'aller plus loin par rapport à l'analyse précédente effectuée à l'échelle de la population. Ces travaux ont confirmé qu'un stress froid à 0 °C (sans formation de glace) induit une rigidification de la membrane dans les deux souches qui n'est pas corrélée à la mort cellulaire. Une rigidification de la membrane en condition de stress osmotique a également été mise en évidence dans le cas de la souche résistante *L. bulgaricus* ATCC 11842. A l'inverse, la membrane de la souche sensible ne s'est pas rigidifiée de façon significative sous une contrainte osmotique létale. Plus intéressant encore, les hétérogénéités inter- et intra-cellulaires ont été quantifiées pour la première fois dans ce travail. La souche sensible s'est ainsi révélée plus hétérogène que la souche résistante aux niveaux inter- et intra-cellulaires, avec augmentation de domaines rigides. L'application d'un traitement hyperosmotique a eu pour effet d'augmenter cette hétérogénéité dans le cas de la souche sensible avec une multiplication du nombre de domaines rigides ainsi que leur augmentation en taille le long de la membrane de cellules individuelles. Ces résultats corroborent l'existence d'interactions perturbatrices entre le saccharose et la membrane de la souche sensible, proposées à partir des données de FTIR.

L'analyse des cellules bactériennes à haute résolution a également été réalisée par microspectroscopie IRTF et en milieu aqueux pour un examen des cellules en conditions natives ; le rayonnement infrarouge étant non invasif (**CHAPITRE IV**). Deux niveaux de résolution ont été obtenus : soit des groupes d'environ 10^{3-4} cellules (niveau intermédiaire entre les mesures à l'échelle de la population et de la cellule unique), soit des cellules individuelles avec une résolution spatiale de 1 x 1 µm². Dans les deux cas, les bandes de vibration caractéristiques de l'eau, qui submergent les bandes de vibration qui nous intéressent (celles émanant des composants bactériens) dans les spectres bruts, ont pu être éliminées de manière optimisée grâce au développement d'un programme de soustraction dédié. La première approche combinait l'utilisation de microchambres et de porte-échantillons spécifiques, les maintenant hermétiquement fermées. De cette façon, en minimisant et en contrôlant le chemin optique, la soustraction de l'eau des spectres a pu être effectuée. Cela a permis d'accéder à une large région spectrale pour l'analyse des échantillons (protéines, glucides et molécules phosphorylées) et de quantifier l'hétérogénéité des populations de cellules. En particulier, les productions de *L. bulgaricus* CFL1 ont ainsi pu être différenciées.
La deuxième approche, consistant à sonder des bactéries individuelles, a résulté d'un développement technique original, entrepris par le personnel de la ligne de lumière SMIS. En effet, les analyses à haute résolution spatiale par spectroscopie IRTF se limitaient jusqu'à présent aux grandes cellules eucaryotes en solution ou aux cellules bactériennes séchées. Une configuration de microscopie inversée couplée au mode de spectroscopie en réflexion totale atténuée (ATR) a donc été conçue sur mesure et connectée au rayonnement synchrotron. En utilisant des hémisphères ATR à indice de réfraction élevé et une chambre permettent d'accueillir des échantillons liquides, il a été possible de minimiser la quantité d'eau sondée et

ainsi d'enregistrer les spectres IRTF de cellules individuelles de *L. bulgaricus* en solution. Avec une telle configuration optique, la profondeur de pénétration du rayonnement infrarouge est extrêmement faible et a principalement ciblé l'enveloppe de *L. bulgaricus* CFL1 et *L. bulgaricus* ATCC 11842. La région spectrale portant des informations relatives aux protéines a pu être analysée et a révélé la présence de structures secondaires protéiques plus hétérogènes dans le cas des cellules cryosensibles que dans le cas des cellules cryorésistantes.

En résumé, ces travaux ont confirmé que la résistance à la cryopréservation de la bactérie lactique *L. bulgaricus* dépend fortement de la souche considérée et des conditions de culture. Ils ont souligné que les pertes de cultivabilité et d'activité acidifiante après congélation-décongélation peuvent être principalement attribuées aux effets délétères du stress osmotique résultant de la cryoconcentration en solutés extracellulaires lors de la formation de la glace. De plus, ces travaux ont identifié l'implication décisive de l'enveloppe cellulaire dans la résistance de *L. bulgaricus* à de telles contraintes environnementales, notamment la composition et l'organisation de la membrane et de la paroi cellulaire. L'analyse multi-échelle réalisée tout au long de ce travail, en particulier par le biais d'expériences à haute résolution utilisant le rayonnement synchrotron, était novatrice et a révélé l'existence d'un lien entre hétérogénéité inter-cellulaire (de la fluidité membranaire et de la conformation des protéines) et cryosensibilité. De plus, l'hétérogénéité de la fluidité membranaire est apparue plus prononcée au niveau intra-cellulaire dans les cellules cryosensibles. Par conséquent, l'identification des souches, des conditions de culture, de récolte et de cryopréservation conduisant à des populations homogènes de cellules résistantes constitue un défi pour l'industrie laitière afin de produire et de stabiliser des ferments hautement viables et fonctionnels après décongélation.

La caractérisation des populations bactériennes cryorésistantes et cryosensibles à l'aide de techniques analytiques complémentaires a permis d'avoir une vision d'ensemble des différents types de biomolécules impliqués dans la cryorésistance bactérienne, et ainsi de mieux comprendre les mécanismes impliqués. Il a été possible d'identifier des molécules (composition en acides gras membranaire) ou des fractions de macromolécules (gènes), de caractériser des entités cellulaires (fluidité membranaire ; structure secondaire des protéines ; enveloppe cellulaire) et d'associer leur analyse à la fonctionnalité finale des populations bactériennes (cultivabilité et activité acidifiante).

Cette étude a été réalisée en appliquant des techniques plus ou moins invasives. Les données sur l'activité biologique (pour rendre compte de la cultivabilité et de l'activité acidifiante) ont donc été obtenues dans des conditions natives et les données de spectroscopie IRTF en environnement aqueux. En revanche, la fixation des cellules par séchage à l'air (microspectroscopie Raman), l'utilisation de fluorophores se fixant au niveau de la membrane et de radiations UV ionisantes (anisotropie de fluorescence), ou des procédures d'extraction (extraction accélérée par solvant – ASE – des lipides membranaires) ont pu introduire des modifications chimiques dans les échantillons. Cette considération doit être gardée à l'esprit pour réaliser des interprétations judicieuses des résultats.

La spectroscopie IRTF dans la région du rayonnement infrarouge moyen (4000 à 400 cm^{-1}) a donné accès à un éventail de résolutions spatiales. En combinant différents modes d'analyse à une source thermique ou

synchrotron, et en ayant recours à des techniques d'échantillonnage et à des procédures de soustraction de l'eau pour l'analyse d'échantillons aqueux, il a été possible de personnaliser l'utilisation de la spectroscopie IRTF pour la pleine exploitation de son potentiel analytique. Cependant, la non-spécificité de la spectroscopie IRTF peut également être un inconvénient qui nécessite l'utilisation de techniques complémentaires et souvent plus invasives. Ainsi, la combinaison de différentes techniques d'analyse présentant différents avantages et inconvénients apparaît ici comme étant l'approche idéale et nécessaire pour fournir une caractérisation d'échantillons biologiques la plus exhaustive et pertinente possible.

université PARIS-SACLAY
ÉCOLE DOCTORALE
Agriculture, alimentation, biologie, environnement, santé (ABIES)

Titre : Etude des stress liés au procédé de cryopréservation *via* une approche globale et multi-échelle chez la bactérie lactique *Lactobacillus delbrueckii* subsp. *bulgaricus*

Mots clés : Bactéries lactiques, cryopréservation, stress osmotique, propriétés biophysiques membranaires, hétérogénéité, rayonnement synchrotron

Résumé : La cryopréservation engendre des dégradations variables de l'activité biologique et des fonctionnalités des bactéries lactiques, notamment chez *Lactobacillus delbrueckii* subsp. *bulgaricus*, un starter de l'industrie laitière. Le but de ce travail a été d'identifier les marqueurs cellulaires de cryorésitance et de cryosensibilité afin de mieux comprendre les mécanismes de dégradation sous-jacents et d'améliorer les performances industrielles des bactéries lactiques. La cryopresérvation a ici été considérée comme une combination de deux stress majoritaires : froid et osmotique. Une attention particulière a été portée à l'analyse de la membrane cellulaire, un site majeur de dégradation lié à la congélation, mais également à la paroi cellulaire et aux protéines. De plus, les cellules ont été analysées à différentes échelles d'observation, de la population jusqu'à la cellule unique, afin de quantifier l'hétérogénéité des propriétés cellulaires existant au sein de populations. Dans une première partie de ce travail, des conditions de culture ont été comparées pour identifier deux souches de *L. bulgaricus* présentant des résistances contrastées vis-à-vis de la congélation. Une analyse génomique comparative des souches a également été menée dans le but de fournir des pistes de compréhension de ces comportements différents. Dans une seconde partie, des propriétés membranaires des cellules ont été évaluées en réponse aux stress froid et osmotique : composition en acides gras, organisation au niveau des chaînes d'acides gras et des têtes phospholipidiques, et fluidité. Leur fluidité membranaire a également été caractérisée à une échelle subcellulaire par microscopie de fluorescence au moyen du rayonnement synchrotron, permettant la quantification des hétérogénéités inter- et intra-cellulaires. Enfin, un développement technique et méthodologique a été entrepris afin de permettre l'analyse de bactéries individuelles en milieu aqueux par spectroscopie infrarouge à transformée de Fourier, et ainsi leur signature biochimique en conditions natives. Ces approches complémentaires et multidisciplinaires ont révélé l'existence de propriétés et d'organisation différentes de la membrane des deux souches de *L. bulgaricus*. Différents types d'interaction entre les molécules cryoprotectrices du milieu extracellulaire et la membrane des deux souches a été proposé, pouvant être à l'origine des dommages causés à la souche sensible. De plus, une hétérogénéité plus importante au sein de la population sensible a été identifiée, attribuée à des différences en termes de composition biochimique et d'organisation au niveau de la membrane et de la paroi. Finalement, ce travail suggère quelques marqueurs cellulaires d'évaluation de la cryorésistance des bactéries lactiques, et fournit des méthodes de caractérisation de l'hétérogénéité biochimique au sein des populations. Ceux-ci pourraient être appliqués à l'étude de toute autre étape critique du procédé de production des bactéries lactiques, et pourraient être utiles pour aller vers la production de ferments homogènes au niveau de leur résistance.

Title : Study of the cryopreservation-related stresses in the lactic acid bacterium *Lactobacillus delbrueckii* subsp. *bulgaricus* through a global and multi-scale approach

Keywords : Lactic acid bacteria, cryopreservation, osmotic stress, membrane biophysical properties, heterogeneity, synchrotron radiation

Abstract : Cryopreservation leads to variable degradation of the biological activity and functionality among lactic acid bacteria (LAB), particularly *Lactobacillus delbrueckii* subsp. *bulgaricus*, a dairy starter of industrial relevance. The aim of this work was to identify cellular markers of cryoresistance or cryosensitivity for better understanding the mechanisms of cell cryoinjury and increasing LAB industrial performances. Cryopreservation was here considered as a combination of cold and osmotic stresses. A particular focus was given to the analysis of the cell membrane, recognised as a primary site of cryoinjury, but also of the cell wall and proteins. Moreover, cells were analysed from the population level down to the single-cell level to quantify the heterogeneity of cell properties within populations. In the first part of this work, bacterial cultivation conditions were compared to identify two *L. bulgaricus* strains with markedly different cell cryoresistance. Moreover, a comparative genomic analysis of the strains was performed to provide some clues for the explanation of their different behaviours. In the second part of this work, the membrane properties were evaluated in response to the cold and osmotic stresses: fatty acid composition, organisation of fatty acyl and phospholipid headgroups, and fluidity. Subcellular membrane fluidity was also characterised by fluorescence microscopy using synchrotron radiation, enabling the quantification of inter- and intra-cellular heterogeneities. Finally, original methodological and technical developments were undertaken to achieve the analysis of individual bacterial cells in an aqueous environment by Fourier transform infrared (FTIR) spectroscopy, for the analysis of the biochemical signature of cells under native conditions. These complementary multidisciplinary approaches revealed different properties and organisation of the membrane of both *L. bulgaricus* strains. It was proposed that different types of interaction between cryoprotectants of the extracellular matrix and the membrane of both strains could be at the origin of cryoinjury for the sensitive strain. Moreover, a high population heterogeneity characterised the cryosensitive strain, ascribed to differences in terms of biochemical composition and organisation of the membrane and cell wall. Altogether, this work suggests some cellular markers to evaluate LAB cryoresistance and provides methods to characterize population biochemical heterogeneity. These could be applied to any other stressful step of their production process, and should be useful for future production of homogeneous populations of resistant LAB.

Université Paris-Saclay
Espace Technologique / Immeuble Discovery
Route de l'Orme aux Merisiers RD 128 / 91190 Saint-Aubin, France